September 2020
Vol. 4 - n. 2 Suppl.

2532-3997

Substantia

An International Journal of the History of Chemistry

ABOUT WATER: Novel Technologies for the New Millennium

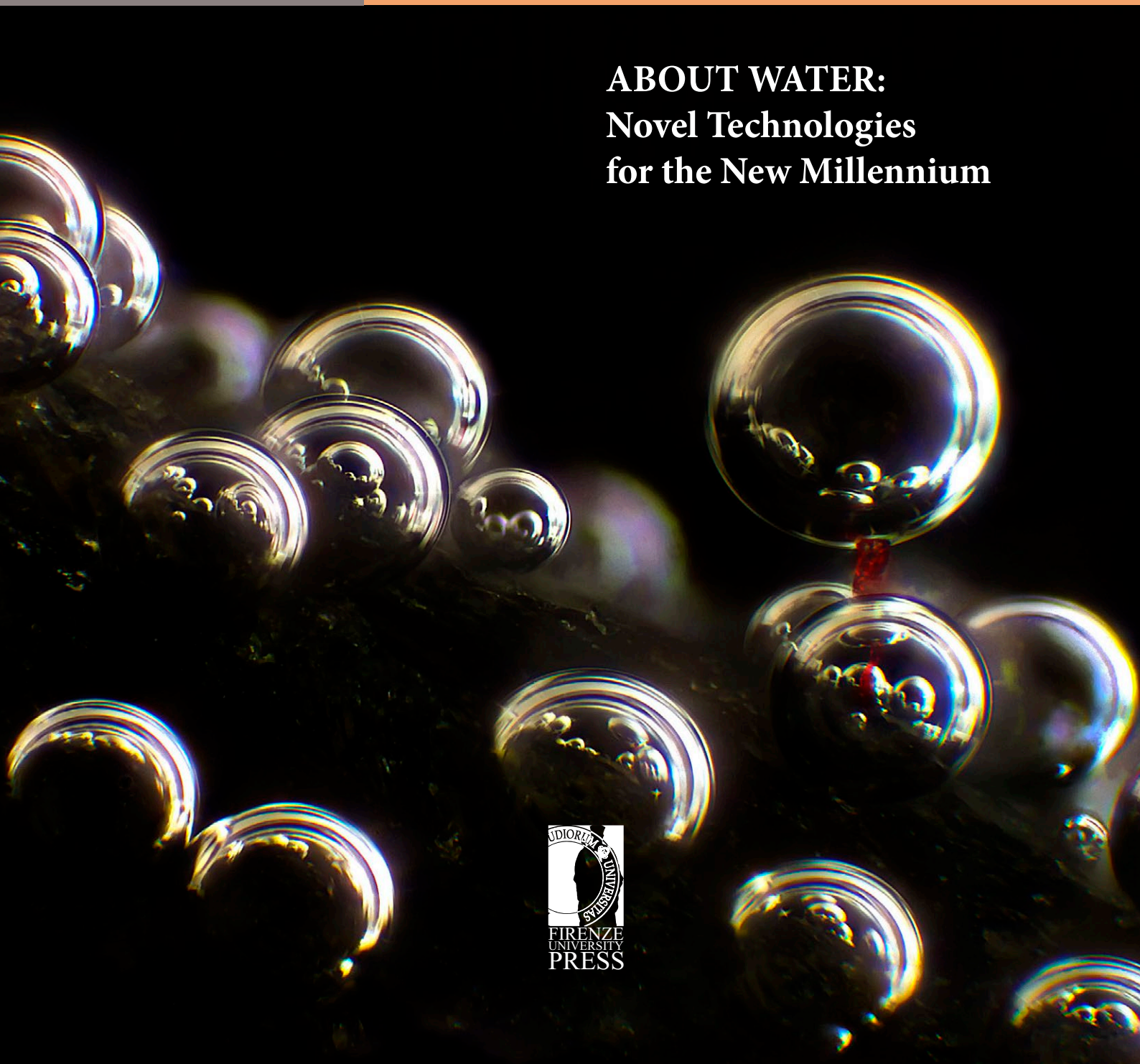

FIRENZE UNIVERSITY PRESS

Substantia

An International Journal of the History of Chemistry

Vol. 4, n. 2 Suppl. - 2020

Firenze University Press

***Substantia*. An International Journal of the History of Chemistry**

Published by
Firenze University Press – University of Florence, Italy
Via Cittadella, 7 - 50144 Florence - Italy
http://www.fupress.com/substantia

Direttore Responsabile: **Romeo Perrotta**, University of Florence, Italy

Cover image: Reflected light image stacking micrograph (magnification 10x) of bubbles and single cloth fiber (red) on a rock surface by Walter A. Piorkowski, South Beloit, Illinois, USA. Courtesy of Nikon Small World (Honorable Mention, 2018 Photomicrography Competition, https://www.nikonsmallworld.com).

Substantia is honoured to declare the patronage of:

museo galileo
Istituto e Museo di Storia della Scienza

Fondazione Prof. Enzo Ferroni ONLUS Firenze

Università degli Studi Firenze
Dipartimento di Chimica "Ugo Schiff"

Società Chimica Italiana

With the financial support of:

Breakthrough Water Technologies

Substantia
An International Journal of the History of Chemistry

No walls. Just bridges

Substantia is a peer-reviewed, academic international journal dedicated to traditional perspectives as well as innovative and synergistic implications of history and philosophy of Chemistry.
It is meant to be a crucible for discussions on science, on making science and its outcomes.
Substantia hosts discussions on the connections between chemistry and other horizons of human activities, and on the historical aspects of chemistry.
Substantia is published *open access* twice a year and offers top quality original full papers, essays, experimental works, reviews, biographies and dissemination manuscripts.
All contributions are in English.

Substantia
An International Journal of the History of Chemistry

Firenze University Press
www.fupress.com/substantia

Citation: B.W. Ninham, R.M. Pashley, (2020) Overview. *Substantia* 4(2) Suppl.: 5-8. doi: 10.36253/Substantia-1155

Data Availability Statement: All relevant data are within the paper and its Supporting Information files.

Competing Interests: The Author(s) declare(s) no conflict of interest.

Overview

Barry W. Ninham[1], Richard M. Pashley[2,*]

[1] *Department of Applied Mathematics, Research School of Physical Sciences, Australian National University, Canberra, Australia*
[2] *School of Science, University of New South Wales, Northcott Drive, Campbell, Canberra, Australia*
*Corresponding author: r.pashley@adfa.edu.au

It is an indisputable observation, beyond climate change: that the urgent development of simple new technologies, to ensure the supply of quality fresh water for cities and towns, industry and agriculture, presents an existential challenge for humanity.

Several novel technologies that fill that need show that the job is not impossible. They are summarized in this volume. They are environmentally friendly and inexpensive.

They include techniques for seawater desalination, wastewater sterilization – including viruses –, selective removal of heavy metals from industrial wastewater, efficient concentration of wastewater slimes to recycle water, and the prevention of water cavitation for much cheaper transport. Other new techniques like high temperature reactions achieved in low temperature water, and low energy desalination are in the wings. Borrowing from biology, new and edible class of surfactants is environmentally friendly, and can replace standard surfactants in present usage. The new technologies are cheap and scalable.

They became possible once we realised that the theories of physical, colloid, surface and electrochemistry are deeply flawed due to sins of omission and commission. Those of commission have to do with erroneous treatment of molecular forces in solution and their specificity (Hofmeister effects). Those of omission are due to neglect of effects of dissolved gas. Both are ignored in classical and textbook theories. The Greeks taught us there were 4 elements, earth (salt), water, fire (heat) and air. We forgot the air, even Descartes, who might instead of his saying: "I think, therefore I am", might have better said: "I breathe, therefore I am," The inclusion of gas changes the world of physical chemistry and opens up new vistas.

DESALINATION

Seawater desalination offers an unlimited source of fresh water, the demand for which we are increasingly unable to meet. Different desalination techniques are already commercially available. It is unlikely that they can be

improved further in terms of energy efficiency as well as operational simplicity to meet the needs of an ever expanding industrial scale. Some of these techniques have not been changed for half a century, reverse osmosis membranes being the most familiar. Their limitations are well known.

Two novel desalination processes are described here. The first is the bubble column evaporator (BCE), which is simple, scalable and requires low maintenance. The BCE operates primarily by direct contact of the seawater with heated gas. In a further development, helium carrier gas consumes less energy than other processes and can be recycled in a closed system. High overall heat- and mass-transfer is achieved. The BCE process can be used extensively in many applications such as desalination, water/wastewater treatment and even for the thermolysis of solute decomposition (e.g. ammonium bicarbonate).

A new way of decomposing and recycling ammonium bicarbonate in aqueous solution has been developed using a membrane-transport process with both dense and porous hollow-fiber membranes. The decomposition of ammonium bicarbonate solutions occurs via contact through a permeable membrane, of the solutions pre-heated to 80°C with a continuous counter-flow of dehumidified air at room temperature. In this process, ammonia (NH_3) and carbon dioxide (CO_2) gases permeate through the membrane and are thereby separated from the feed solution; they can then be collected into aqueous solution for recycling.

The BCE method also offers a fast and robust way to decompose ammonium bicarbonate solutions and readily meets industrial-scale requirements. Combined with this, we have produced a novel, sustainable ion exchange desalination process based on low cost resin regeneration. It uses ammonium bicarbonate solution in place of the usual, and expensive, acid and base washing.

Regeneration using this salt further allows the use of novel ion exchange resins which contain the cation and anion exchanging groups in close proximity, that is, nanometers apart rather than millimeters apart. These resins are more efficient and can be regenerated *in situ* without exposure to either acid or base solutions. This offers a second energy-efficient desalination method. It is a serious competitor for, and indeed superior to reverse osmosis desalination on all fronts and is close to large scale implementation.

WATER TREATMENT

The treatment of water contaminated with hazardous heavy metal ions, is also needed to supply clean water. These metal ions are produced naturally or through industrial processes, and can infiltrate water supplies for general or agricultural uses. Naturally occurring arsenic is a massive problem for millions of people world-wide. New techniques are required to remove hazardous ions from drinking water, especially at low-level concentrations.

One potential technique is ion flotation, and with environmentally friendly, meaning biodegradable, surfactants. In principle these should be highly efficient and specific absorbers of hazardous ions from aqueous solutions. In biology, enzymes have an exquisite capacity to select and bind specific ions.

So taking that lesson from biology, we have taken cysteine, which is a natural amino acid, and has a high affinity to bind with a range of contaminant ions, to explore what can be done. As an example, the Na^+ salt of the N-octanoyl-cysteine surfactant showed highest efficiency in the ion flotation process. It has a high water solubility and exhibits extensive foaming in a typical flotation chamber over a wide pH range. In a batch ion-flotation process, this surfactant was able to remove 97–99% of lanthanum, arsenic and various divalent heavy metals present at 5ppm levels in contaminated water, in a simple, single-stage physiochemical process. This surfactant showed significantly lower efficiency for the removal of iron, selenium and gold ions and hence these studies also show how the ion-flotation process could be used to remove specific ions selectively from mixed ion solutions. The most promising aspect of the selectivity achieved is probably for future developments involving rare earth separation and the treatment of nuclear wastes.

The design of environmentally friendly surfactants that have specific ion binding properties is a long standing aim of the chemical industry, and something devoutly to be wished for.

Our “exhibit one” surfactant is such an environmentally acceptable compound. It can be readily decomposed into cysteine (an amino acid) and octanoic acid (or caprylic acid), both of which can be taken as a dietary supplement). The surfactant, as an efficient and specific collector, has the potential for wide usage in both ion and froth flotation. The surfactant has also been shown to have a high affinity to bind with ions like copper, lead, arsenic. It is promising in the treatment of mining wastewater sites contaminated by such ions worldwide. Naturally occurring arsenic contamination in drinking water is a huge problem in various countries and this surfactant is a winner not yet harnessed for the task.

A novel, efficient synthesis method has been developed to produce the N-octanoyl-cysteine surfactant.

This gives cheap high product yields with a simple and straight forward method. The high synthesis yield of this product is important, as it offers an environmentally acceptable agent for the removal of a range of heavy-metal ions from contaminated water and soil.

More importantly, it could also be used in general household-detergent/personnel-cleaner formulations and even in toothpastes! Replacement of standard surfactants like sodium dodecyl sulfate and a myriad quaternary ammonium or related cationic surfactants is urgent. Their manufacture from petroleum products is a large part of industrial CO_2 production in Europe.

In addition, the surfactant could be used to facilitate the removal of PFAS compounds from soils. The PFAS surfactants are negatively charged, but often bind to negatively charged particles of sand, clay and humic acid-coated materials, and microorganisms via bridging multivalent cations. Hence, it could be more environmentally acceptable to use this biodegradable surfactant, which would combine cation chelation properties with foam fractionation separation of surface-active (e.g. PFAS) components in soils.

STERILIZATION, CARBON DIOXIDE AND VIRUSES

Inactivation of viruses has been an insuperable inhibition to the use of recycled water. Hence the ubiquity of plastic bottled water in cities. Current processes such as UV irradiation, chlorination, ozonolysis and even treatment with bacteriocides, such as quaternary ammonium surfactants, all produce varying levels of potentially toxic by-products and subsequent environmental issues. We have said goodbye to all that. In a surprising development, we found an environmentally friendly technology for sterilizing water by doing just that. The technology bubbles heated, un-pressurized carbon dioxide (or even exhaust gases) through contaminated wastewater in a bubble column. The process kills both waterborne bacteria and viruses close to 100%! The technique is extremely cost effective, with no by-products to bother about, and has already been successfully scaled-up industrially. Substantial success so far achieved in solving the problem of pathogens is here extended. A novel technique based on the use of a continuous, high density flow of carbon dioxide bubbles, over a range of temperatures – depending on application, can effectively sterilize wastewater – without the risk of harmful byproducts. Efficient use of hot, waste combustion gases can be used for wastewater sterilization and at the same time produce pure, condensed product water using a bubble column evaporator. In the near future, testing of COVID-19 susceptibility may also prove interesting and might lead to further sterilization applications for this simple technique (See Postscript for rapid progress here).

DE-WATERING SLIMES

Industrial wastewater slimes are currently treated in several ways, e.g. flocculation, filtration, hydrocyclone treatment, centrifugation, all of which raise issues and problems associated with each particular process. We have developed a novel method based on the use of hot gas bubbles which both fluidize slimes whilst at the same time efficiently removing water vapour which can then be condensed as a pure water product. The bubble column evaporator enables slime de-watering up to levels where the dispersions are only maintained in a fluid state by the continuous flow of hot gases. This facilitates the industrial use of this process via the continuous deposition into flat open drying trays where the material is deposited in solid form for ultimate evaporative drying and disposal. Our surprising observations with heated helium gas might further dramatically improve the efficiency of the process, with the incorporation of helium recycling.

At the end we found a good method to inhibit scaling in pipelines. And this has opened up new insights into the core of physical chemistry –the energy sources of reactivity in ordinary and biochemistry (See Postscript).

CAVITATION PREVENTION

Another novel process has been developed which completely prevents the cavitation caused by the rapid rotation of a propeller in water. Cavitation has a deleterious effect on the efficiency of fluid transmission, and generally leads to material degradation in hydraulic systems. A major part of transport costs by shipping is due to cavitation. Currently, the main approaches by industry to reduce the effects of cavitation are to select operating conditions, use geometric designs that reduce the occurrence of cavitation, or use hard materials to resist wear caused by cavitation. For example, the maximum shaft speed of propellers is typically limited to ensure that cavitation does not occur at the blades.

In the recent advance described here, a novel method of releasing de-gassed water towards the low-pressure side of a propeller was developed. This forms a boundary layer completely preventing cavitation. This is extraordinary, simple and has game changing implications.

The prevention of cavitation and associated noise has widespread practical implications for commercial shipping and the navy; it improves energy efficiency and reduces propeller damage, and also can have a dramatic effect on the effective operating speed of ships and submarines. Following proven laboratory scale tests, a multidisciplinary research approach involving fluid engineers, propeller designers, ship-makers with expertise in cavitation is now required to develop this innovation for large scale applications. We wish them well in the enterprise.

The novel technologies presented in this volume offer promising new environmentally friendly processes for desalination, water treatment, water sterilization, and the total prevention of cavitation. Some of these technologies have already been patented. Each of these innovations has been brought to the stage where further development might lead to full commercialization with global implications.

Substantia
An International Journal of the History of Chemistry

Firenze University Press
www.fupress.com/substantia

Citation: B.W. Ninham, R.M. Pashley (2020) *Introduction and Background*. About Water: Novel Water Technologies in the New Millennium. *Substantia* 4(2) Suppl.: 9-17. doi: 10.36253/Substantia-1123

Data Availability Statement: All relevant data are within the paper and its Supporting Information files.

Competing Interests: The Author(s) declare(s) no conflict of interest.

Introduction and Background
About Water: Novel Water Technologies in the New Millennium

Barry W. Ninham[1], Richard M. Pashley[2,*]

[1] *Department of Applied Mathematics, Research School of Physical Sciences, Australian National University, Canberra, Australia*
[2] *School of Science, University of New South Wales, Northcott Drive, Campbell, Canberra, Australia*
*Corresponding author: r.pashley@adfa.edu.au

A year ago, May 24, 2019 was the 500th anniversary of the death of Leonardo da Vinci. Visionary water projects on a grand scale were one of his lifelong passions. They were never fulfilled. Substantia offers this volume on new water technologies that work, in celebration of the life of da Vinci, the artist and genius of Florence.

These technologies are simple and cheap. They embrace desalination, sterilization of wastewater, including killing of viruses, selective heavy metal ion removal and harvesting.

And a simple solution to a major world economic problem. that of cavitation in ship propellers.

Our claims are startling and apply to real world conditions, that is, in concentrated and complex environments. They are not restricted to ideal, dilute solutions. They are presently inexplicable within the confines and boundaries of classical physical and colloid chemistry. It has been increasingly apparent that this venerable enabling discipline that underpins chemical engineering and biology suffers from sins of omission and commission. Once those strictures are removed whole new opportunities open up. Examples of these we want to exhibit here.

ABOUT WATER

In the early centuries of our Christian-Roman civilisation it is reported by Gibbon in *Decline and Fall of the Roman Empire*, that the bazaars of Byzantium, Alexandria and Antioch all buzzed with debate on the Nature of the Trinity. The matter was settled by the guidance of Constantine himself at the Council of Nicea in 351 AD and, as we know, against the heresy of Arius.

At the present time the corresponding, though Godless, debate concerns the anticipated catastrophe of climate change. Regardless of which Creed tri-

umphs here, pro climate change or sceptic, it is apparent that without clean water mankind is in for a terrible time.

The motivation is indisputable. Without clean water our future prospects, recalling the Biblical ten plagues of Egypt[1], are dire.

1. The History of Water in Civilisations has been documented with elegance and erudition by Mark Henry. We defer to his exceptional paper.[1]

2. Water and Climate Change in Prehistory

What is missing in Henry's paper are some sobering water related catastrophes of prehistory. It has recently been discovered that the Blue Nile did not flood for 30 years, during the Middle Kingdom of Egypt. The disaster was one from which Egyptian civilisation never quite recovered, not to speak of cannibalism, the loss of many cities and Nile tributaries. Similar events consumed civilisations of the middle east on the Euphrates and Tigris. The mighty Oxus of antiquity it now seems might even have been so large that it passed through the then Sea of Aral to the Caspian and on to the Black Sea. Its banks were lined with lost cities all the way to Afghanistan. Alexander's army it seems might have been able to row all the way to Central Asia.[2]

The sea of Aral has dried up permanently in the last 50 years due to Soviet exploitation of the Oxus for irrigating second grade cotton.

The Darling river in Australia, that country's longest river dried up this year for the same reason. The British Aswan dam, massively expanded by the Soviets has stopped the Nile from flooding – a catastrophe for Egypt and the 500 km dam so formed, for the Sudan. The Blue Nile is now dammed in Ethiopia with who knows what catastrophes are to follow in Egypt, as for Turkey's dam at the head of the Euphrates.

The Black Sea only filled up about 8000 years ago, taking out an entire civilisation in the process.

3. A Perennial Problem with Water

Why ice floats on water, without which life could not have evolved, was the subject of celebrated debate commissioned by Cosimo II de' Medici. It took place in Florence for a few days around Nov 5, 1611, between Galileo and an Aristotelian Professor. Galileo lost the debate, although he never admitted it. In almost a role reversal, a hubris-filled Galileo argued as an Aristo-Platonist, while his opponent appealed to experiment.[3]

The occasion was marked again 400 years later in Florence with an international conference.[4] The matter remains unresolved. The only work that comes close to solving the problem is the little-known paper.[5]

This is not accepted, as it is unconventional and not understood by a too conservative clientele obsessed with simulation as a valid occupation, and not familiar with older theories.

4. Water and Oil

The first experiment published was on clay tablets that dates back to the time of Hammurabi (a famous Akkadian ruler from the area which is now Iraq) around 18th century before Christ. The priests studying oil on water spreading (pouring water in oil and oil in water) were among other things interested in predicting the future. For instance, if one small and one large drop emerged a male child would be born. There were lots of scientifically interesting results in this early publication such as a study on spreading and retraction; the formation of droplets and globules; and interference colors. The clay tablet is one of the first scientific publications known.[6]

The other experiment relevant was also reported by Tabor and also published in the Journal of Colloid & Interface Science paper. It was a translation of an experiment published on cuneiform clay tablets found in the library of the ruined palace at Nineveh of the King Asshurnabanipal around 750 BC. The tablets were brought back to Oxford by George Smith who discovered also the story of Noah and the Flood and of Gilgamesh there. The priests studying oil on water spreading were more interested in applications to necromancy than present fashionable pursuits. More recently, and on a stronger scientific footing, Lord Rayleigh re-did Benjamin Franklin's studies of oleic acid spreading on the surface of a South London pond to make the first quite accurate estimate of molecular size. Franklin started the experiment but got bored and went off to a house of ill repute.

5. Carbon Dioxide and Natron the Oldest Technology. Temperature a Factor

After sodium chloride, natron, sodium bicarbonate, is probably the first industrial scale chemical used by mankind. Natron, in ancient Egypt was essential for mummification. The still little understood, peculiar hydration properties of the bicarbonate ion, in contact with air, affects both tissue dehydration and preserves by sterilization against bacterial degradation.

---

[1] God's punishment of the Egyptians from whom the enslaved Israelites who escaped across the Red Sea is given in the Jewish Passover services. They consisted of ten plagues: Blood, Boils, Frogs, Hail, Vermin, Locusts, Murrain (an infection of mucous membrane of intestines of sheep and cattle (substitute swine flu) Pestilence, Slaying of first born, Darkness.

The magic of the bicarbonate ion has remained, along with the likewise unexplained problems of Roman and other cements. The foundation of physical chemistry can arguably be marked by Berthollot's observation that reactions are temperature dependent.[7] He saw soda lime instead of the expected calcium carbonate on the banks of the Nile River during Napoleon's scientific expedition to Egypt in 1792.[7] This was and is very surprising. Under the high temperature of the sun (> 60 °C) when the salt is precipitated from a mix of Na^+, Ca^{2+}, Cl^-, and HCO_3^- ions in the flood waters the hydration is different from that at 25 °C. But at the very high temperatures in excess of 60 °C the natural precipitate is sodium bicarbonate.

This profoundly important observation is still universally forgotten, and seems never to have been repeated. Wet sodium bicarbonate is extremely effective in cleaning surfaces. It cuts peptide bonds of proteins bound to saucepans.

Carbon dioxide bubbles in a salt water column are extremely effective in killing viruses as well as bacteria![8-10] This is the key to sterilizing and recycling water as is amply illustrated further in papers that follow. The technique is developing fast and successfully for commercial use.

6. Water, Country Clubs and the British Empire

For over two centuries the third largest contributor to the economy of the State of Massachusetts was ice from a small lake in the village of Wenham, south of Boston. Very pure water from a small lake froze gradually in winter, so slowly that the ice contained no trapped air and was crystal clear. The ice was sawn up into blocks, covered with hessian bags, and transported by sailing ship around the British Empire from London to the colonies, from India to Jamaica.

During the journey, 2/3 of the ice melted. No self-respecting Englishman would ever drink his gin and tonic without Wenham ice. This affectation persists. It is claimed that gas free water tastes differently. Perhaps it does. The same can today be achieved using a freeze-thaw vacuum system but is perhaps somewhat less exotic.

7. The 4 H's: In Search of Hydration

The words hydration, hydrophobic, hydrophilic, hydrogen bond are as elusive to pin down as they are universally used. So are other words that are part of the fabric of physical chemistry. The meaning of the four H words, and others like pH, buffers, surface potentials, water structure are not something a researcher wants to delve into too much. Yet delve into them we must. The 12 member IPAC Commission on pH, for example, recommends that one cannot place any faith in a pH measurement in a salt solution above 0.1 Molar concentration. Similarly any biologist knows that once a protocol is working, you never play around with the buffer.

Such facts are well known but ignored, and with justification. Because if we do ask questions outside the classical canon we enter a perfect storm. At the other extreme, and for different reasons, pH measurements on ultra-pure water are also very difficult to make.

To make that explicit:

7a. Water "structure": Bernal's ideas

The perennial debate on very long ranged water structure vs short range order – hydration – is of long standing. There is no molecular theory of liquids like that underlying statistical mechanical theories of gases or solids. For gases the molecular distribution function is uniform. For solids, the distribution function which is the basis for perturbation is a periodic distribution function (crystal lattice).

Bernal's ideas on the dynamic zeolite-like topology of structures with many membered hydrogen bonded water molecule rings perhaps comes closest to capturing the essence.[11]

7b. Water Structure and Hydration

While we cannot yet define what we mean by "water structure" the soda lime phenomenon of # 5 is a clear demonstration that it exists. The specific "affinity" of hydrated cations and anions is different at low and high temperatures.

Indeed, it turns out that water in not "hydrogen bonded" above about 89-90 °C.

If we change water structure by adding an indifferent background electrolyte or sugars or urea, then precipitation of salt crystals, e.g. $Mg(OH)_2$ can be made to vary from microns to nanoparticles to zero in size, as water structure imposed by the background solute changes.[12]

Changing hydration (water structure) with temperature or surfactants affects protein structure and function.[13, 14] Other explicit examples of water structure show up in micellar and microemulsion phase diagrams and with gels.[15-17]

7c. Young, Laplace, vs Poisson and Maxwell and Hydration

Interfacial tensions and colloidal particle interactions both involve surface induced hydration (or surface water structure). That is a matter of thermodynamics, quantified in principle by Gibbs. Thomas Young's classic work ignored this. Debates about this have continued,

starting with Laplace vs. Poisson (1832) and a definitive article by J Clerk Maxwell,[18] (1876) to the present day. At soft surfaces, rough or dynamic on a molecular scale, like phospholipid membranes, these "hydration" forces are repulsive and decay exponentially with a range of the order of the size of a molecule, for water about 3 Å.[17]

At hard surfaces "depletion" forces due to molecular granularity are oscillatory and also repulsive. Molecular granularity includes, for example, micelles that can stabilise emulsions. The periodicity is here of the order of the size of the "pseudo molecules", here micelles.[19] Similar effects occur with proteins in solution. Our confidence in what we know about water is tempered by the fact that we do not know and cannot predict even the sign of the potential at the air-water interface due to the hydronium vs. hydroxide disposition at the air-water interface.[20]

7d. Hydrogen Bonding and other Heresies

The concept of a hydrogen bond derives from a perturbation calculation of the interaction between two hydrogen atoms. This has been extended to apply to interactions between two atoms in a sea of its neighbours, an inherently many body problem. Evidently it is nonsense. The strength of what is assigned to a "hydrogen bond" can vary between 0.1 to 10 kT!

The same confusion has become standard for "dipole–dipole" interactions. Thus, the "Keesom force" between two rotating water or protein molecule dipoles is inversely proportional to temperature T. But in a condensed medium it is proportional to temperature due to many body effects.

The distinction made between hydrogen bonding, hydration, van der Waals, permanent dipole or ion dipole forces is completely artificial and erroneous.

It is an artefact of the (mathematical) expansion of an arbitrary distribution of mass or charge into a multipolar Taylor series.

8. Very Long Ranged Hydrophobic Interactions

Very long ranged hydrophobic interactions between similar surfaces were first measured and reported by Israelachvili and Pashley in 1982[21, 22] based on their experiments using the Surface Forces Apparatus (SFA), which was developed by Israelachvili. Two symmetrical, cleaved and smooth mica surfaces were coated with a hydrophobic surfactant monolayer and the forces between them was measured in various aqueous electrolyte solutions. Comparing these measured forces with the expected van der Waals attractive forces, indicated that there was an additional attractive force, acting over a range of several nanometers, which was identified as a 'long range hydrophobic attraction.' Since then, these attractive forces have been measured at separations up to several hundred nms. The origin of these forces has generated much debate, with the likelihood that their unexpectedly long range is probably related to dissolved gas cavitation created between the hydrophobic surfaces, evidence for which was also observed in the original studies.[22, 23]

There are other mechanisms all lumped together in this single mysterious word. Some are due to capillary action.[24] Some are due to co-operative electrostatic surface molecular correlations and some due to permanent dipolar surface correlations between zwitterionic lipids.[25] And some are due to polymer bridging between surfaces.

Some are due to nanobubbles. To confuse matters all depend on dissolved atmospheric gas. Many of these forces disappear when dissolved gas is removed from water![26]

9. Deconstructing Colloid Science, Physical Chemistry and Electrochemistry

As is evident above, the classical theories, even in the continuum solvent approximation are fundamentally flawed. This is due to sins of omission and commission, about which much has been revealed over these past 20 years. See[26] and references therein.

Classical theory begins with an ansatz that treats electrostatics and dispersion forces separately. Double layer forces are treated by a nonlinear theory Poisson Boltzmann or HNC say, while dispersion forces are treated by a linear theory (Lifshitz, Hamaker). See Ref. 4.

This ansatz violates thermodynamics, both the Gibbs adsorption isotherm and the gauge condition on the electromagnetic field. A consequence is that Hofmeister, "specific ion" effects, are ignored. (When the theory is done correctly, they are not.) The result is that practically all force measurements (with the exception of those measured at long range and in very dilute solution) are incorrect and inferences on hydration are also wrong.

Subtracting two partial incorrect theories, double layer and dispersion (van der Waals) forces from an experimental measurement means that the assignment of the residual to "hydration" or specific ion effects is meaningless. So all measurements based on the incorrect theory like pH, pKas, zeta potentials, membrane potentials, ion pumps, activities and interfacial potentials can be incorrect and can be badly so.

10. Dissolved Gas a Hidden Variable. Cavitation

There is worse to come. It turns out that dissolved atmospheric gas, we mean not just oxygen or CO_2, but

nitrogen too, has a profound effect. Remove the gas and "hydrophobic" forces go away. Emulsions become stable.[26] Hofmeister effects reverse and we enter a new world. Simulation does not help and is very misleading. This is because it cannot handle dissolved gas in water. It compares model, gas-free, water or electrolytes or proteins with REAL water and solutions that do contain dissolved gas.

Newton tried to measure molecular forces but gave up, in Art 31 of the Principia, I think, saying "surface combinations were owing". This is not the main problem for us.

11. Why not Simulation?

It is impossible to find an answer by computer simulation. The reason will recur. It has nothing to do with the inadequacy and incorrect nature of the molecular potentials used.

The reason is that real water contains dissolved gas. This changes the physico-chemical properties of water drastically. So any computer simulation that does not include dissolved gas is not appropriate to, and does not apply to, real water which does. If it does claim agreement with experimental properties, it is comparing apples with oranges and is wrong.

It is reasonable to think that dissolved atmospheric gas could be ignored.

Consider that the total number of gas molecules in air at 20 °C and 1 atm is 0.041 moles/L = 2.5×10^{19} molecules /mL.

The dissolved gas content in water in equilibrium with normal atmospheric pressure at 20 °C is:

Oxygen: 0.0093 g/L = 0.00029 moles/L =1.75×10^{17} molecules /mL.

Nitrogen: 0.0148 g/L = 0.00053 moles/L = 3.17×10^{17} molecules /mL.

Total gas molecules in water is 0.00085 moles/L = 5.1×10^{17} molecules /mL.

The number of water molecules in liquid water is 55 moles/L. Hence, they differ by a factor of about 10^5.

Such a small number of impurity molecules would be impossible to deal with in a simulation. (This is around the CMC of a surfactant like SDS in 0.3 M salt).

But it really does matter!

In another important example: acceptable or potable water has to be at least 99.99% pure, that is less than 1.0 mM NaCl! Small 'contaminants' matter but so can drinking ultra-pure water, which can cause death by hyponatremia or water poisoning by reducing sodium levels in your blood. Sports electrolyte drinks prevent this. The famous medical doctor Paracelsus told us this about too much water. As already remarked, the origins of long ranged hydrophobic interactions most likely lie with the presence of dissolved gas also.

The tensile strength of water depends on 'inert' dissolved atmospheric gas molecules. They act in the same way as impurities in a solid to reduce its strength according to a well known theory of Griffiths. The tensile strength of water is two orders of magnitude less than that we would calculate from molecular forces. It gives rise to cavitation, which only occurs because of the presence of dissolved gases. The energy cost of cavitation on shipping is a huge economic impost on society. So control by removal of gas will yield enormous energy savings. We will see how it can be accomplished in what follows.

12. Water, Salt and Bubbles

The debacle has hardly begun. This, perhaps simplest of all experiments remains unexplained:[27]

Gas passed through a porous frit ascends as bubbles in a column of water. They collide, and fuse to form bigger bubbles. The column stays clear (like a fish tank). If a salt like NaCl is added, above a critical concentration centred around 0.17 M the bubbles do not fuse. The column becomes a densely packed foam of tiny bubbles. The critical concentration is the same ionic strength as that of the blood of land animals and that of the Permian ocean from which we emerged. The reason is not incidental and irrelevant.

To make matters worse, for some salts no such effect is observed. Bubbles happily fuse in salt solutions up to 6 M. There are rules without exceptions that show which ion pairs give rise to fusion and which do not, and also rules for mixtures.

This is still a complete mystery that has defied explanation and has been ignored for over 30 years. It is a phenomenon that the new technologies of this volume exploit.

12. Nanobubbles and Bubble Fusion

A history of nanobubbles is given in Reference 29. By these we mean gas filled entities of the order of a nanometer in size or above. They are if we like the analogue of micelles. It was argued until recently that they could not exist as stable entities, although what "stable" meant is unclear. That consensus was arrived at by applying macroscopic concepts to nanometric objects to which macroscopic arguments cannot apply. It is now agreed that nanobubbles do exist in salt water regardless of theory.[28-30]

Gas containing small bubble structures have been much studied by laser spectroscopy and appear to be involved in enzyme catalysis via cavitation, in the active sites of enzymes.[31] Their formation and stability in elec-

trolytes is long lived above 0.17 M and probably explains the bubble-bubble fusion inhibition phenomenon.

13. Jellyfish

Just as old as the problem of why ice floats on water, or why bubbles do not fuse in salt water is that of the very existence of jellyfish, and other soft bodied multicelled animals. These emerged in the Ediacaran Era 570 million years ago before the Cambrian Era. It was first raised by Gorter and dismissed by the establishment at a Faraday Conference in 1930.[1] The problem is that jellyfish contain <<1-2% non-aqueous matter. Any such matter is confined to digestive and reproductive regions. If that is so the jellyfish carapace must be essentially pure water. This rubbery solid matter exists surrounded by an ocean that contains at least 3% salts. Its existence – Chinese people preserve and eat it – defies the laws of osmotic pressure; and the diffusion equation.[1]

On the face of it, there is little to answer the inference that here is a new state of water with very long ranged macrostructure. That could be resolved by some straightforward experiments. Like measurement of conductivity and careful elemental composition studies. The existence of jellyfish – for 600 million years defies conventional wisdom and yet the problem continues to be ignored except by brave souls like J. Pollack. (See however remarks below on very long range forces between conducting polymers.)

14. The Polywater Debacle

The jellyfish conundrum is resolved by some by postulating the existence of a new state of water structures over tens of thousands of nanometers. Such a "solution" is a tautology. It was a trap into which the renowned Russian colloid scientist fell into with the discovery of the much derided "polywater". For an account of this and associated events see Ref 32. Polywater does exist but is due to polymeric impurities. Between conducting thin linear charged polymers there are very long range, many body interactions, which are a hidden driver of organisation and recognition.[26,33-35]

The same forces occur for polyelectrolytes and also for DNA.[36] They have been known almost since the discovery of van der Waals dispersion forces and ignored.

15. Problems and Solutions

We can continue in this mould, listing words without limit that remind us that the foundations are insecure – chirality, magnetic fields, clouds and rain, for a start. The surface tension of water? Forget it.

The problems associated with water seem to have become deeper with the increasing reliance on, and now dominance of unreasonable Aristo-Platonic approaches to chemistry. These abjure experiment in favour of simulation with fixed concepts that assign insight to mindless computer games. These can sometimes fit data but never predict. It is a curious constraining and lazy reversion to medievalism.

We can consider this reversion a catastrophe or an opportunity. Awareness of the defects of present theory allows us to throw off the shackles. The major source of hubris and of omission in theories is that of air, the fourth ᵗelement of the Greeks.

In retrospect, Descartes might better have said: "I breathe; therefore I am" instead of his famous impotent Platonic assertion: "I think: therefore I am".

Thales of Miletus, the oldest known Greek scientist, thought the world consisted in two parts: water and God.

16. Desalination and Aristotle

The technology is not new. Aristotle described a desalination technique in the 4th century BC in Meteorologica. There's even a mention of desalination (although vague) in the Bible (Exodus 15:22-26).

"Desalination has been around for millennia if you count the evaporation techniques pioneered by the ancient Greek. Sailors in the 4th century BC boiled salt water and then captured the steam. When cooled, steam condenses into distilled water that's free of virtually all contaminants."

https://ideas.ted.com/would-you-drink-desalinated-seawater-recycled-sewage-water-get-ready-to-find-out/

Plans for desalination—removing salt from seawater—date back to 4th century B.C. from ancient Greek philosopher Aristotle, according to livescience.com. Action was put into place around 200 A.D. when sailors desalinated seawater with boilers on their ships.

https://www.pumpsandsystems.com/desalination-projects-picking-challenges-remain

17. Leonardo da Vinci's View

It is impossible to assert with confidence what people meant by words written in a different world 500 years ago. Leonardo's science seems to have been sniffily dismissed because he did not know Latin and Greek, Plato and Aristotle, the mantles of the Renaissance Cogniscenti. But he seems to have been of the same view as Roger Bacon and Kant. And as d'Arcy Thompson said:

> *Kant said of the chemistry of his day and generation that it was a science but not a Science – in that the criterion of true science lay in its relation to mathematics.*[37]

(By that he included physics too). He tells us too that Leonardo da Vinci (1452 – 1519) who died 500 years ago thought the same:[38]

Nissuna umana investigazione si pò dimandare vera scienzia s'essa non passa per le matematiche dimostrazioni, e se tu dirai che le scienzie, che principiano e finiscono nella mente, abbiano verità, questo non si concede, ma si niega, per molte ragioni, e prima, che in tali discorsi mentali non accade esperienzia, sanza la quale nulla dà di sé certezza.

(No human enquiry can call itself a true science unless it proceeds by means of mathematical demonstrations**, and if you claim that the sciences that begin and end in the mind possess some truth, this is not conceded, but is denied for several reasons, the first being that in such mental arguments no experience occurs, without which nothing is certain)**.

And Xenophanes said:

The gods have not revealed all things from the beginning.
But men seek and so find out better in time,

Let us suppose these things are like the truth.

But surely no man knows or ever will know
The truth about the gods and all I speak of.
But even if he happens to tell the perfect truth, he does not know it, but appearance is fashioned over everything.

We borrowed Xenophanes words of motivation and inspiration from Morris Klines' marvellous book 'Mathematics: The Loss of certainty.'

This present volume takes air with salts and water and puts them to work for novel water technologies, regardless of theory. We take that as our text and so to work.

Postscript Since this essay was written the very long range forces between conducting cylinders, or polyelectrolytes have begun to surface as serious hidden variables, in phenomena associated with physiology in the previously mysterious endothelial surface layer[28] and other anomalous properties that occur with the fuel cell polymer Nafion.[39-40]

These developments, connected to Chinese acupuncture confirm the perpetual fact that water always surprises.

REFERENCES

1. M. Henry, The state of water in living systems: from the Liquid to the Jellyfish in Aqua Incognita. *Why Ice Floats on Water and Galileo 400 years on,* pp 51-99 Connor Court Publishing Pty Ltd. Copyright **2014** Pierandrea Lo Nostro and Barry W Ninham Eds.
2. The route of the ancient shipping route from Greece through the Karakum desert of Turkmenistan and beyond to the lost city of Alexandria on the old Oxus in Afghaistan has been explored and rediscovered by Australian photo journalist David Adams.
3. S. J. Louis Caruana in Aqua Incognita From Water to the Stars: A reinterpretation of Galileo's style and Dava Sobel*, Galileo's Daughter.*
4. *Aqua Incognita Why Ice Floats on Water and Galileo 400 Years on.* Editors: P. Lo Nostro and B. W. Ninham, **2014**, 516 pp. Connor Court publishers Ballarat, Victoria.
5. S. Andersson, B. W. Ninham, Why Ice Floats on Water, *Solid State Science*, **2003**, 5 (5), 683-693.
6. D. Tabor, Quotes from British Museum, Cuneiform Texts from Babylonian Tablets in British Museum, Vol. 5, Plate IV, 22446, London, 1898, *J. Colloid Interface Sci.*, **1980**, 75, 240 – 245
7. Scientific Aspects of the French Egyptian Expedition 1798-1801 Author(s): Charles Coulston Gillispie Source: Proceedings of the American Philosophical Society, Vol. 133, No. 4 (Dec, 1989), pp. 447- 474, Published by: American Philosophical Society Stable, Accessed: 07-01-2016 12:50 UTC.
8. A. G. Sanchis, R.M. Pashley, B.W. Ninham, Water sterilisation using different hot gases in a bubble column reactor, *J. Environ. Chem. Eng.,* **2018**, 6, 2651-2659.
9. A. G. Snachis, R. M. Pashley, B. W. Ninham, Low temperature MS2 (ATCC15597-B1) virus inactivation using a hot bubble column evaporator (HBCE), *Colloids Surf. B Biointerfaces,* **2016**, 151, 1-10.
10. A. G. Sanchis, R. M. Pashley, B. W. Ninham, Virus and bacteria inactivation by CO_2 bubbles in solution, *NPJ Clean Water,* **2019**, v2 Number 1.
11. S. T. Hyde, Aqua reticulata: topology of liquid water networks, *in Aqua Incognita*, 145-175.
12. R. Giorgi, C. Bozzi, L. Dei, C. Gabbiani, B. W. Ninham, P. Baglioni, Nanoparticles of $Mg(OH)_2$: Synthesis and Application to Paper Conservation, *Langmuir,* **2005**, 21 (18), 8495-8501.
13. A. E. Voinescu, P. Bauduin, C. Pinna, D. Touraud, B. W. Ninham, W. Kunz, Similarity of salt influences on the pH of buffers, polyelectrolytes and proteins, *J. Phy. Chem. B*, **2006**, 110 (17), 8870-8876.

14. R. Waninge, M. Paulsson, T. Nylander, B. W. Ninham, P. Sellers, Binding of sodium dodecyl sulphate and dodecyl trimethyl ammonium chloride to beta –lactoglobulin: A Calorimetric Study, *Int. Dairy J.*, **1998**, 18 (2), 141-148.
15. I. Lisiechi, M. B. Orling, L. Motte, B. W. Ninham, M. P. Pileni, Synthesis of copper nanosize particles in anionic reverse micelles: Effect of the addition of a cationic surfactant on the size of the crystallites, *Langmuir*, **1995**, 11 (7), 2385-2392.
16. P. Andre, A. Filankembo, I. Lisiecki, C. Petit, T. Gulik-Krzywicki, B.W. Ninham, M. P. Pileni, Supra-aggregation: Microphase formation in complex fluids, *Adv. Mater.*, **2000**, 12, 119-123.
17. The literature on hydration and controlled nanoparticle synthesis in cationc microemulsions is very large now. The Authors' book provides an entry point *Molecular Forces and Self Assembly In Colloid, Nano Sciences and Biology*, Cambridge UP, 2010, B. W. Ninham and P. Lo Nostro.
18. J. Clerk Maxwell: Capillary Action. Encyclopaedia Britannica, 9th ed.; **1876**. See also his "Collected Works".
19. R. M. Pashley, B. W. Ninham, Double-layer forces in ionic micellar solutions, *J. Phy. Chem.,* **1987**, 91 (11), 2902-2904.
20. T. Duignan, D. F. Parsons and B. W. Ninham Hydronium and Hydroxide at the Air–Water Interface with a Continuum Solvent Model, *Chem. Phys. Lett*, **2015**, 635, 1-12.
21. J. N. Israelachvili, R. M. Pashley, The hydrophobic interaction is long-range, decaying exponentially with distance, *Nature*, **1982**, 300, 341-342.
22. J. N. Israelachvili, R. M. Pashley, Measurement of the hydrophobic interaction between two hydrophobic surfaces in aqueous electrolyte solutions, *J. Colloid Interface Sci.*, **1984**, 98, 500-514.
23. R. M. Pashley, P. M. McGuiggan, B. W. Ninham, D. F. Evans, Attractive forces between uncharged hydrophobic surfaces: Direct measurements in aqueous solutions, *Sci.*, **1985**, 229, 1088-1089.
24. V. V. Yaminsky, S. Ohnishi, B. W. Ninham. Long-Range Hydrophobic Forces are due to Capillary Bridging. In: Handbook of Surfaces and Interfaces of Materials, Academic Press: New York, **2001**, 4, 131-227.
25. P. Kekicheff. *Adv. Coll. Interface Sci,* **2019**, 270, 191-215.
26. B. W. Ninham, R. M. Pashley, P. Lo Nostro, Surface forces: Changing concepts and complexity with dissolved gas, bubbles, salt and heat, *Curr. Opin. Colloid Interface Sci.*, **2016**, 27, 25-32.
27. V. S. J. Craig, B. W. Ninham, R. M. Pashley, The Effect of Electrolytes on Bubble Coalescence in Water, *J. Phy. Chem.*, **1993**, 97 (39), 10192-10197.
28. B. P. Reines, B. W. Ninham, Structure and function of the endothelial surface layer: unraveling the nano-architecture of biological surfaces, *Quarterly Reviews of Biophy.*, **2019**, 52, 1–11.
29. M. Alheshibri, J. Qian, M. Jehannin, V. S. Craig, A history of nanobubbles, *Langmuir*, **2016**, 32(43), 11086-11100.
30. N. F. Bunkin, , B. W. Ninham, P. S. Ignatiev, V. A. Kozlov, A. V. Shkirin, A. V. Starosvetskij, Long living nanobubbles of dissolved gas in aqueous solutions of salts and erythrocyte suspensions, *J. Biophotonics*, **2011**, 4(3), 150-164.
31. Kim, H.-K., E. Tuite, B. Norden, B. W. Ninham, Co-ion dependence of DNA nuclease activity suggests hydrophobic cavitation as a potential source of activation energy, *Eur. Phys. J.*, **2001**, 4, 411-417.
32. B. V. Derjaguin, J. Theo, G. Overbeek, Their Times, and Ours, Barry W. Ninham, *Substantia,* **2019**, 3(2), 65-72. P. Lo Nostro, B. W. Ninham, After DLVO: Hans Lyklema and the keepers of the faith, *Adv. Colloid Interface Sci.*, **2020**, 276, 102082.
33. B. Davies, B. W. Ninham, P. Richmond, Van der Waals forces between thin cylinders: new features due to conduction processes, *J. Chem. Phys.*, **1973**, 58(2), 744-750.
34. N. F. Bunkin, P. N. Bolotskova, S. V. Gudkov, Y. Juraev, M. S. Kiryanova, V. A. Kozlov, B. W. Ninham, R. S. Safronenkov, A. V. Shkirin, E. V. Uspenskaya, Structure and Properties of the Exclusion zone of Nafion: Swelling in a constrained volume, *ACS Omega*, **2020**.
35. N. F. Bunkin, A. V. Shkirin, V. A. Kozlov, B. W. Ninham, E. V. Uspenskaya, S. V. Gudkov, Near-surface structure of Nafion in deuterated water, *J. Chem. Phys.*, **2018**, 149, 164901.
36. K. L. Jimenez-Monroy, N. Renaud, J. Drijkoningen, D. Cortens, C. van Haesendonck, W. J. Guedens, J. V. Manca, L. D. A. Siebbeles, F. C. Grozema, P. H. Wagner, High Electronic Conductance through Double-Helix DNA Molecules with Fullerene Anchoring Groups, *J. Phys. Chem. A,* **2017**, 121, 1182-1188.
37. D. W. Thompson, *Growth and Form*. Cambridge University Press, **1917**.
38. L. Da Vinci, Treatise on Painting, Codex Rurbinas Latinus, transl. and annotated by P. P. McMachon, Princeton University Press, **1956**.
39. N. F. Bunkin, P. N. Bolotskova, S. V. Gudkov, Y. Juraev, M. S. Kiryanova, V. A. Kozlov, B. W. Ninham, R. S. Safronenkov, A. V. Shkirin, E. V. Uspenskaya,

Structure and Properties of the Exclusion zone of Nafion: Swelling in a constrained volume, *ACS Omega*, **2020**.
40. N. F. Bunkin, A. V. Shkirin, V. A. Kozlov, B. W. Ninham, E. V. Uspenskaya, S. V. Gudkov, Near-surface structure of Nafion in deuterated water, *J. Chem. Phys.*, **2018**, 149, 164901.

Substantia
An International Journal of the History of Chemistry

Firenze University Press
www.fupress.com/substantia

Citation: B.W. Ninham, M. Shahid, R.M. Pashley (2020) A Review and Update of Bubble Column Evaporator Processes. *Substantia* 4(2) Suppl.: 19-32. doi: 10.36253/Substantia-823

Data Availability Statement: All relevant data are within the paper and its Supporting Information files.

Competing Interests: The Author(s) declare(s) no conflict of interest.

A Review and Update of Bubble Column Evaporator Processes

Barry W. Ninham[1], Muhammad Shahid[2], Richard M. Pashley[2,*]

[1] *Department of Applied Mathematics, Research School of Physical Sciences, The Australian National University, Canberra, Australia*
[2] *School of Science, University of New South Wales, Northcott Drive, Campbell, Canberra, Australia*
*Corresponding author: r.pashley@adfa.edu.au

Abstract. This paper gives an updated review of the bubble column evaporator (BCE) and its various new processes. These include recent work on helium gas desalination and high temperature inlet gas decomposition. The BCE process offers a continuously produced source of high gas-water interface and consequently provides high overall heat and mass transfer coefficients. Very different results have been obtained using nitrogen, oxygen, carbon dioxide and helium inlet gases. Although the bubbling process itself is both simple to use and apply, our understanding of the fundamental physical and chemical principles involved is surprisingly limited and there are many issues yet to be explained. Recently the process has been used to develop new methods for the precise determination of enthalpies of vaporisation (ΔH_{vap}) of concentrated salt solutions, as an evaporative cooling system, a sub-boiling thermal desalination unit, for sub-boiling thermal sterilization, for low temperature thermal decomposition of different solutes in aqueous solution and for the inhibition of particle precipitation in supersaturated solutions. These novel applications can be very useful in many industrial practices, such as desalination, water/wastewater treatment, thermolysis of ammonium bicarbonate (NH_4HCO_3) for the regeneration in forward osmosis and refrigeration related industries. The background theories and models use to explain the BCE process are also reviewed and this fundamental knowledge is applied to the design of BCE systems and to explain recently explored applications, as well as potential improvements. Many other prospective applications of the BCE process are also reported in this paper.

Keywords: bubble column evaporator, sub-boiling, bubble inhibition, thermolysis, desalination, heat of vaporisation, supersaturation.

1. INTRODUCTION TO THE BUBBLE COLUMN EVAPORATOR (BCE)

Double, double toil and trouble; Fire burn: and, cauldron, bubble. The three witches of Shakespeare's play McBeth: *Act 1V, Scene 1* (1606) seem to be the first to have used hot bubble columns effectively. However, the witches use of various outrageous potions distilled from animals would be forbidden in our present politically correct society. Nonetheless bubble column evapo-

rators or BCEs are simple devices that have emerged as facilitators of powerful new technologies for aqueous systems in:

- Desalination (seawater and groundwater).
- Water sterilization (recycled water with no surviving pathogens including viruses).
- Thermolysis of solutes in aqueous solution (destruction of drugs, facilitation of high temperature reactions).
- Inhibition of salt precipitation in concentrated salt solutions.
- Evaporative air conditioning systems for buildings.

The first three are now proven processes, and cheap at industrial scales. They represent encouraging progress in the search for clean water, arguably the biggest problem facing the world.

2. BUBBLE COLUMN EVAPORATORS AS CONVENTIONAL EQUIPMENT

By itself the bubble column evaporator (BCE) is a good and faithful and apparently boring tool of Chemical Engineering. It employs gas-liquid interfaces to drive fundamental processes involving heat and mass transfer. Bubble columns are devices in which a gas, often dry air, is pumped through a porous sinter disc to form gas bubbles in contact with the column solution. They are continuously replenished. Dry gas bubbles in the column solution may be used simply to mix the liquid phase homogenously to attain uniform temperature distribution or to saturate dissolved gases in the column solution. Substances can also be transferred from one phase to the other, for example, when liquid reaction products are stripped from a gas, where both mass and heat transfer processes can occur simultaneously.[1]

Heat transfer using shell and tube heat exchangers is a fundamental chemical engineering process by which heat is transported between two fluids via a material having high thermal conductivity (i.e. copper, Cu). Heat transfer may also be accomplished directly by mixing the solution and the heating fluid (for example, water and hot air bubbles), to give so-called direct-contact evaporators. This concept of heat transfer via hot bubbles was first demonstrated by Collier in a patent, published in 1887.[2] The first commercial plant was installed in the USA in the early 20th century.[3] There has been much attention on the industrial uses of bubbles columns in the chemicals industry, including a volume in *Chemical Engineering Technology* in 2017.[4] Much work has also been carried out on the difficult area of numerical modelling of turbulent bubble column reactors.[5]

Advantages of bubble columns, using direct-contact heat transfer, compared to other multiphase reactors are several: (a) less maintenance required due to the absence of moving parts, (b) higher effective interfacial areas and overall mass transfer coefficients can be achieved, (c) higher heat transfer rates per unit volume of the reactors can be attained, (d) solids can be handled without any erosion or plugging problems, (e) less floor space is occupied and bubble column reactors are less costly, (f) slow reactions can be carried out due to high liquid residence time,[6] and (g) the product can be recovered from the reaction mixture without additional separation operations.[1] Finally, and a glaringly obvious technology still to be exploited, high temperature reactions can be carried out at the surface of bubbles whilst maintaining a relatively low temperature in the liquid column.

3. EXTRAORDINARY SALT INDUCED BUBBLE FUSION INHIBITION

3.1. New Opportunities for the BCE

The BCE is easy to use. But a theoretical understanding of processes involved is still embryonic. It becomes more difficult to understand when a new phenomenon is thrown into the mix. This is the phenomenon of bubble coalescence inhibition with addition of salt. This was first used experimentally by Russian mineral coal flotation engineers more than 100 years ago. The addition of sufficient salt inhibits bubble-bubble fusion, produces smaller bubbles, and the efficiency of flotation was improved.[7] More recently, aqueous bubble column evaporators have been used for a range of new applications based largely on the unexpected effects of many salts and sugars on inhibiting bubble-bubble coalescence in water, in combination with limited bubble rise rates and rapid water vapour uptake into the bubbles.[8-13]

The percentage of bubbles that fuse as a function of salt concentration as they ascend the column and the transition from 100% fusion on collision to zero fusion occurs over a narrow concentration range centered at the same 0.175 M for 1:1 salts. Similarly for others like 2:1, 1:2, 3:1, 3:2 electrolytes and so on but at different concentrations. However, for other salts no such effect occurs.[11,14-15] There are a set of rules that assign each ion pair to either class, and that allow prediction for outcomes with mixtures.[11,14] There are no exceptions. The phenomenon occurs also for different isomers of sugars and other solutes.[11] There is no theoretical explanation.[14-15] Classical theories of molecular forces (e.g. DLVO forces) would predict that increased salt ought to

reduce double layer forces between bubbles and enhance, not inhibit bubble fusion. With non-ionic solutes no electrostatic theory is relevant anyway.

Even more remarkable is that the fact that the ionic strength of blood is exactly the same critical concentration. There are good physiological reasons for this has recently been discovered.[16] It is also the same concentration as that estimated for the Permian ocean when land animals emerged.

The absence of any theoretical explanation for the bubble coalescence phenomenon has not inhibited the development of a wide range of useful techniques. These include:

- A new method for the precise determination of enthalpies of vaporisation (ΔH_{vap}) of concentrated salt solutions;[10,15]
- Evaporative cooling;[10]
- A new method for thermal desalination;[17-19]
- A novel method for sub-boiling, thermal sterilization;[20-22]
- A novel method for the low temperature thermal decomposition of different solutes in aqueous solution[8] and
- A new approach to aqueous precipitation in a controlled manner[23] (see Fig. 1).

In addition to these methods, the thermal design of a bubble column condenser has also been studied for the production of high quality water as condensate.[24-26]

Bubble coalescence behaviour is vital in water-based cleaning processes, ore-flotation, food processing, gas–oil separations, absorption and distillation.[27] As discussed above, bubble coalescence inhibition depends critically on salt type as well as concentration.[11, 28] Salt solutions that do inhibit coalescence have recently been used in many applications, as illustrated in Fig. 1.

All attempts to explain the inhibition problem and its salt dependence with theory have failed. That is not surprising as the theories of forces in colloid science suffer from sins of omission and commission that are now as well documented as they are ignored.

These are:

1. The ansatz of separability of electrostatic and dispersion forces. This violates two fundamental laws of thermodynamcs, even in the continuum solvent model, and dismisses specific ion effects.
2. Hydrophobic interactions are ill defined and depend on dissolved gas.[29]

We can speculate that the theories fail because of the omission, not just of dissolved gas, but of the capacity of dissolved gas to self assemble into dynamic microstructures, just as do surfactants. Nanobubbles seem to have critical nanobubble concentration CNC, which is salt and salt concentration dependent, just as do the CMCs of surfactants. Such nanobubbles would inhibit fusion by depletion forces and adsorption at the mac-

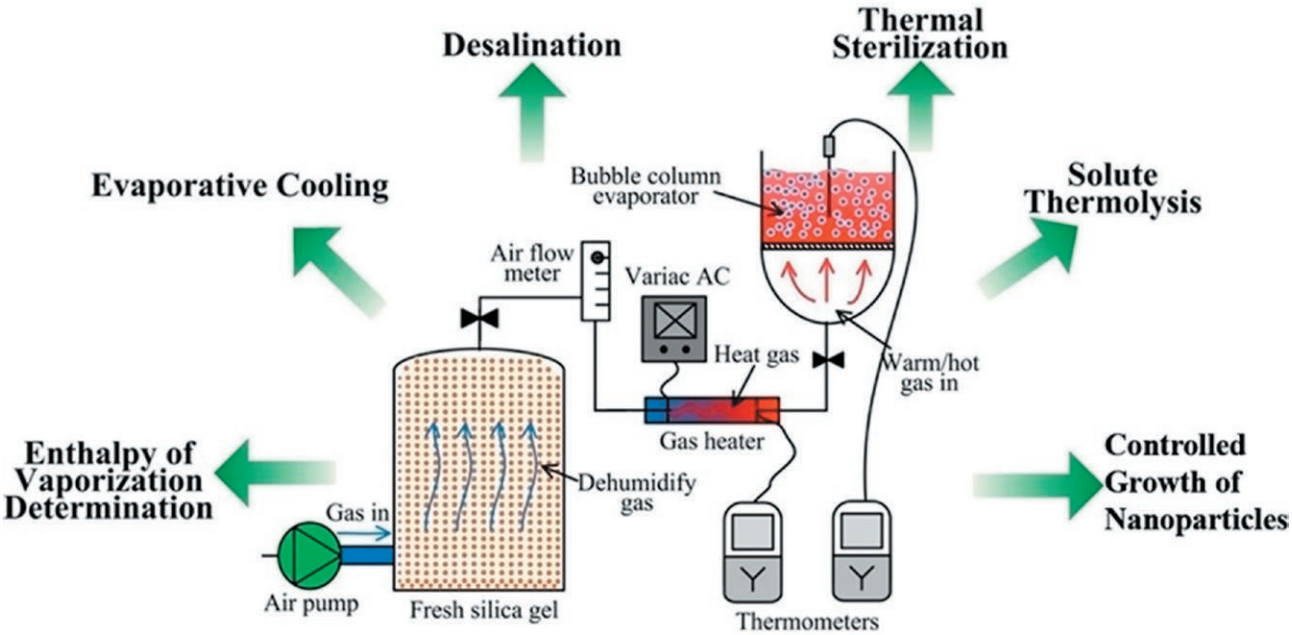

Figure 1. Different applications of the BCE process (reprinted by permission of the publisher, Taylor&Francis Ltd, http://www.tandfonline.com, from M. Shahid et al. 2015).[8]

robubble surfaces. For a history of nanobubbles see Ref 30. The bubble coalescence process is not obvious partly because it is also dependent on dynamic effects, since bubbles slowly forced together always coalesce in aqueous salt solution.

3.2. Bubble evaporation layer model

The deficiencies of the classical theories of forces does not inhibit us from applying thermodynamics to explore some important aspects of bubble column evaporators. The bubble evaporation layer model presented here is based on the estimated thickness of a heated water layer formed transiently around the surface of an initially dry, hot bubble. Some of this water layer must be evaporated into the bubble to produce saturated vapour pressure, at that temperature. This surface bubble layer thickness is a function of temperature and bubble diameter. It will be useful in considering heat and mass transfer processes for desalination, sterilization and other applications. The bubble layer thickness (t_{bl}) varies with temperature, and this model can be described by the following equation for situations where the evaporated film thickness is much less than the radius of the bubble:

$$t_{\mathrm{bl}} = \frac{1}{3} r \frac{\rho_{\mathrm{w}}^{v}(T_{\mathrm{c}})}{\rho_{\mathrm{w}}} \tag{1}$$

where r is the radius of a bubble; $\rho_{\mathrm{w}}^{v}(T_{\mathrm{c}})$ is the water vapour density at the steady state column temperature and ρ_w is the liquid water density. Eq. (1) shows that the bubble layer thickness is a function of steady state column temperature. As an example, for water the average evaporation layer thickness would be about 23 nm for an inlet dry air temperature of 200 °C, forming 1 mm radius bubbles.

3.3. Bubble surface hot layer model

Water vapor is transported through the surface of a hot, dry bubble as it enters a BCE. Simultaneously heat will also flow to a thin water layer surrounding the bubble, as the bubble approaches steady state and cools to the temperature of the column solution. A transient hot water film will be produced around the bubbles flowing into a BCE and this layer can be used to effect changes within the solution. It is therefore useful to consider the likely thickness of this heated layer as a function of inlet air temperature. These thermal effects appear to play a key role for heat transfer processes like sterilization[20-22] and solute thermal decomposition.[8] The maximum extent of the layer can be estimated for a given inlet air temperature. The estimate assumes that there is a linear decrease in the temperature of the surrounding water film from the bubble temperature to the column solution temperature. The thermal energy supplied to heat the water film must be supplied by cooling of the freshly released bubble. (Note that the millimetre bubble surface can be considered to be flat relative to the thin, nanometre thickness of the heated water layer).

In this simple model we consider the intermediate state when the inlet bubble (initially at a high temperature T_{i}) has cooled from T_{i} to T_{b} (assumed to be 100 °C) and the heat transferred to the thin water film surrounding the bubble is sufficient to produce this temperature profile in the film. This amount of heat is the same as that required to heat a film of thickness δ from the column solution temperature T_{c} to the average film temperature $(T_{\mathrm{b}}+T_{\mathrm{c}})/2$. The bubble layer thickness varies with bubble radius, the temperature of the inlet gas and the steady state column solution temperature. A rough estimate of the heated layer thickness can be calculated using the thermal energy balance equation:[8,20]

$$C_p \Delta T r = 3 C_s \Delta t \delta \tag{2}$$

where C_{p} and C_s are the air and solution (or water) specific heat capacities in J/m^{3}K, respectively, and $\Delta t = \frac{T_b+T_c}{2} - T_c$ and $\Delta T = T_i - T_b$ are the transient temperature increase in the solution layer and the temperature reduction within the cooling bubbles, respectively. (Note that in this approximate equation the value of C_p should be taken as that at the average temperature of the cooling bubbles, i.e. at $T=(T_i+T_b)/2$ and the value of C_s should be that at $T=(T_b+T_c)/2$).

The volume of a layer of thickness δ around a bubble is given by $4\pi r^2\delta$, when δ is much smaller than r. Hence the cooling of the bubble by ΔT must determine the thickness δ. In addition, if we also assume that there is a 50% heat loss due to water vaporisation, then the thickness of the active hot region can be roughly estimated. For example, this approximate calculation indicates that for 1mm radius (dry) air bubbles, at an inlet temperature of about 200 °C, on cooling to 100 °C, forms a transient heated water film around the rising bubbles of about 50 nm thickness.

This transient layer of heated water around the bubbles must be responsible for the sterilization effects[20-22] and solute thermal decomposition effects[8] recently reported when using inert gases, such as nitrogen. However, in addition to these thermal effects some gases also have specific properties which can also produce effects

on solutes and microorganisms in bubble columns. For example, recent results have shown that CO_2 inlet gas can be more effective at virus and bacterial sterilization and can even be effective at low temperatures.[34] The use of hot, pure O_2 inlet gas can also be used to enhance solute oxidation processes, whilst maintaining a relatively low BCE solution temperature.

3.3. Bubble water vapour equilibration

It has been observed that fairly large air bubbles (1-3 mm) in water, which are used in the BCE method, become non-spherical and oscillate both in shape and trajectory, thus enhancing the rate at which water vapour equilibrates within the bubbles.[35] It is remarkable that water vapour saturation within these bubbles is attained in a few tenths of a second. It does so because of these oscillations and the circulatory fluid flow induced inside the bubbles due to shear forces generated at the surface of bubbles. This produces rapid water vapour transfer within the bubbles.[36] The vapour transfer is much faster that that expected for quiescent diffusion, which would require several seconds to reach equilibrium according to Fick's law. This rapid vapour transfer must correspond to a similarly fast rate of transfer of heat to the surrounding column solution. It is these factors that form the basis for several recent applications (see Fig. 1) of the BCE process.

3.4. Bubble rise velocity

Bubble rise behaviour in water, even for single isolated air bubbles, is surprisingly complex[35,36] and depends on bubble diameter, sphericity and water purity.[37] The presence of many other bubbles within a BCE makes this situation even more complex and this has not been well studied. The rise of a bubble in a liquid is a function of many parameters viz. bubble characteristics (diameter and shape), properties of gas-liquid systems, and operating conditions, temperature, cleanliness etc.

It was demonstrated by Leifer et al.[35] that the motion of intermediate (single, isolated) bubbles ranging from 1-3 mm diameter is produced by the combination of two oscillation types, trajectory oscillations (zig-zag or helical), and shape or deformation oscillations (ellipsoidal). These gas bubbles actually rise at a limited rate of between about 15 and 35 cm s^{-1} in quiescent water because they undergo trajectory and shape oscillations which reduce their rise rate.[38]

Quinn et al.[39] reported that the shape and velocity of ellipsoidal bubbles appears to oscillate in a fashion linked with increasing solute concentration. Increased solute concentration creates more spherical bubbles with reduced rise velocity and a unique bubble shape. The rise velocity relationship is independent of solute type.

It was also explained by Gonzaleztello et al.[40] that surfactants modify the surface of a bubble predominately through the adsorption of a monolayer. This produces a more rigid interface and so enhances fluid drag. The rise velocity in these solutions is less than for clean bubbles of the same diameter.

Luo et al.[41] have studied the rise velocity of single bubbles in liquid-solid suspensions at pressures up to 17 MPa and temperatures up to 88 °C, over the bubble diameter range from 1 to 20 mm. It was found that the bubble rise velocity decreased with increasing pressure and with decreasing temperature. The decrease of bubble rise velocity was mainly due to the variations of gas density and liquid viscosity with pressure and temperature.

Many researchers have described several factors affecting bubble rise velocity.[37] But the detailed understanding of bubble rise velocity and its associated parameters with regards to the bubble column evaporator method (BCE) is yet to be thoroughly explained.

Stokes' law was derived for spherical objects moving under high Reynolds number and with zero slip boundary condition and gives rise rates substantially higher than those observed for air bubbles in water. Unfortunately, the addition of slip boundary conditions would give even higher rise rates, such as those obtained using the Hadamard-Rybczynski (H-R)[42] equation (see Fig. 2 (a)). The Levich[43] formula gives results more closely resembling experimental rates and this is also given in Fig. 2. Eq (3) represents the general formula for the theoretical bubble rise calculation but unfortunately, none of these equations give an accurate explanation of air bubbles in the 1-3 mm diameter range of interest.[35, 44] The general formula is given by the equation:

$$U_\infty = k \frac{\rho_w g a^2}{\eta} \tag{3}$$

where U_∞ is the bubble rise velocity in an infinite liquid, η is the coefficient of viscosity of the liquid, ρ_w is the density of the liquid, g is the gravitational constant, a is the gas bubble radius and k is a constant (2/9 for Stokes equation, 1/3 for the Hadamard-Rybczynski equation and 1/9 for the Levich equation) (see Fig. 2 (a)). The three typical equations, discussed earlier, have closer agreement with the experimental results summarised by Klaseboer et al. in Fig. 2 (b)[45] when bubble diameters are less than about 1.0 mm.

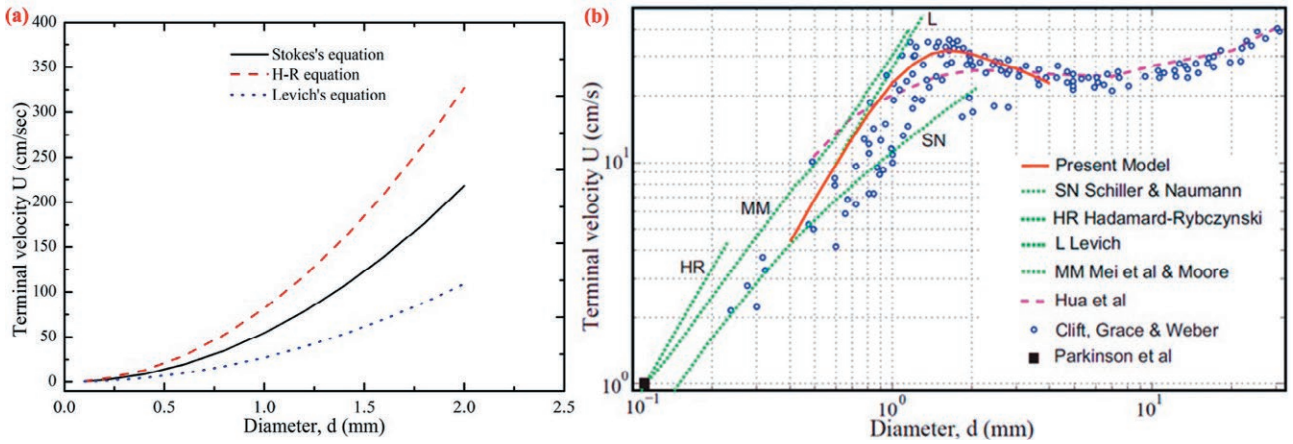

Figure 2. The relationship between rise velocity of isolated bubbles and bubble diameter using typical equations (a) and from models results (b) published by Klaseboer E. et al.[45] (Reprinted from Ref. 45, with permission from Elsevier).

The complex behaviour of bubble rise rates for isolated bubbles in the diameter range >1 mm will be further complicated by multiple collisions within a densely packed bubble column, where coalescence is inhibited by the presence of added salts.

3.5. Thermal energy balance in the BCE

Consideration of the steady state thermal energy balance within a BCE, containing salt solutions can be used to explain the process whereby the heat supplied from the entering warm bubbles (per unit volume of gas leaving the column) is balanced by the heat required for vaporisation, to reach the equilibrium water vapour pressure within these bubbles. This principle is based on the steady state volumetric balance within a bubble column, which has been used for the determination of the enthalpy of vaporisation (ΔH_{vap}) of concentrated salt solutions,[9-10,18] and is described by the following Eq. (4):

$$\Delta T \times C_p(T_e) + \Delta P = \rho_v(T_e) \times \Delta H_{vap}(T_e) \quad (4)$$

where $C_p(T_e)$ is the specific heat per unit volume of the gas flowing into the bubble column at constant pressure; T_e is the steady state temperature near the top of the column; ρ_v is the water vapour density at T_e, which can be calculated from the water vapour pressure of salt solutions at the steady state temperature, using the ideal gas equation; ΔT is the temperature difference between the gas entering and leaving the column; ΔP is the hydrostatic differential pressure, between the gas inlet into the sinter and atmospheric pressure at the top of the column. This represents the work done by the gas flowing into the base of the column until it is released from the solution.

This equation was first published in 2009 by Francis and Pashley[10] for low vapour pressure aqueous solutions, that is, at low column temperatures of about 283 K. The equation's accuracy and precision was further tested in later studies[9,18] at room temperature. The units used throughout the equation are Jm^{-3}, which relates directly to the thermal energy transfer or work done per unit volume of gas flow passing through the column, at the steady state temperature of the column. Once the steady state is reached, then assuming no heat losses to the environment, the cooling of each bubble entering the column exactly balances, on average, the latent heat required to vaporize water to reach the equilibrium vapour pressure with that bubble, at that steady state temperature. This thermal energy and work done per unit volume of gas, means that once the steady state temperature is reached, the balance given in equation (4) is independent of gas flow-rate. However, the time taken to reach the steady state temperature will depend on the gas flow rate.

In a more recent variation of this energy balance equation, use of the heat capacity per unit volume, C_p, in volume-based units was replaced by the corresponding heat capacity per unit weight of gas (i.e. 1.005 J g^{-1} K^{-1} over 270-330 K[46] for dry air), which is fairly constant with temperature. This gives a new version of the thermal balance equation:

$$[\Delta T \times C_p^g(T_e) \times m_g] + \Delta P = \rho_v(T_e) \times \Delta H_{vap}(T_e) \quad (5)$$

where m_g is the mass of air (or gas) in gram per cubic meter. This can be obtained using the molar mass of air (28.96 g mol^{-1}) where the absorbed water vapour is subtracted from the total number of moles of gas within the

bubble per unit volume, using the ideal gas equation, at T_e and 1 atmosphere pressure. It should be noted that the mass of air or gas within a bubble remains constant as the bubble passes through the column. This equation appears to encompass a logical and reasonable thermophysical energy balance to describe the BCE process, especially at higher column solution temperatures, where the water vapour pressure will be more significant.

This model assumes that while bubbles are capturing water vapour and rising in the solution from their initial dry state to 100% water vapour saturation at T_e, they will expand further due to the water vapour captured into the bubbles but only the initial (and constant) mass of gas can supply heat to the column, to produce this level of evaporation.

In both balance equations ΔH_{vap} includes the work done by vapour expansion. However, for high gas temperatures and short bubble residence times, removing the water vapour expansion work produces a better fit when using Eq. (5) to give Eq. (6), which is adapted for no work of water vapour expansion and corresponds to the following equation:

$$[\Delta T \times C_p^g(T_e) \times m_g] + \Delta P = \rho_v(T_e) \times [\Delta H_{vap}(T_e) - P\Delta V(T_e)] \quad (6)$$

Hence, it appears that high temperature bubbles in short height column solutions (~5 cm) and short residence times appear to show no expansion due to vapour uptake (see Fig. 3). On the other hand, low temperature experiments appear to correspond to a steady state condition in terms of not only temperature but also the bubbles' vapour expansion. It is interesting that at low temperatures, Eq. (6) produces low errors for calculated ΔH_{vap} values, similar to those produced from Eq.(4) and Eq.(5), because the $P\Delta V$ term has no significant effect on the calculation. It should be noted that since bubbles reach vapour and temperature equilibrium within a few tenths of a second, the column height becomes important. In this work we define a medium height column to be one where this equilibrium is just attained.

It should be noted that use of C_p^g, the heat capacity of the dry air under constant volume conditions (0.718 J g^{-1} K^{-1} for 270-330 K[46]) in place of the corresponding C_p^g values gives inaccurate ΔH_{vap} values at both high and low column solution temperatures. This indicates that atmospheric work done on the contracting, cooling bubbles must be transferred to the column and so must be included in the energy balance equations.

Based on the results obtained and the analysis of energy balances in the BCE, the original balance Eq.(4) was found to be accurate for the determination of ΔH_{vap} values of salt solutions over a wide range of temperatures. In comparison, Eq.(5) can only be used at low temperatures and Eq. (6) is applicable to the special case of high inlet gas temperatures and short bubble residence times. Although the original Eq. (4) was derived for low temperatures, around room temperature, we have since shown that it also works well for very hot inlet gases.[18] This is because any given bubble released into the column at high temperature (T_i) will contract until it reaches the column solution equilibrium temperature T_e. The heat supplied by the bubble (of volume V_b at temperature T) to the column, as it contracts, is given by the sum of $C_p(T) \times V_b(T)$ over the temperature range T_i to T_e (i.e. ΔT). However, because the mass of gas in any given bubble remains constant, the value $C_p(T) \times V_b(T)$ is also constant for any bubble and hence the heat transferred to the column is given by $C_p(T_e) \times \Delta T$, per unit volume, as given in Eq.(4).

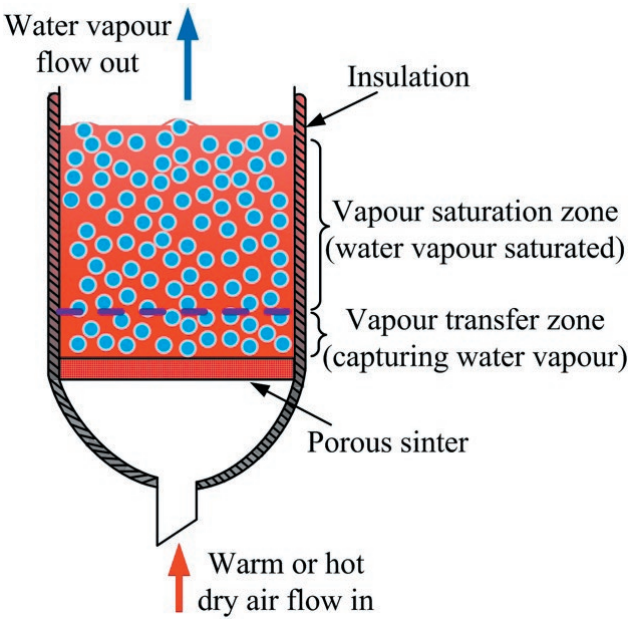

Figure 3. Schematic diagram of a bubble column (reprinted by permission of the publisher, Taylor&Francis Ltd, http://www.tandfonline.com, from M. Shahid et al. 2015).[8]

The results obtained using inlet air temperatures at around 275 °C and for solutions ranging from 0.5-6 m NaCl indicate that the amount of water carried over varied with different NaCl concentrations, relative to the expected vapour carry over, obtained from the variable theoretical column temperature (i.e. since the theoretical column temperature varies with increasing NaCl concentrations) and the corresponding vapour pressure. At the highest NaCl concentration, 6 m, the calculated energy utilization at 275 °C was found to be about 29

MJ m^{-3} which indicates that the BCE process can be an energy effective method, especially at higher solution concentrations and hence could be used for industrial applications.

4. APPLICATIONS OF THE BUBBLE COLUMN EVAPORATOR (BCE)

The gas-liquid direct-contact bubble column evaporator is characterized by a continuously replenished, high gas-liquid interfacial area, which subsequently offers higher mass and heat transfer coefficients due to non-isothermal[3] (i.e. localized evaporation) nature of the BCE. It could be applied in many large scale industrial applications. We now spell out in detail current applications of the bubble column evaporator (BCE) in aqueous systems:

4.1. Determination of ΔH_{vap} values for concentrated aqueous solutions using the BCE method

Bubble coalescence inhibition and rapid vapour transfer both offer a novel application of the BCE process for the precise measurement of ΔH_{vap} values for concentrated salt solutions [3,6,15] where the vapour pressure values of salt solutions are known. ΔH_{vap} values can be obtained from the volumetric energy balance within the column, operating under steady state conditions, as defined by equation (4), at ambient temperatures. In recent work[9,17], ΔH_{vap} values of various salt solutions at different concentrations have been obtained with accuracies, on average, within around 0.5-1.0% compared to the literature values for several salt solutions and demonstrate a measurement precision of between 0.1% and 0.9%. For relatively low column temperature studies, around room temperature, the two balance equations, discussed earlier, give similar results, i.e. within the 0.5-1.0% range, on average.

The accuracy and precision of these ΔH_{vap} measurements was recently further improved using vacuum insulation (which reduced thermal transfers with the room environment) of the bubble column and an automatic data acquisition system for temperature readings.[17] Under the steady state of the BCE system, hundreds of temperature data can be acquired by computer within 0.5-1 hour and hence a large number of ΔH_{vap} values can be produced using these energy balance equations. These ΔH_{vap} values[17] were found to pass the Kolmogorov-Smirnov test[47] with high probabilities after standardization of data and supported the null hypothesis, that is, the normal distribution. Typical examples are shown in the frequency histograms given in Fig. 6.[18] Narrow confidence intervals (95%), say always around ±0.02 kJ mol^{-1}, also demonstrated the high precision of the BCE method for ΔH_{vap} measurement, as well as supporting the basic physics of the energy balance equation. At relatively higher operating or steady state temperatures, around 40 to 50°C, the BCE method was still found to be suitable for determining ΔH_{vap} values of the salt solutions.

4.2. BCE for evaporative cooling

The steady state operating temperature of an aqueous solution in a bubble column can be calculated using the volumetric energy balance equation (4). The relation between inlet gas temperature and column top temperature using known ΔH_{vap} values and vapour pressure values for salt solutions or pure water, can be calculated for pure water and salt solutions. The steady state column solution temperature within the BCE is a function of the temperature of the inlet gas.[9,10] This cooling effect has led to the suggestion that the BCE process could be used as a simple evaporative cooling system for buildings. This was earlier proposed by M.J. Francis and R.M. Pashley and published in 2009.[10]

When the BCE process is used with some types of salt solutions, which have coalescence inhibition effects on the bubbles,[28] it will produce a high volume fraction of small bubbles which will enhance the water vapour transfer into the bubbles. The solution with dissolved salt (NaCl) at 0.5 M has a more efficient evaporative cooling effect and hence halves the time for the column to reach steady state conditions. As an example, inlet dry air at a temperature of 50 °C will cool the 0.5m NaCl column solution to less than 20 °C.

4.3. Seawater desalination using the bubble column evaporator

The dynamic BCE method has higher overall mass transfer and heat transfer coefficients, compared with the quiescent system.[1] In this novel bubble column desalination system, water vapour can be captured and transported using a simple BCE system operated at temperatures well below the boiling point. The inhibition of bubble coalescence in salt solutions enables the design of a bubble column with a high volume fraction of small air bubbles, continuously colliding but not merging. This produces a uniform and efficient exchange of water vapour into the bubbles, which together with the high bubble rising velocity, due to its shape and trajectory based oscillations, allows water vapour to be rapidly

absorbed into bubbles, condensed and then collected as pure water.[17]

The BCE method for seawater desalination, was examined and patented in 2013.[48] The process is, of course, a reduced version of the natural phenomenon in which air is used as a carrier gas for desalting seawater through the rain cycle. However, the BCE process is based on the unexpected property of seawater in stopping air bubble coalescence[11,28] because this facilitates a high packing volume of air bubbles, which are persistently colliding but are prevented from coalescing by the presence of salts. In addition, the bubbles produced in the 1-3 mm diameter range are ideally suited for rapid water vapour uptake.[35] These factors form the basis of this enhanced process for the desalination of seawater. In addition, the BCE process offers an efficient vapour transfer mechanism in a continuous flow, with the evaporative bubble column operating below the boiling point. This method provides a very high surface area of air/water interface continuously produced and managed, naturally, by gas bubbling in salt water, such as seawater, to improve the efficiency of evaporation and transportation of the water saturated vapour producing drinking water from seawater.[36]

In the first reported experiments,[17] seawater was first heated to 70 °C then air bubbles ranging from 1-3 mm diameter were produced via a glass sinter (porosity No.2) and was passed continuously through heated seawater. After bubbling for 60 min, the temperature of the solution in the column had fallen to about 52 °C. The starting and finishing temperatures were used to estimate the theoretical yield expected for complete collection and condensation of the water vapour, at the average temperature of the column. The electrical conductivity of the bubble column solution was reduced from 49 mS cm^{-1} (seawater) to 6 μS cm^{-1} (well below the levels required for acceptable drinking water).[17] One of the advantages is that renewable sources of energy (i.e. solar energy system) could easily be coupled with a bubble column system.[17]

4.4. Enhanced supersaturated bubble column desalination

In these experiments hot, dry, air bubbles ranging from 150 to 275°C at about 23 L min^{-1} were first passed through an empty dry BCE column and then a known mass of the solution was quickly added. However, in these experiments 200 g of 0.5 m NaCl was added with and without 0.002 g of a non-ionic surfactant ($C_{12}EO_8$). The temperature of the solution was then measured every minute throughout the 30 min bubbling runs. After 30 min, the column and remaining solution was detached and weighed. Since the dry weight of the column was also known, the total amount of water vapour removed in each experiment was easily measured.[17] The results obtained show that increasing the temperature of the inlet air increases the water vapour carryover expected from the column solution vapour pressure and the air volume passed. The results obtained also showed that with added surfactant the carryover increased even more.

It seems likely that the use of the non-ionic surfactant, octaethylene glycol monododecyl ether ($C_{12}EO_8$), provides a monolayer coating at the surface of bubbles.

Thus, it appears that the packed mono-layer of surfactant molecules allows water vapour transport into the bubbles but inhibits this vapour from re-condensing on the interior, now hydrophobic, walls of the bubbles. Hence, the surfactant layer acts like a "Surface molecular diode", which facilitates water vapour transport in one direction. This supersaturation of the air bubbles then produces increased water vapour carryover.[17]

4.5. Enhanced bubble column desalination using helium as a carrier gas

Helium as inlet gas can increase the BCE performance more than 3.3 times higher compared with expected equilibrium vapour pressure, which is significant. It suggests that He as a carrier gas could be a promising solution for efficient seawater desalination.

It was suggested previously[48,49] that a suitable clathrate-forming carrier gas might be used to vaporize water not as individual molecules but in clusters and so remove the high thermal energy required for vapour phase desalination. A clathrate-forming gas partially dissolved in the aqueous solution would equilibrate with the gas in the bubbles and produce water clusters in the highly turbulent water. So providing conditions that favour enhanced evaporation with lower temperatures.[48] Helium produces different lattice structures to capture water molecules in gas form with multiple cages over a wide range of pressure and temperature. This was found by employing optimising dynamic method to determine free Gibbs energy of the He clathrate hydrates produced. Results showed that among different He clathrate hydrates, sI hydrate and filled ice II are relatively metastable comparing to sII hydrate form.[50]

Another possible explanation for the high performance of helium in the BCE desalination is based on the simple idea that the continuous flow of heated He sparge gas breaks down a small proportion of the hydrogen bonding network within water molecules due to its small size. This would also reduce the ΔH_{vap} value. For example, a decrease in hydrogen bonding of 3.6 to 3.2, due to

a modest increase in temperature, of 0 to 70 °C, corresponds to a decrease in ΔH_{vap} of about 3 kJ/mol.[19] The effect of this reduction can be roughly estimated using fundamental thermodynamics.

That is from the standard equations of equilibrium:

$$\Delta G=\Delta H-T\Delta S \text{ and} \quad (7)$$

$$\Delta G^0=-RTlnK_{eq} \leftrightarrow K_{eq}=\exp(-\frac{\Delta G^0}{RT}) \quad (8)$$

It can be assumed that the entropy difference of conversion water to gas (liquid↔gas) will be constant for either air or He. So, any difference in vaporization entropy change for the two gases will be insignificant, that is: d(ΔS)=0 and Eq. (8) becomes:

$$d(\Delta G)=d(\Delta H_{vap}) \quad (9)$$

Given this and the water density ratio of He comparing to air ($K_{eq}=\frac{\rho^w_{He}}{\rho^w_{air}}=3.3$), Eq. (9) becomes:

$$K_{eq}=\frac{\rho^w_{He}}{\rho^w_{air}}=3.3=\exp(-\frac{d(\Delta H_v)}{RT}) \quad (10)$$

In this equation, R is the gas constant and T is the average column temperature, and average $d(\Delta H_{vap})$ is calculated to be -3 kJ mol^{-1}. The expected ΔH_{vap} values for different column temperatures is, on average, about 43.4 kJ mol^{-1}, so with He experiments, a 7% reduction of ΔH_{vap} is sufficient to explain the enhanced water vapour carryover.[19]

4.6. Comparison and benefits

The main advantages of the BCE desalination system are its simplicity, resilience to feed water purity and the fact that it is a continuous and controlled, non-boiling process. These are clear advantages over the two most common seawater desalination processes currently used, that is seawater reverse osmosis (SWRO) and thermal desalination (such as MSF). There is little room left for improvement in SWRO but thermal desalination methods can still be substantially improved. Methods such as the BCE which represent low capital investment do not rely on rare materials or complex manufacturing and ready use of waste heat and sustainable energy sources, such as wind power, offer fewer constraints than the other common processes.

The main advantages in the BCE system for water desalination are listed below.

- The BCE collects water vapour throughout the entire body of the salt solution as compared to MSF, which uses only the surface of the heating plates as the main water vapour transfer site.
- The BCE process is uniform and controlled because it does not involve boiling.
- Very fast vapour collection of a few tenths of a second for 1-3 mm diameter bubbles.
- High rising velocity of saturated bubbles within the BCE system.
- Air flow produces continuously renewed bubbles and high surface area of evaporating surfaces.
- No requirement for feedwater pre-treatment as in SWRO.
- System is self-cleaning via the flotation process.
- Sub-boiling process easier to control compared with MSF and doesn't produce scaling.
- Can concentrate to a much higher level, up to 6 m NaCl, than either SWRO or MSF, i.e. produces higher recovery rate.
- Simple design will give low capital cost compared with MSF.
- Single stage and continuous process produces high quality water.
- Well suited for sustainable wind power for air flow generation and use of waste industrial hot gases.
- Does not need vacuum pumps to reduce pressure and boiling point, compared with MSF.
- Use of heated gas inflow offers an ideal process for control of column temperature and hence evaporation rate.

4.7. Water sterilization using the BCE

The high heat transfer coefficients created within the BCE system can be used to thermally destroy biological organisms well below the boiling point and it has recently been established that sterilization occurs due to transitory impact of biological species with hot gas bubbles by collisions with the heated air-water interface, although the column temperature remains low and actually even favours the growth of bacterial colonies present in typical contaminated water.[21-22]

In the first BCE sterilization study,[22] hot gas bubbles up to 150 °C were used and in a more recent study bubbles up to 250 °C[21] were passed into a water column via a glass sinter with 40-100 μm pores. The effects of exposure on sterilizing water were examined with different time intervals and typical results showed that only 2 min flow of 250 °C air was required to destroy almost all of the coliforms in the solution. The degree of sterilization was determined using natural lake water heavily contaminated with coliforms from waterfowl and land run-off. These coliform counts, obtained through the membrane filtration method, were used to measure the degree of sterilization using hot gas bubbling under

a range of conditions but in all cases where the column solution temperature never exceeded the optimum growing temperature for the coliforms.[21-22]

The presence of a salt that inhibits bubble coalescence in the solution serves to preserve finer bubbles of the heated gas, enhancing the number of bubble collisions with the biological species by ensuring a higher gas-liquid contact surface area and higher surface area per gas volume which leads to improved sterilization rates.

The use of added NaCl enhances the rate of water sterilization as air bubbles more typically in the approximate size range of 1 to 3 mm diameter increase the probabilities of bubble collisions with typically small microorganisms ranging from 2 to 5 μm in size. It is worth mentioning that after 2 mins very few coliform colonies were still observed for columns with added NaCl in the solution, which produced the smaller bubbles.

4.8. Thermolysis of solutes in aqueous solution

Thermal sterilization studies with the BCE led to the suggestion that this process could also facilitate thermal decomposition of some solutes in aqueous solutions, even at lower solution temperatures and at a faster rate than is normally produced via the direct heating of a bulk solution. Studies of the use of the BCE process for the thermal decomposition of solutes have recently been reported.[8,52] This study examined the thermal decomposition of ammonium bicarbonate (NH_4HCO_3) in aqueous solution. This salt has been used for important applications, such as a draw solution in Forward Osmosis [53] and, more recently, in the regeneration of ion exchange resins.[54] A second solute in widespread use is potassium persulfate ($K_2S_2O_8$) which was also studied in aqueous solutions. This salt is often used as a radical initiator for the process of emulsion polymerization.[55]

4.8.1. Decomposition of NH_4HCO_3 solutions

Typical decomposition results obtained using different solution conditions[8] clearly demonstrate that the BCE process is much more efficient for NH_4HCO_3 decomposition, especially compared with the standard method, which is, using a stirred water bath at the same solution temperature, of 45 °C. For example, in the BCE process, 90% thermal decomposition of NH_4HCO_3 was obtained after 30 min of bubbling of 150 °C air through 0.5m solutions.[8]

The initial high (2 m) concentration of NH_4HCO_3 used in these BCE experiments was found to inhibit bubble coalescence, producing small bubbles. However, after 30 min of the BCE process, the significant reduction in NH_4HCO_3 concentration produced larger bubbles of the same diameter as those observed in pure water, which also confirms the decomposition of NH_4HCO_3 salt into ammonia and carbon dioxide gases.[8]

4.8.2. Proposed Mechanism of BCE Solute

Pre-heated gas bubbles introduced and passed through the aqueous solution, must produce a transient hot surface layer around each rising bubble. The transient hot surface layer will have a higher temperature than the average temperature of the aqueous solution. We believe that it is the interaction of the solute with this transient hot surface layer which results in the thermal decomposition of the solute, even when the average temperature of the aqueous solution remains below the temperature at which it would normally cause thermal/chemical decomposition of the solute. For situations where thermal decomposition is either required very quickly or at reduced temperature, the BCE method offers a new approach.

4.9. Inhibition of particle growth in a BCE

At first, it might appear that the BCE process, with continuous water evaporation via the rising dry bubbles, could be used to slowly increase supersaturation levels and hence cause precipitation. However, it was discovered[23] using aqueous $CaCl_2$ and K_2SO_4 mixtures that the BCE process actually has a significant inhibition effect on the precipitation process, and as these particles grow the turbidity was monitored with time during the precipitation. In this case, with no added foreign nucleating particles, turbidity values within the BCE solutions were fairly constant with time over more than 300 mins, even though in quiescent solutions, at this same supersaturation level, significant particle growth was observed much earlier.

These results suggest that the high density of rising bubbles might disrupt sub-nuclei or molecular clusters in the solution during precipitation and, in addition, the charged surfaces of the bubbles might have a big perturbation on interacting ions involved in nucleation and growth. A similar phenomenon was reported by J. W. Mullin and K. D. Raven[56-57] who found that an increase in the intensity of agitation does not always lead to an increase in nucleation, which might be explained by assuming that agitation can disrupt sub-nuclei or molecular clusters in the solution. Stirred systems are also

complex in that, for example, different types of impellers can have a significant effect on other process parameters of crystallization[58] and can lead to the production of different crystal shapes.[59]

4.10. Other potential applications

The BCE process, in addition to its applications in wastewater concentration, could at the same time be used to inactivate different types of viruses and enzymes in the wastewater. The BCE hot air system could also possibly be used for the sterilization of dairy and dairy based products and could even be used for the production of chiral compounds. In addition, the bubble column system could be effective in treating water-based foods, beverages, blood and blood related products and it might also be employed in specific stages for the treatment of pharmaceutical products. The BCE could also be used for carbon capture by adding surfactant to produce a continuous flow of CO_2 foam from hot waste industrial gases. This foam could be transported and then buried under pressure to reduce total volume and foam cell size for long term storage.

5. CONCLUSIONS

This updated review article examines the theoretical background and the applicability of the BCE process to several important industrial applications. The design and development of the BCE are established on the two main features (1) higher overall mass transfer coefficient and (2) efficient heat transfer coefficient, which is a prerequisite for different bubble column evaporator applications. It is argued that a thorough and in-depth understanding of the BCE system, when used with aqueous solutions, is critically dependent on the physical properties of water. Further detailed studies would be required to develop large scale industrial applications of this technique.

ACKNOWLEDGEMENT

The authors would like to thank the Australian Research Council for funding this project.

LIST OF PARAMETERS, DEFINITIONS AND UNITS

(ΔH_{vap}): enthalpy of vaporization (kJ/mol)
CMC: critical micelle concentration of a surfactant (M)
t_{bl}: bubble layer thickness (m)
$\rho_w^v(T_c)$: is the water vapour density at the steady state column temperature (T_c) (in mol/m^3)
r: radius of the bubble (m)
ρ_w: is the liquid water density (mol/m^3)
C_p and C_s: are the air (at constant pressure) and solution (or water) specific heat capacities (in J/m^3 K)
Δt: estimated transient temperature increase in the solution layer surrounding the bubbles (K)
ΔT: temperature reduction within the cooling bubbles (K)
δ: estimated heated layer thickness around partially cooled hot bubble (m)
T_i: initial bubble temperature (K)
T_b: temperature of partially cooled bubbles (in K) assumed to be equal to 100 °C
T_c: column solution temperature (K)
U_∞: is the bubble rise velocity in an infinite liquid (m/s)
η: is the coefficient of viscosity of the liquid (Nsm^{-2})
ρ_w: is the density of the liquid (kg/m^3)
a: is the gas bubble radius in eqn (3) (m)
g: is the gravitational constant (9.81m/s^2)
k: in eqn (3) is a bubble rise constant
$C_p(T_e)$; is the specific heat per unit volume of gas at constant pressure and at temperature T_e (J/m^3 K)
T_e: steady state temperature of the solution in a bubble column (K)
$\rho_v(T_e)$: is the water vapour density at temperature T_e (mol/m^3)
$\Delta H_{vap}(T_e)$: is the enthalpy of vaporization of water at temperature T_e (J/mol)
ΔT: is the temperature difference between the gas entering and leaving the column (K)
ΔP: is the hydrostatic differential pressure, between the gas inlet into the sinter and atmospheric pressure at the top of the column (Pa)
$C_p^g(T_e)$: mass heat capacity of gas at temperature T_e (J/kg K)
m_g : is the mass of air (or gas) per cubic meter at T_e (kg/m^3)
P : gas pressure (Pa)
ΔV: change in gas volume at temperature T_e (m^3)
C_v^g: the heat capacity of gas under constant volume conditions (J/m^3 K)
C_p^g: the heat capacity of gas under constant pressure conditions (J/m^3 K)
V_b: volume of a bubble (m^3)
r^w_{He}: water vapour density from helium sparged solution (mol/m^3)
r^w_{air}: water vapour density from air sparged solution (mol/m^3)
R: gas constant (J/K mol)

REFERENCES

1. P. Zehner, M. Kraume, Bubble columns, *Ullmann's Encyclopedia of Industrial Chemistry*, **2000**.
2. A. H. Luedicke, B. Hendrickson, G. M. Pigott, A method for the concentration of proteinaceous solutions by submerged combustion, *J. Food Sci.,* **1979**, 44, 1469-1473.
3. C. P. Ribeiro, P. L. C. Lage, Gas-Liquid Direct-Contact Evaporation: A Review, *Chem. Eng. Technol.,* **2005**, 28 (10), 1081-1107.
4. M. Schluter, A-M. Billet, S. Herres-Pawlis, Reactive Bubbly Flows, *Chem. Eng. Technol.,* **2017**, 40 (8), 1384.
5. J. B. Joshi, K. Nandakumar, G. M. Evans, V. K. Pareek, M. M. Gumulya, M. J. Sathe, M. A. Khanwale, Bubble generated turbulence and direct numerical simulations, *Chem. Eng. Sci*., **2017**, 157, 26–75.
6. Y. T. Shah, B. G. Kelkar, S. P. Godbole, W. D. Deckwer, Design parameters estimations for bubble column reactors, *AIChE Journal,* **1982**, 28 (3), 353-379.
7. V. I. Klassen, V. A. Mokrousov, *An introduction to the theory of flotation*, London: Butterworths, **1963**.
8. M. Shahid, X. Xue, C. Fan, R.M. Pashley, Study of a novel method for the thermolysis of solutes in aqueous solution using a low temperature bubble column evaporator, *J. Phys. Chem. B,* **2015**, 119 (25), 8072–8079.
9. C. Fan, M. Shahid, and R. M. Pashley, Studies on bubble column evaporation in various salt solutions, *J. Sol. Chem.,* **2014**, 43 (8), 1297-1312.
10. M. J. Francis, R. M. Pashley, Application of a Bubble Column for Evaporative Cooling and a Simple Procedure for Determining the Latent Heat of Vaporization of Aqueous Salt Solutions, *J. Phys. Chem. B,* **2009**, 113 (27). 9311-9315.
11. V. S. J. Craig, B. W. Ninham, R. M. Pashley, The effect of electrolytes on bubble coalescence in water, *J. Phys. Chem.,* **1993**, vol. 97(39), 10192-10197.
12. Hierarchies of forces: The last 150 years, *Advances in Colloid & Interface Science*, **1982**, 16 (1), 3-15.
13. Proceedings of the *IUTAM-IUPAC Symposium on Interaction of Particles in Colloidal Dispersions,* Canberra, March **1981**.
14. V. S. J. Craig, Bubble coalescence and specific-ion effects, *Curr. Opin. Colloid Interface Sci.,* **2004**, 9 (1), 178-184.
15. S. Marcelja, Short-range forces in surface and bubble interaction, *Curr. Opin. Colloid Interface Sci.,* **2004**, 9 (1), 165-167.
16. B. P. Reines, B. W. Ninham, Structure and Function of the Endothelial Surface Layer: unravelling the nano-architecture of biological surfaces. *Quarterly Reviews of Biophysics*, **2019**, 52, 1-11.
17. M. J. Francis, R. M. Pashley, Thermal desalination using a non-boiling bubble column, *Desalin. Water Treat.,* **2009**, 12 (1-3), 155-161; M. Shahid, R. M. Pashley, A study of the bubble column evaporator method for thermal desalination, *Desalination,* **2014**, 351, 236-242.
18. C. Fan, R.M. Pashley, Precise Method for Determining the Enthalpy of Vaporization of Concentrated Salt Solutions Using a Bubble Column Evaporator, *J. Sol. Chem.,* **2015**, 44 (1), 131-145.
19. M. Taseidifar, M. Shahid, R. M. Pashley, A study of the bubble column evaporator method for improved thermal desalination, *Desalination,* **2018**, 432, 97-103.
20. X. Xue, R. M. Pashley, A study of low temperature inactivation of fecal coliforms in electrolyte solutions using hot air bubbles, *Desalin. Water Treat.*, **2015**, 1–11.
21. M. Shahid, A study of the bubble column evaporator method for improved sterilization, *J. Water Process. Eng.,* **2015**, 8, 1-6.
22. M. Shahid, R. M. Pashley, M. Rahman, Use of a high density, low temperature, bubble column for thermally efficient water sterilization, *Desalin. Water Treat.,* **2014**, 52, 4444–4452.
23. C. Fan, R. M. Pashley, The controlled growth of calcium sulfate dihydrate (gypsum) in aqueous solution using the inhibition effect of a bubble column evaporator, *Chem. Eng. Sci.,* **2016**, 142, 23-31.
24. P. N. Govindan, G. P. Thiel, R. K. McGovern, J. H. Lienhard, M. H. Elsharqawy, *Bubble-Column Vapor Mixture Condenser*, US8523985, Google Patents.
25. G. P. Narayan, J. H. Lienhard, Thermal Design of Humidification–Dehumidification Systems for Affordable Small-Scale Desalination, *IDA J. Desalin. Water Reuse,* **2012**, 4 (3), 24-34.
26. M. Schmack, H. Goen, and A. Martin, A Bubble Column Evaporator with Basic Flat-plate Condenser for Brackish and Seawater Desalination, *Environ. Technol.,* **2015**, 37 (1), 74–85.
27. P. Ghosh, Coalescence of air bubbles at air–water interface, *Chem. Eng. Res. Des.,* **2004**, 82 (7), 849-854.
28. V. S. J. Craig, B. W. Ninham, R. M. Pashley, Effect of electrolytes on bubble coalescence, *Nature,* **1993**, 364 (6435), 317-319.
29. B. W. Ninham, R. M. Pashley, P. Lo Nostro, Surface forces: Changing concepts and complexity with dissolved gas, bubbles, salt and heat, *Current Opinion in Colloid & Interface Science,* **2016**, 27, 25-32.
30. M. Alheshibri, J. Qian, M. Jehannin and V. S. J. Craig, A history of nanobubbles. *Langmuir,* **2016**, 32(43), 11086-11100.

31. E. C. W. Clarke, D. N. Glew, Evaluation of the thermodynamic functions for aqueous sodium chloride from equilibrium and calorimetric measurements below 154 °C, *J. Phys. Chem. Ref. Data,* **1985**, 14, 489, 1985.
32. D. E. Garrett, *Handbook of lithium and natural calcium chloride*, London: Academic Press, **2004**.
33. D. R. Lide, T. J. Bruno, CRC handbook of chemistry and physics: CRC Press, Boca Raton, **2012**.
34. A. G. Sanchis, R. M. Pashley, B. W. Ninham, Virus and bacteria inactivation by CO_2 bubbles in solution, *NPJ Clean Water*, **2019**, 2.
35. I. Leifer, R. K. Patro, P. Bowyer, A study on the temperature variation of rise velocity for large clean bubbles, *J. Atmos. Ocean. Tech.,* **2000**, 17(10), 1392-1402.
36. R. M. Pashley, M. J. Francis, M. Rzechowicz, Unusual properties of water: Effects on desalination processes, *Water,* **2008**, 35 (8), 67-71.
37. A. A. Kulkarni, J. B. Joshi, Bubble formation and bubble rise velocity in gas-liquid systems: A review, *Industrial & Engineering Chemistry Research,* **2005**, 44(16), 5873-5931.
38. R. Clift, J. Grace, M. Weber, Bubbles, drops and particles New York, Academic Press, **1978**.
39. J. J. Quinn, M. Maldonado, C. O. Gomez, J. A. Finch, Experimental study on the shape–velocity relationship of an ellipsoidal bubble in inorganic salt solutions, *Minerals Engineering,* **2014**, 55, 5-10.
40. P. Gonzaleztello, F. Camacho, E. Jurado, M. P. Paez, Influence of surfactant concentration on the final rising rate of droplets, *Canadian J. Chem. Eng.*, **1992**, 70(3), 426-430.
41. X. Luo, J. Zhang, K. Tsuchiya, L. S. Fan, On the rise velocity of bubbles in liquid-solid suspensions at elevated pressure and temperature, *Chem. Eng. Sci.,* **1997**, 52(21), 3693-3699.
42. K. W. K. Li, and A. Schneider, Rise velocities of large bubbles in viscous Newtonian liquids, *J. American Ceramic Soc.,* **1993**, 76(1), 241-244.
43. V. G. Levich, S. Technica, *Physicochemical hydrodynamics*: Prentice-hall Englewood Cliffs, NJ, **1962**.
44. D. Y. Chan, E. Klaseboer, R. Manica, Film drainage and coalescence between deformable drops and bubbles, *Soft Matter,* **2011**, 7(6), 2235-2264.
45. E. Klaseboer, R. Manica, D. Y. Chan, B. C. Khoo, BEM simulations of potential flow with viscous effects as applied to a rising bubble, *Eng. Anal. Bound. Elem.,* 2011, 35(3), 489-494.
46. E. W. Lemmon, R. T. Jacobsen, S. G. Penoncello, D. G. Friend, Thermodynamic properties of air and mixtures of nitrogen, argon, and oxygen from 60 to 2000 K at pressures to 2000 MPa, *J. Phys. Chem. Ref. Data,* **2000**, 29(3), 331.
47. F. J. Massey Jr, The Kolmogorov-Smirnov test for goodness of fit, *J. Amer. Statist. Assoc.*, **1951**, 46(253), pp. 68-78.
48. R. M. Pashley, *Method for desalination*, US20090120877; Google Patents.
49. E. W. Hough, M. J. Rzasa, B. B. Wood, Interfacial Tensions at Reservoir Pressures and Temperatures; Apparatus and the Water-Methane System, *Journal of Petroleum Technology,* **1951**, 192, 57-60.
50. R. V. Belosludov, Y. Y. Bozhko, O. S. Subbotin, V. R. Belosludov, H. Mizuseki, Y. Kawazoe, V. M. Fomin, Stability and Composition of Helium Hydrates Based on Ices Ih and II at Low Temperatures, *J. Phys. Chem. C,* **2014**, 118(5), 2587-2593.
51. C. Fan, A Study of Some Physical Properties of Concentrated Salt Solutions Using the Bubble Column Evaporator, PhD Thesis. School of Physical, Environmental and Mathematical Sciences, The University of New South Wales, **2016**.
52. R. M. Pashley, X. Xue, C. Fan, M. Shahid, *Method for assisting thermally-induced changes*, AU2015901956, 2015.
53. J. R. McCutcheon, R. L. McGinnis, M. Elimelech, A novel ammonia—carbon dioxide forward (direct) osmosis desalination process, *Desalination,* **2005**, 174(1), 1-11.
54. N. P. G. N. Chandrasekara, and R. M. Pashley, Study of a new process for the efficient regeneration of ion exchange resins, *Desalination,* **2015**, 357, 131-139.
55. M. Okubo, T. Mori, The decomposition of potassium persulphate used as initiator in emulsion polymerization, *Makromolekulare Chemie. Macromolecular Symposia*, 1, Wiley Online Library, **1990**, 143-156.
56. J. W. Mullin, K. D. Raven, Influence of mechanical agitation on the nucleation of some aqueous salt solutions, *Nature,* 1962, 195, 35-38.
57. J. W. Mullin, K. D. Raven, Nucleation in Agitated Solutions, *Nature,* **1961**, 190(4772), 251.
58. W. Beckmann, *Crystallization: Basic Concepts and Industrial Applications*, Weinheim: John Wiley & Sons, **2013**.
59. I. Mukhopadhyay, V. P. Mohandas, G. R. Desale, A. Chaudhary, P. K. Ghosh, Crystallization of Spherical Common Salt in the Submillimeter Size Range without Habit Modifier, *Ind. Eng. Chem. Res.,* **2010**, 49(23), 12197-12203.

Substantia
An International Journal of the History of Chemistry

Firenze University Press
www.fupress.com/substantia

Citation: T. Gettongsong, M. Taseidifar, R.M. Pashley (2020) New Resins for Ion Exchange Applications and a Process for Their Sustainable Regeneration. *Substantia* 4(2) Suppl.: 33-37. doi: 10.36253/Substantia-824

Data Availability Statement: All relevant data are within the paper and its Supporting Information files.

Competing Interests: The Author(s) declare(s) no conflict of interest.

New Resins for Ion Exchange Applications and a Process for Their Sustainable Regeneration

Tanita Gettongsong, Mojtaba Taseidifar, Richard M. Pashley*

School of Science, UNSW Canberra, Northcott Drive, Canberra, Australia
*Corresponding author: r.pashley@adfa.edu.au

Abstract. The report is concerned with the design and synthesis of a mixed bead resin for high salt level desalination. The resin allows for the simultaneous exchange of both anions and cations, within the same polymer. This improves the efficiency of desalination at seawater levels. A novel process for sustainable and low energy desalination for brackish water has already been achieved via ion exchange resins as explained below. The advance in resin technology improves a novel membrane process with closed–cycle regeneration of the resin. It is a superior alternative to reverse osmosis.

Keywords: thermal decomposition, bubble column evaporator, zwitterionic polymer resin, desalination, ion-exchange resin, ammonium bicarbonate, hollow fibre membrane.

1. INTRODUCTION

Current desalination techniques like distillation and reverse osmosis (RO) are so energy intensive processes that they are often marginal economically.[1] A promising alternative discussed in this volume comprises mixed cation and anion ion-exchange resins, that remove salt. It offers several advantages in desalination, such as low-input pressure, simple setup, high efficiency and also does not require an extensive pre-treatment. Success requires removal of the salt and regeneration of the resin by the ammonium bicarbonate technology described [2-4] and further below.

Ion exchange beads, in typical commercial applications, are mixed and widely used in order to adsorb different ions onto their surfaces. The process has been used over many years in various water treatment processes, and consumes less energy than distillation and reverse osmosis. However, it has limited capacity to remove and adsorb ions in seawatwer and even fairly concentrated brackish water. An ion-exchange resin reaches a 'spent' point, at which the majority of the ion-receiver sites on the surface of the beads are depleted and no longer adsorb ions in aqueous solution. This problem can be resolved by maintaining separation of cationic and anionic beads following by regeneration of each with large volumes of strong acid and strong base. This limits the economic viability of the technique for desalination applications.[2,5]

Our published results[2] have shown that ammonium bicarbonate (AB) can regenerate the spent resin without the need for separation of cationic and anionic resins and also the use of strong acid and strong base regeneration. Ammonium bicarbonate (AB) is a thermolytic salt, which is capable of decomposing in aqueous solution at low temperatures, ranging between 35 and 80 °C.[6] The decomposition is described by below reaction:

$$NH_4HCO_{3\,(aq)} \triangleq NH_{3\,(g)} + CO_{2\,(g)} + H_2O \quad (1)$$

Using an AB solution as regenerant resolves the regeneration issue, and apparently for the first time. Ammonium bicarbonate is unique in having the necessary properties for regeneration. The decomposition of the product AB solution also provides drinking water, as well as re-forming the resin.[5]

This work relates to use of mixed bead resin for high salt level desalination and also potential processes for regeneration of the resin. The resin material produced the polyampholytic hydrogel and zwitterionic resins to simultaneously exchange ions and cations in desalination at salt concentrations approaching seawater levels, and the regeneration process is comprised of washing the resin with high concentration of ammonium bicarbonate solutions. The recovery of the latter compound can be performed using either, a closed cycle hollow fibre membrane system or by using a suitable bubble column evaporator (BCE). These methods offer the advantage of re-using the ammonium bicarbonate as an *in situ* regenerator for the mixed bead resin desalination system.

2. MATERIAL AND METHODS

2.1. Materials

Certified reagent grade chemical (>99% purity) ammonium bicarbonate (NH_4HCO_3) was supplied by Sigma-Aldrich and was used without further purification. Aqueous solutions were prepared using deionized, ultrafiltered water (Milli-Q).

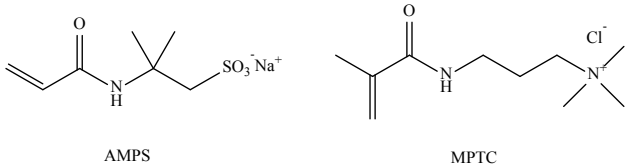

Figure 1. Chemical structures of the cationic and anionic monomers used to produce the polyampholytic hydrogel.

For the decomposition experiment using a bubble column evaporator, a glass sinter column (Büchner type, Pyrex® Borosilicate, VWR) with 120 mm diameter filled with 250 mL solution was used. The inlet air temperature was varied using a Tempco air heater (300W) with a thermocouple temperature monitor and an AC Variac electrical supply. The gases (air and nitrogen) were produced by cylinder (Coregas Pty Ltd, Australia) and a BOC gas flow meter.

2.2. Synthesis of strong acid and strong base polymer resins

The resin is synthesised by synthesis of two different strong acid and strong base resins. The resins comprise a chemical cross-linked polyampholytic resin and a crosslinked zwitterionic polymer, both resins containing strong acid and strong base on the same polymer.

2.2.1. A chemical cross-linked polyampholytic resin materials

2.2.1.1. Materials

2-acrylamido-2-methylpropanesulphonic acid sodium salt solution (AMPS) (anionic monomer), 3-(methacryloylamino) propyl-trimethylammonium chloride solution (MPTC) (cationic monomer), ethylene glycol dimethacrylate (EGDMA) (crosslinking agent), 25% glutaraldehyde (GA) and alpha-glutaric acid (initiator) were used for synthesis. Several salts: 98% sodium chloride, 99% sodium sulphate, magnesium chloride (AR grade) and magnesium sulphate (AR grade) were used to study swelling and conductivity and absorption properties. Chemical structures of AMPS and MPTC compounds are shown in Figure 1. All chemicals were purchased from Sigma-Aldrich, Australia as a reagent grade. 365 nm, 230 Volts, 8 Watts UV-lamp and 365 nm Ultraviolet Crosslinker replacement tubes were purchased from John Morris Scientific Pty Ltd.

2.2.1.2. Methods

Several different reaction cells were tested for the UV polymerisation process to produce the polymer. The most suitable method was based on using an array of glass tubes of 1 cm diameter and 0.8 cm inner-diameter and of 10 cm length. Cross-linked polyampholytic resins were synthesised within the glass tubes using the one-step copolymerisation of an anionic monomer, a cationic monomer and a crosslink agent (EGDMA). 2-oxoglutaric acid was used as initiator. Cross-linked polyampholytic resins were produced with a range of

different composition ratio. The ratio of momoners are shown in Table 1. 0.5 M NaCl was used to fill the reaction cell. The UV reactions used 8 Watts at 250 volts, with a 365 nm ultraviolet lamp, for 15 hours. After reaction, the product was immersed in water for 1 week to allow the product to equilibrate and to wash out the residue unreacted chemicals.

2.2.2. A crosslinked zwitterionic polymer

2.2.2.1. Materials

p-Phenylene diamine and glutaraldehyde in dimethyl formamide (DMF) and 1,3-propane sultone in DMF were used as reactants for synthesis of the zwitterionic compounds. All chemicals were purchased from Sigma-Aldrich, Australia as a reagent grade.

2.2.2.2. Methods

This resin was prepared using 5 mmol of p-phenylene diamine in 20 mL of DMF and 5 mmol of glutaraldehyde in 20mL of DMF were prepared separately in a different beaker. The solution was mixed and refluxed at 80°C for 1 hr. Then, 15 mmol of 1,3-propane sultone in 10 mL of DMF was added in the reaction and refluxed at 70°C for 3 hr. The final product was washed several times with hot water to remove residual unreacted chemicals. Figure 3 shows the chemical structure of the zwitterionic polymer.

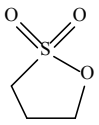

1,3-propane sultone

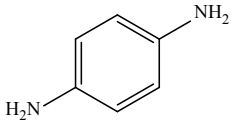

p-Phenylene diamine

Figure 2. Chemical structures of the cationic and anionic monomers used to produce the zwitterionic resins.

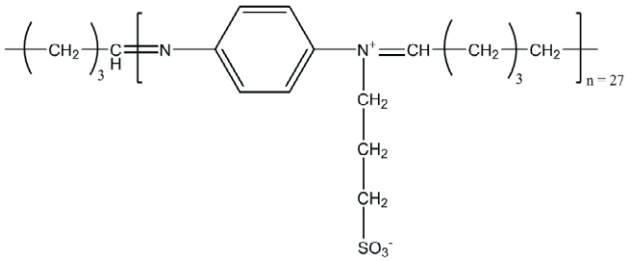

Figure 3. The zwitterionic polymer compound.

Table 1. The different molar ratios of reactant chemicals used for the polyampholytic resin syntheses.

Monomers		Crosslink agent	Initiator*
AMPS	MPTC		
1	1	0	1
1	1	0	4
1	1	1	1
1	1	1	4
1	1	2	1
1	1	2	4

*note that the initiator concentrations 1- 4 refers to the ratio of monomer and 0.25% mole of initiator (i.e. for '1', with '4' corresponding to 1%).

2.3. Bubble column evaporator system as an example for the ammonium bicarbonate recovery

Laboratory grade air and nitrogen separately was heated at 275 °C using a Tempco air heater (300 W) with a thermocouple temperature monitor and an AC Variac electrical supply to produce high-surface-area gas/water interface into a 120mm diameter open-top glass column (Büchner type, Pyrex® Borosilicate, VWR) filled with 250 mL of the ammonium bicarbonate solution. The bubble column evaporator apparatus used to study improved decomposition with a high-temperature gas (air) flow is shown in our previous work.[7] The actual temperature of the dry gas flowing into the solution was measured at the centre of the sinter by a Tenmars thermometer (±1.5 °C) without any solution in the column. The gases (air and nitrogen) were produced from cylinders (Coregas Pty Ltd, Australia) and a BOC gas flow meter was used to measure flow rates. The temperature of the column solution was also continuously monitored using a thermocouple positioned at the centre of the column solution. The air flow at temperatures of 300–600 °C was needed to produce gas temperatures just above the glass sinter up to 275 °C, and this necessitated the use of steel and brass connectors for the downstream output from the heater and the use of FM Insulation Rock Wool as an insulating material.

Using the measured electrical conductivities of the NH_4HCO_3 solutions at different time intervals, the percent decomposition of NH_4HCO_3 at time (t) in the either membrane or the bubble column evaporator process was calculated using the formula:

$$Decomposition\% = [1 - \frac{[NH_4HCO_3]_t}{[NH_4HCO_3]_0}] \times 100 \quad (2)$$

Where $[NH_4HCO_3]_t$ is the concentration of NH_4HCO_3 at time (t) during the decomposition operation and

$[NH_4HCO_3]_0$ is the initial concentration of NH_4HCO_3, just before pouring the solution into the membrane contactor or the bubble column evaporator. Electrical conductivity values of all the solutions were measured using a EUTECH CON 700 Conductivity Bench.

3. RESULTS AND DISCUSSION

3.1. Polyampholytic and polyzwitterionic resins

Ion adsorption equilibria were studied for both resins using monovalent (NaCl) and divalent ($MgSO_4$) salt solutions. Typical results for the polyampholytic resin are shown in Figure 4 This graphs the absorption of salts by crosslink hydrogels. Similar adsorption isotherms were obtained with the polyzwitterionic resin, with a maximum NaCl adsorption of about 28 mmol/g (dry wt). Both resins indicate enhanced adsorption capacity compared with typical results obtained using commercial mixed-bed strong acid-strong base systems. These give about 5 mmol NaCl/g (dry wt). The high adsorption rates show an increased efficiency of using the new resins in desalination compared to commercial resins. In addition, the latter resins are expected to have a shorter operating lifespan due to their regeneration using strong acid strong base This damages their polymeric structures.

The results in Figure 4 were obtained based on the electrical conductivities for different solutions when they were exposed to different ion exchange resins. These results are given below in Table 2-5.

3.2. AB decomposition using the bubble column evaporator

Some typical decomposition results (using air and nitrogen) obtained under different solution conditions

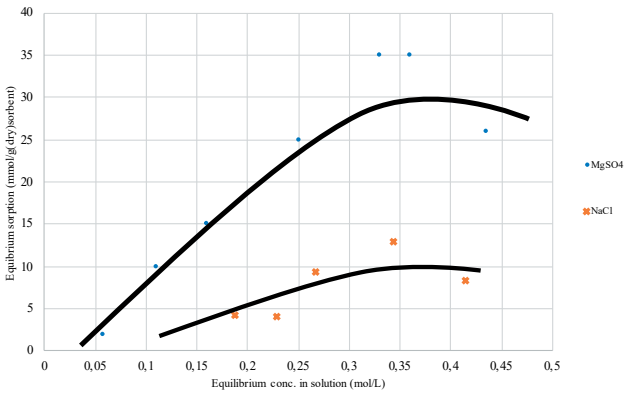

Figure 4. Adsorption of cross-linked polyampholytic resins equilibrated in NaCl and $MgSO_4$.

Table 2. Electrical conductivity results for the hydrogel polymer dry sample (weight 0.05 g) in 50 mL NaCl solution.

Concentration (M)	Conductivity (mS/cm)	
	Before	After
0.2	19.14	18.74
0.25	23.2	22.8
0.3	27.3	26.4
0.4	34.9	33.7
0.5	41.3	40.5

Table 3. Electrical conductivity results for the zwitterionic polymer dry sample (weight 0.05 g) in 50 mL NaCl solution.

Concentration (M)	Conductivity (mS/cm)	
	Before	After
0.1	10.43	10.34
0.3	27.5	24.8
0.5	35.4	34.1

Table 4. Electrical conductivity results for 0.2 M salts solution (Conductivity in solution).

	Conductivity (mS/cm)			
	day 0	day 1	day 2	day 3
NaCl	18.98	18.66	18.62	18.38
$MgSO_4$	15.96	15.92	15.82	15.69
DI water	0.0025	0.01329	0.037	0.053

Table 5. Electrical conductivity results for 0.2 M salts solution (Conductivity in gel)

	Conductivity (mS/cm)			
	day 0	day 1	day 2	day 3
NaCl		15.64	16.73	16.3
$MgSO_4$		13.5	13.75	14.03
DI water		0.0363	0.042	0.0573

are given in Figure 5. These results clearly demonstrate that the improved bubble column evaporator process is much more efficient for NH_4HCO_3 decomposition than the standard method using simple stirred heating (i.e. without bubble column evaporator) at the same solution temperature of around 57 °C. The results in Figure 5 obtained for different stirring conditions showed that

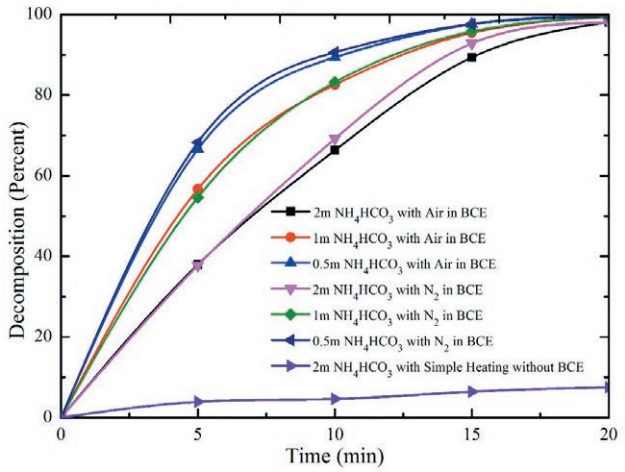

Figure 5. Percent decomposition of NH_4HCO_3 solutions at different concentrations in the bubble column evaporator (with an inlet gas (air and nitrogen) temperature of 275 °C and column solution temperature of 57 °C) compared with simple heating in a stirred vessel at around 57 °C.

the decomposition rates for simple heating (without bubble column evaporator) remained the same, which indicates that the continuous mixing by the bubbling process in the bubble column evaporator did not itself contribute to the NH_4HCO_3 decomposition.

During the experiments, it was also observed that the presence of NH_4HCO_3 at concentrations above about 0.5 m inhibited bubble coalescence to a similar degree as 0.17 M NaCl,[8] and that fine (1-3 mm diameter) bubbles were produced in the bubble column evaporator process. The thermal decomposition of ammonium bicarbonate solutions into ammonia and carbon dioxide gases and the resulting reduction in NH_4HCO_3 concentration can clearly be seen by the increase in bubble size.

4. CONCLUSION AND FUTURE WORK

An ion exchange resin was used for high salt level water desalination, with the resin comprising either a chemically cross-linked ampholytic polymer resin or a cross-linked zwitterionic polymer resin, on the same polymer chain, wherein the ampholytic polymer resin and the zwitterionic polymer resin each contain strong acid and base groups on the same polymer chain.

The current laboratory system could be scaled up and optimised either with a commercial mixed-bed resin (strong acid/strong base mixed resin) or a novel mixed bead resin of the type used in this study but using ammonium bicarbonate for the closed-cycle regeneration of the resin, which offers an energy efficient desalination process. The resin regeneration process could also be combined with the bubble column evaporator method in order to recycle ammonium bicarbonate in a simple and efficient way. This can potentially be used as a new method to treat brackish groundwater in remote communities to replace current techniques, such as, reverse osmosis and thermal distillation which both have expensive maintenance requirements and are more difficult to establish.

5. ACKNOWLEDGMENT

The authors gratefully acknowledge the Australian Research Council for funding this research.

6. REFERENCES

1. I. C. Karagiannis, P. G. Soldatos, Water desalination cost literature: review and assessment, *Desalination*, **2008**, 223, 448-456.
2. N. P. G. N. Chandrasekara, R. M. Pashley, Regeneration of strong acid/strong base mixed-bed resins using ammonium bicarbonate (AB) for a sustainable desalination process, *Desalination*, **2017**, 409, 1-6.
3. N. P. G. N. Chandrasekara, R. M. Pashley, Study of a new process for the efficient regeneration of ion exchange resins, *Desalination*, **2015**, 357, 131-139.
4. N. Tarannum, M. Singh, Synthesis and characterization of zwitterionic organogels based on Schiff base chemistry, *J. Appl. Polym. Sci.*, **2010**, 118, 2821-2832.
5. N. P. G. N. Chandrasekara, R. M. Pashley, Enhanced ion exchange capacity of polyampholytic resins, *Sep. Purif. Technol.*, **2016**, 158, 16-23.
6. G. W. Gokel, Dean's handbook of organic chemistry, McGraw-Hill, New York, **2004**.
7. M. Shahid, X. Xue, C. Fan, B. W. Ninham, R. M. Pashley, Study of a novel method for the thermolysis of solutes in aqueous solution using a low temperature bubble column evaporator, *J. Phys. Chem. B*, **2015**, 119, 8072–8079.
8. V. S. J. Craig, B. W. Ninham, R. M. Pashley, The effect of electrolytes on bubble coalescence in water, *J. Phys. Chem.*, **1993**, 97, 10192-10197.

Substantia
An International Journal of the History of Chemistry

Firenze University Press
www.fupress.com/substantia

OPEN ACCESS

Citation: T. Gettongsong, M. Taseidifar, R.M. Pashley, B.W. Ninham (2020) Novel Resins for Efficient Desalination. *Substantia* 4(2) Suppl.: 39-48. doi: 10.36253/Substantia-826

Data Availability Statement: All relevant data are within the paper and its Supporting Information files.

Competing Interests: The Author(s) declare(s) no conflict of interest.

Novel Resins for Efficient Desalination

Tanita Gettongsong[1], Mojtaba Taseidifar[1], Richard M. Pashley[1,*], Barry W. Ninham[2]

[1] *School of Science, University of New South Wales, Canberra, Northcott Dr, Campbell Australia*
[2] *Department of Applied Mathematics, Research School of Physical Sciences, The Australian National University, Canberra, Australia*
*Corresponding author: r.pashley@adfa.edu.au

Abstract. This paper reports the synthesis and properties of new polymer resins containing strong acid and base groups for optimising applications in desalination. Several polyampholytic gels were synthesised with a ratio of 1:1 of strong acid (sulphonate) and strong base (quaternary ammonium) groups and a zwitterionic resin with a 1:1 strong acid and base ratio. The physico-chemical properties of these highly charged resins were studied in electrolyte solutions over a range of pH values, in particular: effects of chemical cross-linking, water and electrolyte swelling; bulk electrical conductivities and surface charging properties in different pH values. The results from absorption of NaCl showed that the resins have considerable potential for more effective desalination than other resin-based techniques.

Keywords: Zwitterionic polymer resin, polyampholytic resins, desalination, ion-exchange resin, ammonium bicarbonate.

INTRODUCTION

One of several themes of this Substantia volume on novel technologies for water processing concerns desalination. It has been shown that mixed cationic and anionic ion exchange resins can be used to great effect in a new desalination process. This is far more efficient in all aspects (in excess of 30%) to the present best reverse osmosis (RO) and other techniques in use. The claim may seem extravagant. But it is the result of extensive evaluation by a major international company that builds RO plants worldwide. Our aim here is to seek to improve this new ion exchange based technology even further.

If we can build an ion exchange resin in which cationic and anionic exchange sites are on the same polymer, nanometers apart only, that in principle should do the job. Few such synthetic polymers are known. Hydrogels are composed of three-dimensional networks of polymers made of natural or synthetic materials that possess a high degree of flexibility. They have the ability to swell or de-swell, and to retain a significant fraction of water within their structure. In this study we have developed a new method to synthesise polyampholytic hydrogels containing strong acid and strong base

ionic groups. The chemical and physical properties of highly charged hydrogels are of interest besides because of their potential as controllable shape materials.[1] Shape can be controlled in several ways: by moderating the electrostatic interaction between the strong acid and base groups, their degree of hydration and hydrophobicity and also by the extent of chemical cross-linking within the resin. The range of control variables, including chemical composition make these materials of interest for their mechanical and electrical properties, their water absorption/swelling properties and their potential for selective solute separation. Especially because of the proximity of the cation and anion groups, the Hofmeister effect and other specific ion effects offer wide flexibility beyond electrostatics alone. The combination of chemical bonding as well as hydration/hydrophobic interactions and van der Waals forces offers a remarkably diverse range of materials with wide-ranging properties, and hence applications to specific ion separation.[2,3]

THE BACKGROUND TO HYDROGELS

By definition a hydrogel is a polymeric material which swells significantly when immersed in aqueous solution. These polymers can be covalently or ionically crosslinked to control this swelling.[4] Hydrogels typically have water contents over 80% (by wt). Non-crosslinked polyampholytic compounds can show gel-like properties due to ionic cross-links that are formed by one molecule with other polymer chains, which induces enhanced plasticity and higher yield stress. These compounds will completely dissolve in aqueous concentrated salt solutions (e.g. 4 M NaCl) at high temperatures (> 50 °C), typically within days.[1] This has been assumed to be because the electrostatic binding between the numerous oppositely charged groups, holding the matrix together, is weakened by the presence of an excess of oppositely charged ions in an immersing solution and also with increasing the temperature. Prima facie this is not so. Because even without salt the effective Debye length is so small that electrostatic forces will be screened. With 4 M salt they are irrelevant. For many applications it is important to introduce controlled chemical cross-linking and swelling. The current study takes this issue on board for several hydrogels and, for comparison, a typical non-swelling polyzwitterionic resin.

Polyampholytes have already been used as additives in papermaking to improve strength.[5] They are being considered for some biological replacement applications[6] and for controlled drug release.[7] Recently, polyampholytic hydrogels have also been employed for the efficient removal of heavy metal ions from contaminated wastewater.[8] These applications are facilitated by the highly accessible open structure of these swollen polymers in water.[9] It was shown first by Chandrasekar and Pashley[10] that commercial strong acid and strong base mixed resins might be used to advantage for desalting water; the exhausted resin being regenerated by a process involving ammonium bicarbonate (AB) rather than acid and base washing.[10] See also other papers in this volume for detailed application.

Polyampholytic latices have small particle sizes that are similar to the polyampholytic resins. Typically, they contain weak acid and base carboxylic and tertiary amine groups. They have been recently synthesised and they show high ability to adsorb different divalent metal ions such as Ca(II), Cd(II), Cu(II), Mg(II), Ni(II), Pb(II) and Zn(II).[11] Another study has shown that these latices can exchange both cations and anions.[12] Similar ionic exchange properties are found in protein molecules as well as in biomolecules, which have both cationic and anionic sites to adsorb multivalent ions of either sign.[13-15] There are a variety of factors that affect ion adsorption properties of polyampholytic ion exchange resins; including pH of the electrolyte solution[16,17], temperature[18,19], ionic strength of the electrolyte solutions[20,21], the ratio of acid to basic groups and the affinities of specific counter ions.[22-24]

The polyampholytic latices are zwitterionic, and usually show a pH where they have net zero charge (pzc), or an isoelectric point (IEP). In order to assign an effective IEP of such latices that throws light on the behaviour of adsorption sites present on the particles, surface charge measurements and ionization models can be used.[25-27]

Hydrogel based compounds synthesised with 2-acrylamido-2-methylpropane sulfonic acid (AMPS) have attracted extensive attention due to their strong ionizable sulfonate group. AMPS dissociates completely over a wide pH range, so the hydrogels derived from it show pH independent swelling properties.[28, 29] Hydrogels containing amide and sulfonic groups, can form coordinate bonds with metal ions for water purification.[30] Ayman et al.[31] prepared acrylamide (AM) and AMPS based hydrogel. They found that these hydrogels can take up several heavy metal ions, such as Cu (II), Cd (II) and Fe (III) from aqueous solutions. The recovery of hydrogels was also produced by immersion in acidic media. Yan et al.[32] synthesised a series of homogeneous cross-linked uncharged and sulfonated hydrogel membranes using poly(ethylene glycol diacrylate) (PEGDA) copolymerized with AMPS. Different concentrations of sodium chloride solutions were used to determine the

uptake of ion content (Na^+ and Cl^-) based on charge density measurements on the membranes.

A NOVEL DEVELOPMENT IN HYDROGELS

All the studies mentioned above dealt only with the physical properties of the final hydrogels without considering a way to regenerate them. Therefore, interest has focused on finding novel sorbents with high adsorption capacities, fast adsorption/desorption rate, and easy separation and regeneration. The present work offers a novel regeneration process for depleted resins, using ammonium bicarbonate, that can regenerate the resins. Since it can also be readily decomposed into ammonia and carbon dioxide gases, this offers a reusable compound for the adsorption/desorption regeneration process. That is, without the need to use acid and base regeneration.

This property is unique to ammonium carbonate and is the basis of our desalination process. The work is motivated by a novel patented ion-exchange water desalination process with PCT application number: PCT/AU2019/P110031.[33]

The main subject of the patent is a cross-linked organic polymer containing mixed beads of both positively and negatively charged ions at the nano scale. By integrating the positively and negatively charged ions on the one polymer, the ions are much closer together, at a nano scale, which substantially improves their absorption capacity.

The innovation relates to the application of a new, simple and low-cost method for continuously removing salt from the resin (i.e. resin regeneration process). The use of an environmentally inert ammonium bicarbonate (AB) wash avoids the requirement for the depletion of expensive chemical reagents (i.e. acids and bases) or for heat required for resin regeneration. These are major advances.

These two innovations open up the possibility for other high-value applications of the technology, in addition to desalination applications, such as selective solute removal from contaminated water, for example, heavy metal ions and PFAS ions.

MATERIALS & METHODS

3-(methacryloylamino) propyl-trimethylammonium chloride (MPTC) and 2-acrylamido-2-methylpropane sulfonic salt solution (AMPS) were used as strong acid cationic and strong base anionic monomers, respectively. Alpha-ketoglutaric acid was used as the initiator. Ethylene glycol dimethacrylate (EGDMA), and 25% glutaraldehyde (GA) were used during the synthesis as the chemical crosslinking agent. To synthesise the zwitterionic polymer compounds N'N'-methylene bisacrylamide, PEG 400 and 1,3-propane sultone were used as monomers.

Several salts: 98% sodium chloride, 99% sodium sulphate, magnesium chloride (AR grade) and magnesium sulphate (AR grade) were used to study swelling and conductivity properties. All chemicals were used as purchased from Sigma-Aldrich, Australia without further purification. Electrical conductivity values of all the solutions were measured using a EUTECH CON 700 Conductivity Bench. A Zetasizer Nano instrument (Malvern Instruments Ltd.) was used to study the size distribution of the dry ground resin particles and the zeta-potentials of these particles dispersed in various electrolyte solutions. The chemical structures of the monomers used to produce the polyampholytic hydrogels are show in Figure 1.

The synthesised resins were characterised by micro-elemental analysis using Vario MICRO cube elemental analysers (Elementar Analysensysteme GmbH, Germany) and by Fourier-transform Infrared spectroscopy (FTIR) in KBr from 400–4000 cm^{-1}, using a Jasco FT/IR-6000 FTIR Spectrometer.

Polyampholyte Hydrogel Synthesis Method

Polyampholyte hydrogels were synthesized using a one-step copolymerization process. A mixed aqueous solution (monomers and initiator) was prepared and poured into the several reaction cells. It was found that glass cells with 0.5 cm tube diameter and 9.5 cm long were suitable for the polymerisation reaction. The fraction of chemicals in the reaction have been studied in different ratios, as shown in Table 1. They were each irradiated with 365 nm UV light, 8 Watts, (John Morris Scientific Pty Ltd.) for 15 hr at a distance of 5 cm. After polymerization, the product was immersed in a large amount of water for 1 week to reach equilibrium and to wash away the residual, unreacted chemicals. Parameters were varied for the polymerization reaction; for example, the time for irradiation, distance between reaction cell and UV light source, as well as the ratio of chemical reactants and crosslinking agents. In the crosslinking processes, the product was treated by reflux reaction with glutaraldehyde and by UV copolymerization with added EGDMA.

For our study, several reaction cells were designed and developed for the polymerization reaction, as shown in Figure 2. Firstly, a rectangular metal sheet made from

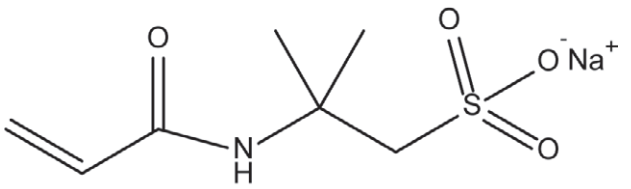

AMPS*

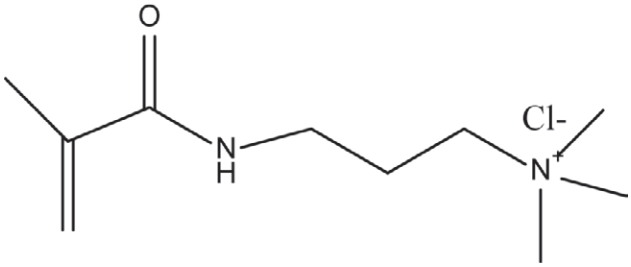

MPTC**

(a) Monomers for synthesis of polyampholytic hydrogel
*2-Acrylamido-2-methyl-1-propanesulfonic acid sodium salt solution
**3-(methacryloylamino) propyl-trimethylammonium chloride

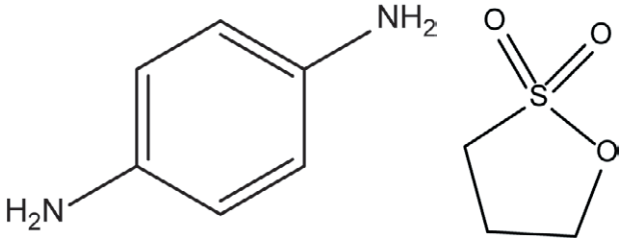

p-Phenylene diamine 1,3-propane sultone
(b) Reactants for synthesis of zwitterionic resins

Figure 1. Chemical structures of the monomers used to produce: (a) the polyampholytic hydrogel and (b) the zwitterionic resins.

Table 1. The ratio of monomers (molar ratio), initiator and crosslinking agent used in various synthesis reactions. In this table the initiator concentrations 1-4 refer to the ratio of monomers and 0.25% mole of initiator (i.e. for '1', and with '4' corresponding to 1%).

AMPS	MPTC	2-oxoglutaric acid	EGDMA
1	1	1	-
1	1	4	-
1	2	1	-
2	1	1	-
1	1	1	1
1	1	4	2
1	1	1	2
1	1	4	2

tin and an upper plate glass cover was used, as recommended in the literature. However, the results showed that tin metal also reacts with the chemicals. Therefore, an all-glass rectangular reaction cell was developed. Nevertheless, atmospheric gases still diffused into the mixture during UV polymerisation and affected the reaction. Oxygen gas is known to react with radicals and can change the polymerisation reaction. An array of glass tubes with closed-off ends to reduce gas inlet diffusion was therefore used and this was found to be the most suitable reaction cell for the UV polymerisation reaction.

Zwitterionic Resin Synthesis Method

The "zwitterionic" polymer shown in Figure 3 was synthesised using 5 mmol of p-phenylene diamine (0.54 g) in 20 mL of dimethylformamide (DMF) together with

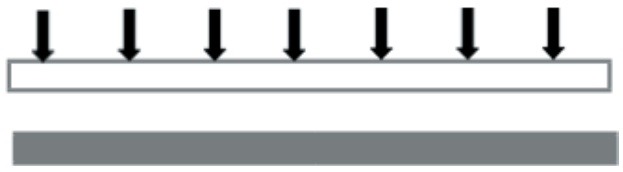

a) Rectangular metal sheet

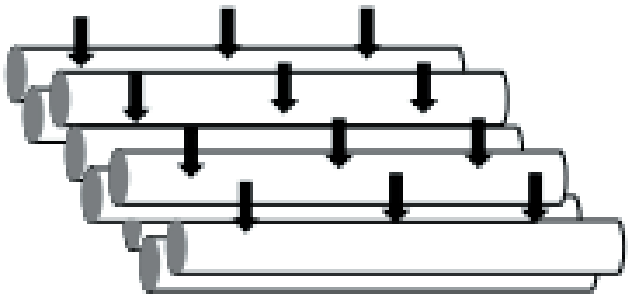

b) Array of glass tubes

Figure 2. This schematic figure shows the different types of reaction cells that were designed and developed in the study. (a) rectangular metal and glass sheet with the reactive monomer liquid in the space between (b) an array of glass tubes with closed-off ends, with the reactive monomer liquid enclosed in the tubes.

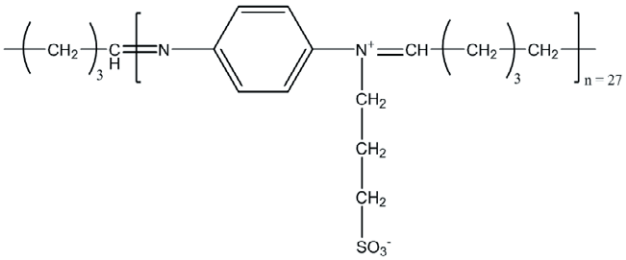

Figure 3. The chemical structure of the pseudo zwitterionic polymer studied here, as quoted in[34].

5 mmol of glutaraldehyde (0.47 mL) in 20 mL of DMF, prepared separately in a different beaker. The solutions were mixed and refluxed at 80 °C for 1 hr. Then, 15 mmol of 1,3-propane sultone (1.32 mL) in 10 mL of DMF was added to the reaction and refluxed at 70 °C for 3 hr. The final product was washed several times with hot water to remove residual chemicals. The product was found to have a black gel-like form. The reason behind the colour is unclear, perhaps due to absorption of all light by the product, because of the aromatic ring of the product which has HOMO-LUMO energy gaps that absorbs light in the visible wavelengths (400–700 nm), causing the black appearance. From the molecular diagram it is clear that the C3 chain connecting the sulphonate to the imine N cation is not of sufficient length to allow close contact between the oppositely charged groups. This supports the view that this is indeed a zwitterionic polymer. However, it should also be realised that this polymer is not actually a pure zwitterionic polymer in any case because of the presence of a second imine group, which will readily become protonated in aqueous solutions below pH 10. This is due to the pK_a value of the imine group, which is around 10. In typical aqueous solutions this polymer will therefore actually be a 2+/1- ionic polymer and on dissolution will also act to increase the solution pH.

Powdered Resin Samples Preparation

The products of the various polyampholyte hydrogels and the zwitterionic resin compound were allowed to completely dry in a fume cupboard at room temperature. A mortar and pestle dry-grinding system was used to produce finely ground particle samples of each dry resin. The resins were all in the water-washed state, prior to drying, to maintain maximum electrostatic binding of the polymer matrix and hence solid rigidity, to enhance dry-grinding efficiency.

FT-IR Results

The FT-IR spectra was obtained for both resin samples and are given in Figure 4. Broad absorptions

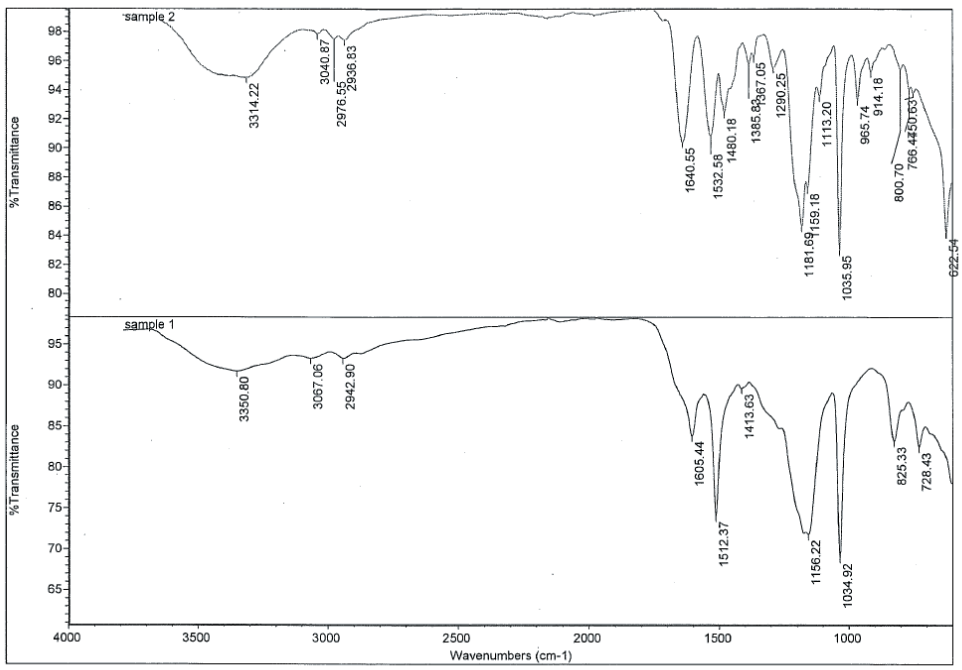

Figure 4. FT-IR spectra for zwitterionic resin (Sample 1) and hydrogel resin (Sample 2).

around 3400 cm^{-1} indicate free O-H. The absorptions at 2900–3000 cm^{-1} are due to the C-H asymmetric stretch. The carboxybetaine was characterised by absorptions at 1181 cm^{-1} (C-CO-C) stretched band in Sample 2 for the hydrogel resin. Also 1640 cm^{-1} indicates C=O stretching in this sample. The aromatic ring stretching absorptions (C=C and C=N) for the Sample 1 (zwitterionic resin) can be seen in the range 1413-1605 cm^{-1}. The characteristic absorption for sulfonate groups present in both resins, appear at 1034 cm^{-1}, 1035 cm^{-1} and 1640 cm^{-1}, which are highly intense.[34]

RESULTS AND CHARACTERISATION

Several polyampholytic hydrogels, produced without chemical crosslinking, were made from a ratio of 1:1 (AMPS: MPTC) with initiator. These resins readily produced a clear film on drying but were also easily dispersed in water, losing their structure, as illustrated in the example in Figure 5.

Several polyampholytic hydrogels were formed with chemical crosslinking using EGDMA and GA. These were added to the polymerisation reaction mixture to reduce the aqueous swelling properties of the hydrogels. An example of a suitable ratio of polyampholyte hydrogel with crosslinking agent is 1 : 1 : 2 : 1 (AMPS : MPTC : EGDMA : initiator). Note that in this scheme '1' for the initiator refers to a level of 0.25 %. The polymerisation results obtained show that chemically crosslinked hydrogels prevent the release of the constituent polymer chains when immersed in water, while still allowing substantial aqueous uptake or swelling.

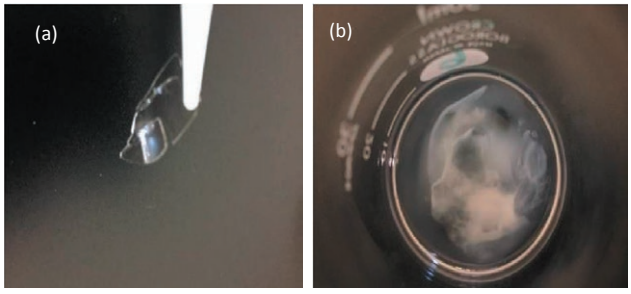

Figure 5. These photographs illustrate that the polyamplolytic hydrogels formed without the use of chemical crosslinking agents formed clear plastic films when dry (a) and then when equilibrated with excess water (b), the polymer chains completely dispersed.

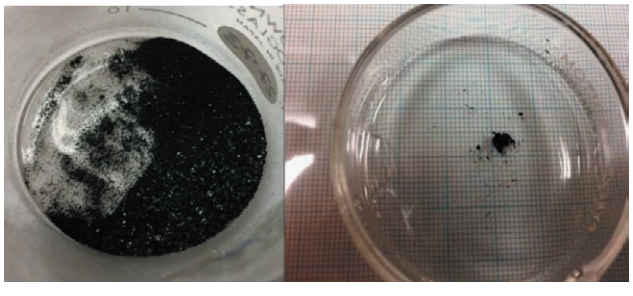

Figure 6. The product of the zwitterionic synthesis dry product (on left) and the after 24 hours water-swelling (on right).

By comparison, the zwitterionic polymer containing similar charged groups, that is sulphonate and quaternary ammonium groups, produced a black powder which showed little or no swelling in water, as illustrated in Figure 6. The results of a swelling study showed that both zwitterionic polymer products did not show any significant swelling in either pure water or a range of electrolyte solutions.

These observations are consistent with the extent of chemical cross-linking expected in the final product and the hydrophobicity of these polymers. A qualitative evaluation of the relative hydrophobicity of the powdered resin samples can be achieved using a simple 'water float test'. Small amounts of both the cross-linked hydrogel (dry ground into powder) and the zwitterionic resin (dry ground) powder were carefully sprinkled onto the surface of water. These observations indicate that the zwitterionic resin is much more hydrophobic, which is also consistent with its lack of swelling when immersed in water. By comparison, the hydrogel resin both swells substantially in water and is water wet, and so readily enters the aqueous phase.

The finely dry-ground resin samples were dispersed by simple stirring in water and 1mM NaCl solution at room temperature and the particle size distributions were measured using a Malvern Zetasizer light scattering instrument (model ZS). In addition, the zeta potentials of the dispersed particles of each resin were measured in 1 mM NaCl solution, at room temperature. Typical results obtained are shown in Table 2.

The elemental analysis for two polymer resins show similar results for N, H and S atoms in their chemical structures, except that the zwitterionic resin had a higher level of carbon compared to the hydrogel resin. This is because the zwitterionic sample comprises a higher level of carbon in its aromatic rings. These results are averaged based on two analyses for each sample and the average values are given in Table 3.

A summary of typical results obtained using the two powdered resin samples dispersed in 1mM NaCl in different pH values at room temperature is given in Table 2. The results indicate that the polyampholytic particles are typically clumped together in water. This cannot be due to electrostatic binding between the positive and negative charged groups on facing polymer particles

Table 2. Particle size distribution (radius in nm) and zeta potential (mV) of the two polymer resins in different pH solutions. Note that all the samples were prepared in 1mM NaCl solution and pH adjusted using 0.1 M NaOH and 0.1 M HCl solution.

pH	Size (r / nm)		Zeta potential (mV)	
	Hydrogel	Zwitterionic	Hydrogel	Zwitterionic
3	915	3849	-8.79	-5.65
6	1194	14700	-9	-19.2
9	9142	9180	-15.9	-17.5

Table 3. Total elemental analysis of two synthesised polymer resins.

	%C	%H	%N	%S
Zwitterionic	53.44	5.81	8.98	5.40
Hydrogel	43.92	8.60	8.69	6.24

alone and must involve some specific hydration effects. It is known from extensive work on microemulsions, force measurements between surfactant bilayers and NMR that the quaternary ammonium group has two tightly bound water molecules of hydration. Bromide, chloride, iodide and fluoride all bind strongly, and the ion pair is effectively neutral. These anions displace divalent sulphate ions. On the other hand sodium binds very strongly to the sulphonate group whereas other cations do not. So we expect that addition of NaCl to the dispersion will weaken this inter-polymer-polymer binding, due to reduced hydration and polymer bridging forces. Polymer swelling could not cause the large particle size differences seen in Table 2.

Addition of salt should increase the swollen size of individual particles, as reported by Kudaibergenov and Ciferri, 2013.[9] But as for above the effect can be expected to be ion specific. Osmotic pressure effects caused by the 1 mM NaCl solution will only be about 0.05 atm, which is too small to cause any significant dewatering of the resin particles. The standard argument for the overall negative zeta potential of the hydrogel particles in 1 mM NaCl solution, shown in Table 2, supposes that this is expected for polymers with similar densities of positive and negative charged groups because the Na^+ ion is more strongly hydrated than the Cl^- ion and so is less readily adsorbed onto the particle surface.

Biological cells and the common, natural inorganic particles, such as quartz and clays, are negatively charged for the same reason. However the classical theory is erroneous but usually reasonable at very low salt.[35-37] We persist with the classical colloid science approach keeping in mind that it can be misleading.

The zwitterionic resin particles were found to have a lower (in magnitude) negative zeta potential, see Table 2. This is consistent with the additional imine group present on this zwitterionic molecule (see Figure 3). It will protonate, depending on pH, and so should reduce the overall negative potential.

A comparison of water swelling of the cross-linked (1:1:2:1 sample) polyampholytic hydrogel in pure water and in various 0.2 M electrolyte solutions was studied visually. The solutions were equilibrated for 24 hr at room temperature. The results showed that water content was typically found to be around 90% for chemically cross-linked gels immersed in a range of electrolyte solutions. These swelling results indicate that pure water produced the greatest swelling and that all of the salts reduced the swelling to a similar extent relative to pure water. And that there appeared to be no significant specific ion effects on the degree of swelling, even when the osmotic pressure of the solution was increased, say for $MgCl_2$ and Na_2SO_4 solutions. At least the differences between the monovalent sodium and divalent magnesium are not significant. (That need not be so for other cations like nickel, or anions in the Hofmeister series that have not yet been tested.)

CONDUCTIVITY VALUES

Bulk electrical conductivities of the swollen gels were measured and compared with bulk solution values for: water, NaCl and $MgSO_4$ solutions, over a 3-day period. These results, given in Tables 4-7, showed that the conductivity was reduced in the swollen gels by around 10 percent for each solution. In other words, there appeared to be no specific ion effects and the gels with a high-water content, gave electrical conductivities, even the two different electrolytes, roughly consistent with their water volume fraction. These results reflect the high-water content of these hydrogels.

That these single polymer resins can make useful ion exchange resins is clearly demonstrated by their ability to absorb NaCl from solution, as shown by the results given in Table 4. The absorption trend shows that the zwitterionic resin offered a significant absorption capacity from 1 to 28 mmol/g for NaCl solution from 0.1 M to 0.3 M, respectively. While the hydrogel resin absorption capacity increased from 4 to 9 mmol/g for the two NaCl solutions.

These results compare favourably with the most efficient commercially available, mixed-bed, strong acid and strong base resin systems, which absorb NaCl from aqueous solution at a level typically of about 2.5 mmol/g.

Table 4. Electrical conductivity results for the hydrogel polymer dry sample (weight 0.05 g) in 50 mL NaCl solution (with an average experimental error of about ± 0.05 mS/cm).

Concentration (M)	conductivity (mS/cm)	
	Before	after
0.2	19.1	18.7
0.25	23.2	22.8
0.3	27.3	26.4
0.4	34.9	33.7
0.5	41.3	40.5

Table 5. Electrical conductivity results for the zwitterionic polymer sample (weight 0.05 g) in 50 mL NaCl solution (with experimental error ± 0.05 mS/cm).

Concentration (M)	conductivity (mS/cm)	
	Before	after
0.1	10.4	10.3
0.3	27.5	24.8
0.5	35.4	34.1

Table 6. Electrical conductivity results for 0.2 M salt solutions (Conductivity in solution) with experimental error ± 0.05 mS/cm.

	Conductivity (mS/cm)			
	day 0	day 1	day 2	day 3
NaCl	18.9	18.7	18.6	18.4
$MgSO_4$	15.9	15.9	15.8	15.7
DI water	0.002	0.013	0.04	0.05

Table 7. Electrical conductivity results for 0.2 M salt solutions (Conductivity in gel) with experimental error ± 0.05 mS/cm.

	Conductivity (mS/cm)			
	day 0	day 1	day 2	day 3
NaCl		15.6	16.7	16.3
$MgSO_4$		13.5	13.7	14.0
DI water		0.04	0.04	0.06

ADDITIONAL COMMENTS

In the course of this work it was realised that the 'zwitterionic' polymeric resin compounds containing amide groups reported by Tarannum and Singh[34] have been erroneously defined as zwitterionic. In fact, they are anionic resins only. This is because the nitrogen atom in the amide group will not be protonated under normal solution conditions. It can actually be protonated only in very strong acid solution. That is, the zwitterionic structure reported in the literature can only be formed in very strong acid solution. For all practical uses the resin acts as an anionic, sulphonated, resin. The pK_a of the conjugate acid nitrogen in an amide group present in the hydrogel resin, is about -0.5, which means that an acid with 3 M concentration is required to protonate the amide group in this resin to form a zwitterionic compound. Adsorption isotherms for the zwitterionic resins showed a maximum NaCl adsorption of about 28 mmol/g (dry wt.), while for the same concentration of NaCl, hydrogel resins had adsorption levels of about 9 mmol/g (dry wt.). In addition, as also mentioned earlier, the other zwitterionic compound, used in this work, will have a protonated imine group in most aqueous solutions, in addition to the zwitterionic (sulphate/quaternary ammonium) group. Hence, this compound is also not a 'true' zwitterionic polymer.

Table 8. The resin absorption capacities (+/- 0.5 mmol/g) estimated from the measured absorption from aqueous NaCl solutions (i.e. 0.1 and 0.3 M).

Resin	mmol/g of absorption	
	0.1M	0.3M
Hydrogel	4.3	9.3
Zwitterionic	1.0	28.1

This work was designed to extend the efficiency of a novel patented ion-exchange water desalination process. [33] In this patent, ammonium bicarbonate (AB) solution has been used to regenerate depleted mixed bed ion exchange resins for subsequent use in desalinating salt solutions. A bubble column evaporator (BCE) can then be used to decompose the AB product solution into drinking water, ammonia (NH_3) and carbon dioxide (CO_2) gases; this is the subject of another work published in this special issue of Substantia. The gases can then be collected into a cool aqueous solution for reuse in further regenerating the resin.

A commercial-in-confidence report on this patent was prepared by the international engineering company *Arcadis* for *Breakthrough Water Technology* on behalf of a major International Gold Mining Group. The results in this report show that this method is likely to be up to 30% more efficient and less energy consuming than current reverse osmosis (RO) and ion-exchange desalination processes. We will be working on this method to scale up the technique for commercial usage. This project aims to establish in a larger scale pilot unit for further testing, evaluation and development.

CONCLUSIONS

A new UV method to produce polyampholytic hydrogels was developed. It was found that it is very difficult to chemically cross-link the gels to reduce swelling in water. Interestingly, the gels have a high-water content and their electrical conductivities, even in different electrolytes, are consistent with their water volume fraction. Strong acid and strong base polyampholytic gels have some unusual chemical and physical properties. We also found that some zwitterionic resins reported in the literature have been erroneously classified. The results are encouraging. There is clear advantage for desalination applications for a resin with cationic and anionic ion exchange sites angstroms apart on the same polymer. By comparison, with conventional mixed cationic and anionic beads, presently available and evaluated and proposed for desalination, as is outlined in this volume, the oppositely charged groups can be millimeters apart. While we have seen in earlier papers that the mixed cationic and anionic resins are much more efficient than reverse osmosis, the new structures would be more efficient still. Some further study to confirm the robustness of the regeneration process is necessary to confirm its expected successful availability as an efficient desalination system.

A Final Comment. Because of the very large variation in specific ion binding capacities of both the quaternary ammonium and sulphonate moieties of the gel it might be expected, that combined with the ammonium bicarbonate process, it might well have applications beyond ordinary desalination per se.

There are very major problems with natural drinking water contamination with fluoride. and the perennial problem of nitrate and phosphate ions in runoff water in agriculture.

We hope to tackle these issues subsequently.

ACKNOWLEDGMENTS

The authors would like to thank Dr. Mokhlesur Rahman for his support and suggestions on the synthesising procedures. The authors also would like to thank Dr. Remi Rouquette of Macquarie University for the elemental analysis and the FTIR analysis.

REFERENCES

1. T.L. Sun, T. Kurokawa, S. Kuroda, A.B. Ihsan, T. Akasaki, K. Sato, M.A. Haque, T. Nakajima, J.P. Gong, Physical hydrogels composed of polyampholytes demonstrate high toughness and viscoelasticity, *Nat Mater*, **2013**, 12(10), 932-7.
2. L. Su, S. Khan, J. Fan, Y.-N. Lin, H. Wang, T.P. Gustafson, F. Zhang, K.L. Wooley, Functional sugar-based polymers and nanostructures comprised of degradable poly(d-glucose carbonate)s, *Poly. Chem.*, **2017**, 8(10), 1699-1707.
3. D. Tatini, F. Sarri, P. Maltoni, M. Ambrosi, E. Carretti, B.W. Ninham, P. Lo Nostro, Specific ion effects in polysaccharide dispersions, *Carbohydr. Polym.*, **2017**, 173, 344-352.
4. C.A. Finch, Polymers in aqueous media: Performance through association. Advances in Chemistry Series No. 223 Edited by J. E. Glass, ACS, Washington, *Polym. Int.*, **1991**, 25(1), 61-62.
5. M.A. Hubbe, O.J. Rojas, D.S. Argyropoulos, Y. Wang, J. Song, N. Sulić, T. Sezaki, Charge and the dry-strength performance of polyampholytes: Part 2. Colloidal effects, *Colloids Surf., A:Physiochem. Eng. Aspects*, **2007**, 301(1), 23-32.
6. A.B. N. Alepee, M. Daneshian, B. De Wever, E. Fritsche, A. Goldberg, J. Hansmann, T. Hartung, J. Haycock, H.T. Hogberg, t4 workshop report: State-of-the-art of 3D cultures (organs-on-a-chip) in safety testing and pathophysiology, *Altex*, **2014**, 31(4), 441-477.
7. J. H. Chen, C. C. Tsai, Y.Z. Kehr, L. Horng, K. Chang, L. Kuo, *An Experimental Study of Drag Reduction in a Pipe with Superhydrophobic Coating at Moderate Reynolds Numbers*, in *ICEM 14 – 14th International Conference on Experimental Mechanics*. EPJ Web of Conferences Poitiers, France, **2010**.
8. C. Zhang, C. Lai, G. Zeng, D. Huang, C. Yang, Y. Wang, Y. Zhou, M. Cheng, Efficacy of carbonaceous nanocomposites for sorbing ionizable antibiotic sulfamethazine from aqueous solution, *Water Res.*, **2016**, 95, 103-112.
9. S.E. Kudaibergenov, A. Ciferri, Natural and Synthetic Polyampholytes, 2, *Macromol. Rapid Commun.*, **2007**, 28(20), 1969-1986.
10. N.P.G.N. Chandrasekara, R.M. Pashley, A model for ion-exchange behaviour of polyampholytic resins: Using polystyrene polyampholytic latex, *Colloids Surf., A:Physiochem. Eng. Aspects*, **2017**, 516, 39-47.
11. D.S. Eldridge, R.J. Crawford, I.H. Harding, The role of metal ion-ligand interactions during divalent metal ion adsorption, *J. Colloid Interface Sci.*, **2015**, 454, 20-26.
12. A. Homola, R.O. James, Preparation and characterization of amphoteric polystyrene latices, *J. Colloid Interface Sci.*, **1977**, 59(1), 123-134.
13. E. Ruckenstein, M. Manciu, *Stability of dispersions*, in *Nanodispersions: Interactions, Stability, and*

Dynamics, Springer New York: New York, NY, **2010**, 201-324.
14. S. Salgin, U. Salgin, S. Bahadir, Zeta potentials and isoelectric points of biomolecules: The effects of ion types and ionic strengths, *Int. J. Electrochem. Sci.*, **2012**, 7(12), 12404-12414.
15. S. Perez-Amodio, P. Holownia, C.L. Davey, C.P. Price, Effects of the ionic environment, charge, and particle surface chemistry for enhancing a latex homogeneous immunoassay of C-reactive protein, *Anal. Chem.*, **2001**, 73(14), 3417-3425.
16. I.H. Harding, T.W. Healy, Adsorption of aqueous cadmium(II) on amphoteric latex colloids: I. General kinetics and thermodynamics, *J. Colloid Interface Sci.*, **1985**, 107(2), 362-370.
17. I.H. Harding, T.W. Healy, Adsorption of aqueous cadmium(II) on amphoteric latex colloids: II. Isoelectric point effects, *J. Colloid Interface Sci.*, **1985**, 107(2), 371-381.
18. M. Chanda, S.A. Pillay, A. Sarkar, J.M. Modak, A thermally regenerable composite sorbent of crosslinked poly(acrylic acid) and ethoxylated polyethyleneimine for water desalination by Sirotherm process, *J. Appl. Polym. Sci.*, **2009**, 111(6), 2741-2750.
19. N.P.G.N. Chandrasekara, R.M. Pashley, Study of a new process for the efficient regeneration of ion exchange resins, *Desalination*, **2015**, 357, 131-139.
20. B.A. Bolto, R. McNeill, A.S. MacPherson, R. Siudak, D.E. Weiss, D. Willis, An Ion-Exchange Process with Thermal Regeneration. VI. Factors Influencing the Titration Curve Shape of Weak Electrolyte Resins, *Australian J. Chem.*, **1968**, 21(11), 2703-2710.
21. D.E. Weiss, B.A. Bolto, R. McNeill, A.S. MacPherson, R. Siudak, E.A. Swinton, D. Willis, An Ion-Exchange Process with Thermal Regeneration. IV. Equilibria In A Mixed Bed of Weak-Electrolyte Resins, *Australian J. Chem.*, **1966**, 19(5), 765-789.
22. D. Weiss, B. Bolto, R. McNeill, A. MacPherson, R. Siudak, E. Swinton, D. Willis, An ion-exchange process with thermal regeneration. II. Properties of weakly basic resins, *Australian J. Chem.*, **1966**, 19(4), 561-587.
23. D.E. Weiss, B.A. Bolto, R. McNeill, A.S. MacPherson, R. Siudak, E.A. Swinton, D. Willis, An ION-Exchange Process with Thermal Regeneration. III. Properties of Weakly Acidic ION-Exchange Resins, *Australian J. Chem.*, **1966**, 19(4), 589-608.
24. V.K. Koul, A.K. Gupta, Uptake of sodium chloride by mixture of weakly acidic and weakly basic ion exchange resins: equilibrium and kinetic studies, *Chem. Eng. Sci.*, **2004**, 59(7), 1423-1435.
25. J.T. Duniec, J.N. Israelachvili, B.W. Ninham, R.M. Pashley, S.W. Thorne, An ion-exchange model for thylakoid stacking in chloroplasts, *FEBS Letters*, **1981**, 129(2), 193-196.
26. R.M. Pashley, DLVO and hydration forces between mica surfaces in Li^+, Na^+, K^+, and Cs^+ electrolyte solutions: A correlation of double-layer and hydration forces with surface cation exchange properties, *J. Colloid Interface Sci.*, **1981**, 83(2), 531-546.
27. F. Makavipour, R.M. Pashley, A study of ion adsorption onto surface functionalized silica particles, *Chem. Eng. J.*, **2015**, 262, 119-124.
28. S. Durmaz, O. Okay, Acrylamide/2-acrylamido-2-methylpropane sulfonic acid sodium salt-based hydrogels: synthesis and characterization, *Polym.*, **2000**, 41(10), 3693-3704.
29. L. Zhang, A. Eisenberg, Formation of crew-cut aggregates of various morphologies from amphiphilic block copolymers in solution, *Polym. Adv. Technol.s*, **1998**, 9(10-11), 677-699.
30. A. El-Hag Ali, H.A. Shawky, H.A. Abd El Rehim, E.A. Hegazy, Synthesis and characterization of PVP/AAc copolymer hydrogel and its applications in the removal of heavy metals from aqueous solution, *Europ. Polym. J.*, **2003**, 39(12), 2337-2344.
31. A.M. Atta, H.S. Ismail, A.M. Elsaaed, Application of anionic acrylamide-based hydrogels in the removal of heavy metals from waste water, *J. Appl. Polym. Sci.*, **2012**, 123(4), 2500-2510.
32. N. Yan, D.R. Paul, B.D. Freeman, Water and ion sorption in a series of cross-linked AMPS/PEGDA hydrogel membranes, *Polym.*, **2018**, 146, 196-208.
33. R.M. Pashley, M. Taseidifar , T. Gettongsong, *Resin for desalination and process of regeneration*, PCT, Google Patents, **2019**.
34. N. Tarannum, M. Singh, Synthesis and characterization of zwitterionic organogels based on Schiff base chemistry, *J. Appl. Polym. Sci.*, **2010**, 118(5), 2821-2832.
35. B.W. Ninham, R.M. Pashley, P. Lo Nostro, Surface forces: Changing concepts and complexity with dissolved gas, bubbles, salt and heat, *Curr. Opin. Colloid Interface Sci.*, **2017**, 27, 25-32.
36. F. Cugia, M. Monduzzi, B.W. Ninham, A. Salis, Interplay of ion specificity, pH and buffers: insights from electrophoretic mobility and pH measurements of lysozyme solutions, *RSC Advances*, **2013**, 3(17), 5882-5888.
37. A. Salis, L. Cappai, C. Carucci, D.F. Parsons, M. Monduzzi, Specific Buffer Effects on the Intermolecular Interactions among Protein Molecules at Physiological pH, *J. Phy. Chem. Lett.*, **2020**, 11(16), 6805-6811.

Substantia
An International Journal of the History of Chemistry

Firenze University Press
www.fupress.com/substantia

OPEN ACCESS

Citation: M. Shahid, M. Taseidifar, R.M. Pashley (2020) A Study of the Bubble Column Evaporator Method for Improved Ammonium Bicarbonate Decomposition in Aqueous Solutions: Desalination and Other Techniques. *Substantia* 4(2) Suppl.: 49-55. doi: 10.36253/Substantia-833

Data Availability Statement: All relevant data are within the paper and its Supporting Information files.

Competing Interests: The Author(s) declare(s) no conflict of interest.

A Study of the Bubble Column Evaporator Method for Improved Ammonium Bicarbonate Decomposition in Aqueous Solutions: Desalination and Other Techniques

Muhammad Shahid, Mojtaba Taseidifar, Richard M. Pashley*

School of Science, University of New South Wales, Northcott Drive, Canberra, Australia
*Corresponding author: r.pashley@adfa.edu.au

Abstract. A bubble column was used to study the improved thermal decomposition of NH_4HCO_3 in aqueous solution using a continuous flow of hot gas bubbles of optimum sizes (1-3 mm) produced via controlled bubble coalescence to maintain bubble size. The rapid transfer of heat from small, hot (dry) gas bubbles to the surrounding water, i.e. into a transient hot surface layer, was used as an effective and energy efficient method of decomposing ammonium bicarbonate in aqueous solution. It is shown that the continuous flow of (dry) hot gases, even at 275 °C, only heat the aqueous solution in the bubble column to about 57 °C, at which it was also established that NH_4HCO_3 has a negligible decomposition rate even with long-term exposure to this solution temperature. Hence, the effects observed appeared to be caused entirely by the effective collisions between the hot gas bubbles and the solute. It was also established that the use of high gas inlet temperatures can reduce the thermal energy requirement to only about 50% (i.e. about 575 kJ/L) of that reported in previous studies and less than 25% of solution boiling.

Keywords: non-boiling decomposition, bubble coalescence, transient collisions, ammonium bicarbonate.

1. INTRODUCTION

1.1. Significance of solute decomposition

This paper is concerned with optimising a range of applications that use water, be they desalination, sterilisation, reactions and more using a bubble column evaporator. The overarching goal of water treatment by decomposition is to remove unwanted substances or solutes from water affordably and robustly. For example, the decomposition of ammonium bicarbonate (with chemical formula NH_4HCO_3) in aqueous solution is an important and energy-intensive process in the application of forward osmosis[1] and, in the regeneration of ion-exchange resins.[2] For the latter application, the ion-exchange resins comprising carboxylic acid and tertiary amine groups for desalination

can be thermally regenerated using the BCE process at a lower energy cost than with conventional methods. More recently, Shahid et al.[3] studied that solutes, ammonium bicarbonate (NH_4HCO_3) and potassium persulphate ($K_2S_2O_8$) can be thermally decomposed in aqueous solutions using a bubble column evaporator (BCE) process at sub-boiling condition (around 45 °C). Fulks et al.[4] and Gokel[5] studied, ammonium bicarbonate decomposition in solution over the temperature range 30–85 °C. Complete decomposition into ammonia, carbon dioxide and water was observed above 60 °C. The main decomposition reaction is:

$$NH_4\,HCO_{3\,(aq)} \triangleq NH_{3\,(g)} + CO_{2\,(g)} + H_2O \quad (1)$$

The decomposition rate of this solute can be readily measured from simple electrical-conductivity measurements. The decomposition of ammonium bicarbonate using the hot-gas BCE process is examined in this study.

1.2. Significance of the bubble column evaporator (BCE)

The bubble column evaporator (BCE) offers a good illustration of the use of a gas-liquid interface to drive fundamental processes involving heat and mass transfer. Bubble columns are devices in which a gas, often dry air, is pumped through a multi-porous sinter disc to form gas bubbles which are continuously replenished and come into intimate contact with the column solution. Dry gas bubbles in the column solution may be used simply to mix the liquid phase homogenously to attain a uniform temperature distribution or to saturate dissolved gases in the column solution. Substances can also be transferred from one phase to the other, for example when liquid reaction products are stripped from a gas: both mass- and heat-transfer processes can occur simultaneously.[6]

Recently, aqueous bubble column evaporators have been used for a range of new applications. These exploit the long known, but still unexplained effect of bubble bubble coalescence inhibition that occurs systematically with many salts. The effect is both ion pair and concentration dependent. In combination with the effect are size dependent bubble rise rates and rapid water-vapour uptake into the bubbles.[3,7-9] These phenomena together offer a variety of applications. The most striking of these we have developed are in desalination. Some of a wide range of other useful applications of the BCE[10] are: a new method for the precise determination of enthalpies of vaporisation (ΔH_{vap}) of concentrated salt solutions;[7,11] evaporative cooling;[8] a new method for thermal desalination;[12-14] a novel method for sub-boiling thermal sterilization;[7,15-19] a novel method for the low-temperature thermal decomposition of different solutes in aqueous solution;[3] a new approach to aqueous solute precipitation in a controlled manner.[20] The efficient removal of heavy metal ions in an ion-specific, ion-flotation process is a specially noteworthy advance.[21] In addition, a bubble column condenser has also been designed for the production of high-quality water as condensate.[22-24]

1.3. Proposed mechanism of BCE thermal decomposition

The application of the BCE process opens up a new approach to the thermal decomposition of degradable salts in aqueous solution. The hot surface layer produced transiently on the surface of hot bubbles (see Figure 1) created in the BCE appears to play a significant role in providing high heat- and mass-transfer efficiency, since the BCE is a direct-contact evaporator.[25] Degradable chemicals exposed to this hot layer can be efficiently decomposed. In addition, gaseous products are rapidly captured by the rising bubbles, due to the internal gas/vapour rotational flow produced within the rising bubbles.

Here the effectiveness of the BCE as a method for solute decomposition was assessed and quantified. Experiments were conducted using ammonium bicar-

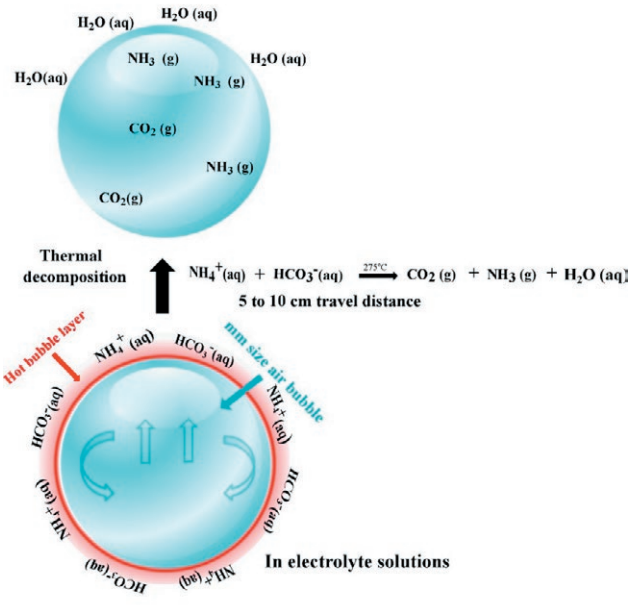

Figure 1. Schematic diagram of BCE thermal decomposition using a hot-air bubble layer. (Reprinted with permission from Ref. 3. Copyright 2015 American Chemical Society).

bonate at high inlet gas temperatures and a comparative study of energy cost was determined.

2. MATERIALS AND METHODS

2.1. Materials

Certified reagent-grade (≥ 99% purity), ammonium bicarbonate (NH_4HCO_3) was supplied by May & Baker Ltd and used without further purification. Aqueous solutions were prepared using deionized, ultrafiltered water (Milli-Q). At room temperature, the deionized water had a conductivity < 2.0 μS/cm and a natural equilibrium pH of 5.7. All concentrations are given in molality (m) units.

2.2.2. Electrical conductivity measurements in standard NH_4HCO_3 solutions

Ammonium bicarbonate solutions were prepared in the range: 0.5 to 2 m. Electrical conductivity values of all the solutions were measured using a Thermo Fisher Scientific (Waltham, MA, USA) conductivity meter at 25 °C.

2.3. BCE system for thermal decomposition

A high-surface-area gas/water interface was produced continuously by pumping dry gases (laboratory grade air and nitrogen separately), through a 40–100 micron pore-size glass sinter into a 120 mm diameter open-top glass column (Büchner type, Pyrex® Borosilicate, VWR) filled with 250 mL solution. The BCE apparatus used to study improved decomposition with a high-temperature gas (air) flow is shown in Figure 2. This system enables the use of inlet dry gas temperatures of more than 275 °C. The inlet air temperature was varied using a Tempco air heater (300W) with a thermocouple temperature monitor and an AC Variac electrical supply. The actual temperature of the dry gas flowing into the solution was measured at the centre of the sinter by a Tenmars thermometer (±1.5 °C) without any solution in the column. The gases (air and nitrogen) were produced by cylinder (Coregas Pty Ltd, Australia) and a BOC gas flow meter. The temperature of the column solution was also continuously monitored using a thermocouple positioned at the centre of the column solution. The air flow at temperatures of 300–600 °C, was needed to produce gas temperatures just above the glass sinter up to 275 °C, and this necessitated the use of steel and brass connectors for the downstream output from

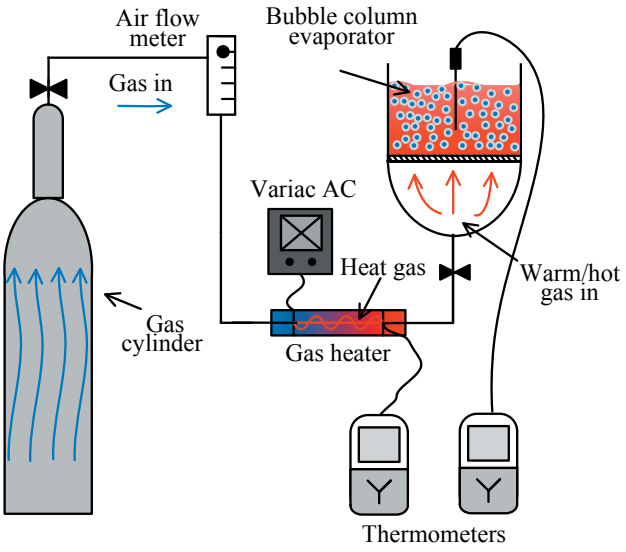

Figure 2. Schematic diagram of the bubble column evaporator (BCE) for solute decomposition. (Reprinted with permission from Ref. 3. Copyright 2015 American Chemical Society).

the heater and the use of FM Insulation Rock Wool as an insulating material.

For comparison, the effects of solution temperature on the decomposition of NH_4HCO_3 solutions was studied over time using stirred samples in a Tamson (Beiswijk, The Netherlands) heating bath at temperatures matching those of the BCE tests. During these experiments, samples were regularly taken out from the column and water bath, and their electrical conductivities and pH values measured using a EUTECH CON 700 pH 700 Bench meter (Eutech Instruments Pte Ltd.).

3. RESULTS AND DISCUSSION

3.1. Thermal decomposition of ammonium bicarbonate solutions using a BCE

3.1.1. Measurement of the electrical conductivity of NH_4HCO_3 solutions at different concentrations

As the NH_4HCO_3 salt thermally decomposed into NH_3 and CO_2 gases, the concentration of NH_4^+ and HCO_3^- reduced in the aqueous solution. So the decomposition process could be monitored through the measurement of the electrical conductivity of the samples taken from the bubble column.

The pH of aqueous solutions were also measured and found to be basic.

As hot dry bubbles enter the column, water vaporisation occurs, and water vapour passes into the bubbles.

The amount of vaporised water removed, m_v (g) after time t (sec), during a typical BCE process was estimated using the following relation:

$$m_v = r_f \frac{\frac{T_e}{T_f}}{\frac{P_e}{P_f}} t\rho_v^w \quad (2)$$

where, r_f (L/s) is the room-temperature gas flow rate, measured just prior to the heater, about 22.5 L/min in this study; T_c, T_f are the gas temperatures (in K) at the top of the column solution and at the flow meter; and P_c, P_f are the corresponding pressures at the same positions. These are the factors used to estimate the "bubble column flow rise" rate. Here ρ_v^w is the water-vapour density in g/L at the temperature of the solution at the top of the column, which was calculated from the vapour pressure of the solution using the ideal gas equation.

Using the measured electrical conductivity of the NH_4HCO_3 solutions at different time intervals, the percent decomposition of NH_4HCO_3 at time (t) in the BCE process was calculated:

$$Decomposition\% = [1 - \frac{[NH_4HCO_3]_t}{[NH_4HCO_3]_0}] \times 100 \quad (3)$$

Here $[NH_4HCO_3]_t$ is the concentration of NH_4HCO_3 at time (t) during the BCE operation and $[NH_4HCO_3]_0$ is the initial concentration of NH_4HCO_3, just before pouring the solution into the bubble columns.

3.1.2. Decomposition of NH_4HCO_3 Solutions

Some typical decomposition results (using air and nitrogen) obtained under different solution conditions are given in Figure 3. These results clearly demonstrate that the improved BCE process is much more efficient for NH_4HCO_3 decomposition than the standard method using a simple stirred heating (without BCE) at the same solution temperature, here around 57 °C. The results in Figure 3 obtained for quite different stirring conditions showed that the decomposition rates for simple heating (without the BCE) remained the same. This shows that the continuous mixing by the bubbling process in the BCE did not itself contribute to the NH_4HCO_3 decomposition. Different concentrations of NH_4HCO_3 were also studied, as shown in Table 1.

It was observed that the presence of NH_4HCO_3 at concentrations above about 0.5 m inhibited bubble coalescence to a similar degree as that at 0.17M. (This critical concentration is the same for all 1:1 salts like NaCl that exhibit the fusion inhibition phenomenon[9]) It was also observed that fine (1–3 mm diameter) bubbles were produced in the BCE process (see Figure 4a). It was clear from the photos taken during the decomposition of 2 m NH_4HCO_3 solution that, after bubbling for 10 min, the average bubble size started to increase (Figure 4b). That is expected as electrolyte concentration reduces.[9] Finally, after almost complete decomposition of NH_4HCO_3 at around 20 min, the bubble size became the same as in pure water. This provides explicit visual indication of the complete decomposition of ammonium bicarbonate in the aqueous solution (Figure 4c). The thermal decomposition of ammonium bicarbonate solutions into ammonia and carbon dioxide gas and the resulting reduction in NH_4HCO_3 concentration reflects the increase in bubble size.

Table 1. Decomposition efficiency for an initial solution of 2 m NH_4HCO_3 solution using a heated (dry) air inlet in the BCE process.

Time (min)	Column Solution Temperature (°C)	Electrical Conductivity (mS/cm)	pH
0	Room Temp.	85	7.74
5	54.2	52.1	9.25
10	56.7	28.3	9.44
15	57.1	8.95	9.33
20	57.8	1.57	8.87

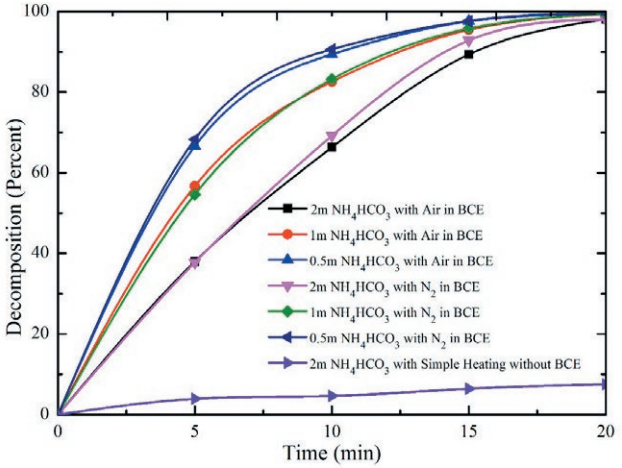

Figure 3. Percent decomposition of NH_4HCO_3 solutions at different concentrations in the BCE with an inlet gas (air and nitrogen) temperature of 275 °C and column solution temperature of 57 °C and in a stirred vessel for simple heating at around 57 °C.

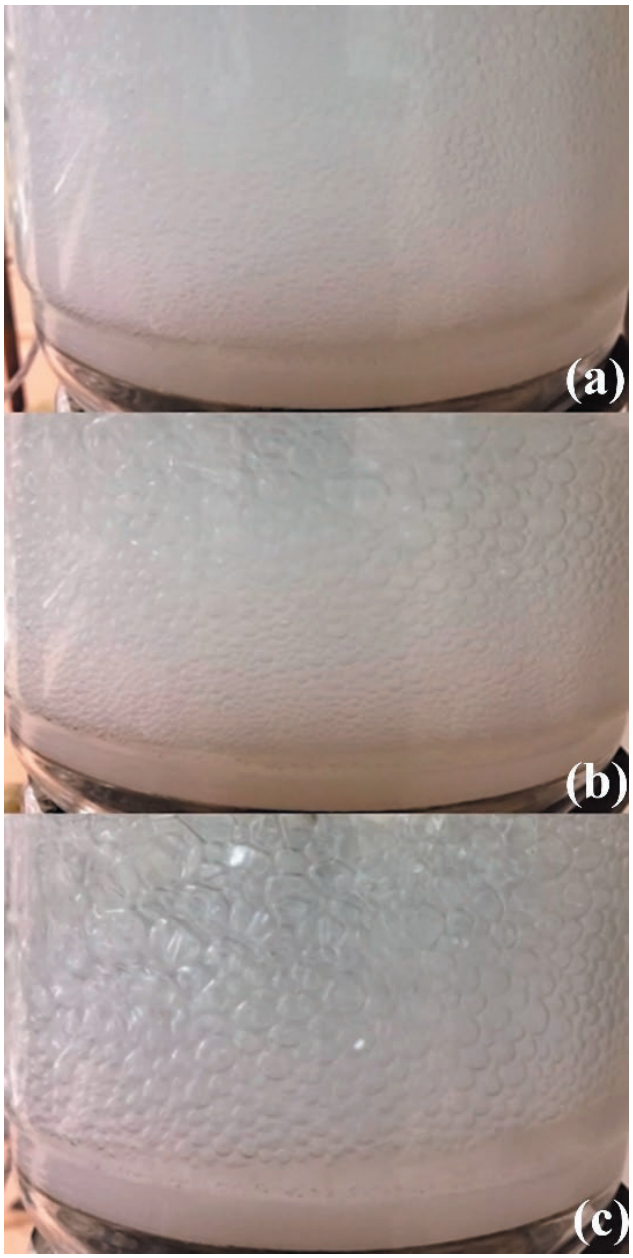

Figure 4. Photographs of the bubble sizes in NH_4HCO_3 solutions in a BCE with an inlet of (dry) air at 275 °C, at experimental times: (a) 0 min (b) 10 min; and (c) 20 min.

3.1.3. Effect of initial bubble temperature on NH_4HCO_3 decomposition in a BCE

It appears that the decomposition of NH_4HCO_3 in aqueous solutions within a hot air BCE system occurs due to the hot surface layer initially present around the stream of hot air bubbles released from the frit. We consider the likely thickness of this transient heated layer as a function of inlet air temperature. The maximum extent of the layer can be estimated for a given temperature, assuming that it is uniform, from the total heat available from the freshly released bubble. For example, for a 1mm bubble we can estimate the maximum layer thickness of water heated to, say, 80°C by the bubbles with an initial release temperature of about 150 °C (i.e. the inlet gas temperature) as follows.

This bubble layer thickness varies with bubble size (V) and the temperatures of the inlet air, the steady state column temperature and the average temperature of the heated surface film surrounding the bubbles. The maximum heated layer thickness can be estimated using the thermal energy balance equation:

$$C_p \Delta T V = C_{water} \Delta t 4\pi r^2 \rho_w z \quad (4)$$

where C_p, C_{water} are the air and water heat capacities, in units of J/(m^3×K) and J/(kg×K), respectively, and ρ_w is the liquid water mass density (in kg/m^3). Δt, ΔT are the transient temperature increase in the water layer and the temperature reduction within the cooling bubbles, in units of K, respectively.

The volume of a layer of thickness z around a bubble is given by $4\pi r^2 \rho_w z$, when z is much smaller than r. Hence the cooling of the bubble by ΔT must determine the thickness z. For example, for bubbles cooling by 100 °C, the maximum heated water layer thickness, heated from 20 to 80 °C, is about 70 nm. So ammonium bicarbonate could be decomposed in this surface region, as illustrated in Figure 5. When the inlet gas temperature is increased, the thickness of the surface hot water layer would also be increased, provided the mean temperature of the film and other assumptions are fixed. Consequently, the volume of the decomposition area (in the hot bubble layer) is correspondingly increased, leading directly to improved decomposition.

It is useful to estimate the thermal energy cost to produce decomposition of an ammonium bicarbonate solution. We have done this by passing 22.5 L/min of air heated to 275 °C through a bubble column for 20 mins with 1-3 mm size bubbles. Different concentrations of ammonium bicarbonate solution were used. The heat capacity C_p at a constant pressure of air in units of J/gK can be calculated from gas heat capacity per mole. This is fairly constant with temperature. At 275 °C this corresponds to about 1.017 J/gK respectively. For a flow rate of 22.5 L/min, this requires a total heat to raise the temperature of gas from 20 to 275 °C of about 144 kJ per 250 mL of solution or 575 kJ/L. By comparison, heating a litre of ammonium bicarbonate solution using different inlet gas temperatures is shown in Figure 6.

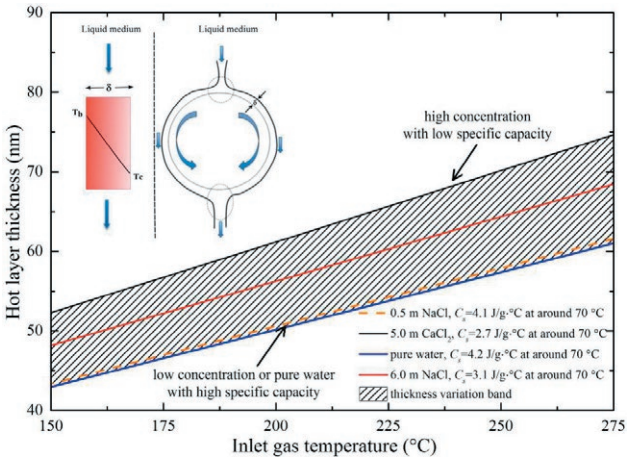

Figure 5. Relationship between the temperature of the inlet gas and the estimated thickness of the transient hot bubble surface layer around a 1 mm radius bubble in pure water, 0.5 m NaCl and 5.0 m $CaCl_2$. Reprinted by permission of the publisher (Taylor &Francis Ltd, http://www.tandfonline.com) from Ref. 10.

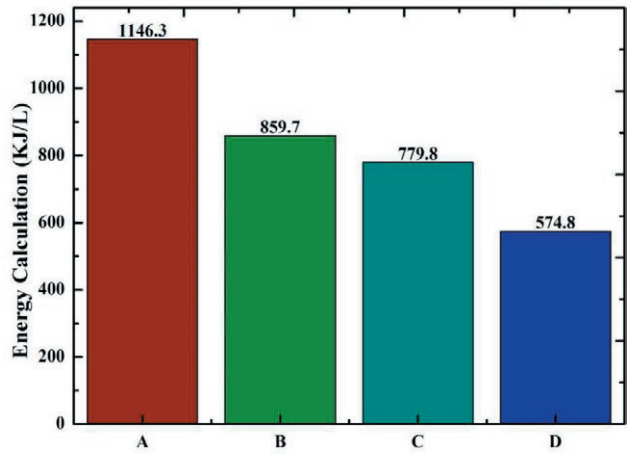

Figure 6. Comparison of thermal energy cost using air as carrier gas; A indicates energy cost at 150 °C inlet gas temperature using 2 m AB solution; B shows at 150 °C inlet gas temperature with 1 m AB solution; C illustrates at 150 °C inlet gas temperature with 0.5 m AB solution and D explains energy cost at 275 °C using 2 m AB solution.

4. CONCLUSIONS AND FUTURE WORK

A method for sub-boiling, thermal decomposition of ammonium bicarbonate solutions was presented. This is a considerable improvement on standard methods. We have shown that a bubble column can rapidly exchange heat from hot gas bubbles to the nearby water surrounding the bubbles. This can be used as an effective and energy efficient method of decomposing ammonium bicarbonate in solution. It can be readily scaled up to treat industrial ammonium bicarbonate draw solutions used in forward osmosis desalination.

An important inference is this: The BCE process, in addition to those applications already mentioned, might also be used to destroy unwanted solutes. Hormones and pharmaceutical compounds present in wastewater present intractable problems for city water recycling. Conventional technologies do not effectively treat these contaminants. Antibiotic residues from human consumption or intensive farming can contribute to the development of antibiotic-resistant bacteria. Protozoa, residual pharmaceutical compounds and hormones are believed to have potential risks to humans and the environment. Examples of such treatments with CO_2 are given in other papers in this volume. The possibilities of achieving very high temperatures within bubbles say with oxygen to carry out reactions at low cost are open.

4. NOMENCLATURE

Abbreviations

AB	Ammonium bicarbonate
BCE	Bubble column evaporator

Symbols

°C	Degree Celsius
M	Concentration in mol/L
m	Concentration in mol/kg
n	Number of moles
T	Temperature
ΔH_{vap}	Enthalpy of vaporisation
ΔP	Pressure difference between inside and outside of the bubble
ΔT	Temperature difference between inlet gas and bubble column solution

5. ACKNOWLEDGMENT

We would like to thank the Australian Research Council for funding this project.

6. REFERENCES

1. J. R. McCutcheon, R. L. McGinnis, and M. Elimelech, A novel ammonia—carbon dioxide forward (direct) osmosis desalination process, *Desalination*, **2005**, 174(1), 1-11.

2. N. P. G. N. Chandrasekara and R. M. Pashley, Study of a new process for the efficient regeneration of ion exchange resins, *Desalination*, **2015**, 357, 131-139.
3. M. Shahid, X. Xue, C. Fan, B.W. Ninham, and R.M. Pashley, Study of a novel method for the thermolysis of solutes in aqueous solution using a low temperature bubble column evaporator, *J. Phys. Chem. B*, **2015**, 119 (25), 8072–8079.
4. G. Fulks, G. B. Fisher, K. Rahmoeller, M. C. Wu, E. D'Herde, J. Tan, *A review of solid materials as alternative ammonia sources for lean NOx reduction with SCR*, **2009**, SAE Technical Paper.
5. G. W. Gokel, *Dean's handbook of organic chemistry*. McGraw-Hill New York, **2004**, 71375937.
6. P. Zehner and M. Kraume, Bubble columns, *Ullmann's Encyclopedia of Industrial Chemistry*, **2000**.
7. C. Fan, M. Shahid, R.M. Pashley, Studies on bubble column evaporation in various salt solutions, *J. Sol. Chem.*, **2014**, 43(8), 1297-1312.
8. M. Francis, R. Pashley, Application of a Bubble Column for Evaporative Cooling and a Simple Procedure for Determining the Latent Heat of Vaporization of Aqueous Salt Solutions, *J. Phys. Chem. B*, **2009**, 113(27), 9311-9315.
9. V. S. J. Craig, B. W. Ninham, R. M. Pashley, The effect of electrolytes on bubble coalescence in water, *J. Phys. Chem.* , **1993**, 97(39), 10192-10197.
10. M. Shahid, C. Fan, R. M. Pashley, Insight into the bubble column evaporator and its applications, *Int. Rev. Phys. Chem.* , **2016**, 35(1), 143-185.
11. C. Fan and R. M. Pashley, Precise Method for Determining the Enthalpy of Vaporisation of Concentrated Salt Solutions Using a Bubble Column Evaporator, *J. Sol. Chem.*, **2015**, 44(1), 131-145.
12. M. J. Francis, R. M. Pashley, Thermal desalination using a non-boiling bubble column, *Desalin. Water Treat.*, **2009**, 12(1-3), 155-161.
13. M. Shahid, R. M. Pashley, A study of the bubble column evaporator method for thermal desalination, *Desalination*, **2014**, 351, 236-242.
14. M. Taseidifar, M. Shahid, R. M. Pashley, A study of the bubble column evaporator method for improved thermal desalination, *Desalination*, **2018**, 432, 97-103.
15. X. Xue and R.M. Pashley, A study of low temperature inactivation of fecal coliforms in electrolyte solutions using hot air bubbles, *Desalin. Water Treat.*, **2015**, 1–11.
16. M. Shahid, A study of the bubble column evaporator method for improved sterilization, *J. Water Process. Eng.*, **2015**, 8, 1–6.
17. A. G. Sanchis, M. Shahid, and R. M. Pashley, Improved virus inactivation using a hot bubble column evaporator (HBCE), *Colloids and Surfaces B: Biointerfaces*, **2018**, 165, 293-302.
18. A. G. Sanchis, R. M. Pashley, B. W. Ninham, Virus and bacteria inactivation by CO_2 bubbles in solution, *NPJ Clean Water*, **2019**, 2(1), 5.
19. M. Shahid, R. M. Pashley, M. Rahman, Use of a high density, low temperature, bubble column for thermally efficient water sterilisation, *Desalin. Water Treat.*, **2014**, 52, 4444–4452.
20. C. Fan, R. M. Pashley, The controlled growth of calcium sulfate dihydrate (gypsum) in aqueous solution using the inhibition effect of a bubble column evaporator, *Chem. Eng. Sci.*, **2016**, 142, 23-31.
21. M. Taseidifar, F. Makavipour, R. M. Pashley, A. F. M. M. Rahman, Removal of heavy metal ions from water using ion flotation, *Environ. Technol. Innov.*, **2017**, 8, 182-190.
22. P. N. Govindan, G. P. Thiel, R. K. McGovern, J. H. Lienhard, M. H. Elsharqawy, *Bubble-Column Vapor Mixture Condenser*. Google Patents.
23. G. P. Narayan, J. H. Lienhard, Thermal Design of Humidification–Dehumidification Systems for Affordable Small-Scale Desalination, *IDA J. Desalin. Water Reuse*, **2012**, 4(3), 24-34.
24. M. Schmack, H. Goen, and A. Martin, A Bubble Column Evaporator with Basic Flat-plate Condenser for Brackish and Seawater Desalination, *Environ. Technol.*, **2015** 37(1), 74–85.
25. C. P. Ribeiro, P. L. C. Lage, Gas-Liquid Direct-Contact Evaporation: A Review, *Chem. Eng. Technol.*, **2005**, 28(10), 1081-1107.

Substantia
An International Journal of the History of Chemistry

Firenze University Press
www.fupress.com/substantia

OPEN ACCESS

Citation: A. Garrido Sanchis, B.W. Ninham (2020) Very High Efficiency of *E. coli* Inactivation by Body Temperature CO_2 Bubbles: in Pursuit of Mechanism. *Substantia* 4(2) Suppl.: 57-67. doi: 10.36253/Substantia-1030

Data Availability Statement: All relevant data are within the paper and its Supporting Information files.

Competing Interests: The Author(s) declare(s) no conflict of interest.

Very High Efficiency of *E. coli* Inactivation by Body Temperature CO_2 Bubbles: in Pursuit of Mechanism

Adrian Garrido Sanchis[2,*], Barry W. Ninham[1]

[1] *Department of Applied Mathematics, Research School of Physical Sciences, The Australian National University, Canberra, Australia*
[2] *School of Sciences, University of New South Wales, Canberra, Australia*
*Corresponding author: a.garridosanchis@adfa.edu.au

Abstract. A CO_2 bubble column (CBC) has been developed as a body-temperature lab-scale water sterilization process for the inactivation of pathogens. Both CO_2 and combustion gas bubbles inactivated *Escherichia coli* C-3000 (ATCC15597) with extraordinary efficiency in solutions with low alkalinity. The mechanisms of inactivation were not known. To characterise the phenomena a new first-order kinetic equation that correlates *E. coli* inactivation rates with a total alkalinity of the solutions has been developed as a first step towards understanding. This leads us to propose a new mechanism of inactivation.

Keywords: *E. coli*, water reuse, carbon dioxide, combustion gas, alkalinity.

1. INTRODUCTION

Water-borne pathogens remain one of the leading risks to public health worldwide. The World Health Organisation (WHO) estimated that over 30 million cases of diseases and millions of deaths could be caused by pathogen-infected water sources, globally, each year.[1]

The inactivation of microorganisms like bacteria and viruses in aqueous solutions is a perpetual challenge. For example, pathogenic bacteria present in water used in food or pharmaceutical manufacture can cause product contamination. In a bigger scenario wastewater from agricultural or industrial uses or water obtained from environmental flows, contains pathogenic microorganisms that need to be inactivated before the water is used for industrial or agricultural purposes or drinking water. This is an existential problem for humanity.

Present methods for inactivating viruses, bacteria, and other microorganisms include heat, irradiation (e.g. ultraviolet treatment), treatment with chemicals (e.g. ozone), high-pressure treatment, and filtration (e.g. membrane filtration). Many of these methods, especially, heat treatment, are energy-intensive. More energy-efficient treatment technologies are desperately needed.

High density and high-pressure CO_2, known as dense phase carbon dioxide (DPCD), is being used as a non-thermal disinfection alternative.[2,3]

Our process is different. We have previously studied CO_2 sterilization effects at atmospheric pressure in a bubble column on *E. coli* and viruses. The process has been implemented commercially. We found that for both pathogenic groups the sterilization effects increase with the temperature.[4] It is of much interest that inactivation becomes optimal above 38 degrees, body range temperature.

Carbon dioxide, being a greenhouse gas, is assigned some responsibility for global warming. But it is also literally vital for plant growth. Recently it has been shown likely to be Nature's way of controlling viral infection in the human body, following from these CO_2 antiviral properties a recent study has identified the use of body temperate humidified CO_2 as a possible early therapy to mitigate infection in COVID-19 patients.[5, 6] Many alternatives to reduce CO_2 emissions have been proposed, apart from planting trees and controlling bushfires. Geological sequestration in depleted gas and oil reservoirs, ocean storage, seaweed production, CO_2 mineralization are just a few.

Sterilisation by CO_2 has been widely used throughout history. After sodium chloride, natron, sodium bicarbonate is probably the first industrial-scale chemical used by mankind. Natron, in ancient Egypt, was essential for mummification. The still and little understood peculiar hydration properties of the bicarbonate ion in contact with air affects both tissue dehydration and sterilization against bacterial degradation.

The magic of the bicarbonate ion has remained, with the still unexplained problem of Roman and other cement formation. The foundation of physical chemistry can arguably be marked by Berthollot's observation that reactions are temperature dependent: He saw soda-lime, sodium carbonate rocks instead of the calcium carbonate on the banks of the Nile River during Napoleon's scientific expedition to Egypt in 1792. The normal precipitation of calcium carbonate from a sodium chloride calcium carbonate solution is reversed at high temperatures of the drying Nile flood in summer. The astute chef and detergent companies know that wet sodium bicarbonate is extremely effective in cleaning. It cuts peptide bonds of proteins bound to saucepans or dishes. But why?

1.1. Nature of the Present Studies

The work here presented studies the *E. coli* inactivation effect of CO_2 at different alkalinity levels at 38 °C (human body temperature range) and atmospheric pressure.

Alkalinity is defined as the ability of water to resist changes in pH when acids or bases are added to the solution or the capacity of water to neutralize acids. The CO_2-carbonate system describes which of the four forms of total inorganic carbon (molecular aqueous CO_2, Carbonate ion, CO_3^{-2}, Bicarbonate ion, HCO_3^-, or Carbonic acid, H_2CO_3) is the dominant species as a function of pH.[7,8]

We have analysed our results within the boundaries of the accepted theory of physical chemistry of solutions. This allowed the development of a new first-order kinetics equation that correlates *E. coli* inactivation rates with total alkalinity when bubbling CO_2 or combustion gases in a bubble column at atmospheric pressure and body temperature. But while it fits the data it does not account for why the process is efficient. We are then led to such an explanation outside the confines of classical theory.

2. MATERIALS AND METHODS

2.1. Coliform bacteria

Escherichia coli is a gram-negative bacterium with a straight cylindrical rod shape of 1.0-2.0 μm size.[9] *E. coli* are harmless, can be found in the intestines of healthy humans and animals but some are pathogenic to the host. As a result of fecal contamination, it can be found in water and soil. Its presence in water is used as an indicator to monitor water quality.[10]

The strain *E. coli* C-3000 (ATCC15597) is a biosafety Level-1 organism[11] which was selected as a representative model for bacterial contamination in water.[12,13]

Spinks at al.[14] demonstrated that pathogenic bacteria are inactivated in a temperature range of 55 to 65 °C. Other studies found that *E. coli* presents the first signs of thermal inactivation at temperatures over 55 °C, with high inactivation rates at 60 °C.[15]

An overnight *E. coli* C-3000 (ATCC 15597) culture was grown in 10 mL broth (see section 2.3 for more details) without agar at 37 °C for 18–20 hours in a Labtech digital incubator, model LIB-030M, while shaken at 110 rpm by a PSU-10i orbital shaker.

2.2. Experimental solutions

Solutions with different alkalinity levels (see Table 1) were prepared and sterilized by autoclaving in an Aesculap 420 at 15 psi and 121–124 °C, for 15 minutes.[16]

A standard **secondary-treated synthetic sewage** medium (Organisation for Economic Co-operation and

Development (OECD) medium) was prepared according to water-quality guidelines and standards.[17,18] The official Journal of the European Community for Secondary-treated Water Quality has the following requirements for discharges from urban wastewater-treatment plants: 125 mg/L of COD; 2 mg/L of total phosphorus; and 15 mg/L of total nitrogen.[19] This solution was designed to meet the European standards by using the following ingredients in a liter of boiled tap water or Milli-Q water (depending on the experiment): 120 mg of peptone; 90 mg of meat extract (replaced here by Bovril® according to recommendations in Biology of Wastewater Treatment[20]); 30 mg of urea; 13 mg of dipotassium hydrogen phosphate; 7 mg of sodium chloride; 2 mg of calcium chloride dehydrate; and 2 mg of magnesium sulfate heptahydrate.

Two NaCl solutions with concentrations of 0.001 M and 0.17 M NaCl (NaCl ≥ 99% purity, obtained from Sigma-Aldrich) in Milli-Q water, a 0.01 M $CaCl_2$ solution ($CaCl_2$.≥ 99% purity, obtained from Sigma-Aldrich) in Milli-Q water and tap water. These concentrations were chosen to coincide roughly with the physiological concentration of humans and to typical environmental conditions faced by the bacterium.

To ensure the full elimination of chlorine from tap water it was previously boiled for 30 minutes, therefore *E. coli* (C3000) was not affected by the disinfecting action of chlorine.

2.3. E. coli growth media

The plate count method[21] is commonly used for the detection of *E. coli* in, both wastewater and marine water. The degree of contamination in water is assessed based on the ability of bacteria to propagate forming colonies in a layer of agar.[22]

For each bacterial-growth experiment, two broths were prepared (A and B).

Broth A was prepared with 1 g of yeast extract, 6 g of NaCl, 13 g of tryptone, and 1,000 mL of Milli-Q water. This medium was aseptically distributed into two vessels containing 1.41% agar and no agar, respectively; the agar used in the experiments was molecular-biology grade from Sigma-Aldrich. The medium was heated to boiling to dissolve the agar and sterilized by autoclaving for 15 minutes in an Aesculap 420 at 15 psi and 121–124 °C.

Broth B was used to improve the viability of the bacteria. It was prepared by adding 0.010 g of thiamine and 1 g of glucose to 50 mL of Milli-Q water and filtered through a 0.22 μm filter for its sterilization. Once cooled to 50 °C, it was added aseptically to broth A in a proportion of 1:19.

The resulting 1.34% agar medium was poured into 100mm × 15mm Petri dishes and dried above a Bunsen burner to maintain local environmental sterility until the agar was not too dry nor too moist.[23]

2.4. CO_2 Bubble column (CBC) process

The CBC process used two different gases: CO_2 and combustion gases. A flow of 24 L/min of CO_2 was pumped through the electrical heater that maintained the gas temperature just above the sinter surface at 38°C for the CO_2 experiments. When using combustion gases, the exhaust pipe of an LPG gas generator (Greenpower 2.5 kW) was attached to an isolated metal pipe with a valve that provided an exhaust-gas flow rate of 27 L/min through the bubble column reaching a temperature of 58 °C just above the sinter surface. The base of the bubble column evaporator was fitted with a glass sinter (type 2) of 135 mm diameter and pore size 40–100 μm.

Once the experimental solutions (0.17 M NaCl, 0.01 M $CaCl_2$, 0.001 M NaCl, secondary treated synthetic sewage made with Milli-Q water and tap water) were poured into the column, the temperature of the solution was measured with a thermocouple in the center of the column. Hot bubbles of both gases passed through the sinter into the 300 ml solution, inactivating *E. coli*.

The sterilization effects of other gases like air, argon, and nitrogen on *E. coli* have been discussed[24], they are not significant compared with CO_2 bubbles, especially at low temperatures.

2.5. Experimental setup and procedure

The CBC treated 0.17 M NaCl, 0.01 M $CaCl_2$, 0.001 M NaCl, secondary treated synthetic sewage made with Milli-Q water, and tap water containing *E. coli* C-3000 (ATCC15597) at inlet CO_2 temperature of 38 °C, and combustion exhaust gas from an LPG generator at 60 °C.

The plate count method[25,26,27] was used to assess the viability of *E. coli*. Samples were collected from 10–15 mm above the central area of the bubble column. Each sample of 0.1 mL was spotted in triplicate.

Alkalinity measures the acid-neutralizing ability of dissolved substances in water and is equivalent to the amount of strong acid required to lower the pH of the solution from an initial value to about 4.2. The total alkalinity of each solution, in mg/L $CaCO_3$, was determined by the amount of 0.02 M HCl added in a titration until a pH electrode (ThermoFisher Scientific) measured an end pH of 4.2. The initial pH of the sample of each of the 6 solutions was less than 8.3 therefore the alkalin-

ity was calculated with the carbonate ion concentration multiplied by a factor of two since each [CO_3^{-2}] ion neutralised two protons[28], see Table 1.

2.6. Data analysis

The linear decay model was used to study the inactivation of *E. coli* over time in CBC.[24,29,30] The evaluation of viable *E. coli* in the samples was performed using the plate count agar (PCA) method.[23,26,31] Plate counts numbers indicate the number of *E. coli* colonies that grow on the surface of a solid and translucid agar media in a Petry dish. The mean and standard deviation of each triplicated sample was obtained using bacteria survival factor, $\log_{10}(CFU/\ CFU_0)$, where CFU_0 is the initial number of colony-forming units (CFU) per sample and CFU is the number of *E. coli* colonies per sample after a set exposure time to the CO_2 bubbles.[32]

When analysing the data we assumed that the inactivation of *E. coli* by CO_2 in different alkaline solutions follows first-order kinetics. We proposed a model that uses the decimal reduction time (D-value) to measure how the alkalinity of a given solution can influence *E. coli* inactivation. The D-Value is defined as the time, in minutes, needed to inactivate 90% (i.e. 1-log) loss of *E. coli*.

D-values were calculated using a linear exponential decay model.

$$\log(CFU_t)=\log(CFU_0)-\frac{t}{D} \quad [1]$$

$$\log\left(\frac{CFU_t}{CFU_0}\right)=-\frac{t}{D} \quad [2]$$

Here, is the number of *E. coli* colonies at time t, = the initial number of *E. coli* colonies, *D*= the decimal reduction time, -(1/D) = the slope of the curve.

3. RESULTS AND DISCUSSION

3.1. CBC process inactivating E. coli at 38 °C and one atmosphere

Zhong et. al.[33] observed that when bubbling CO_2 in different electrolyte solutions, their pH dropped until it reached a steady value in less than 10 minutes; this value was different for each solution. Similar behavior was observed when CO_2 gas at 38 °C and combustion gases were bubbled for 10 minutes through six different solutions (0.17 M NaCl, 0.01 M $CaCl_2$, 0.001 M NaCl, secondary treated synthetic sewage made with Milli-Q water and tap water) in the bubble column (see Table 1). The absorption of CO_2 into different solutions increases when CO_2 gas is bubbled through the sintering area in a bubble column; many bubbles are produced with a large CO_2-liquid contact surface that is continually produced.

When CO_2 dissolves in water 99% stays as the dissolved molecular gas and less than 1% as carbonic acid (H_2CO_3 (equations 1 and 2) which reduces the pH of the solution (see Table 1). Carbonic acid dissociates into bicarbonate ion (HCO_3^-) and carbonate ion (CO_3^{2-}) (see equations 3 and 4).[34]

$$CO_2(g)\rightarrow CO_2(aq) \quad [3]$$

$$CO_2(aq)+H_2O(l)\leftrightarrows H_2CO_3(aq) \quad [4]$$

$$H_2CO_3(aq)\leftrightarrows H^+ + HCO_3^-(aq) \quad [5]$$

$$HCO_3^-(aq)\leftrightarrows H^+ + CO_3^{2-}(aq) \quad [6]$$

This is the reason why the pH of every solution dropped (see Table 1) and was different from that of the other solutions.[34]

When a 24 L/min flow of CO_2 passes through a single glass tube immersed in a beaker containing *E. coli* in 300 mL of 0.17 M NaCl the big bubbles of 1-3 cm diameter do not inactivate the pathogens.[4] However, when the same flow of CO_2 gas at the same temperature in the same solution is bubbled through a sintering area in a bubble column *E. coli* inactivation occurs. The bubble column produces many small CO_2 bubbles (1-3 mm diameter). The consequent CO_2 dissolution rate increases due to the large CO_2-liquid contact surface that is constantly produced. Mass transfer from the CO_2 to the liquid depends highly on the interfacial area (α).[4] This increases the amount of CO_2 dissolved in the solution and produces a similar sterilization effect to what can be achieved by raising the pressure in dense phase carbon dioxide (DPCD) processes. *The overwhelming advantage of the bubble column delivery is that only atmospheric pressure is required.*

A possible mechanism previously described[4], could explain in part why *E. coli* (doesn't work for viruses) can be inactivated by bubbling CO_2 at body temperature in a bubble column. It is that the pH decreases when CO_2 dissolves in a solution and this acidification of the solution increases the binding of bicarbonate ion to bacterial membrane phospholipid head groups. The resulting change in the head group area and membrane structure to an open mesh phase then allows free diffusion of CO_2 through the bacterial membranes. The CO_2 inside the cell produces an intracellular pH decrease that exceeds the cell's buffering capacity, resulting in cell inactiva-

tion.[35,36] Orij et al. observed that *Saccharomyces cerevisiae* cell division rate is controlled by intracellular pH changes and low intracellular pH could reduce the cell division.[37] This idea has a degree of plausibility and may well contribute to bacterial inactivation. However, it does not explain the inactivation of viruses.

When CO_2 was bubbled at 38 °C through 0.17M NaCl and 0.001 M NaCl solutions (made with Milli-Q water) in the bubble column evaporator, for both solutions, 0.6-log of *E. coli* inactivation was observed after 10 minutes due to the high CO_2 surface area in the solution (see Fig. 1). This occurred even though the two solutions had very different bubble densities. When using secondary-treated synthetic sewage and 0.01 M $CaCl_2$ (both made with Milli-Q water), a 0.2-log and 0.3 log reduction of *E. coli* was achieved respectively after 10 minutes (Fig. 1a and Table 1). However, when the same experiment was conducted with boiled tap water and with secondary-treated synthetic sewage (made with boiled tap water), no inactivation was observed after 11 minutes (Fig. 1a).

When combustion gas from a generator (with 12.5–14% of CO_2)[38] at 60°C was used in the bubble column experiments an *E. coli* inactivation rate of 2.6-log in 0.17 M NaCl solutions (made with Milli-Q water) was observed after 10 minutes.[24] However, when using secondary-treated synthetic sewage (made with boiled tap water) no inactivation was detected after the same period (Fig. 1b). This is consistent with the hypothesis that reduced pH buffering capacity aids inactivation. Within the combustion gas, other products than CO_2, H_2O, and N_2 could be present due to minor components and impurities in the fuel and different fuel/air ratios. These gases are carbon monoxide (CO), hydrogen (H_2), sulfur oxide (SO_2), and mono-nitrogen oxides (NO*x*) such as NO and NO_2.[38] Even with the presence of these gases, no inactivation was observed.

The tap water used in this work had a total alkalinity of 87.4 mg $CaCO_3$/L (Table 1), and an initial pH of 8 and therefore can act as a buffer solution. After bubbling CO_2 the pH was reduced to 4.9 for the pure tap water and 5.4 for the secondary-treated synthetic sewage, with an alkalinity of 94.5 mg $CaCO_3$/L (Table 1). This pH is too high to allow the penetration of the CO_2 through the membranes, with a consequent lack of *E. coli* inactivation when using the CBC process in solutions with high alkalinity.

Milli-Q-water-based solutions had a reduced buffer capacity of only 6 mg $CaCO_3$/L (Table 1), reaching low pH values of 4 for NaCl and $CaCl_2$ based solutions. For Milli-Q-water based secondary-treated synthetic sewage the pH reached 4.4 and the total alkalinity value was 27.7 mg $CaCO_3$/L (Table 1); this solution contains different salts that can slightly increase its alkalinity, with a consequent reduction in inactivation.

3.2. Effect of alkalinity on E. coli inactivation when bubbling CO_2 and combustion gases

Decimal reduction times (D-values) (Table 1), calculated from inactivation values, have been used to understand the effect of alkalinity on *E. coli* inactivation. To do this, we compared *E. coli* inactivation performance of the CBC when using body temperature CO_2 with that of combustion gases for six solutions (0.17 M NaCl, 0.01 M $CaCl_2$, 0.001 M NaCl, secondary treated synthetic sewage made with Milli-Q water and tap water) with different alkalinity values, see Fig. 2.

The correlation between the log of the D-values and the corresponding total alkalinity is shown in Fig. 2 and Table 1. A D-value is a time needed to inactivate 90% (i.e. 1-log) of the *E. coli*. To measure the impact of alkalinity on *E. coli* inactivation when bubbling CO_2 we have proposed

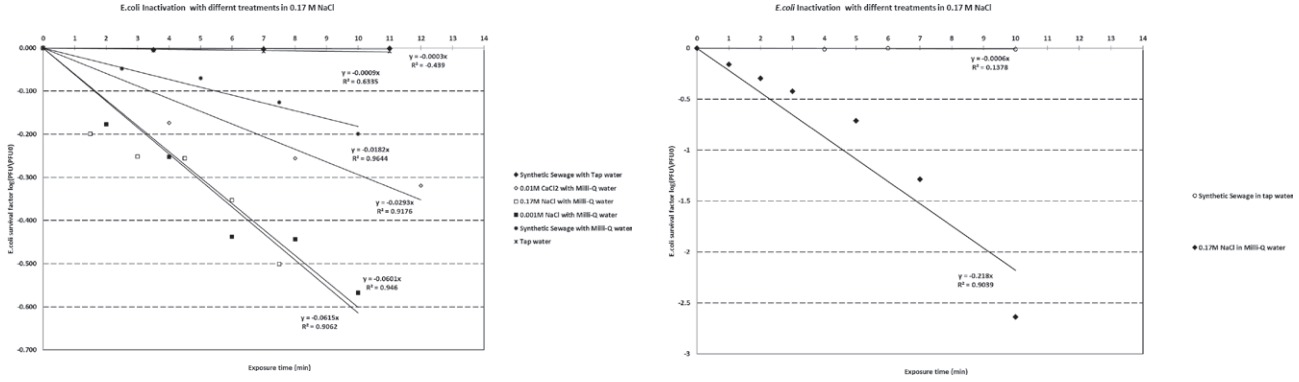

Figure 1. (a) Comparison of *E. coli* inactivation with CO2 at 38 °C in a bubble column in 6 different solutions; (b) *E. coli* inactivation with combustion gas at 60 °C in a bubble column in 2 different solutions.

Table 1. Initial and final pH values after bubbling CO_2 and combustion gas in 6 different solutions, amount of 0.02 M HCl to reduce the pH of the solutions to 4.2, alkalinity in mg/L of $CaCO_3$ and D-values.

Solution	pH initial	pH final	ml of HCl 0.02 M to reach pH 4.2	ml of HCl 0.02 M to reach final pH	Total Alkalinity (mg/L of $CaCO_3$) (to reach a pH of 4.2)	Equivalent (mg/L of $CaCO_3$) (to reach final pH)	D-value (min)	Log10 (D-value, min)
CO_2 gas at 38°C								
0.001M NaCl in Milli-Q water	5.78	4	0.9	1.3	6	8.7	16.3	1.21
0.17M NaCl in Milli-Q water	5.86	4	0.9	1.3	6	8.7	16.6	1.22
0.01M $CaCl_2$ in Milli-Q water	5.94	4	1	1.5	6.7	10	34.1	1.53
Tap water	8	4.9	13.1	12	87.4	80.1	2,000	3.30
Secondary-treated synthetic sewage made with tap water	7.63	5.4	14.3	10.5	95.4	70.1	3,333	3.52
Secondary-treated synthetic sewage made with Milli-Q Water	6.83	4.4	4	2.6	26.7	17.3	54.9	1.74
Combustion gas at 60 °C								
Secondary-treated synthetic sewage made with tap water	7.63	6.5	14.3	5.4	95.4	36	1,666	3.22
0.17M NaCl in Milli-Q water	5.86	4	0.9	1.3	6	8.7	4.6	0.66

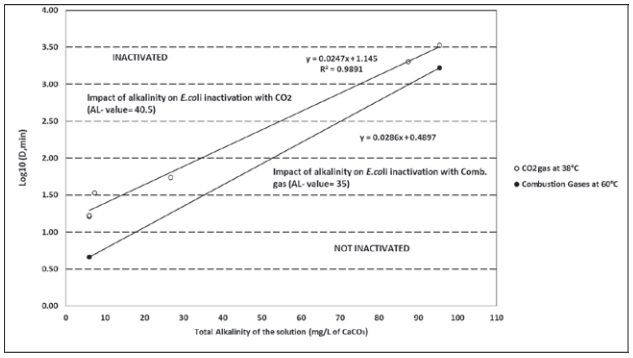

Figure 2. Minimum CO_2 bubbling times at different alkalinity values to achieve 1-log bacteria inactivation in 6 different alkaline solutions. Above and to the right of the lines the pathogens will be sterilized by 1-log.

the new AL-value. The AL-value gives the total alkalinity required to change the D-value by a factor of 10 and reflects the alkalinity impact on *E. coli* inactivation. The smaller the AL-value, the greater the sensitivity to low alkalinity.

Figure 2 compares the impact of alkalinity on *E. coli* inactivation between CO_2 and combustion gases. Above and to the right of the lines *E. coli* will be inactivated by at least 1-log.

From the AL-values obtained with CO_2 (AL=40.5) and combustion gases (AL=35), it can be seen that the inactivation for both gases showed a similar alkalinity-dependent behavior (Fig. 2). A reduced AL-value of 35 to 40.5 mg/L of $CaCO_3$ suggests that when bubbling both gases inactivation rates of *E. coli* will highly depend on the alkalinity of the solution, see Table 1 and Figure 1.

For alkalinity values in the range, 5–95 mg $CaCO_3$/L, combustion gases presented higher *E. coli* inactivation rates than when using pure CO_2, with D-values of 16.3 min at 6 mg $CaCO_3$/L for pure CO_2 and 4.6 min at 6 mg $CaCO_3$/L for combustion gases. At higher alkalinity values both gases needed longer times to achieve 1 log *E. coli* inactivation, combustion gases required 1,666 min at 95.4 mg $CaCO_3$/L, pure CO_2 needed 3,333 min at 95.4 mg $CaCO_3$/L (Fig. 2 and Table 1).

For both gases, *E. coli* inactivation can be increased by reducing the alkalinity of the solution. Solutions with a low buffer capacity, low alkalinity, after bubbling CO_2, or combustion gases in the bubble column for 10 minutes significantly reduced their pH as observed in our experiments (Table 1). This reduced pH could affect microbial cell inactivation, since cell membranes stop protons from penetration but also make them more permeable to other substances, like CO_2, due to the chemical modification on the phospholipid bilayer of the membranes.[35,36] When CO_2 penetrates inside of the bacteria dissolves in the intracellular fluid producing carbonic acid (H_2CO_3) what triggers an intracellular pH decrease that exceeds the cell's buffering capacity, resulting in cell inactivation.[35,36]

3.3. Development of an inactivation model based on alkalinity

Based on the evidence (see Figure 3) that *E. coli* inactivation in different alkaline solutions when bubbling 38

°C CO_2 and combustion gases follows first-order kinetics we proposed a new *E. coli* inactivation equation that considers the alkalinity of different solutions.

3.4 Disinfection Kinetics model

The disinfection efficiency of bubbling CO_2 or combustion gases at low temperatures through a solution with *E. coli* depends on the total alkalinity of the solution. A new model that includes alkalinity based on the Chick-Watson first-order equation has been developed in this work.

E. coli inactivation follows the first-order kinetics, thus the model results in the following equation:

$$\frac{dCFU}{dt} = -k\ CFU \quad [7]$$

where the *E. coli* population (CFU) varies with processing time (t) at a constant rate (k).

The New Model based on the decimal reduction time (D-value) and the new AL-value explains how the alkalinity of a given solution can influence *E. coli* inactivation when CO_2 or combustion gases, that contain CO_2, are bubbled through at atmospheric pressure. The D-value is defined as the time, in minutes, needed to inactivate 90% (i.e. 1-log) of *E. coli*.

D-values were calculated using a linear exponential decay model.

$$\log S(t) = \log\left(\frac{CFU_t}{CFU_0}\right) = -\frac{t}{D} \quad [8]$$

where $S(t)$ is the survival fraction after a time (min), is the number of *E. coli* colonies at time t, = the initial number of *E. coli* colonies, D= the decimal reduction time, -(1/D) = the slope of the curve (see Figure 3).

For this work, we have defined a new parameter, the AL-value, that is the reduction in alkalinity needed to reduce the D-value by 1-log when bubbling CO_2 in a bubble column at body temperature (38°C) and atmospheric pressure. It measures the impact of alkalinity on *E. coli* inactivation.

Thus:

$$\log D_1 = \frac{1}{AL}(A_1 - A_2) + \log D_2 \quad [9]$$

$$AL = \frac{A_1 - A_2}{\log D_1 - \log D_2} \quad [10]$$

Where, A_1 first alkalinity of the interval, A_2 second alkalinity of the interval, and D_1 and D_2 are the D-values at A_1 and A_2.

Equation 5 is obtained from Fig. 3, where A is alkalinity.

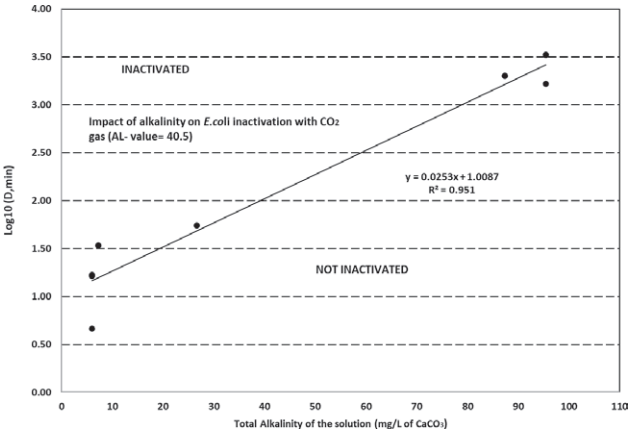

Figure 3. Minimum CO_2 and combustion gas bubbling times at different alkalinity values to achieve 1-log bacteria inactivation in 6 different alkaline solutions. Above and to the right of the lines the pathogens will be sterilized by 1-log.

$$\log D = 0.0253A + 1.0087 \quad [11]$$

From quations 2 and 5.

$$\log\left(\frac{CFU_t}{CFU_0}\right) = \frac{-t}{e^{(0.0253\ A\ +\ 1.0087)}} \quad [12]$$

Where, CFU_t is the number of *E. coli* at time t, CFU_0= the initial number, A= is the alkalinity of the solution in mg/L of $CaCO_3$ (see Figure 3).

4. POSSIBLE MECHANISMS OF STERILISATION

4.1. Negotiating the Quagmire: Nanobubbles

We began this and previous works[4,24] with the remarkable discovery that CO_2 bubbles at body temperatures are extremely efficient sterilising agents for both bacteria and viruses. The technology is being implemented at industrial scales. Potential applications are legion. The use of recycled water in cities has been prohibited in large part because viruses could not be easily removed from drinking water. A recent discovery in physiology has revealed the structure and function of the ubiquitous endothelial surface layer (ELS), unknown for 150 years.[39]

It is a micron thick foam of carbon dioxide nanobubbles. CO_2 is being produced by metabolism. and passes through a molecular frit that is the polymeric glycocalyx to form nanobubbles. This mimics our bubble column apparatus and vice versa. The ESL foam repels red cells and protects organs from invasion by bacteria, neutrophils, low-density lipoproteins, and a legion of

other invaders, good and bad. Viruses like COVID-19 have to run the gauntlet of this layer of nanobubbles on their way out to the adjoining bloodstream and exit with CO_2 nanobubbles via the lungs. The issue of CO_2 sterilisation takes on a wider import as Nature's gift to protect us from the disease. The question of what factors combine to account for the mechanism of sterilisation then takes on a decided imperative. The results of the experiments we have been able to subsume in the single first-order kinetic equation of Section 3.3. We now have to see if we can extract any sense and hints at mechanism from this. In attempting to do so we have negotiated our way through a swamp of misinformation. By this, we mean the classical foundations of physical chemistry that inform our intuition suffer from serious sins of omission and of commission. [40] These are due to the omission of specific ion (Hofmeister) effects, of dissolved gas: and the organization and reactivity of nanobubbles. Their universal presence has been a hidden variable that controls reactivity in solution. They are the energy source via free radicals that drive in polymerization[41], and enzymatic reactions.[42,43] Their presence has been revealed and studied extensively by laser spectroscopy over many years.[44-46] Nanobubbles even appear on mechanical shaking and contain highly reactive hydrogen peroxide and of course on sonication.[47-49]

4.2. Available Evidence

With these complications of classical theory in mind we marshall what further evidence we can that could illuminate the issue of mechanism.

Other gases: argon, air, and nitrogen have no deleterious on pathogens at low temperatures. At very high temperatures they do explore in a succeeding paper.[24] Our problem is peculiar to CO_2.

4.3. Sodium bicarbonate.

The astute chef and detergent companies know that the removal of food proteins adhering to utensils is not easily accomplished. It is by using reasonably warm concentrated sodium bicarbonate solution. This involves active nanobubbles nucleated at the surface that cut peptide bonds. It is also aided by Berthelot's 1795 observations on the Nile of precipitation of sodium carbonate rather than calcium carbonate. The ion exchange at and above 50 degrees removes calcium and weakens adhesive bonds. This occurs with the destruction of proteins and their adhesion in the protective coats of both bacteria and viruses.

With bacteria the lipids of the exterior membranes of both gram-positive and gram-negative types fall apart above 50-60 degrees because of the same change in head group hydration with temperature – apart from the obvious change in hydrocarbon chain packing.

4.4. pH changes with salt and salt concentration

We have already remarked on apparently peculiar specific differences in pH with different salts with bubbling CO_2 through the solution. This artifact occurs for solutions with CO_2 and those without. They are because the classical theory of pH and buffers assumes that electrostatic forces alone are operating. Specific Hofmeister effects arise when the theory is corrected to include dispersion force acting ions, anion cations, and buffer ions. Further complications of buffers show up explicitly in[42]. But also listed below of course all classical measurements ignore dissolved gas that also affects matters like the interpretation of surface potentials (pH). Reversal of the Hofmeister series for pH is seen with buffers nominally at the same pH, e.g., phosphate vs cacodylate, nominally pH 7.[50-52]

These are serious complications around which we have to tread carefully. See e.g. for an explicit illustration of obstacles to interpretation caused by the use of classical theory.[53] This reports studies of growth rates of *Staphylococcus aureus* and *Pseudomonas aeruginosa* as a function of salt concentration for a large range of anions spanning the Hofmeister series. The variations are enormous and not explainable in the usual framework of colloid science.[53]

4.5. Finally a Mechanism of Sterilisation

So armed for pitfalls of theory, we can tread carefully towards an understanding of what is going on.

Essentially this: Nanobubbles are formed through the turbulent passage of CO_2 through the bubble column frit. They are stabilised by the adsorption of ions and proteins from the bubble column solution. The nanobubbles will have a dynamic highly reactive surface containing bicarbonate and carbonate ions in amounts depending on alkalinity that determines the proportion of each.

Carboxylates form due to surface reactions with solutions depending on solution constituents. If in high enough concentration these will react with peptides of bacterial (and viral) coats, resulting in destruction. This is consistent with the astute chef and detergent companies cleaning recipe.

5. CONCLUSIONS

Pure CO_2 gas or combustion gases can be used in the bubble column to effectively inactivate *E. coli* C-3000 (ATCC15597) in the water at atmospheric pressure and ambient temperatures. The efficiency of the process appears to depend on the alkalinity of the solution.

CO_2 bubbles will have a dynamic highly reactive surface containing bicarbonate and carbonate ions in amounts depending on the alkalinity of the solution that determines the proportion of each. Carboxylates form due to surface reactions with solutions on solution constituents. If in high enough concentration, especially in low alkalinity solutions, this will react with peptides of bacterial (and viral) coats, resulting in their inactivation.

We have developed a new first-order kinetics equation that predicts *E. coli* inactivation rates from solutions with different alkalinity when bubbling CO_2 or combustion gases in a bubble column at atmospheric pressure.

6. ADDENDUM

Since this work was written we discovered an excellent paper from 1948 dealing with the Surface Inactivation of Bacterial Viruses and of Proteins by Mark H.Adams.[54] It explores the effects of shaking with different gases but not CO_2 on viruses and proteins. It even compares with the effect of bubbling through a frit. This and references contained therein go back to the beginnings of genuine molecular biophysics and predate the molecular biology DNA revolution. It would be remiss of us not to refer the reader to the beginnings of quantification of the physical effects of gas and nanobubbles, long-forgotten and missing from contemporary physical chemistry.

7. CONTRIBUTIONS

Adrian Garrido Sanchis (principal author) carried out the lab experiments, performed analysis on all samples, interpreted data, and lead the writing of the manuscript.

Barry Ninham acted the part of devil advocate and critic and led his disciple back to the paths of correctness.

8. REFERENCES

1. WHO, *Technical guidance on water-related disease surveillance* 2011, World Health Organization.
2. J.F. Rusling, Environmental Electrochemistry: Fundamentals and Applications in Pollution Abatement By Krishnan Rajeshwar (University of Texas at Arlington) and Jorge G. Ibanez (Universidad IberoAmericana). Academic Press: San Diego. 1996. 776 pp. ISBN 0-12-576260-7, *J Am Chem Soc*, **1998**, 120(45), 11837-11837.
3. G.F.a.M.O. Balaban, *Introduction to Dense Phase Carbon Dioxide Technology*, in *Dense Phase Carbon Dioxide*, B.P. Professional, Editor. 2012. p. 1-4.
4. A. Garrido Sanchis, R. Pashley, B.W. Ninham, Virus and bacteria inactivation by CO2 bubbles in solution, *npj Clean Water*, **2019**, 2(1), 5.
5. B.P. Reines, B.W. Ninham, Structure and function of the endothelial surface layer: unraveling the nanoarchitecture of biological surfaces, *Quarterly reviews of biophysics*, **2019**, 52, e13.
6. A. El-Betany, E. Behiry, M. Gumbleton, K. Harding, *Humidified Warmed CO2 Treatment Therapy Strategies Can Save Lives with Mitigation and Suppression of SARS-CoV-2 Infection: An Evidence Review*. 2020.
7. G.W. VanLoon, S.J. Duffy, Environmental chemistry : a global perspective, **2005**.
8. C. Baird, M. Cann, *Environmental chemistry*. 2012, New York, NY: W.H. Freeman and Company.
9. G. Reshes, S. Vanounou, I. Fishov, M. Feingold, Cell shape dynamics in Escherichia coli, *Biophys J*, **2008**, 94(1), 251-264.
10. R.A. Welch, *The Genus Escherichia*, in *The Prokaryotes: Volume 6: Proteobacteria: Gamma Subclass*, M. Dworkin, et al., Editors. 2006, Springer New York: New York, NY. p. 60-71.
11. ATCC, *Product Sheet Escherichia coli (ATCC 15597)*, ATCC, Editor. 2015.
12. X. Yang, *Introduction*, in *A Study on Antimicrobial Effects of Nanosilver for Drinking Water Disinfection*. 2017, Springer Singapore: Singapore. p. 1-12.
13. I. Gaska, O. Bilenko, S. Smetona, Y. Bilenko, R. Gaska, M. Shur, Deep UV LEDs for Public Health Applications, *Int J High Speed Electron*, **2014**, 23(03n04), 1450018.
14. A.T. Spinks, R.H. Dunstan, T. Harrison, P. Coombes, G. Kuczera, Thermal inactivation of water-borne pathogenic and indicator bacteria at sub-boiling temperatures, *Water Res*, **2006**, 40(6), 1326-1332.
15. McGuigan, Joyce, Conroy, Gillespie, M. Elmore, Solar disinfection of drinking water contained in transparent plastic bottles: characterizing the bacterial inactivation process, *J Appl Microbiol*, **1998**, 84(6), 1138-1148.
16. I. 10705-1, *Water quality - Detection and enumeration of bacteriphages- Part 1*, in *ISO 10705-1*. 1995, International Organization for Standardization: ISO.
17. I. 11733, *Water quality - Determination of the elimination and biodegradability of organic compounds*

in an aqueous medium - Activated sludge simulation test., in *ISO 11733*. 2004, ISO. p. 27.
18. OECD, *OECD Guideline for the Testing of Chemicals*, in *Simulation Test - Aerobic Sewage Treatment: 303 A: Activted Sludge Units - 303 B: Biofilms*. 2001, Organization for Economic Co-operation Development: Paris.
19. EEC, *Concerning Urban Waste Water Treatrment*, E.U. Council, Editor. 1991, EEC: O.J. European Communities. p. 13.
20. N.F. Gray, *Biology of Wastewater Treatment*.
21. S. Massa, M. Caruso, F. Trovatelli, M. Tosques, Comparison of plate count agar and R2A medium for enumeration of heterotrophic bacteria in natural mineral water, *World J Microbiol Biotechnol*, **1998**, 14(5), 727-730.
22. ATCC, *Product Information Sheet for ATCC 15597-B1*, A.T.C.C. (ATCC), Editor. 2005, ATCC. p. 2.
23. ATCC, *Mehtod 1602: Male-specific (F+) and Somatic Coliphage in Water by Single Agar Layer (SAL)*, U.S.E.P.A.O.o. Water., Editor. 2001. p. 30.
24. A. Garrido, R.M. Pashley, B.W. Ninham, Water sterilisation using different hot gases in a bubble column reactor, *J Environ Chem Eng*, **2018**, 6(2), 2651-2659.
25. USEPA, *Method 1602: Male-specific (F+) and Somatic Coliphage in Water by Single Agar Layer (SAL) procedure: U.S. Environmental Protection Agency Report 821-R-01-029, 38 p.* 2001.
26. J. Cormier, Janes, M., A double layer plaque assay using spread plate technique for enumeration of bacteriophage MS2, *J Virol Methods*, **2014**, 196, 86-92.
27. A.M. Kropinski, A. Mazzocco, T.E. Waddell, E. Lingohr, R.P. Johnson, Enumeration of bacteriophages by double agar overlay plaque assay, *Methods Mol Biol*, **2009**, 501, 69-76.
28. P. Zhang, S. Huang, N. Zhang, A.T. Kan, M.B. Tomson, Automated Analytical Method To Determine Solution Alkalinity of Oilfield Brine in the Presence of Weak Organic Acids, *Ind Eng Chem Res*, **2019**, 58(11), 4667-4673.
29. A. Garrido, R.M. Pashley, B.W. Ninham, Low temperature MS2 (ATCC15597-B1) virus inactivation using a hot bubble column evaporator (HBCE), *Colloids Surf B*, **2016**, 151, 1-10.
30. A.G. Sanchis, M. Shahid, R.M. Pashley, Improved virus inactivation using a hot bubble column evaporator (HBCE), *Colloids Surf B*, **2018**, 165, 293-302.
31. M.R.J. Clokie A.M. Kropinski, *Enumeration of Bacteriophages by Double Agar Overlay Plaque Assay*, in *Bacteriophages*, U.o. Leicester, Editor. 2009: Humana Press.
32. K. Seo, Lee, J. E., Lim, M. Y., Ko, G., Effect of temperature, pH, and NaCl on the inactivation kinetics of murine norovirus, *J Food Prot*, **2012**, 75(3), 533-40.
33. H. Zhong, K. Fujii, Y. Nakano, F. Jin, Effect of CO2 Bubbling into Aqueous Solutions Used for Electrochemical Reduction of CO2 for Energy Conversion and Storage, *J Phys Chem C*, **2015**, 119(1), 55-61.
34. W. Knoche, *Chemical Reactions of CO2 in Water*, in *Biophysics and Physiology of Carbon Dioxide: Symposium Held at the University of Regensburg (FRG) April 17–20, 1979*, C. Bauer, G. Gros, and H. Bartels, Editors. 1980, Springer Berlin Heidelberg: Berlin, Heidelberg. p. 3-11.
35. O. Erkmen, *Effects of Dense Phase Carbon Dioxide on Vegetative Cells*, in *Dense Phase Carbon Dioxide*. 2012, Wiley-Blackwell. p. 67-97.
36. H.M. Lin, Z. Yang, L.F. Chen, Inactivation of Saccharomyces cerevisiae by supercritical and subcritical carbon dioxide, *Biotechnol Progr*, **1992**, 8(5), 458-461.
37. R. Orij, M.L. Urbanus, F.J. Vizeacoumar, G. Giaever, C. Boone, C. Nislow, S. Brul, G.J. Smits, Genome-wide analysis of intracellular pH reveals quantitative control of cell division rate by pHc in Saccharomyces cerevisiae, *Genome Biol*, **2012**, 13(9), R80.
38. J.H.S. Richard, C. Flagan, *Fundamentals of air pollution engineering. Chapter 2 Combustion fundamentals.* Prentice-Hall, Inc.: California Institute of Technology. p. 59 - 166.
39. B.P. Reines, B.W. Ninham, Structure and function of the endothelial surface layer: unraveling the nano-architecture of biological surfaces, *Q Rev Biophys*, **2019**, 52, e13.
40. B.W. Ninham, R.M. Pashley, P. Lo Nostro, Surface forces: Changing concepts and complexity with dissolved gas, bubbles, salt and heat, *Curr Opin Colloid Interface Sci*, **2017**, 27, 25-32.
41. M.E. Karaman, B.W. Ninham, R.M. Pashley, Effects of Dissolved Gas on Emulsions, Emulsion Polymerization, and Surfactant Aggregation, *J Phys Chem*, **1996**, 100(38), 15503-15507.
42. H.K. Kim, E. Tuite, B. Nordén, B.W. Ninham, Co-ion dependence of DNA nuclease activity suggests hydrophobic cavitation as a potential source of activation energy, *Eur Phys J E*, **2001**, 4(4), 411-417.
43. B. Feng, R.P. Sosa, A.K.F. Mårtensson, K. Jiang, A. Tong, K.D. Dorfman, M. Takahashi, P. Lincoln, C.J. Bustamante, F. Westerlund, B. Nordén, Hydrophobic catalysis and a potential biological role of DNA unstacking induced by environment effects, *Proceedings of the National Academy of Sciences*, **2019**, 116(35), 17169-17174.
44. N.F. Bunkin, B.W. Ninham, P.S. Ignatiev, V.A. Kozlov, A.V. Shkirin, A.V. Starosvetskij, Long-living nano-

bubbles of dissolved gas in aqueous solutions of salts and erythrocyte suspensions, *J Biophotonics*, **2011**, 4(3), 150-164.
45. N.F. Bunkin, A.V. Kochergin, A.V. Lobeyev, B.W. Ninham, O.I. Vinogradova, Existence of charged submicrobubble clusters in polar liquids as revealed by correlation between optical cavitation and electrical conductivity, *Colloids Surf Physicochem Eng Aspects*, **1996**, 110(2), 207-212.
46. W. Kunz, P. Lo Nostro, B.W. Ninham, The present state of affairs with Hofmeister effects, *Curr Opin Colloid Interface Sci*, **2004**, 9(1), 1-18.
47. S. Gudkov, G. Lyakhov, V. Pustovoy, I. Shcherbakov, Influence of Mechanical Effects on the Hydrogen Peroxide Concentration in Aqueous Solutions, *Phys Wave Phenom*, **2019**, 27, 141-144.
48. Z. Fang, X. Wang, L. Zhou, L. Zhang, J. Hu, Formation and Stability of Bulk Nanobubbles by Vibration, *ACS J Surf Collo*, **2020**, 36(9), 2264-2270.
49. N.F. Bunkin, A.V. Shkirin, B.W. Ninham, S.N. Chirikov, L.L. Chaikov, N.V. Penkov, V.A. Kozlov, S.V. Gudkov, Shaking-Induced Aggregation and Flotation in Immunoglobulin Dispersions: Differences between Water and Water–Ethanol Mixtures, *ACS Omega*, **2020**, 5(24), 14689-14701.
50. M. Boström, V.S.J. Craig, R. Albion, D.R.M. Williams, B.W. Ninham, Hofmeister Effects in pH Measurements: Role of Added Salt and Co-Ions, *J Phys Chem B*, **2003**, 107(13), 2875-2878.
51. A. Salis, M. Cristina Pinna, D. Bilaničová, M. Monduzzi, P. Lo Nostro, B.W. Ninham, Specific Anion Effects on Glass Electrode pH Measurements of Buffer Solutions: Bulk and Surface Phenomena, *J Phys Chem B*, **2006**, 110(6), 2949-2956.
52. H.K. Kim, E. Tuite, B. Nordén, B.W. Ninham, Co-ion dependence of DNA nuclease activity suggests hydrophobic cavitation as a potential source of activation energy, *Eur Phy JE*, **2001**, 4(4), 411-417.
53. P. Lo Nostro, B.W. Ninham, A. Lo Nostro, G. Pesavento, L. Fratoni, P. Baglioni, Specific ion effects on the growth rates of Staphylococcus aureus and Pseudomonas aeruginosa, *Phys Biol*, **2005**, 2(1), 1-7.
54. M.H. Adams, Surface inactivation of bacterial viruses and of proteins, *J Gen Physiol*, **1948**, 31(5), 417-431.

Substantia
An International Journal of the History of Chemistry

Firenze University Press
www.fupress.com/substantia

Citation: A. Garrido Sanchis (2020) Thermal Inactivation of Viruses and Bacteria with Hot Air Bubbles in Different Electrolyte Solutions. *Substantia* 4(2) Suppl.: 69-77. doi: 10.36253/Substantia-832

Data Availability Statement: All relevant data are within the paper and its Supporting Information files.

Competing Interests: The Author(s) declare(s) no conflict of interest.

Thermal Inactivation of Viruses and Bacteria with Hot Air Bubbles in Different Electrolyte Solutions

Adrian Garrido Sanchis

School of Sciences, University of New South Wales, Canberra, Australia
E-mail: a.garridosanchis@adfa.edu.au

Abstract. Inactivation of viruses has been an insuperable inhibition to the use of recycled water. Substantial success in solving the problem has recently been achieved using a hot column evaporator (HBCE). Here we extend the technique to inactivate *E. coli* and MS2 viruses in different electrolyte solutions (0.17M NaCl and 0.01M $CaCl_2$). An increase in the inlet air temperature, from 103 to 250 °C, substantially improved the destruction of both pathogenic groups in either solution. *E. coli* proved to be more susceptible than viruses to inactivation in the HBCE. The phenomenon of inhibition of bubble coalescence above 0.17M for the NaCl solutions makes the HBCE process for this solution more efficient than for $CaCl_2$ solutions. In part, this is because of the higher air/water interfacial area with NaCl.

Keywords: virus, *E. coli*, inactivation, coalescence inhibition, hot bubble column evaporator (HBCE), sterilisation.

1. INTRODUCTION

Inactivation of microorganisms, specifically viruses and bacteria is the central problem for the sterilisation of aqueous solutions for almost any application. Pathogens have to be inactivated before the water can be used for industry or drinking water.

Wastewater from human activities usually contains bacteria like *E. coli and* human enteric viruses like hepatitis and rotavirus. If this water is to be reused, even for example in agriculture, it has to be disinfected.

Familiar methods for inactivating viruses, bacteria, and other microorganisms in aqueous media include heat, chemicals (e.g. ozone), irradiation (e.g. ultraviolet treatment), high-pressure treatment, and filtration (e.g. membrane filtration). Only reverse osmosis (RO) and nano-membrane pore scan block viruses. Heat treatments are energy-intensive. Better cheaper technologies are urgently needed. Such a technology has already been developed.[1] It is a surprisingly simple and successful method that kills viruses. It uses carbon dioxide or combustion gases in a bubble column. The process is now being scaled up for major industrial use. However, why and how it kills pathogens

is still obscure. It is to gain insight into the thermal mechanism that inactivates viruses and bacteria at different inlet air temperatures (103, 150, 200, and 250 °C) that is the goal of this work.

For a more detailed account of bubble column evaporators see the first paper in this volume. Bubble column evaporators (BCE) are typically in the form of cylindrical containers. A gas is introduced at the bottom of the column, via a porous frit. A continuous flow of rising bubbles passes through the liquid.[2] A gas-liquid bubble column provides a heat transfer rate between gas and liquid 100 times more efficiently than via bulk.[3] This heat transfer efficiency in a hot bubble column evaporator (HBCE) has been used in this work to inactivate *E. coli* and the MS2 virus for water reuse, without the need for boiling.[4] It does so by transferring heat from the hot air bubbles to the surfaces of pathogens contained in the solution through collisions.[5] The HBCE process requires less thermal energy than solution boiling because of the lower operating temperature of the solution. (the specific heat capacity per unit of weight, C_p, of air is four times lower than that of water).

Following from a previous work[5] two model solutions were chosen. The first one was 0.17 M NaCl. This is the concentration at which bubble coalescence is fully inhibited[6] and so gives an increased hot air/water interfacial area which should enhance the performance of the HBCE. The second solution at 0.01 M $CaCl_2$ is at a concentration less than that for bubble coalescence inhibition. So gas pathogen surface area is much reduced compared with the NaCl solution. But calcium adsorption by proteins should decreases pathogen surface charge (especially for the viruses) so this might be expected to reduce repulsive electrostatic forces with bubbles and so increase the HBCE inactivation efficiency.

The phenomenon of bubble-bubble interactions in electrolytes has remained unquantified until 1993.[6] Gas passing through a frit at the base of a water column produces bubbles. These ascend the column, the bubbles collide, fuse, and become larger. The column stays clear. However, when NaCl is added, and above an effective physiological concentration of 0.17 M, suddenly the bubbles no longer fuse. The column becomes dense with the production of a high-density of bubbles (typically 1–3 mm diameter).[6] The same phenomenon is responsible for the foaminess of the ocean, and the lack of foam production in freshwater.

The phenomenon occurs for a wide variety of electrolytes, always at the same effective concentration 0.17 M or the equivalent Debye length for all salts 1:1 2:1 2:2 3:1… and mixtures. For another class of electrolytes, there is no effect of salt on fusion inhibition.

2. MATERIAL AND METHODS

2.1. Experimental solutions.

Monovalent (1:1) and divalent (2:1) electrolyte solutions of 300 ml were prepared and sterilised by autoclaving in an Aesculap 420 at 15 psi, and 121-124 °C for 15 minutes. A NaCl concentration of 0.17 M NaCl or higher (≥ 99% purity, obtained from Sigma-Aldrich) in Milli-Q water, prevents bubble coalescence and increases the performance of the HBCE process by producing a higher air/water interfacial area. See ref[6] for detailed results.

0.01 M $CaCl_2$ solutions (≥ 99% purity, obtained from Sigma-Aldrich) in Milli-Q water do not reduce bubble coalescence, these solutions were chosen to reduce the virus and bacteria charge, perhaps reducing repulsion between bubbles and pathogens potential of increasing the HBCE inactivation efficiency, without affecting MS2 viability in this salt solution.[5,7]

2.2. Media preparation for experiments with E. coli.

The plate count method is commonly used for the identification of *E. coli* in marine water, treated drinking water, and wastewater. The water quality is assessed based on the ability of *E. coli* colonies to propagate in a layer of agar in the form of colony-forming units (CFU).[26,34]

For each experiment, 1 liter of medium was prepared from two solutions (A and B).

Solution A was composed of 6 g of NaCl, 13 g of tryptone, 1 g of yeast extract, and 1,000 ml of Milli-Q water. A pH value o 6.9 was measured with a Thermos Scientific Orion Star A214 pH meter. This solution was aseptically dispensed into two vessels, broth media, without agar, and the other one containing 1.41% agar (molecular biology-grade from Sigma-Aldrich). To dissolve the agar, the solution was heated to boiling and then sterilized by autoclaving in an Aesculap 420 at 15 psi, and 121-124 °C, for 15 minutes.

Solution B was used to enhance *E. coli* growth. This solution was prepared by adding 0.010 g of thiamine and 1 g of glucose to 50 ml of Milli-Q water and filtered through a 0.22 μm filter for its sterilization and then was aseptically added to solution A (in a proportion of 1:20), once cooled to 50 °C.

The 1.41 % agar solution was poured into 100 × 15 mm Petri dishes which were placed within the sterile field area around the Bunsen burner created by the updraft of the flame.[26]

2.3. Media preparation for experiments with viruses.

A specific optimized Double Layer Plaque Assay technique was used to assess the concentration of active MS2 viruses. This plaque assay method is commonly used for the detection of MS2 in treated drinking water, wastewater, and marine water. The water quality is assessed based on the ability of bacteriophages to kill the host bacteria and allow phages (circular zone of infected cells) to propagate in a confluent lawn of bacterial host cells, immobilized in a layer of agar.[8,9,10,11]

The Double Layer Plaque Assay requires an adequate growth medium to achieve better visibility and higher consistency. [10, 11] The medium is not commercially available. Therefore, it was prepared for each experiment in the form of two solutions, A and B. Solution A contains 15 g of tryptone, 1.5 g of yeast extract, 12 g of NaCl, and 1,425 ml of Milli-Q water. A pH value of 6.9 was measured with a Thermos Scientific Orion Star A214 pH meter. This solution was dispensed aseptically into three vessels with different amounts of agar (1% for the bottom agar, 0.5 % for the top agar, and no agar for the broth media). The agar used in these experiments was molecular biology-grade, obtained from Sigma-Aldrich. These solutions were first heated to boiling to dissolve the agar and then sterilized by autoclaving in an Aesculap 420 at 15 psi, and 121-124 °C, for 15 minutes.

Solution B was used to improve the visibility of the viruses. This solution was prepared by adding 1.5 g of glucose, 0.441 g of $CaCl_2$, and 0.015 g of thiamine to 75 ml of Milli-Q water and filtered through a 0.22 μm filter for its sterilization and then was aseptically added to solutions A (in a proportion of 1:20), once cooled to 50 °C.

The bottom agar was poured into 100 mm x 15 mm Petri dishes which were dried within the sterile field area around the Bunsen burner created by the updraft of the flame, to maintain local environmental sterility, until the agar was not too dry or too moist.[9]

2.4. Bacterial strain Escherichia coli C-3000 (ATCC 15597)

E. coli is a gram-negative bacteria with a straight cylindrical rod shape of 1.0-2.0 μm size.[12] It is found in the gastrointestinal tract of animals and humans. *E. coli* strains can be harmless or pathogenic to the host. As a result of fecal contamination, they can be found in water and soil. Therefore, it was selected as a representative model for bacteria in water[13,14] for the *E. coli* inactivation experiments and also for the virus sterilization experiments, as the MS2 virus-host.[11] *E. coli* C-3000 (ATCC15597) is a biosafety level 1 organism [15] and can be used as the MS2 virus-host.[11]

For a successful plaque assay, for virus inactivation experiments, the *Escherichia coli* C-3000 (ATCC 15597) must be in an exponential growth phase. This was achieved by growing two separate bacterial cultures: an overnight culture and a log phase culture.[10,11,16] The overnight culture was grown in 10 ml of broth media at 37 °C for 18-20 hours in a Labtech digital incubator; model LIB-030M, while shaking at 110 rpm with a PSU-10i orbital shaker. This overnight culture resulted in high numbers of bacteria in the culture and was used as a reference standard.

For a successful plate count, the concentration of *E. coli* from the overnight culture was calculated by serially 10-fold diluting 0.50 ml of *E. coli* overnight culture into a tube containing 4.50 ml sterile saline solution.[10]

To start the log phase *E. coli* culture, 1 ml of the overnight culture was transferred into 25-30 ml of broth media and incubated for 3 h at 37 °C, with gentle shaking at 110 rpm. To prevent loss of F-pill by the cells, they were then quickly cooled in a refrigerator, at 5 °C. A UV-VIS spectrometer, UVmini-1240, was then used to measure the optical density (OD) of the log phase *E. coli* culture. OD readings at 620 nm of between 0.8 and 1.1 indicated that the culture can be used in the plaque assay for the virus experiments and as a standard for the *E. coli* experiments.

2.5. Viral strains MS2 (ATCC 15597-B1)

A freeze-dried vial of MS2 bacteriophage was acquired from the American Type Culture Collection (ATCC). Bacteriophage MS2 (ATCC 15597-B1) was replicated using *Escherichia coli* C-3000 (ATCC 15597) according to the International Standard ISO 10705-1[16] and the Ultraviolet Disinfection Guidance Manual of the United States Environmental Protection Agency.[17] MS2 is a bacteriophage member of a class called group I. Its entire genome has been sequenced. It is a positive-sense, single-stranded RNA molecule of 3,569 nucleotides and it has an icosahedral structure. The virus has a hydrodynamic radius of about 13 nm.[18]

The concentration of the MS2 bacteriophage was calculated by adding 1.0 ml of broth media to the vial and serially 10-fold diluted 10 times by passing 0.50 ml of the bacteriophage into a tube containing 4.50 ml of broth medium.[10] 0.20 ml of the 4 hours host (log phase *E. coli* culture) and 10 mL of 0.5% top agar layer were poured over the Petri dishes with 1% bottom agar, dried around the Bunsen burner, 0.1 mL aliquots of 10^{-6} to 10^{-11} dilutions were inoculated on the surface of 14 Petri dishes.

After overnight incubation, 18-24 hours at 37 °C, individual plaques were countable and the concentration of the MS2 Bacteriophage was calculated using the equation:

Undiluted spiking suspension in PFU / mL = (PFU1 + PFU2… PFUn)/(V1 + V2…. Vn) [1]

Where PFU is the number of plaque-forming units from plates, Vn is the volume (in ml) of each undiluted sample added to the plates containing countable plaques and n is the number of useable counts.

2.6. Hot bubble column evaporator process (HBCE)

In the HBCE process, 27 l/min of ambient air was pumped through a silica gel desiccator, for dehumidification, and from there the dry air was passed through an electrical heater that maintained a hot air temperature, just above the sinter surface, of 103 °C 150 °C, 200 °C or 250 °C, depending on the experiment. The base of the bubble column evaporator was fitted with a 40-100 µm pore size glass sinter (type 2) of 135 mm diameter.

Once the solutions with known concentrations of virus and *E. coli* were prepared, two rounds of experiments (one for viruses and the other one for bacteria) were conducted in the HBCE. The temperature of the hot air (103 °C, 150 °C, 200 °C, 250 °C for this study) was measured, before the introduction of the solutions in the column, with a thermocouple above the sinter in the center of the dry column. The hot air passed through the sinter, in the form of bubbles, into the 300 ml solutions (0.17 M NaCl and 0.01 M $CaCl_2$). This inactivated the pathogens (MS2 viruses and *E. coli)* and heated the solution to a steady-state temperature (of 34 to 55 °C, depending on the inlet air temperature).

2.7. Disinfection experiments

A total of 18 viral and bacterial sterilization experiments were conducted in two solutions: 0.17 M NaCl and 0.01 M $CaCl_2$ at 4 different inlet air temperatures (103 °C, 150 °C, 200 °C, and 250 °C) in the HBCE.

The evaluation of bacteriophage and *E. coli* results was performed by the plaque assay and plate count methods (respectively).[8,10,19]

For each experiment, the target number of pathogens per 0.1 ml aliquot was 290. The following equation [4] was used to determine the spiking volume (that is, the volume that was taken from the virus/bacteria stock):

$$S = \frac{T * B}{C} \quad [2]$$

where S is the virus/bacteria stock volume (ml) added to 300 ml of solution, T is the target number of pathogen per sample, B is the total number of samples in 300 ml and C is the concentration (pathogen/ml) in the virus/bacteria dilution to be used for spiking.[17]

Once the solutions with the known concentration of pathogens were prepared the inactivation experiments at different temperatures were conducted in the HBCE. 1 ml samples were collected from 10 to 15 mm above the central area of the sinter. For each sample, 0.1 ml was spotted in triplicate following the double layer or the plaque count technique,[17] the same procedure that was used to determine the concentration of the MS2 bacteriophage or *E. coli*.

2.8. Zeta potential measurements

Zeta potential measurements were performed using a nano zeta sizer (Zetasizer Nano ZS Malvern Instruments Ltd.)[20] to study the MS2 virus and *E. coli* surface charge in various electrolyte solutions containing 10^8 MS2 viruses/ml or 10^8 *E. coli* C-3000/ml. Trapped air bubbles in the zeta cells were carefully avoided in the disposable zeta cells used to conduct the zeta measurements.

2.9. Data analysis

The linear decay model was used to study the time dependence of inactivation of pathogens (MS2 virus or *E. coli*). Plate counts were performed for all 18–21 plates from each of the experiments. The mean and standard deviation of each triplicated sample were obtained using bacterial survival factor, $\log_{10}(N_t/N_0)$, where N_0 is the initial number of pathogens per sample and N_t is the number of pathogens after a set exposure time in minutes.[21]

The decimal reduction time (D-value) was used to measure the temperature impact on both pathogenic groups (virus and bacteria). This can also be defined as the time needed to inactivate 90% (i.e. 1-log) of *E. coli* or virus (heat resistance). The Z-value is the temperature change required to change the D-value by a factor of 10.

D-values and Z-values were calculated using a linear exponential decay model or Thermal Death Model.[22]

$$\log(N_t) = \log(N_0) - \frac{t}{D} \quad [3]$$

$$\log\left(\frac{N_t}{N_0}\right) = -\frac{t}{D} \quad [4]$$

Where, D = the decimal reduction time, -(1/D) = the slope of the curve.

The Z-value is the increase in temperature needed to reduce the D-value by 1-log. It measures the impact of

a change in temperature on *E. coli* or virus inactivation. Thus:

$$Z = \frac{T_1 - T_2}{logD_1 - logD_2} \quad [5]$$

Where, T_1 is the first temperature of the interval, T_2 second temperature of the interval, and D_1 and D_2 are the D-values at T_1 and T_2.

3. RESULTS AND DISCUSSION

3.1. Theoretical model estimate of thickness and temperature of the transient hot water layer around the hot bubbles used in the inactivation of viruses and bacteria

The HBCE process successfully sterilised water contaminated with *E. coli* and MS2 viruses using hot air bubbles in two different solutions (0.17 M NaCl and 0.01 M $CaCl_2$). This inactivation process appears to be triggered by collisions between the bacteria and viruses with the hot air bubbles.[5,23,24] In the HBCE, a thin layer of heated water must also be formed transiently around the surface of the hot air bubbles, once they are released into the column. The thickness and the temperature of this thin, transient layer can be roughly estimated and it appears that this may be an important parameter to understand inactivation rates of virus and *E. coli* occurring at the HBCE. The collisions between these heated water layers, as well as the hot air in the bubbles themselves, is considered as the fundamental mechanism proposed for pathogen inactivation (*E. coli* and virus).[24,5]

During the HBCE experiments the inlet air temperature was always between 103 and 250 °C and the estimated average temperature of the heated water layers was in a range of 66 to 70 °C (see Table 1). By comparison, the column solution temperatures were always significantly lower (i.e. from 32 to 55 °C) (Fig. 1).

In the theoretical model, the temperature and the thickness of the hot water layer around the surface of a 1 mm diameter air bubble were estimated roughly for a range of inlet air temperatures using the formula:

$$T_{avg} = \frac{100 + T_c}{2} \quad [6]$$

where T_{avg} (in °C) is the average (transient) temperature of the hot water layer surrounding the air bubble and T_c (°C) is the steady-state temperature of the solution in the HBCE, with the assumption that the hot air bubbles had cooled from their initial inlet temperature to 100 °C when they first enter the bubble column.

The thickness of the transient has been estimated by balancing the heat supplied by the cooling bubble with

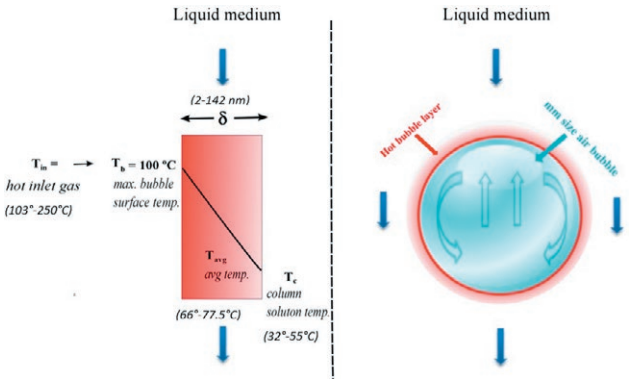

Figure 1. Model used to estimate the thickness and temperature of the hot layer around the air bubble at different inlet air temperatures.

Table 1. Estimated thickness and temperature of the transiently heated water layer around the air bubbles at different inlet air temperatures.

Inlet Gas Temperature T_{in} (°C)	Column Solution Temperature T_c (°C)	Density of Water (g/cm^3)	Hot Layer Thickness δ (nm)	Average Temperature of Hot Layer T_{avg} (°C)
103	32	0.99053	2	66
150	45	0.99022	39	72.5
200	51	0.98758	87	75.5
250	55	0.98569	142	77.5

the heat required to raise the film to this average temperature (see Table 1). Thus, since the volume of the film V is given by:

$$V = 4\pi r^2 z \quad [7]$$

where r is the bubble radius with a constant value of 0.001 m, z the layer thickness around the bubble and $r >> z$, this thermal energy balance is given by.[25]

$$C_p \Delta T V = C_{water} \Delta t 4\pi r^2 \rho_w z \quad [8]$$

where C_p air heat capacities per unit volume, C_{water} is the air heat capacity per unit weight, is the liquid water mass density, ΔT is the cooling of the air bubble (from inlet temperature to 100 °C) and Δt is the transient temperature increase in the water layer, relative to the column solution temperature.

In practice, likely, at least half of the heat supplied by the cooling bubble will be used in evaporating water into the bubble, and hence the calculated, roughly estimated, film thicknesses should be about halved.

Table 2. D and Z values for *E. coli* and MS2 virus in 2 different solutions (NaCl and $CaCl_2$).

Pathogen	Solutions	D-values at different inlet air temperatures (min.)					Z-values (°C)
		102 °C	150 °C	195 °C	205 °C	250 °C	
Virus	0.17M NaCl		121.95		29.41	6.15	77
	0.01M CaCl2		75.19		23.75	15.5	145
E. coli	0.17M NaCl	65.36	9.31	3.87			76
	0.01M CaCl2	33.00	18.73		3.51		105

Table 3. Zeta potential and bubble coalescence values for virus and bacteria in NaCl and $CaCl_2$ solutions.

Pathogen	Solution	% Coalescence	Zeta Potential (mV)
Virus	0.17 M NaCl	0	-6.32
	0.01 M $CaCl_2$	94	-2.55
E. coli	0.17 M NaCl	0	-12.50
	0.01 M $CaCl_2$	94	-12.20

When the inlet gas temperature increases, so does the thickness of the surface hot water layer around the bubble surface (Fig. 1). Consequently, the volume of the inactivation area is increased and this should make the inactivation rate more effective. Typical results from this model are given above (Table 1). Therefore, the inlet air temperature has a direct relation with pathogen inactivation as will be shown.

3.2. Temperature effects on pathogen inactivation in the HBCE in two different solutions

The impact of temperature for MS2 viruses and *E. coli* inactivation in the HBCE process at 103 °C, 150 °C, 200 °C and 250 °C inlet air temperatures was studied using two solutions: 0.17 M of NaCl and 0.01 M $CaCl_2$ (Table 2).

3.3. Solution comparison.

A 0.17 M solution of NaCl will inhibit bubble coalescence and so will increase the interfacial area of the bubbles within a bubble column [6], whereas the other solutions of 0.01 M $CaCl_2$ do not produce bubble coalescence inhibition [4, 26] (Table 3). Higher bubble interfacial areas were expected to increase will increase the chances of a collision between pathogens and hot air bubbles so improving virus and bacteria inactivation rates.

The Zeta potential for viruses presented lower values for $CaCl_2$ than for NaCl solutions. Presumably, this can be attributed to the absorption of calcium on the MS2 virus. *E. coli* did not present this selective absorption so that a similar Zeta potential was observed for both electrolyte solutions for this pathogenic group (see Table 3).

To understand the effect of hot air on different solutions (0.17 M NaCl vs 0.01 M $CaCl_2$) when thermally inactivating pathogens, such as MS2 virus and *E. coli*, decimal reduction times (D-values) at four inlet air temperatures, 50 °C intervals, were obtained (Table 2). The correlation between the log of the D-values and the corresponding temperature was represented in Fig. 2 and 3. A D-value is the time needed to inactivate 90% (i.e. 1-log) of the pathogens. To measure the heat resistance of these pathogens, Z-values have been calculated. The Z-value gives the temperature required to change the D-value by a factor of 10 and reflects the temperature impact on a pathogen (*E. coli* and MS2 virus in our study). The smaller the Z-value, the greater the sensitivity to heat.

Figures 2 and 3 show the minimum air bubbling times, at different temperatures, needed to achieve 1-log pathogen (virus and bacteria) inactivation in 0.17 M NaCl and 0.01 M $CaCl_2$ solutions. Above and to the right of the lines the pathogens will be sterilised by 1-log.

At low inlet air temperatures, between 100 and 150 °C, both pathogenic groups MS2 viruses and *E. coli* present higher inactivation rates in $CaCl_2$ than in NaCl solutions with D-values of 33.00 and 75.19 min for *E. coli* and virus in $CaCl_2$ solutions and 121.95 and 65.36 min for NaCl solutions (see Table 2 and Figures 2 and 3). For an intermediate range of temperatures, 150 to 200 °C NaCl solutions show better inactivation rates for *E. coli* with D-values of 9.31 min. than do $CaCl_2$ solutions do for viruses with D-values of 23.75 min. At higher temperatures, 200 to 250 °C, both solutions presented similar inactivation rates for *E. coli* with D-values in a range of 3.5 to 3.8 min. For viruses, NaCl solutions inactivated almost 3 times faster than $CaCl_2$ solutions with a D-value of just 6.15 min. (see Table 2 and Figures 2, and 3).

Virus (Z-value= 145 °C) and *E. coli* (Z-value= 105 °C) inactivation in $CaCl_2$ solutions is less temperature dependent than in NaCl solutions with Z-values of 77 °C for virus and 76 °C for *E. coli* See Table 2.

The effect of 0.17 M NaCl on the inhibition of bubble coalescence makes the HBCE process more temperature-dependent (reduced Z-values of 77 °C) than when

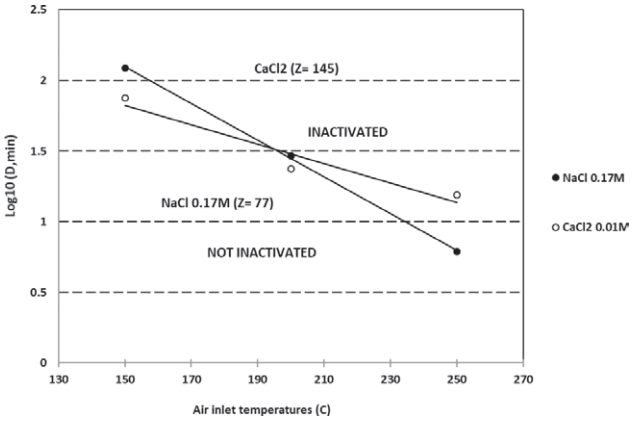

Figure 2. Comparison of the impact of temperature on MS2 virus inactivation between 0.17M NaCl and 0.01M $CaCl_2$ solutions.

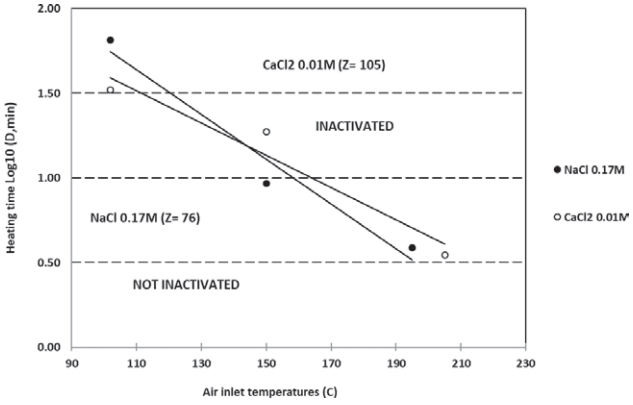

Figure 3. Comparison of the impact of temperature on *E. coli* inactivation between 0.17M NaCl and 0.01M $CaCl_2$ solutions.

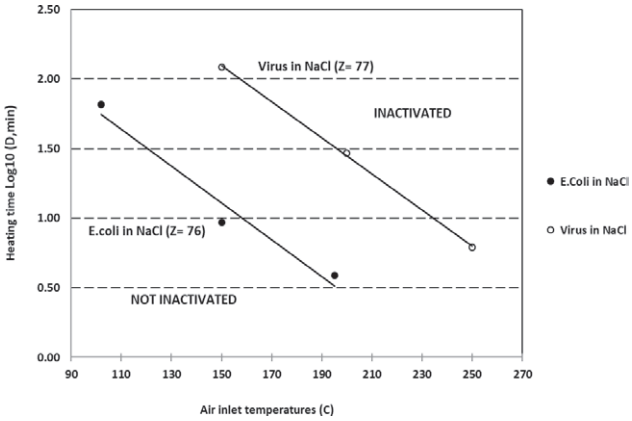

Figure 4. Comparison of the impact of temperature on *E. coli* and MS2 virus in 0.17M NaCl solutions.

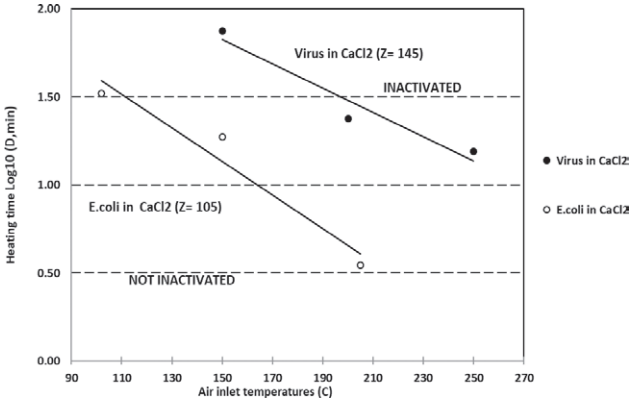

Figure 5. Comparison of the impact of temperature on *E. coli* and MS2 virus in 0.17M $CaCl_2$ solutions.

using $CaCl_2$ solutions. It can reasonably be assumed that this is due to the higher air/water interfacial bubble area produced. Consequently, there will be an increase in the volume of the transiently heated layer around the bubbles (see Table 1). When this volume increases, the chances of collision between pathogens and hot air bubbles will also increase with the consequent improvement in heat transfer.

3.4. Pathogenic group comparison

The World Health Organisation (WHO) studied the sterilization properties of hot liquids for thermal inactivation of bacteria and viruses in their guidelines for drinking-water quality.[27] WHO concluded that water temperatures above 60 °C effectively inactivate both pathogenic groups and when the temperature range lies between 60 and 65 °C, the inactivation of bacteria

For *E. coli* and MS2 virus inactivation in the HBCE was improved by increasing the inlet air temperatures from 103 to 250 °C. The thermal inactivation effect is more effective when the inlet air temperature increases. This is probably because of a thicker and hotter transient heated water layers created around the rising air bubble surface[28] (see Table 1). *E. coli* and viruses will be thermally inactivated by the collisions with this layer.

To understand the temperature effect of inlet air for thermal inactivation of pathogens (MS2 virus and *E. coli*) decimal reduction times (D-Values) at four different inlet gas temperatures, at intervals of 50 °C, were obtained and the correlation between log of the D-values and the corresponding temperature was represented in Figures 4 and 5. Again, D-values and Z-values have been calculated to assess the temperature impact on the pathogens.

Figures 4 and 5 show the minimum hot air bubbling times at different temperatures to achieve 1-log pathogen

(virus and bacteria) inactivation in 0.17 M NaCl and 0.01 M $CaCl_2$ solutions. Above and to the right of the lines the pathogens will be sterilised by 1-log.

For both solutions and for the entire range of temperatures *E. coli* was inactivated much faster than MS2 virus, therefore, *E. coli* proved to be more sensitive to hot air bubbles than MS2 virus (Fig. 4).

At 150 °C inlet air temperatures *E. coli* presented D-values of 9.31 min. in NaCl solutions and 18.73 min. in $CaCl_2$ solutions while the D-values for MS2 virus at the same temperature were 121.75 min. in NaCl and 75.19 min in $CaCl_2$ (Figures 4 and 5, Table 2). When inlet air temperature raised to 200 °C D-values for *E. coli* were 3.87 min in NaCl and 3.51 min in $CaCl_2$ for virus these values were much higher with 29.41 min for NaCl solutions and 23.75 in $CaCl_2$.

We can infer then that in the HBCE process, viruses and *E. coli* are inactivated when they are immersed in the hot water layer around the hot air bubbles or the bubbles themselves. The results agree with WHO with a faster inactivation for bacteria than for viruses, at similar water temperature [27]. But this phenomenon is considerably enhanced by using the HBCE for both solutions. Thus, the inactivation rates for viruses are much slower than for bacteria even though the gas temperature range for the virus (150 to 250 °C) was higher than for the bacteria (103 to 205 °C). This difference, might in part, due to the large size/momentum effect of *E. coli* compared with viruses. In a turbulent regime within the HBCE, the significantly larger momentum of *E. coli* cells is more likely to enable direct contact with the hot air phase what will increase their inactivation. A more likely contributor is the destruction of phospholipid bilayers of the bacteria with high temperatures.

4. CONCLUSIONS

This work has shown that viral and bacterial inactivation in the HBCE process can be substantially improved by raising the inlet air temperature, from 103 °C to 250 °C. According to the hot water layer theoretical model, when the inlet gas temperature increases, so will the thickness and the temperature of the transient heated water layer around the rising air bubble surface, and this appears to facilitate pathogen inactivation.

When thermal processes are used for water sterilization faster inactivation is always observed for bacteria than for viruses, at similar water temperatures. This phenomenon is considerably enhanced when using the HBCE independently of the solution.

The effect of 0.17 M NaCl on the inhibition of bubble coalescence makes the HBCE process more temperature-dependent than with $CaCl_2$ solutions by producing a higher air/water interfacial area and a better heat transfer.

5. ACKNOWLEDGMENTS

The author thanks Professors Ric Pashley and Barry Ninham for their helpful suggestions and advice and review.

6. REFERENCES

1. A. Garrido Sanchis, R. Pashley, B. Ninham, Virus and bacteria inactivation by CO_2 bubbles in solution, *npj Clean Water*, **2019**, 2(1), 5.
2. N. Kantarci, F. Borak, K.O. Ulgen, Bubble column reactors, *Process Biochem*, **2005**, 40(7), 2263-2283.
3. W.D. Deckwer, On the mechanism of heat transfer in bubble column reactors, *Chem Eng Sci*, **1980**, 35(6), 1341-1346.
4. M. Shahid, R.M. Pashley, R.A.F.M. Mohklesur, Use of a high density, low temperature, bubble column for thermally efficient water sterilization, *Desalin Water Treat*, **2013**, 52(22-24), 4444-4452.
5. A. Garrido, R.M. Pashley, B.W. Ninham, Low temperature MS2 (ATCC15597-B1) virus inactivation using a hot bubble column evaporator (HBCE), *Colloids Surf B*, **2016**, 151, 1-10.
6. V.S.J. Craig, B.W. Ninham, R.M. Pashley, Effect of electrolytes on bubble coalescence, *Nature*, **1993**, 364(6435), 317-319.
7. M. Brennecke, *Virus aggregation final*, in *Laboratorie de Chimie Environnementale (LCE)*. 2009, Ecole Polytechnique Federale de Lausanne. p. 47.
8. J. Cormier, M. Janes, A double layer plaque assay using spread plate technique for enumeration of bacteriophage MS2, *J Virol Methods*, **2014**, 196, 86-92.
9. M.R.J. Clokie, A.M. Kropinski, *Enumeration of Bacteriophages by Double Agar Overlay Plaque Assay*, in *Bacteriophages*, U.o. Leicester, Editor. 2009: Humana Press.
10. ATCC, *Mehtod 1602: Male-specific (F+) and Somatic Coliphage in Water by Single Agar Layer (SAL)*, U.S.E.P.A.O.o. Water., Editor. 2001. p. 30.
11. ATCC, *Product Information Sheet for ATCC 15597-B1*, A.T.C.C. (ATCC), Editor. 2005, ATCC. p. 2.
12. G. Reshes, S. Vanounou, I. Fishov, M. Feingold, Cell shape dynamics in Escherichia coli, *Biophys J*, **2008**, 94(1), 251-264.

13. X. Yang, *Introduction*, in *A Study on Antimicrobial Effects of Nanosilver for Drinking Water Disinfection*. 2017, Springer Singapore: Singapore. p. 1-12.
14. I. Gaska, O. Bilenko, S. Smetona, Y. Bilenko, R. Gaska, M. Shur, Deep UV LEDs for Public Health Applications, *Int J High Speed Electron*, **2014**, 23(03n04), 1450018.
15. ATCC, *Product Sheet Escherichia coli (ATCC 15597)*, ATCC, Editor. 2015.
16. I. 10705-1, *Water quality - Detection and enumeration of bacteriphages- Part 1*, in *ISO 10705-1*. 1995, International Organization for Standardization: ISO.
17. U.S.E.P. Agency, *Preparing and Assaying Challenge Microorganismos*. 2006. p. 267- 277.
18. K. Valegard, L. Liljas, K. Fridborg, T. Unge, The three-dimensional structure of the bacterial virus MS2, *Nature*, **1990**, 345(6270), 36-41.
19. M.R.J. Clokie, A.M. Kropinski, *Enumeration of Bacteriophages by Double Agar Overlay Plaque Assay*, in *Bacteriophages*, U.o. Leicester, Editor. 2009: Humana Press.
20. M.I. Ltd., *Zetasizer Nano User Manual*, M.I. Ltd., Editor. 2009. p. 312.
21. K. Seo, Lee, J. E., Lim, M. Y., Ko, G., Effect of temperature, pH, and NaCl on the inactivation kinetics of murine norovirus, *J Food Prot*, **2012**, 75(3), 533-40.
22. J. Smelt, S. Brul, *Thermal Inactivation of Microorganisms*. Vol. 54. 2014. 1371-85.
23. A. Garrido, R.M. Pashley, B.W. Ninham, Water sterilisation using different hot gases in a bubble column reactor, *J Environ Chem Eng*, **2018**, 6(2), 2651-2659.
24. X. Xue, R.M. Pashley, A study of low temperature inactivation of fecal coliforms in electrolyte solutions using hot air bubbles, *Desalin Water Tret*, **2015**, 1-11.
25. M. Shahid, C. Fan, R.M. Pashley, Insight into the bubble column evaporator and its applications, *Int Rev Phys Chem*, **2016**, 35(1), 143-185.
26. C. Fan, M. Shahid, R.M. Pashley, Studies on Bubble Column Evaporation in Various Salt Solutions, *J Solution Chem*, **2014**, 43(8), 1297-1312.
27. WHO - Geneva, World Health Organization, *Guidelines for drinking-water quality*, W.H. Organization, Editor. 2007. p. 38.
28. A.G. Sanchis, M. Shahid, R.M. Pashley, Improved virus inactivation using a hot bubble column evaporator (HBCE), *Colloids Surf B*, **2018**, 165, 293-302.

Substantia
An International Journal of the History of Chemistry

Firenze University Press
www.fupress.com/substantia

Citation: M. Ziaee, M. Taseidifar, R.M. Pashley, B.W. Ninham (2020) Selective Removal of Toxic Ions from Water/ Wastewater: Using a Novel Surfactant. *Substantia* 4(2) Suppl.: 79-88. doi: 10.36253/Substantia-830

Data Availability Statement: All relevant data are within the paper and its Supporting Information files.

Competing Interests: The Author(s) declare(s) no conflict of interest.

Selective Removal of Toxic Ions from Water/ Wastewater: Using a Novel Surfactant

Mohammad Ziaee[1], Mojtaba Taseidifar[1], Richard M. Pashley[1], Barry W. Ninham[2,*]

[1] *School of Science, University of New South Wales, Northcott Drive, Canberra, Australia*
[2] *Department of Applied Mathematics, Research School of Physical Sciences, The Australian National University, Canberra, Australia*
*Corresponding author: barry.ninham@anu.edu.au

Abstract. Pollution of drinking water by toxic heavy-metal ions is a matter of concern worldwide. These ions occur naturally, and also from environmental spills, radioactive wastes and other industrial waste. Arsenic and lead are typical examples. A novel green surfactant, purpose designed, and environmentally friendly is shown to be extremely effective and specific for heavy metal ion removal. This is a considerable step forward on previous technologies. Surfactants have been used universally to remove organic and inorganic contaminants from water. But little selectivity has been achieved. After usage, the residual surfactants are discharged into surface waters or sewage systems. This causes environmental pollution. In this review, three surfactants from different classes (novel green surfactant, synthetic chemical surfactant and biosurfactant) are compared in terms of their efficiency in flotation, removal of different heavy-metal ions, biodegradability, and toxicity level, including their advantages and disadvantages.

Keywords: ion flotation, green surfactant, chemical synthetic surfactant, biosurfactant, water treatment, toxic heavy metals.

1. INTRODUCTION

Low but toxic amounts of heavy metal ions like arsenic occur naturally in drinking water. It is a long-standing problem. It affects millions of people. There has been little progress towards its solution. Similar environmental issues of increasing concern are: wastewater from mining operations, battery and electronic manufacturing, the paper industry, radioactive waste disposal, which all pose massive challenges. The discharge of such waste waters into rivers and lakes affect aquifers, discharge into the ocean and can cause serious problems to marine life and to public health.[1,2]

Heavy metals such as chromium (Cr), cobalt (Co), lead (Pb), cadmium (Cd), mercury (Hg), nickel (Ni), zinc (Zn) and copper (Cu) are not biodegradable and they can accumulate in human tissues. Cobalt and chromium are a big problem with joint replacement surgery, and horse racing! Another

example: although zinc is essential for normal function of both eukaryotic and prokaryotic cells and other different human tissues, excessive amounts of zinc cause skin irritation and vomiting.[3] Another ion, copper is an important element in human metabolism; however, excessive ingestion of copper can lead to spasms, vomiting, and even death.[4]

Heavy-metal ions like radioactive strontium and radium in low concentration are among the most damaging in nuclear waste. So new techniques that allow removal, and especially selective removal of contaminating heavy metal ions, wherever they occur, is a matter of highest importance. The urgent need for separation technologies for rare earth metals for the computer industry reinforce this.

In the medical field, a large amount of research has focused on establishing critical heavy metal levels in the human body. For instance, nickel, lead, mercury, cadmium, and chromium can be carcinogenic and cause serious problems for normal human organ function.[5-7]

The existence of heavy metal ions in industrial wastewater, a matter of global concern, has led to stricter environmental regulations. Much research on the removal of heavy metal ions from water has been aimed at several different methods: membrane technology, adsorption, ion exchange, chemical precipitation, and flotation. Of these, flotation is a technique of much promise. This method is able to remove heavy metal ions using bubbles and a 'collector' in the aqueous phase. In the context of minerals beneficiation, collectors are usually surfactant molecules. They are used in froth flotation of particulates, metal rich minerals that attach to surfactant coated air bubbles. They typically leave unwanted substances like silica and clays behind in the flotation process.

There are several processes that use this technique: froth flotation, dissolved air flotation, precipitation flotation, and ion flotation that are well described in references.[8,9]

Ion flotation derives from the mineral separation industry. It is a technique also capable of removing organic and inorganic contaminants either in anionic or cationic forms from wastewaters.[10] Currently, ion flotation is in use for the recovery of precious metals, ion separation, and wastewater treatment because of its low energy consumption, inexpensive ancillary devices, flexibility, and a negligible amount of sludge.[11,12] A simple schematic of a laboratory scale ion flotation process is depicted in Figure 1 and shown in the graphical abstract.

The conventional picture of how froth flotation separation of mineral particles works has it that surfactants adsorb onto finely ground hydrophilic mineral particles, selectively converting the required mineral to possess a hydrophobic surface. The continuous flow of a high density of bubbles captures the coated hydrophobic particles and carries them off into the collected foam. Naturally hydrophobic particles, such as talc and some mineral sulphides, float naturally, whereas most minerals are hydrophilic and will not float unless coated with an adsorbed layer of surfactant. The selective and controlled hydrophobicity of the mineral particles in a mixture, facilitates the successful selectivity of the froth flotation separation process.

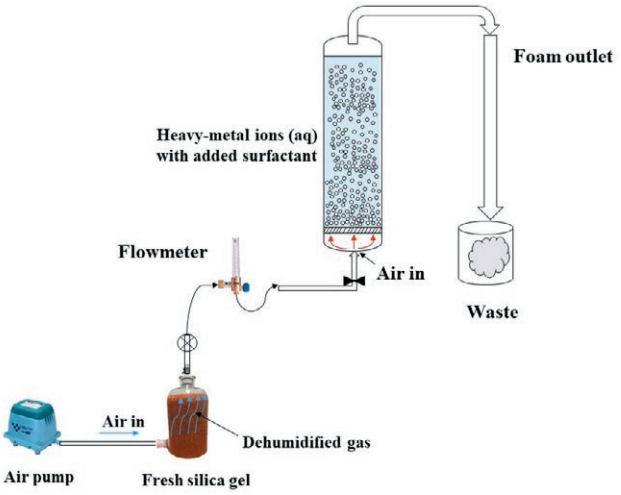

Figure 1. Schematic diagram of the column setup for ion flotation process.

Our interest is in ion flotation for which the simplest explanation is different but closely related to froth flotation. The important process is that surfactants adsorb to bubbles below the CMC, to provide a monolayer to which the heavy metal ions to be collected adsorb specifically and as the bubbles rise, the surfactant-ion complex can be collected in the froth. At the same time, ions in solution may selectively bind to the surfactant head-group(s) and then be adsorbed at the bubble surface. Whichever process dominates, it works and our aim here is to make the process as specific as possible. In this study, the effectiveness of a novel kind of surfactant designed for specificity in the removal of heavy metal ions has been explored and compared with two other standard surfactants.

2. GREEN SYNTHETIC SURFACTANTS. HINTS FROM BIOLOGY

The promise of flotation techniques has not been matched by expectation so far. The goal of selectivity, of specificity, in harvesting heavy metal ions has remained

an Elusive Eldorado. Taking a lesson from biology, from enzymes, we have synthesised novel surfactants that go some way to achieving improved specificity. There are double pluses in this. The most widely used surfactants are made from petroleum compounds. These surfactants are made by a wide range of industries, which themselves produce toxic products for the environment. Remediation methods of these surfactants include ozonation, UV radiation and catalyst-coupled auto-oxidations, which are of economic concern. In addition, the levels of CO_2 liberated by petrochemical processes for the synthesis of the surfactants was found to be as high as 37% in the EU. Further, cationic surfactants with quaternary ammonium and pyridinium headgroups widely used in many household and pharmaceutical/ medical applications are potent immunosuppressants (see section 3 below).

These difficulties have led to the idea of going green, that is, through the search for a new class of surfactants which are to be obtained from raw renewable materials.[13] Environmentally friendly, or "Green Surfactants" can be obtained from natural and renewable ingredients. They should be biodegradable with low toxicity. There are evolving stricter environmental regulations due to increasing concern about traditional surfactants which create health and environmental /water pollution issues. Our goal in this search for green surfactants that are ion specific is made easier in that Nature has already shown the way. The shape, folding and hydrophobicity that determines structure and function of proteins and enzymes all depend on binding of specific ions to sites with specific dispersion forces and hydration compatibility. There are myriad examples of active sites within enzymes that bind specific, usually divalent, ions that can serve as guides to templates that suggest prototypes for novel synthesised surfactant head groups.

2.1. L-cysteine an exemplar

L-cysteine is an amino acid that is biosynthesised in the human body, mostly in keratin-rich tissues, such as nails, hair, and skin which have the highest level of cysteine.[14] Different cysteine-based green surfactants with suitable hydrocarbon chain lengths can be synthesized by reacting octanoyl chloride and dodecanoyl chloride with cysteine.[15,16]

Such surfactants have many useful properties. They are edible! So, their potential as a soap in industry is immense. For our present problem of heavy metal contamination, then if a slight amount of this surfactant remains in treated water after a flotation process, it will not be harmful for human beings compared to traditional chemical synthetic surfactants. It might even put hair on our chests!

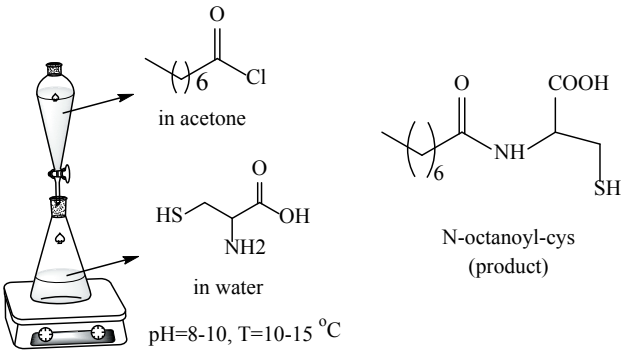

Figure 2. Schematic for the synthesis of octanoyl-cysteine surfactant from octanoyl chloride, in acetone, and L-cysteine in water.[16]

2.2. Reaction synthesis

Below is the standard reaction synthesis method which can be used to obtain different cysteine-based surfactants.[15,16] The obtained surfactant was recrystallised in a mixture of ethanol:water (V:V 50:50) twice before using in the ion flotation experiments.

2.3. Green Surfactant Properties

These surfactants can be naturally decomposed by enzymes known as peptidases and proteases, a process that takes place in the intestine. The process produces octanoic acid and cysteine, which are both natural and have health benefits. Octanoic acid is an organic carboxylic acid, which is found naturally in the milk of various mammals and is a minor component of kernel oil, palm, and coconut oil. Octanoic acid (caprylic acid), can also be taken as a dietary supplement due to its anti-inflammatory and antimicrobial properties. As a consequence, both of the products of this decomposition reaction are compatible with the human body.

2.4. An application to arsenic removal

Cysteine-based surfactants with different chain lengths were developed and used for removal of low level of arsenic from drinking water.[16] Single chain octanoyl-cysteine (s-octanoyl-cys) and single chain dodecanoyl-cysteine (s-dodecanoyl-cys) have been applied as the collectors in a single stage batch ion flotation process. The

Table 1. Ion flotation results for the removal of arsenic ions (5 mg/L or ppm) at pH = 8 using different cysteine-based surfactants (reproduced from[15]). C(surfactant) = 0.01M.

Surfactant	As (ppm) after 30 mins	Removal (%) after 30 mins	As (ppm) after 60 mins	Removal (%) after 60 mins
S-Octanoyl-cys 1st crystallized	0.442	91.2	0.120	97.6
S-Octanoyl-cys 2nd crystallized	0.135	97.3	0.025	99.5
S-Dodecanoyl-cys 2nd crystallized	3.310	33.8	2.34	53.2

results obtained are given in Table 1. The single-chain octanoyl-cysteine surfactant was found to have a relatively high CMC value of 0.1 mol/L and showed significant foaming ability. The corresponding values for dodecanoyl cysteine surfactant were found to be 0.009 mol/L. The dodecanoyl-cysteine surfactant, with the lowest CMC value, also showed the lowest solubility in water and the weakest foaming ability.

It is necessary to avoid forming micelles, in which the surfactant spontaneously forms surfactant aggregates that make the flotation process less efficient. During the ion flotation experiments here , the initial concentrations of these surfactants were used at about 0.1 of their CMC(s), i.e. at levels of 0.01 M and 0.0009 M, respectively.

These experiments were performed at pH = 8 (using NaOH 10% w/w), and an initial concentration of 5 mg/L (ppm) for arsenic, As (V) ions. Based on Table 1, S-octanoyl-cys shows superior affinity with As (V) rather than S-dodecanoyl-cys surfactant. As a consequence, after 60 minutes ion flotation, S-octanoyl-cys was able to remove 97.6% of As (V), while S-dodecanoyl-cys was capable of removing only 53% of the initial arsenic ions from solution.

Most of the research on the binding process of heavy metals to cysteine is limited to computational studies, however there are few experimental studies based on NMR analyses. It has been reported[17] that three cysteine molecules are needed to make the $As(Cys)_3$ complex, coordinated with thiolates. This coordination, resulting in a pyramid trigonal site, makes the interaction between As (III) (arsenite) and sulfhydryl in cysteine group more stabilized; and this demonstrates a possible cause of the toxicity mechanism for arsenic in causing structural distortion of cysteine-based biopolymers. [18] Binding of Cd ions with cysteine was also studied using ^{113}Cd NMR spectrum, which displayed 9 resonances where 8 of them were at the range of 600-700ppm, related to S-thiolate coordination for the Cd ions. While one resonance occurred at 516ppm, which is destabilised and can be interrupted. This resonance relates to C-terminal cluster of Cd ions to the cysteine molecule.[19]

2.5. The effects of the input gas type

The effect of different gases on the efficiency of heavy metal ion removal in the ion flotation process was also examined.[15] Pure nitrogen and dry air were introduced separately to the bubble column to produce bubbles with an average of about 2 mm diameter. The results presented in Table 2 show that air gas was slightly better for ion flotation than nitrogen, removing 99.9% of the arsenic compared with 99.4% for nitrogen (see Table 2). Mercury was found to have the highest removal rate in the presence of nitrogen gas, at 99.9%; with air, 99.6% was removed. Table 2 indicates the results of removing arsenic, lead, and mercury from water using S-octanoyl-cys as the collector and N_2 and air as the inlet gases to produce bubbles.

The results presented in Table 2, illustrate that the green S-octanoyl-cys surfactant is entirely able to remove lead, mercury, and arsenic ions from aqueous solutions, at levels more than 99%. According to the Table, this green surfactant almost gives the same efficiency either using

Table 2. Flotation results for of 5 mg/ L (ppm) of different heavy-metals ions using s-octanoyl-cys, C(surfactant) = 0.01M and pH = 8. (Reproduced from[15]).

Contaminant	Inlet gas	As (ppm) after 30 mins	Removal (%) after 30 mins	As (ppm) after 60 mins	Removal (%) after 60 mins	Ref.
Lead	air	0.399	92.0	0.0467	99.1	15
Lead	nitrogen	0.257	94.9	0.032	99.4	15
Mercury	air	0.024	99.5	0.020	99.6	15
Mercury	nitrogen	0.022	99.6	0.002	99.9	15
Arsenic	air	0.137	97.3	0.006	99.9	20
Arsenic	nitrogen	0.032	99.4	0.029	99.4	20

air or nitrogen gas. This high efficiency is remarkable and suggests that the process could be used to treat water contaminated with heavy metal ions like arsenic (As), which is a naturally occuring toxic element and human carcinogen in countries such as Bangladesh, India, Brazil and China. Its concentration has often been increased in ground water due to industrial waste from mining, metallurgy and also the use of toxic substances such as pesticides, in some parts of the world, leading to even greater levels of contamination of ground water and crops.[21,22]

From these results, it appears that air could be used instead of the relatively expensive pure nitrogen gas to reduce the operation costs of a commercial ion flotation plant. It is notable that according to World Health Organisation (WHO), the acceptable level of heavy-metal ions in drinking water is less than 0.5 mg/L. After 60 minutes ion flotation using the green S-octanoyl-cys surfactant, the concentrations of lead, mercury, and arsenic ions in water are 0.046, 0.02, and 0.029 mg/L, respectively, which are 10 to 25 times lower than the WHO standard level.

Following the excellent results for removal of heavy metal ions by using S-octanoyl-cys as the collector, a wide range of heavy metals were examined in a single batch stage flotation process. Removal of eight common heavy metals: cadmium, chromium, strontium, calcium, gold, mercury, lead, and arsenic were determined after sixty minutes bubbling.[12,15,20] The initial concentration of each single metal ion was 5 mg/L and the initial concentration of used S-octanoyl-cys surfactant was adjusted to 0.01 M. These experiments were carried out at pH = 8 (using NaOH 10% w/w) and the results obtained for each single heavy-metal ion are reported in Table 3.

As the Table shows, there is an excellent affinity between the surfactant and various metal ions in the aqueous solutions. This green biodegradable surfactant is able to adsorb Sr, Cr, As, Hg, Cd, Pb, and Ca ions through a physico-chemical process and remove them from drinking water with high removal rates (%) of 99.8, 99.7, 99.6, 99.4, 99.2, 99.1, and 97.3, respectively. According to Table 3, this natural surfactant has less affinity to bind with gold ions in comparison with other metals examined. It shows a moderate removal rate of 42.4%. Gold ions were used in the form of $AuCl_4^-$ ions.

We have also found[12] that the ion flotation system using S-octanoyl-cys surfactant at an initial concentration of 0.01 M and at pH 8, can successfully remove copper ions at 50 mg/L in aqueous solutions. The results show a high removal rate for copper ions using this surfactant and in the hydrated form of copper ions, in the sulphate salt, even visual observation shows a noticeable visible blue colour at concentrations higher than about 200 mg/L of Cu^{2+}. The results observed for ion flotation of copper ions at 500 mg/L indicates that using the S-octanoyl-cys causes this colour to rapidly disappear, which confirms that the ion-flotation process should be directed towards the development of novel treatment methods for the removal of heavy-metal ions, such as Cu, from mining wastewater.

2.6. Selectivity in mixtures of ions

Extending these results, we have illustrated the removal efficiency and the selectivity of S-octanoyl-cys to remove several ions in a mixed aqueous solution with initial concentrations of 5 mg/L.[12] These experiments were undertaken in the presence of an initial concentration of 0.01 M of the surfactant and pH = 8. After 60 minutes samples were taken. Although this green surfactant showed excellent removal rates for single metal ions in aqueous solution, after ICP-MS analysis for a

Table 3. Ion flotation results of different single heavy metals in aqueous solution using S-octanoyl-cys (C(surfactant, initial) = 0.01M, C(heavy metal ion, initial) = 5 mg/L (ppm), and pH = 8). (Reproduced from[12, 20]).

Single pollutant	C (ppm) after 30 min	Removal (%) after 30 mins	C (ppm) after 60 min	Removal (%) after 60 mins
Cd (II)	0.27	94.6	0.04	99.2
Cr (III)	0.33	93.4	0.001	99.7
Sr (II)	0.03	99.4	0.009	99.8
Ca (II)	0.72	85.6	0.13	97.3
Au (III)	3.12	37.6	3.38	42.4
Hg (II)	0.02	98.5	0.02	99.4
Pb (II)	0.40	92.02	0.05	99.1
As (V)	1.37	72.6	0.02	99.6

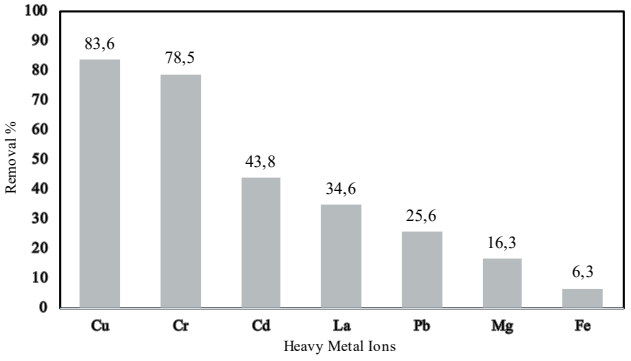

Figure 3. Removal rate of different heavy-metal ions in a mixed aqueous solution using S-octanoyl-cysteine surfactant through a batch stage ion flotation process (Reprinted from Ref. 12, with permission from Elsevier).

mixture of metal ions, the results indicated that some of the metal ions were clearly bound more strongly. The removal rate results for an aqueous solution containing seven heavy-metal ions (Cu, Cr, Cd, La, Pb, Mg, and Fe) are depicted in Figure 3.

Based on the data from ICP-MS analysis, copper and chromium ions also show strong binding affinity to the surfactant with removal rates of 83% and 78%, respectively. However, in comparison with other heavy-metal ions, iron and magnesium ions exhibited less bonding. The removal rates were 16% and 6% for Mg and Fe ions, respectively.

2.7. Other applications

In addition to removal of pollutants from water, there is another significant application for ion flotation. This technique has found its way as a promising separation process with especial interest in heavy metal ions recovery. Therefore, further research on the effectiveness of the green S-octanoyl-cys surfactant has been conducted for separation of iron and lanthanum ions in an aqueous solution. For this purpose, a mixed solution of 5 mg/L of lanthanum and iron ions was studied and ion flotation was undertaken using an initial concentration of 0.01 M of s-octanoyl-cys surfactant at pH = 8. After 60 minutes bubbling, samples of solution remaining in the column were taken and the results are reported in Table 4.

It is evident that besides excellent heavy metal removal capacity of this surfactant, it also can be used to separate or produce specific recovery of some metal ions from a mixed aqueous solution. The Table indicates S-octanoyl-cys surfactant has a stronger binding affinity with lanthanum ions rather than iron ions. As a result, La recovery is almost 12 times more than Fe removal.

3. CHEMICAL SYNTHETIC SURFACTANTS

Chemical synthetic surfactants were initially used by Sebba[23] in a flotation process to concentrate inorganic ions from aqueous solutions. This type of surfactant is widely used in industry since the molecular structures could be designed as they are required. Alkane sulfonate, alkylamine, disodiumalkyl malonate, xanthate, sodium oleate, and sodium dodecyl sulfate (SDS) have been widely applied in ion flotation.[24] Besides the advantage of using chemical synthetic surfactants, there are a number of drawbacks to applying them in industry.

Table 4. Flotation results for a mixed solution of iron and lanthanum, using s-octanoyl-cys surfactant in a batch process. Initial concentration of La and Fe are 5 mg/L. Initial surfactant concentration = 0.01M and pH=8. (Reproduced from[12]).

Mixed Ions	C (mg/L) after 30 min	Removal (%) after 30 min	C (mg/L) after 60 min	Removal (%) after 60 min
Iron	4.78	4.4	4.6	8.0
Lanthanum	1.00	80	0.27	94.6

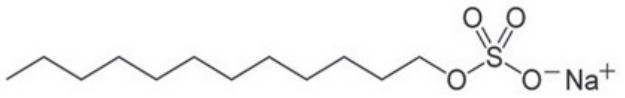

Figure 4. The molecular structure of sodium dodecyl sulfate (SDS) as an anionic chemical synthetic surfactant.[34]

Chemical synthetic surfactants demonstrate considerable biological activity. For instance, anionic chemical synthetic surfactants are able to form bonds with macromolecules such as enzymes, peptides, and DNA which might alter their surface charge and vary the folding of the polypeptide chain. This binding can interfere their normal biological functions.[25,26]

Furthermore, quaternary ammonium compounds are the most common type of cationic surfactants. They are known to bind with the inner membrane of bacteria. As a result, this type of chemical synthetic surfactant can disorganise them and affect their normal functions[27-32] cationic surfactants are potent immunosuppressants, a fact as widely known as it is ignored.

The fact that our cysteine-based surfactants are not toxic and actually edible is highly significant. In addition, non-ionic surfactants demonstrate the ability of binding with phospholipid membranes and different proteins. This binding raises permeability of cellular membranes which can cause cell damage or death due to loss of amino acids and ions.[33]

It is notable that sodium dodecyl sulfate (SDS) is one of the most well-known chemical synthetic surfactant that is used widely in industries. This surfactant is also known as sodium lauryl sulfate. Figure 4 illustrates the molecular structure of this anionic surfactant.

The effectiveness this surfactant in removing heavy-metal ions has been assessed in a number of reports. For example, Yenidünya[34] applied SDS as the collector in an ion flotation process for removing Mn^{2+}, Cu^{2+}, and Zn^{2+} from water. After 60 minutes flotation, 99.8%, 90.5%, and 73.4% of magnesium, copper, and zinc were removed from the aqueous solution. Table 5 shows the results obtained from various studies using SDS for removal of heavy-metal ions through ion flotation. According to Table 5, although a frother and axillary ligand have been used, the achieved removal rates are

Table 5. Using sodium dodecyl sulfate and tea saponin surfactants in the process of ion flotation for removing heavy metal ions from water.

Surfactant	Pollutants	Condition	Removal (%)	Ref.
Sodium Dodecyl Sulphate (SDS)	Zn (II), Mn (II), Cu (II)	C_{metal}:C_{SDS}:$C_{axillary\ ligand}$ =1:5:5, pH = 4	90.5, 99.8, 73.4	35
Sodium Dodecyl Sulphate (SDS)	Cr (III)	C_{SDS} : C_{metal} = 2, pH = 8	91.6	36
Sodium Dodecyl Sulphate (SDS)	Cu (II), Pb (II), Ni (II), Cd (II), Zn (II)	C_{metal}:C_{SDS} = 1, pH = 9	97.5, 87.5, 87, 83, 92.5	37
Sodium Dodecyl Sulphate (SDS)	Cd (II)	C_{SDS} : C_{Cd} =3, pH = 4	94	38
Sodium Dodecyl Sulphate (SDS)	Ni (II), Zn (II)	C_{SDS} : C_{metal} = 13.5, pH = 9.7	99.8, 90.4	39
Sodium Dodecyl Sulphate (SDS)	Cd (II)	C_{SDS} : C_{metal} = 2, pH = 10	99.8	38
Tea Saponin	Cu (II)	$C_{surfactant}$: C_{metal} = 3, pH = 4	81	40
Tea Saponin	Cd (II)	$C_{surfactant}$: C_{metal} = 11, pH = 7.5	8	41
Tea Saponin	Pb (II)	$C_{surfactant}$: C_{metal} = 11, pH = 4.8	12	41

relatively lower than those obtained by S-octanoyl-cys surfactant.

Tea saponin is uncharged with a CMC value of about 0.72 mM.[33] In a recent study,[34] tea saponin was used for removing cadmium, lead and copper ions in aqueous solutions. The highest efficiencies were achieved when the tea saponin ratio to heavy metal was 3:1 at pH = 6. The removal efficiency decreased slightly with increasing in ionic strength obtained by adding NaCl solutions (in the range 0.001-0.004 M).

4. BIOSURFACTANT

Biosurfactants are known as ecosystem friendly compounds, which are found in plants, animals, and microbes etc. Most biosurfactants are found either in anionic or non-ionic form and only a few of them are cationic.[42,43] The lipophilic part of these biosurfactants is usually based on long-chain fatty acids. [4] The hydrophilic sector can be an amino acid, cyclic peptide, carbohydrate, alcohol, or carboxylic acid.[45] Biosurfactants are widely applied as additives in food industry, adsorbents for environmental treatment, and flocculants because of their properties such as biodegradability, low toxicity, and biocompatibility.[46] Due to stricter environmental regulations, biosurfactants would be the promising alternatives to the traditional chemical synthetic surfactants.

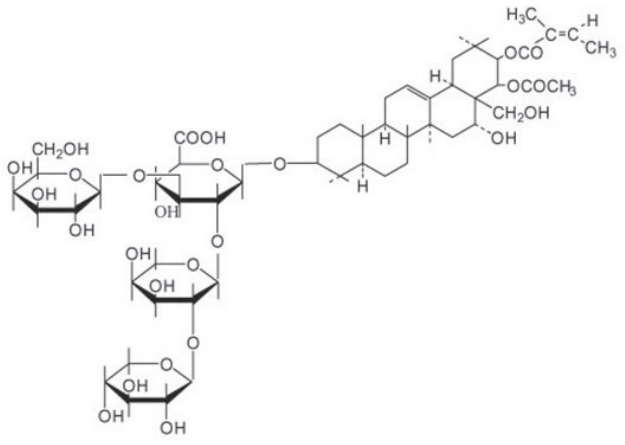

Figure 5. The molecular structure of tea saponin molecule as an example of a non-ionic biosurfactant.[47]

The tea saponin molecule, found in Camellia plants, is a non-ionic surfactant which has been used in soil and water treatments.[47] The molecular structure of this surfactant is depicted in Figure 5.

A very small number of studies have been conducted to ascertain the effectiveness of heavy metal ion removal using tea saponin biosurfactant in the ion flotation technique. Table 5 shows the results obtained for heavy metal removal from water using tea saponin as the collector in an ion flotation process. The removal rates of Cu^{2+}, Cd^{2+}, and Pb^{2+} from water using this surfactant were found to be 81%, 8%, and 12%, respectively. Although tea saponin is a relatively ecosystem friendly biosurfactant, it does not show a satisfactory removal rate for cadmium and lead ions. It is notable that long flotation times and low removal efficiency are the main limits of applying biosurfactants in large-scale water treatment plants. Therefore, more research is required on developing biosurfactants to make them of greater practical value in the water treatment industry.

5. SUMMARY

The Na-octanoyl amino acid-based single-chain cysteine surfactant shows a high-water solubility and high foaming ability over a wide pH range. In a batch ion flotation process, this surfactant was able to remove

97–99% of the initial 5 ppm level of strontium, lanthanum, arsenic and different heavy metal ions at levels typically present in contaminated water, in a simple, single-stage physiochemical process. The surfactant showed significantly lower efficiency for the removal of iron, selenium and gold ions. In a solution mixed with heavy-metal ions, including arsenic, copper, cadmium, magnesium, lanthanum, chromium, lead and iron, the surfactant shows a higher affinity to bind with arsenic, copper and chromium compared with the others. Moreover, the effectiveness of this surfactant for removal of gold ions from aqueous binary mixtures in the presence of iron and mercury ions has been explored. This new surfactant is highly efficient compared with commercial surfactants (e.g., SDS and CTAB) for ion flotation. Importantly, it is also an environmentally acceptable compound. It can be decomposed into cysteine (amino acid) and octanoic acid (caprylic acid), which is taken as a dietary supplement. The surfactant has the potential for wide usage in ion flotation and in froth flotation.[48]

In the ion flotation experiments reported here, the cysteine surfactant concentration was in the range 10 mM (initially) to 5 mM, whereas the initial metal ion concentrations were in the range: 0.1 mM (for light elements ions such as Ca) and 0.025 mM (for the heavy elements, Au, Hg and Pb). Hence, in all cases, the surfactant was always present in the batch column process in excess, relative to the metal ion concentrations.

It should be noted that in this protocol the surfactant, unlike the ions, was not fully depleted from the column during 60 minutes of bubbling time. That is, the surfactant concentration was approximately halved in the column during the bubbling experiments. Hence, the surfactant was always present in the column at a much higher concentration level than the metal ions, during these experiments. These conditions were used to illustrate the relative selectivity of the surfactant for a range of different ions, as shown in the results, from a series of single and mixed ion flotation experiments presented here.

By comparison, in a commercial process much longer ion flotation columns would be used to increase the efficiency of ion collection relative to the surfactant concentration, since the surfactant coated rising bubbles will continue to remove ions from the solution until they have reached saturated adsorption densities.

6. CONCLUSIONS AND FUTURE PROSPECTS

We have shown that ion flotation can be used for the treatment of contaminated waters containing toxic metallic ions. The example given is that of the S-octanoyl-cys surfactant, which can remove a range of low level toxic ions from water. The significant selectivity of this surfactant for some of the ions studied is also most encouraging. It suggests that the ion flotation process could be used to completely separate some specific ion mixtures that pose problems, like rare earth ions. More research and methodological work is needed on how to harvest other valuable ions, such as gold, to reduce the significant costs of current refining processes. The surfactant also showed high efficiency for the removal of relatively high concentrations of copper ions, which could be used as a promising alternative for the treatment of different industrial and mining wastewater.

From a sustainability view-point, the surfactant collected in the foam can be released from the bound ion and then re-used to enable recycling of the surfactant. This surfactant also readily decomposes into products which are acceptable for human ingestion. It is also worth mentioning that the commercial development of this process would have a wide variety of applications and can address the global issue of heavy metal ion presence in drinking water.

A final observation: many enzymes have an active site, a hydrophobic pocket, centred around a specific ion which is generally divalent. The binding is highly specific and the ion sets the required structure of the hydrophobic pocket that allows the enzyme-substrate lock and key process. For example, with the restriction enzyme Hindi 2, the specific ion, e.g magnesium, can be replaced by suboptimal calcium, manganese, copper or nickel. [48] With the suboptimal replacements, the enzyme can still “work”, but not so efficiently and the chain of subsequent reactions is affected. This explains why trace elements are necessary, for both plants and animals, and why small amounts of ions like arsenic are so toxic. That different enzymes bind different trace ions so selectively may provide an entry into a wide range of other novel surfactants.

7. ACKNOWLEDGMENTS

The authors would like to gratefully acknowledge Ms. Rabeya Akter for ICP-MS analysis support within the Mark Wainwright Analytical at the University of New South Wales. The authors also thank Dr Fatemeh Makavipour for her assistance with the arsenic flotation experiments. The author M.Z. acknowledges UNSW Canberra to provide postgraduate research scholarship.

REFERENCES

1. I.Y. El-Sherif, S. Tolani, K. Ofosu, O.A. Mohamed, A.K. Wanekaya, Polymeric nanofibers for the removal of Cr(III) from tannery waste water, *J. Environ. Manage.*, **2013**, 129, 410-413.
2. K. Fischer, H.-P. Bipp, Removal of Heavy Metals from Soil Components and Soils by Natural Chelating Agents. Part II. Soil Extraction by Sugar Acids, *Water, Air, Soil Pollut.*, **2002**, 138, 271-288.
3. C. Mohanna, Y. Nys, Effect of dietary zinc content and sources on the growth, body zinc deposition and retention, zinc excretion and immune response in chickens, *British Poultry Science*, **1999**, 40, 108-114.
4. WHO, Copper in drinking-water, in, WHO, **2004**.
5. WHO, Mercury in Drinking-water, in: Background document for development of WHO Guidelines for Drinking-water Quality, **2005**.
6. Z. Yu, X. Zhang, Y. Huang, Magnetic Chitosan–Iron(III) Hydrogel as a Fast and Reusable Adsorbent for Chromium(VI) Removal, *Ind. Eng. Chem. Res.*, **2013**, 52, 11956-11966.
7. D. Ko, J.S. Lee, H.A. Patel, M.H. Jakobsen, Y. Hwang, C.T. Yavuz, H.C.B. Hansen, H.R. Andersen, Selective removal of heavy metal ions by disulfide linked polymer networks, *J. Hazard. Mater.*, **2017**, 332, 140-148.
8. C.K. Jain, I. Ali, Arsenic: Occurrence, toxicity and speciation techniques, *Water Res.*, **2000**, 34, 4304-4312.
9. P.L. Smedley, D.G. Kinniburgh, A review of the source, behaviour and distribution of arsenic in natural waters, *Appl. Geochem.*, **2002**, 17, 517-568.
10. M.J. Rosen, J.T. Kunjappu, Micelle Formation by Surfactants, in: *Surfactants and Interfacial Phenomena, John Wiley & Sons, Inc.*, **2012**, 123-201.
11. H. Polat, D. Erdogan, Heavy metal removal from waste waters by ion flotation, *J. Hazard. Mater.*, **2007**, 148, 267-273.
12. M. Taseidifar, M. Ziaee, R.M. Pashley, B.W. Ninham, Ion flotation removal of a range of contaminant ions from drinking water, *J. Environ. Chem. Eng.*, **2019**, 7(4), 103263.
13. S. Rebello, A.K. Asok, S. Mundayoor, M.S. Jisha, Surfactants: toxicity, remediation and green surfactants, *Environ. Chem. Lett.*, **2014**, 12, 275-287.
14. S. Shen, X.-F. Li, W.R. Cullen, M. Weinfeld, X.C. Le, Arsenic binding to proteins, *Chem. Rev.*, **2013**, 113, 7769-7792.
15. M. Taseidifar, F. Makavipour, R.M. Pashley, A.F.M.M. Rahman, Removal of heavy metal ions from water using ion flotation, *Environ. Technol. Innov.*, **2017**, 8, 182-190.
16. M. Taseidifar, Environmental applications of a biodegradable cysteine-based surfactant, *Ecotoxicol. Environ. Saf.*, **2020**, 206, 111389.
17. B.T. Farrer, C.P. McClure, J.E. Penner-Hahn, V.L. Pecoraro, Arsenic(III)−Cysteine Interactions Stabilize Three-Helix Bundles in Aqueous Solution, *Inorg. Chem.*, **2000**, 39, 5422-5423.
18. M.C. Teixeira, V.S.T. Ciminelli, M.S.S. Dantas, S.F. Diniz, H.A. Duarte, Raman spectroscopy and DFT calculations of As(III) complexation with a cysteine-rich biomaterial, *J. Colloid Interface Sci.*, **2000**, 315, 128-134.
19. C. Baumann, A. Beil, S. Jurt, M. Niederwanger, O. Palacios, M. Capdevila, S. Atrian, R. Dallinger, O. Zerbe, Structural Adaptation of a Protein to Increased Metal Stress: NMR Structure of a Marine Snail Metallothionein with an Additional Domain, Angew. *Chem. Int. Ed.*, **2017**, 56, 4617-4622.
20. F. Makavipour, R.M. Pashley, A.F.M.M. Rahman, Low-Level Arsenic Removal from Drinking Water, *Global Challenges*, **2019**, 3(3), 1700047.
21. J.F. Ferguson, J. Gavis, A review of the arsenic cycle in natural waters, *Water Res.*, **1972**, 6, 1259-1274.
22. B. Maher, Measuring arsenic in rice – an Australian reference material, *Royal Australian Chemical Institute*, **2015**, pp. 38.
23. F. Sebba, Concentration by Ion Flotation, *Nature*, **1959**, 184, 1062-1063.
24. L.-C. Shen, X.-T. Nguyen, N.P. Hankins, Removal of heavy metal ions from dilute aqueous solutions by polymer–surfactant aggregates: A novel effluent treatment process, *Sep. Purif. Technol.*, **2015**, 152, 101-107.
25. T. Cserhati, E. Forgács, G. Oros, Biological activity and environmental impact of anionic surfactants, *Environ. Int.*, **2002**, 28, 337-348.
26. R. Waninge, M. Paulsson, T. Nylander, B. Ninham, P. Sellers, Binding of Sodium Dodecyl Sulphate and Dodecyl Trimethyl Ammonium Chloride to β-Lactoglobulin: A Calorimetric Study, *Int. Dairy J.*, **1998**, 8, 141-148.
27. G. McDonnell, A.D. Russell, Antiseptics and Disinfectants: Activity, Action, and Resistance, *Clin. Microbiol. Rev.*, **1999**, 12, 147-179.
28. R.B. Ashman, B.W. Ninham, Immunosuppressive effects of cationic vesicles, *Mol. Immunol.*, **1985**, 22, 609-612.
29. R.B. Ashman, R.V. Blanden, B.W. Ninham, D.F. Evans, Interaction of amphiphilic aggregates with cells of the immune system, *Immunol. Today*, **1986**, 7, 278-283.
30. P. Lo Nostro, B.W. Ninham, A. Lo Nostro, G. Pesavento, L. Fratoni, P. Baglioni, Specific ion effects

on the growth rates of Staphylococcus aureus and Pseudomonas aeruginosa, *Phy. Biol.*, **1986**, 2, 1-7.
31. B.W. Ninham, K. Larsson, P. Lo Nostro, Two sides of the coin. Part 1. Lipid and surfactant self-assembly revisited, *Colloids Surf. B: Biointerfaces*, **2017**, 152, 326-338.
32. B.W. Ninham, K. Larsson, P. Lo Nostro, Two sides of the coin. Part 2. Colloid and surface science meets real biointerfaces, *Colloids Surf. B: Biointerfaces*, **2017**, 159, 394-404.
33. T. Cserhati, Alkyl Ethoxylated and Alkylphenol Ethoxylated Nonionic Surfactants: Interaction with Bioactive Compounds and Biological Effects, Environ. *Health Perspect.*, **1995**, 103, 358-364.
34. L. Chang, Y. Cao, G. Fan, C. Li, W. Peng, A review of the applications of ion floatation: wastewater treatment, mineral beneficiation and hydrometallurgy, *RSC Adv.*, **2019**, 9, 20226-20239.
35. X.-L. Yu, Y. He, Development of a Rapid and Simple Method for Preparing Tea-Leaf Saponins and Investigation on Their Surface Tension Differences Compared with Tea-Seed Saponins, *Molecules*, **2018**, 23(7), 1796.
36. X.Z. Yuan, Y.T. Meng, G.M. Zeng, Y.Y. Fang, J.G. Shi, Evaluation of tea-derived biosurfactant on removing heavy metal ions from dilute wastewater by ion flotation, *Colloids Surf., A:Physiochem. Eng. Aspects*, **2008**, 317, 256-261.
37. M. Doğutan Yenidünya, Recovery of Zn(II), Mn(II) and Cu(II) in Aqueous Solutions by Foam Fractionation with Sodium Dodecyl Sulphate in Combination with Chelating Agents, *Sep. Sci. Technol.*, **2006**, 41, 1741-1756.
38. V.S.H. Khoshdast, Efficient chromium removal from aqueous solutions by precipitate flotation using rhamnolipid biosurfactants, *Physicochem. Probl. Miner. Process.*, **2018**, 54, 1014–1025.
39. Ü. Yenial, G. Bulut, Examination of flotation behavior of metal ions for process water remediation, *J. Mol. Liq.*, **2017**, 241, 130-135.
40. A.I. Zouboulis, K.A. Maris, Removal of cadmium from dilute solutions by flotation, *Water Sci. Technol.*, **1995**, 31, 315-326.
41. F.S. Hoseinian, M. Irannajad, A.J. Nooshabadi, Ion flotation for removal of Ni(II) and Zn(II) ions from wastewaters, *Int. J. Miner. Process.*, **2015**, 143, 131-137.
42. T. Pekdemir, S. Tokunaga, Y. Ishigami, K.-J. Hong, Removal of cadmium or lead from polluted water by biological amphiphiles, *J Surfactants Deterg.*, **2000**, 3, 43-46.
43. J. Tang, J. He, X. Xin, H. Hu, T. Liu, Biosurfactants enhanced heavy metals removal from sludge in the electrokinetic treatment, *Chem. Eng. J.*, **2018**, 334, 2579-2592.
44. S. Shekhar, A. Sundaramanickam, T. Balasubramanian, Biosurfactant Producing Microbes and their Potential Applications: A Review, *Crit. Rev. Environ. Sci. Technol.*, **2015**, 45, 1522-1554.
45. E.Z. Ron, E. Rosenberg, Natural roles of biosurfactants, *Environ. Microbiol.*, **2001**, 3, 229-236.
46. C.N. Mulligan, Recent advances in the environmental applications of biosurfactants, *Curr. Opin. Colloid Interface Sci.*, **2009**, 14, 372-378.
47. R. Cohen, D. Exerowa, Surface forces and properties of foam films from rhamnolipid biosurfactants, *Adv. Colloid Interface Sci.*, **2007**, 134-135, 24-34.
48. M. Taseidifar, A.G. Sanchis, R.M. Pashley, B.W. Ninham, Novel water treatment processes, *Substantia,* **2019**, 3(2), 11-17.
49. H. K. Kim, E. Tuite, B. Nordén, B. W. Ninham, Co-ion dependence of DNA nuclease activity suggests hydrophobic cavitation as a potential source of activation energy, *Eur. Phys. J.,* **2001**, 4, 411-417.

Substantia
An International Journal of the History of Chemistry

Firenze University Press
www.fupress.com/substantia

Citation: M. Ziaee, M. Taseidifar, R.M. Pashley, B.W. Ninham (2020) Efficient Dewatering of Slimes and Sludges with a Bubble Column Evaporator. *Substantia* 4(2) Suppl.: 89-94. doi: 10.36253/Substantia-841

Data Availability Statement: All relevant data are within the paper and its Supporting Information files.

Competing Interests: The Author(s) declare(s) no conflict of interest.

Efficient Dewatering of Slimes and Sludges with a Bubble Column Evaporator

Mohammad Ziaee[1], Mojtaba Taseidifar[1], Richard M. Pashley[1,*], Barry W. Ninham[2]

[1] *School of Science, UNSW Canberra, Northcott Drive, Canberra, Australia*
[2] *Department of Applied Mathematics, Research School of Physical Sciences and Engineering, Australian National University, Canberra, Australia*
*Corresponding author: r.pashley@adfa.edu.au

Abstract. The recalcitrant nightmare of de-watering slime/sludge is a major issue, for both industry and the environment. A simple process is developed that solves the problem. It uses a bubble column evaporator (BCE) with heated dry air. The model slime to illustrate the de-watering process was a concentrated dispersion of spherical 5 micron silica particles in pure water. Typical slime samples were de-watered in the range 20-35% colloid/water (w/w) using dry inlet gases pre-heated to temperatures of 150 °C and 250 °C. The BCE process was run at sub-boiling temperatures, with the column solution in the range, 43 and 74 °C, with those two inlet temperatures operating for de-watering the slime**.** A significant bonus is that the pure water vapour produced can be condensed and used as a source of high-quality water for reuse. The BCE process offers simplicity, resilience to slime feed quality, and a pure water biproduct. It also offers a continuous and controlled low-maintenance process. These are clear advantages in de-watering a wide variety of industrial slimes and sludges. In addition, the process involves the passage of a continuous flow of hot dry gases. This causes the dispersion to remain sufficiently fluid to allow easy transportation. However, once the hot gas flow ceased, the dispersion immediately solidified. The success of the bubble column process for dewatering and validation of the mechanism is even more enhanced if helium is used instead of air. It appears that hot helium atoms can disrupt water hydrogen-bonding in the liquid surrounding the hot bubbles and this enhances water vapour collection efficiency. The bubble method appears to offer more than significant advantages over other methods, such as hydrocyclone methods, which are often used to de-water mining wastes.

Keywords: slime and sludge de-watering, bubble column evaporator, silica spheres, helium gas.

1. INTRODUCTION – SLIME AND SLUDGE DE-WATERING

The words sludge or slime are used to mean a high water-content colloidal dispersion that stubbornly resists de-watering. De-watering is a process in which water is separated from the solids, to thicken up the waste for disposal or end-user purposes. This is a problem that poses major eco-

nomic, environmental and safety challenges for a range of sludge types in industries like clay production, phosphate mining, diamond mining, sewage sludges, sand washing, and sludges from paper mills, gold mining, and different metallic ores. As an example, phosphate mining produces clay tailing slurries or sludges which are usually less than 10% solid content. This must be de-watered to a value of at least 40% by an economically acceptable process. Often the solid content has an average particle size equal to or less than 50 microns. This is generally characteristic of suspensions of siliceous and clay solids, and for other minerals, depending on the industrial process.[1,2] Different techniques to de-water sludges are employed in different industries. They include coagulation, flocculation, grinding, heating, applying high voltages and using hydrocyclones. However, each of these techniques has its own drawbacks and they often fail to provide desirable solid content levels. For instance, flocculation and coagulation methods need considerable amounts of chemical agents which might cause environmental, economic and safety concerns.[2,3]

Conventional methods, for example ponding, also suffer from disadvantages. It is time consuming and requires large acreages of land to effectively de-water large volumes of slurries. This also increases land maintenance and remediation costs, also causes environmental and health issues.[2] Hydrocyclones are frequently used in different industries for de-watering of solid-liquid suspensions. Generally, large hydrocyclones are used for separation of particles (larger than 25 μm) from slimes, while smaller hydrocyclones with diameters less than 10mm are usually used to separate fine particles smaller than 10 μm.

The controllability and efficiency of the hydrocyclone method are limited and this method needs to be augmented by further processes like centrifugation to optimise dewatering.[4] Hydrocyclones, in general, are comprised of an inlet, a main body and two outlets. In order to increase the recovery of solids, the feed pressure needs to be increased. Other conditions such as relationship between cutsize, bypass and water recovery determine the performance. Thus, depending on the waste type, they need to be optimised in order to obtain maximum efficiency in de-watering.[5,6] Also, for further improvement of the hydrocyclone process, a centrifuge can also be incorporated. This uses centrifugal forces made by spinning a bowl or basket to separate the sludge solids from the liquid.[7]

In this work a novel method of de-watering slime using a bubble column evaporator (BCE) is developed and evaluated. This can be used for many different sludge thickening applications. The BCE exploits the high interfacial area between gas bubbles and water and acts as a natural semi-permeable membrane. This process uses hot bubbles to allow water vapour to escape but not the solid particles. So far, a wide range of useful applications of the BCE process have been developed by our research group. The list includes: a new method for the precise measurement of enthalpies of vaporisation (ΔH_{vap}) of concentrated salt solutions;[8,9] evaporative cooling;[10] a new method for thermal desalination[11-13] a novel method for sub-boiling thermal sterilization;[9,14-18] a novel method for the low-temperature thermal decomposition of some solutes in aqueous solution;[19] and a new approach to aqueous solute precipitation in a controlled manner.[20] In addition, a bubble column condenser has also been designed for the production of high- quality water as condensate.[21-23] Figure 1 depicts the various applications of the BCE technique we have developed. The green arrows refer to the previous applications developed by the BCE method, while the red arrow refer to the latest application of this method.

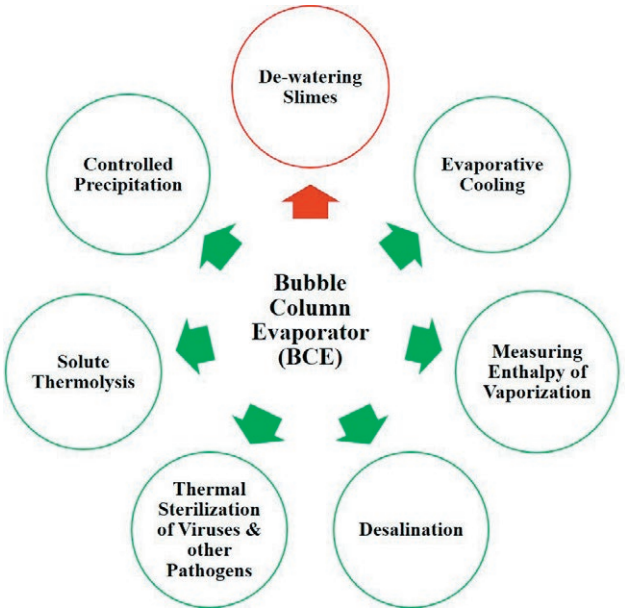

Figure 1. Different applications for the BCE process.

2. MATERIALS AND METHODS

For each experiment 50 g of 5 μm spherical silica powder supplied by US Research Nanomaterials Company was used. Milli-Q water was added to pure 50 g of silica powder to reach 250 g of water-silica mixture. Then, the mixtures were stirred to produce uniform dispersions. The measured turbidity of silica mixtures (20%

weight), was about 40,000 NTU measured by HACH 2100AN Turbidimeter. The concentration of solid particles (slime thickness) in the mixtures were calculated using the following formula:

$$\textit{solid concentration } \% = \frac{\textit{weight of dry solid}}{\textit{total weight of mixture}} \times 100 \quad (1)$$

The BCE process is illustrated schematically in Figure 2. In this work, four experiments were undertaken for de-watering the prepared slime samples using two different gases (dry air, helium) at two different outlet gas temperatures (150 °C, 250 °C).

In each experiment, 250 mL of the prepared slime sample was poured into a 120 mm diameter open-top glass column (Büchner type, Pyrex® Borosilicate, VWR) with a sinter porosity of number 2. The outlet gas temperature was varied using a Tempco air heater (300W) with a thermocouple temperature monitor and an AC Variac electrical supply. A TENMARS thermometer (TM-84N, Taiwan) with the accuracy of ± 1.5 °C was applied on the surface of the sinter to measure the temperature of hot gas introduced to the empty column.

The air gas was produced from an air pump (Hiblow HP40, Philippines) and a BOC gas flow meter was used to measure flow rates. The temperature of the column solution was also continuously monitored using a thermocouple positioned at the centre of the aqueous mixtures. Due to our requirement of a slime gas temperature up to 250 °C, the temperature of the gas heater might reach above 700 °C. That necessitates the use of a steel heater and brass connectors for the downstream, and the use of Rockwool as an insulating material.

The effectiveness of the BCE process was quantified experimentally based on the weight loss of the slime using the following equation:

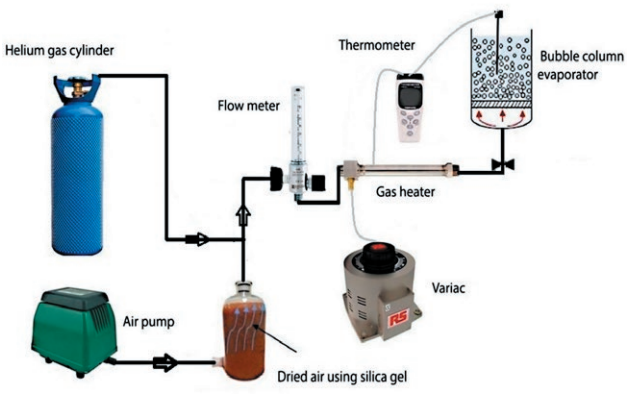

Figure 2. Schematic diagram of BCE system for slimes de-watering.

$$\textit{water loss } \% = \frac{(W1-W2)}{(W1-Wd)} \times 100 \quad (2)$$

where W_1, W_2, and W_d are the initial weight of slime, final weight of slime, and the weight of dry solid compounds, respectively

3. RESULTS AND DISCUSSION

3.1. Results for Air

In the first experiment, 250 g of a silica-water mixture with a concentration of 20% was poured to the column using hot dry air at a temperature of 150 °C. After 45 minutes using hot air with a flow rate of 34 (L/min) for production of hot bubbles in the aqueous mixture, the residual mixture was weighed and the new solid concentration (slime thickness) was calculated using equation (1). The results are presented in Table 1. It shows that the final solid concentration (slime thickness) is 30.5%. Also, the density of the dispersion was increased in this process from 1.05 g/mL to 1.16 g/mL and the operating temperature of the BCE slime remained at about 48-49 °C.

In the second experiment applying dry air at the temperature of 250 °C with a flow rate of 34 L/min over 45minutes, the silica concentration increased from 20 to 34.7%. The temperature of the slime mixture remained in the range of 65-66 °C. The density increased from an initial value of 1.05 to 1.25 g/mL. An example of the bubbling process is shown in the photograph in Figure 3.

3.2. Results for Helium

When helium gas was used for producing bubbles, the helium flow rates were measured using two methods: by weighing the helium cylinder and from calculations based on the helium cylinder pressure differential. The first method gave a flow rate of about 13.9 L/min and the calculations based on the helium cylinder pressure differential led to a flow rate of 10.4 L/min. Therefore, an average value of 12 L/min was used for comparison with the 34 L/min dry air flow. According to the previous studies, helium is a more effective gas in bubbling because of its natural production of smaller bubbles, even in pure water.[13]

In these experiments helium flowed into the BCE column containing 20% silica dispersion at an inlet temperature of 150 °C, flow rate of 12 L/min. After 45 min with the column solution equilibrating at about 41 °C, the silica concentration was increased to 28% and the

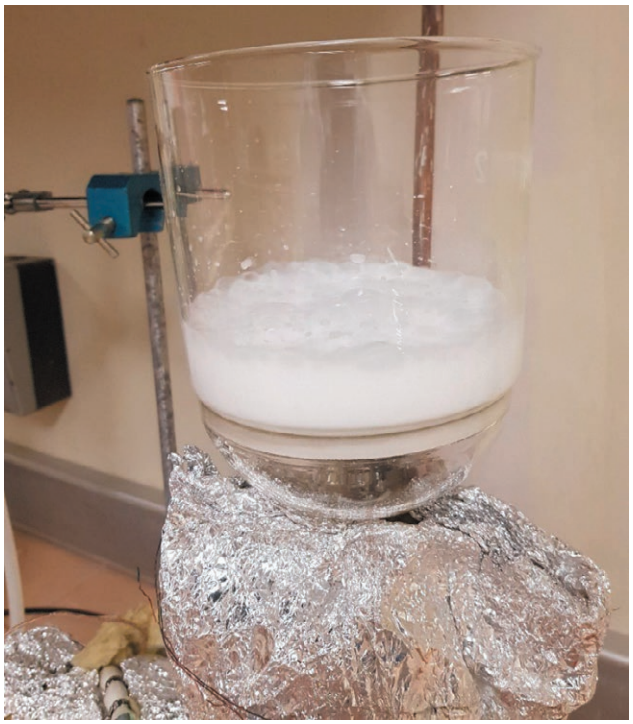

Figure 3. Photograph of the BCE process applied to 20% silica slimes using hot air.

solution density increased from 1.05 g/mL to 1.19 g/mL. When the helium inlet gas temperature was increased to 250 °C at 12 L/min, after 45 min with the column solution equilibrating at about 63°C, the silica concentration (slime thickness) was increased to 32.5% and the solution density increased from 1.05 g/mL to 1.23 g/mL. Table 1 summarises the de-watering results of 20% silica slimes using BCE process with air and helium gases.

At these high silica content levels, the dispersion remained sufficiently fluid for reasonable transport but on stopping the hot inlet gas flow the dispersion immediately solidified.

The values reported in Table 1 are the mean values calculated based on the data obtained after three runs for each single experiment. Besides undertaking experiments using silica-water slime, four experiments have been carried out using both air and helium (at 150 °C and 250 °C) with an industrial slime which had a similar compound composition. The results achieved were very close to the results obtained for de-watering the model silica slime.

Figure 4 shows a Scanning Electron Microscopy (SEM) image of the precipitated silica particles used in this study. This shows that they are of spherical appearance and very fine.

Fine particles (e.g., silica spheres) can stabilise foams even in the absence of surfactants or polymers.[25] Aqueous foams stabilised solely by particles, but these are usually partially hydrophobic and so have an amphiphilic nature.[25] The studies reported here were based on the use of hydrophilic silica particles dispersed in pure water. These micron sized particles would generally act to destabilise foams via water film rupture and hence even with continuous air and helium gas flow no significant level of transient foaming was observed.

Table 1. De-watering of initial 20% silica slime (density of 1.05 g/mL) using BCE process with different gases (air and helium).

	Gas Flow Rate (L/min)	Gas Temperature (°C)	Slime Temperature (°C)	Slime Thickness (%)	Slime Density (g/mL)
BCE with air	34	150	48-49	30.5	1.16
	34	250	65-66	34.7	1.25
BCE with He	12	150	41	28.0	1.19
	12	250	63	32.5	1.23

The relative water loss under different conditions is calculated based on equation (2) and summarised in Figure 5. Regarding the Figure, using helium gas is much more effective than dry air since this level of de-watering was achieved at about one third of the volumetric flow rate compared with air.

In order to compare the efficiency of using different gases for slime de-watering the following equation 3 was used:

$$\frac{E1}{E2} = \frac{Cp2}{Cp1} \times \frac{F2}{F1} \times \frac{water\ loss\ (1)}{water\ loss\ (2)} \tag{3}$$

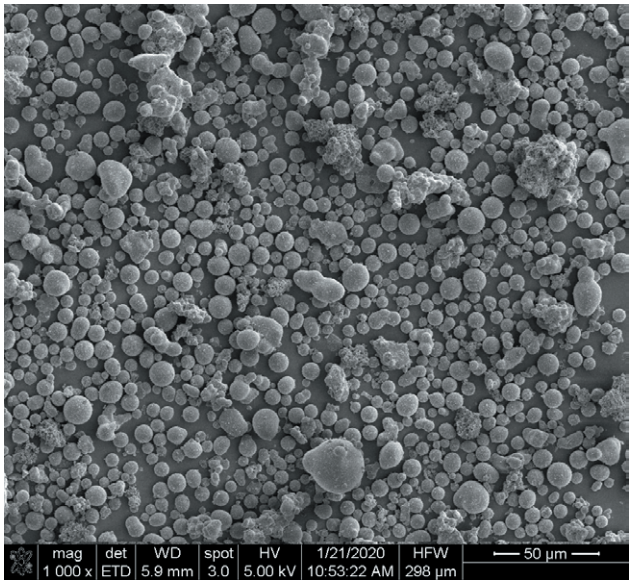

Figure 4. SEM of micro-silica spheres produced by precipitation.

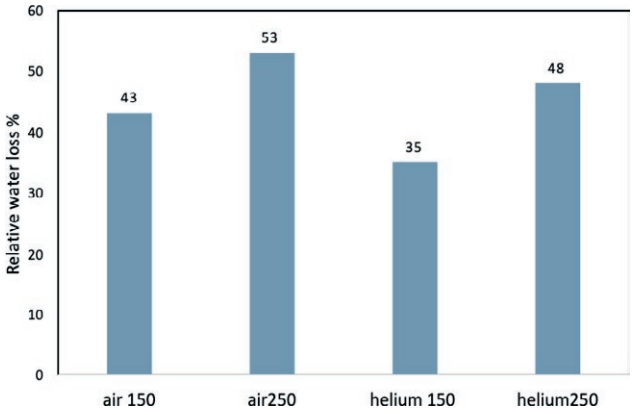

Figure 5. Comparison of the water loss% using air vs helium at 150 °C and 250 °C. Note that the $\frac{helium\ flow\ rate}{air\ flow\ rate} = \frac{1}{3}$.

where E, C_p, F are efficiency of gas carrier, heat capacity of gas at the constant pressure, and gas flow rate, respectively. Also, numbers refer to gas carrier 1 and 2. The water loss factor for each gas carrier can be calculated from equation (2) and the C_p value for air and helium gases are 29.31 and 20.77 (J mole^{-1} K^{-1}), respectively. The E_{Helium}/E_{Air} ratio regarding operational temperatures at 150 °C and 250 °C, gas flow rates, and water loss are 3.25 and 3.62 respectively. This means that to reach an equal level of slime de-watering, helium almost needs less than 1/3 of the energy which air needs.

4. CONCLUSIONS

The BCE system was found to be very effective for slime de-watering. This is major step forward. Its effectiveness was found to depend on the gas temperature. Heated dry air gas at 250 °C was found to be significantly more effective than applying hot dry air at 150 °C to concentrate the slime. It was found that helium gas is more effective than air. We conjecture that this might be due to the very small size of a helium atom with a diameter of 62 pm. Helium atoms can break the hydrogen bonding among water molecules adjacent to the gas-liquid interface and allow easier transfer of water molecules into the rising helium bubbles. (The length of hydrogen bonding among water molecules in the liquid phase is about 1.97 Å).

The BCE method using hot, dry carrier gases offers a promising technique to de-water a wide variety of slimes and slurries produced in different industries. It is simple and robust. This process might offer a novel competitive dewatering process and could be readily scaled up. It offers a robust process which can replace existing techniques such as flocculation, hydrocyclones, and ponding. The BCE technique applied to de-watering also has the very significant additional advantage of producing high quality water from condensation of the sub-boiling water vapour.

5. REFERENCES

1. N.C. Lockhart, Electro-osmotic dewatering of fine tailings from mineral processing, *Int. J. Miner. Process.*, **1983**, 10(2), 131-140.
2. T.J. Laros, Flocculating agent combinations for mineral slime filtration systems, **1990**, Envirotech Corp, United States Patent, Patent No: 4,931,190.
3. P. Pirkonen, B. Ekberg, Chapter Nine – Ultrasonic, *Prog. Filtr. Sep.*, **2015**, 399-421.
4. S. Pasquier, J.J. Cilliers, Sub-micron particle dewatering using hydrocyclones, *Chem. Eng. J.*, **2000**, 80(1), 283-288.
5. J.J. Cilliers, L. Diaz-Anadon, F.S. Wee, Temperature, classification and dewatering in 10 mm hydrocyclones, *Miner. Eng.*, **2004**, 17(5), 591-597.
6. D. Vega-Garcia, P.R. Brito-Parada, J.J. Cilliers, Optimising small hydrocyclone design using 3D printing and CFD simulations, *Chem. Eng. J.*, **2018**, 350, 653-659.
7. G. Chen, P. Lock Yue, A.S. Mujumdar, sludge dewatering and drying, *Drying Technol.*, **2002**, 20(4-5), 883-916.
8. C. Fan, R.M. Pashley, Precise Method for Determining the Enthalpy of Vaporisation of Concentrated Salt Solutions Using a Bubble Column Evaporator. *J. Sol. Chem.*, **2015**. 44(1), 131-145.
9. C. Fan, M. Shahid, R.M. Pashley, Studies on bubble column evaporation in various salt solutions, *J. Sol. Chem.*, **2014**, 43(8), 1297-1312.
10. M. Francis, R.M. Pashley, Application of a Bubble Column for Evaporative Cooling and a Simple Procedure for Determining the Latent Heat of Vaporization of Aqueous Salt Solutions, *J. Phys. Chem. B*, **2009**, 113(27), 9311-9315.
11. M.J. Francis, R.M. Pashley, Thermal desalination using a non-boiling bubble column. *Desalination and Water Treat.*, **2009**, 12(1-3), 155-161.
12. M. Shahid, R.M. Pashley, A study of the bubble column evaporator method for thermal desalination, *Desalination*, **2014**, 351, 236-242.
13. M. Taseidifar, M. Shahid, R.M. Pashley, A study of the bubble column evaporator method for improved thermal desalination, *Desalination*, **2018**, 432, 97-103.
14. X. Xue, R.M. Pashley, A study of low temperature inactivation of fecal coliforms in electrolyte solutions

using hot air bubbles, *Desalination and Water Treat.*, **2016**, 57, 9444-9454.
15. M. Shahid, A study of the bubble column evaporator method for improved sterilization, *J. Water Process. Eng.*, **2015**, 8, 1–6.
16. A.G. Sanchis, M. Shahid, R.M. Pashley, Improved virus inactivation using a hot bubble column evaporator (HBCE), *Colloids Surf. B: Biointerfaces*, **2018**, 165, 293-302.
17. A.G. Sanchis, R.M. Pashley, B. Ninham, Virus and bacteria inactivation by CO_2 bubbles in solution, *NPJ Clean Water,* **2019**, 2, 5.
18. M. Shahid, R.M. Pashley, M. Rahman, Use of a high density, low temperature, bubble column for thermally efficient water sterilisation, *Desalination and Water Treat.*, **2014**, 52, 4444–4452.
19. M. Shahid, X. Xue, C. Fan, B.W. Ninham, R.M. Pashley, Study of a novel method for the thermolysis of solutes in aqueous solution using a low temperature bubble column evaporator, *J. Phys. Chem. B*, **2015**, 119 (25), 8072–8079.
20. C. Fan, R.M. Pashley, The controlled growth of calcium sulfate dihydrate (gypsum) in aqueous solution using the inhibition effect of a bubble column evaporator, *Chem. Eng. Sci.*, **2016**, 142, 23-31.
21. P.N. Govindan, G.P. Thiel, R.K. McGovern, J.H. Lienhard, M.H. Elsharqawy, Bubble-Column Vapor Mixture Condenser, **2013**, United States Patents, Patent No: US 8.523,985 B2.
22. G.P. Narayan, J.H. Lienhard, Thermal Design of Humidification– Dehumidification Systems for Affordable Small-Scale Desalination, *IDA J. Desalination Water Reuse*, **2012**. 4(3), 24-34.
23. M. Schmack, H. Goen, A. Martin, A Bubble Column Evaporator with Basic Flat-plate Condenser for Brackish and Seawater Desalination, *Environ. Technol.*, **2015**, 37(1), 74–85.
24. M. Shahid, C. Fan, R.M. Pashley, Insight into the bubble column evaporator and its applications, *Int. Rev. Phys. Chem.*, **2016**, 35(1), 143- 185.
25. A. Stocco, E. Rio, B. P. Binks, D. Langevin, Aqueous foams stabilized solely by particles, *Soft Matter*, **2011**, 7(4), 1260-1267.

Substantia
An International Journal of the History of Chemistry

Firenze University Press
www.fupress.com/substantia

Citation: A. Wan Nafi, M. Taseidifar, R.M. Pashley, B.W. Ninham (2020) Controlled Growth of Strontium Sulfate Particles in Aqueous Solution: Inhibition Effects of a Bubble Column Evaporator. *Substantia* 4(2) Suppl.: 95-107. doi: 10.36253/Substantia-1031

Data Availability Statement: All relevant data are within the paper and its Supporting Information files.

Competing Interests: The Author(s) declare(s) no conflict of interest.

Controlled Growth of Strontium Sulfate Particles in Aqueous Solution: Inhibition Effects of a Bubble Column Evaporator

Atikah Wan Nafi[1], Mojtaba Taseidifar[1], Richard M. Pashley[1,*], Barry W. Ninham[2]

[1] *School of Science, UNSW Canberra, Northcott Drive, Canberra, Australia*
[2] *Department of Applied Mathematics, Research School of Physical Sciences, The Australian National University, Canberra, Australia*
*Corresponding author: r.pashley@adfa.edu.au

Abstract. In the oil industry, strontium sulfate ($SrSO_4$) scale deposits have long plagued oilfield and gas production operations. This remains an unsolved problem. We here show how the bubble column evaporator (BCE) can be used to control aqueous precipitation from salt solutions. Mixtures of strontium nitrate and sodium sulfate in the BCE system were used to precipitate strontium sulfate at different degrees of supersaturation. The effectiveness of the BCE system was compared to standard mechanical stirring. The precipitation of strontium sulfate in both processes was monitored through turbidimeter, particle counting, Dynamic Light Scattering (DLS) and Scanning Electron Microscopy (SEM). The results show that the BCE system has a significant inhibition effect and so can be used to control precipitation growth rate, even from supersaturated solutions. This remarkable effect also provides new insights into mechanisms of crystallisation, of bubble interactions and mineral flotation.

Keywords: strontium sulfate, aqueous precipitation, nanobubbles, supersaturation, bubble column evaporator, particle growth rates, crystallisation, bubble interactions, mineral flotation.

1. INTRODUCTION

Coatings of partially soluble salts pose significant problems. The growth of deposits on the surface of industrial equipment like boilers, heat exchangers, wastewater treatment plants and in oil and gas drilling operations is always an issue. The scales generally contain sparingly soluble carbonates and sulfates of calcium, barium and strontium. The formation of scale deposits from mixing of two incompatible solutions, such as seawater and natural brines, presents a serious problem in industry, e.g. in the operation of oil fields, desalination plants and geothermal wells. Calcium carbonate and calcium sulfate scales are typical. Strontium sulfate ($SrSO_4$) scale is not so common. However, $SrSO_4$ deposits have long plagued oilfield and gas production

operations. Its removal by fast, spontaneous precipitation remains an unsolved problem in the oil industry, despite significant research efforts.[1-8]

Formation of sulfate scales reduces the diameters of pipes. This causes operational difficulties which may lead to additional capital cost and operating costs.[9-12] Further, severe plugging of equipment causes loss of production, increases the cost of oil extraction and causes many safety issues. According to Howarth et al.[13] wastewater facilities in the oil industry were simply not designed to handle the amount of strontium which can also include radioactive wastes. And indeed, the failure of equipment caused by strontium scale can result in safety issues due to its radioactivity.[14,15] To try to mitigate these detrimental effects, research has focused on several treatment options. These are demineralization systems, thermal evaporation, condensation, and reverse osmosis. However, all these treatment processes suffer from difficulties in operation.[16,17] For instance, the addition of reagents in chemical precipitation methods can result in separation problems, in which the acidic conditions produce toxic gases as by products. So, these processes have to be carefully monitored. $SrSO_4$ scales are categorised as insoluble scales since they are not easily dissolved, and they are also relatively difficult to treat. The addition of acid to treat $SrSO_4$ scales to reduce clogging and build-up of scale poses environmental issues. It also leads to the risk of interruption the whole operation.[18-20] The reverse osmosis membrane technique offers another common treatment method. However, exposure to high salt level concentrations present in feed water can readily block the pores of the membrane sheets and so fouls the expensive membranes. These have to be regularly cleaned or replaced.[21-23] This leads to low efficiency of the process, high maintenance costs and a decrease in the quality of water produced. To protect the membrane and maintain the efficiency of the process, regular feedwater pre-treatment is essential. This again increases costs, besides complicating the process.[24,25] Currently, there are no reports on efficient water treatment which affordably and simply inhibits $SrSO_4$ particle growth.

Prior to disposal, wastewater treatment typically aims to maximize the concentration of contaminant using low cost energy, for example, from industrial-waste vent gases, solar heat or wind turbines. These energy sources could be used with the BCE system, which concentrates wastewater and at the same time inhibits the growth of precipitate particles, as has recently been reported[24,25] in work that precedes ours. It was discovered that precipitation inhibition naturally occurs in the bubble column evaporator process for supersaturated solutions of calcium sulfate. In this process, a continuous, high density, flow of rising bubbles apparently disrupts the growth of nano-particles, even in supersaturated solutions. Comparison with standard mixing methods indicates that the BCE process offers a cost effective and simple method to create precipitation inhibition.[26] There, precipitated particles of $CaSO_4.2H_2O$ were maintained at a steady size of <100 nm within a BCE, whilst stirred solutions, at the same supersaturation rate (of about 32 times the solubility product) formed particles with sizes increasing rapidly above 1 mm.[26]

Apart from scale deposit problems in the oil industry, $SrSO_4$ is a multifunctional inorganic material used in various chemical applications, such as in electronics, ceramics, pigments, cosmetics, paper making and as a compound used for thermo-stimulated luminescence.[27,28] This study is aimed at the determination of suitable treatments to prevent scale formation, and in order to do this it is important to understand in depth the precipitation reaction of $SrSO_4$ in the first place. Studies on the production of fine particles, through precipitation, have received vast attention with a view to controlled production of fine particles. Nanoparticle materials can be obtained by several methods; such as, precipitation, hydrolysis, electrolysis etc. Compared with other methods, the precipitation reaction has potential advantages of homogeneity, high productivity and controllability of the process.[29,30] However, the stirred tanks often used in the precipitation process can produce particles with a broad size distribution due to inhomogeneous mixing combined with rapid and spontaneous reaction of the mixed components.[31,32] The formation of particles of small size is often followed by agglomeration, which hinders the ability to produce fine particles. Few studies on simple, effective, additive-free methods for controlled precipitation have been reported. This paper is one such new method. Some unresolved fundamental issues on mechanisms of crystallisation come up in the course of this research that will leave for later discussion in the Appendix.

One of such experimental studies reports the effect of a magnetic field in combination of temperature on the precipitation of insoluble salts of alkaline earth metals, such as carbonates of calcium, strontium and barium, which were precipitated from supersaturated conditions. The structure of $CaCO_3$ crystals were studied by a combination of X-ray diffraction, optical microscopy and fluorescence. All show that the application of a magnetic field with about 0.4 T, leads to inhibition of particle precipitation.[33] It was discovered that insoluble salts, especially $CaCO_3$, when the solution underwent magnetic treatment for about 15 min before mixing caused a sup-

pression of particle nucleation and increased the crystal size, with a reduction in crystal number density. Precipitation of supersaturated salt solutions can be retarded through a combination of high magnetic fields and high temperature of 60 °C.[34]

In comparison with our experiments, the magnetic field generated in the magnetic stirring system used was likely to be too low to have any significant effect. In addition, it was observed that in the stirring system using a magnetic bar, the particles precipitated readily and in a shorter time and with a higher growth rate.

The BCE process, used in this work, exhibits an excellent ability to control the $SrSO_4$ precipitation. The process employs vigorous mixing to form a uniform solute concentration. From this a more controlled precipitation process was achieved than from a standard mixing method. This study shows that the BCE method can be used to successfully inhibit precipitation of $SrSO_4$ from supersaturated solutions and reduce the rate of particle growth. The inhibition phenomenon is clearly of much wider application than for $SrSO_4$. Based on these experimental results, the BCE process could also be used for reducing precipitation of $SrSO_4$ and other nanoparticles scales that have potential applications especially in the oil and gas industry and in industrial water treatment plants.

2. MATERIALS AND METHODS

2.1. Materials

The salts $Sr(NO_3)_2$ and Na_2SO_4 used in these experiments were analytical reagents with purity level ≥ 99%, purchased from Sigma- Aldrich. Double-distilled water, Milli-Q water and purified bottled drinking water, 'Woolworths Select Mountain Spring', were used to prepare the salt solutions and to produce a low particle count comparison. At room temperature, the Milli-Q water had a conductivity of less than 3.0 μS cm^{-1} and pH of 7.06. All concentrations are given in molarity (M) units at room temperature.

2.2. Precipitation processes

Figure 1 shows a schematic diagram of the BCE system, in which bubbles are sparged into the mixed salt solutions containing $Sr(NO_3)_2$ and Na_2SO_4 and also a standard stirring system to compare the precipitation process for $SrSO_4$ at 25 °C. The air gas is pumped from an air pump (Hiblow HP40, Philippines) that passes through a silica gel column to dehumidify. A flow meter

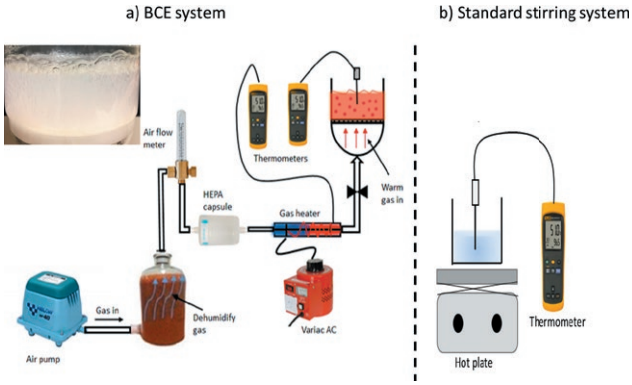

Figure 1. Schematic diagram of the bubble column evaporator (BCE) system and a photograph of a bubble column (a) and standard stirring process (b) for mixing 0.0015^2 M^2 Sr $(NO_3)_2$ and Na_2SO_4.

is used to control the flow rate of the inlet air which was placed after the desiccator. Normal air was used in the BCE, which was pre-filtered using a Whatman large High Efficiency Particulate Air (HEPA) filter capsule to filter inlet air. The inlet air passes continuously through the BCE set up, which was operated within a filtered air, laminar flow cabinet. The HEPA capsule can retain 99% of particles below 0.3 mm. The air flow was passed through the gas heater to provide the required temperature. The heater temperature was controlled by a digital variac power supply and maintained using a thermometer (Control company 4000 Traceable). Then the controlled hot gas flow was pumped into the bubble column containing the mixed salt solution. To start the precipitation process, the concentration of salt solutions was set at a suitable supersaturation level. The bubbles produced in the columns were fairly uniform within the size range of about 2-4 mm.

For comparison with the BCE experiment, a standard stirring experiment using the same salt solutions at the same temperature were operated using different cylindrical magnetic bars with lengths of 2 to 5.5 cm at different stirring rates of 0, 120, 240 and 480 revolutions per min (rpm). The liquid samples from the BCE system and standard stirring systems were taken directly using syringes and filtered through Whatman Millipore 0.22 μm at different times for further characterisation and by analysis of the removed dry particles.

2.3. Analytical methods

The induction and precipitation growth of $SrSO_4$ particles over time were monitored by turbidity measurement (HACH 2100AN Turbidimeter). The solution

turbidity at 0.2 NTU was taken as the onset of precipitation. This is a useful indicator because the clear water and solutions without obvious precipitates normally gave turbidity values less than 0.2 NTU. A Spectrex Laser Particle Counter (model PC-2300) was used to determine the purity of the solutions. The particle counter with detection size range 0.5–100 μm was able to detect the presence of contaminant particles that may affect the precipitation process. The presence of these particles in the solution prepared using distilled water, bottled water and Milli-Q water when filtered by the Whatman Millipore 0.22 μm was tested before each precipitation experiment.

In addition, a Malvern Zetasizer (Model ZS) with detection size range 0.3 nm–10 μm was used to monitor the growth of the precipitated particles. 1 mL samples were collected into polystyrene cells using a syringe for dynamic light scattering measurement using the Malvern Zetasizer. Solution samples were filtered before the DLS analysis when precipitation became visible. Then the filtered samples were kept in the open air to dry completely before examination with a FEI Quanta QEM-SCAN Scanning Electron Microscope (SEM), to study particle morphology.

3. RESULTS AND DISCUSSION

3.1. $SrSO_4$ precipitation

The precipitation process typically starts when the concentration of a compound in solution is greater than its solubility, i.e. from a supersaturated solution. In the case of the reactive precipitation of $SrSO_4$, as in this work, the reaction is given, by convention, as

$$Sr^{2+}_{(aq)} + SO_4^{2-}{}_{(aq)} \rightleftarrows SrSO_{4(S)} \quad (1)$$

The precipitate of $SrSO_4$ is produced when the product of the concentrations of Sr^{2+} and SO_4^{2-} ions is greater than the solubility product. The precipitation of $SrSO_4$ and its morphology was determined using SEM to determine the formation of $SrSO_4$ precipitated from a stirred solution and from a BCE.

The supersaturation degree (denoted S) of a $SrSO_4$ salt solution is defined as:

$$S = \frac{[Sr^{2+}][SO_4^{2-}]}{K_{SP}} \quad (2)$$

Where K_{sp}, the solubility product, equals $[Sr^{2+}]_{eq}$ x $[SO_4^{2-}]_{eq}$ which is the equilibrium product at the solubility limit, assuming ideal conditions. All ion activity coefficients are assumed equal to 1 and hence the activities of all the ions are equal to their concentration. Because of the dilute concentrations involved, this assumption is reasonable. Besides the main factor of supersaturation level, other factors can affect the precipitation process: impurities, temperature, contact time, pH, agitation intensity and overall ionic strength.[35-39] In this study, the main factors were the degree of supersaturation, purity of background solution and the BCE process as it affects precipitation compared with simple solution stirring.

Several studies have discussed the effect of turbulence on morphology, scale deposition and minimal inhibitor concentration.[40, 41] However, there is no consistent finding on the effect of turbulence on scale deposition. Barium sulfate precipitation was conducted under turbulent conditions and compared with lamina precipitates inside oilfield pipes. The results show that there is no difference in sulfate precipitation kinetics without inhibitors (polymeric based additives) in both conditions.[42, 43] The present work using the BCE and standard stirring system was conducted inside a laminar flow cabinet. The results obtained might be developed for application to the $SrSO_4$ precipitation problem in the oil and gas industries.

Particle counts obtained using the Spectrex counter were used to determine the purity of water samples. It was found that the particle count of all types of water samples inside the laminar cabinet are more stable compared to samples exposed to ambient air. These results also showed that the purity of water was ranked as: Milli-Q > Bottled water > Tap water > Distilled water, as expected because the laboratory water distillation system used collected and stored the initially clean distilled water in a vessel which was exposed to atmospheric air.

Based on Spectrex Laser Particle Counter test results reported in Table 1, the normal distilled water contained the highest number of particles, which is more than 227 counts per mL of particles less than 3 μm in size. This value for the salt solutions which are prepared inside laminar flow cabinet using Milli-Q water was increased to 87 counts per mL despite the particle count initially being only 2 counts per mL. These results suggest that, it is almost impossible to achieve a blank solution with zero particles. The lowest consistent particle count was obtained for the salt solution samples prepared using Milli-Q water inside a laminar flow cabinet, and this sample was used as blank solution in this work. In previous work, it was reported that with careful filtration, the particles can be reduced to less than 1000 counts per mL, however it is impossible to achieve zero particles.[44] In addition, it is difficult to prepare systems completely free of fine particles and nucleation sites because

Table 1. Purity of $SrSO_4$ solution based on particle counts and supersaturation degree.

Solution types	Prepared using distilled water (particle counts per ml)	Prepared using Milli Q water (particle counts per ml)	Solution filtered by 0.22μm membrane (particle counts per ml)	Supersaturation degree (S)
Distilled water	227	-	-	-
Milli Q water	-	2	-	-
0.0008 M $Sr(NO_3)_2$ + 0.0008 M Na_2SO_4	608	87	7	1.86
0.001 M $Sr(NO_3)_2$ + 0.001 M Na_2SO_4	629	96	19	2.91
0.0013 M $Sr(NO_3)_2$ + 0.0013 M Na_2SO_4	662	112	30	4.91
0.0015 M $Sr(NO_3)_2$ + 0.0015 M Na_2SO_4	668	126	34	6.54
0.002 M $Sr(NO_3)_2$ + 0.002 M Na_2SO_4	686	138	45	11.63
0.0025 M $Sr(NO_3)_2$ + 0.0025 M Na_2SO_4	698	156	49	18.17
0.005 M $Sr(NO_3)_2$ + 0.005 M Na_2SO_4	704	198	91	72.67

of impurities in supersaturated solutions, which are difficult to remove and act as nucleation catalysts. Also, the walls of the retaining vessel, can catalyse nucleation. The presence of some impurities can even cause inhibition of crystal growth or nucleation and so affect the rate of sulfate precipitation.[45-47]

By filtering the solutions prior to making up the supersaturated solutions, in a laminar flow cabinet, it was possible to reduce particle densities below 50 per mL. This was the typical background level of particles used in this study.

The supersaturation degree of each solution in the Table 1 was calculated based on the solubility product values at 25 °C obtained from the CRC handbook.[48]

The salt solutions of $SrSO_4$ with different types of water source and degree of supersaturation were tested using a standard stirring system at 25 °C with a 3.5 cm length cylindrical stir bar (of 1 cm diameter) at a rate of 120 rpm. The induction time at which turbidity reached 0.2 NTU was recorded. Figure 2 shows that with increase in degree of supersaturation, the onset precipitation time drops down noticeably. The induction time is also affected by the presence of foreign particles. Solutions with the same degree of supersaturation but prepared using distilled water, precipitate in less time compared to salt solutions prepared using Milli-Q water. It was found that $SrSO_4$ solutions in Milli-Q water with lower than 2 degrees of supersaturation had the longest induction time. By comparison, reported results show that the time of the appearance of nuclei (induction time) in water vapour is 10^3 years when the supersaturation degree is at 3.[44]

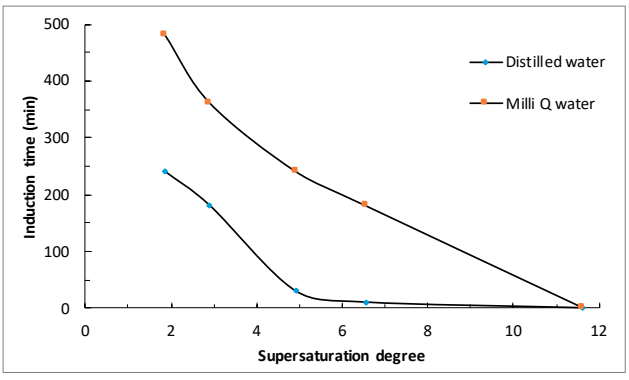

Figure 2. The induction time of $SrSO_4$ precipitation in the solutions with different level of purity and supersaturation degrees by simple stirring (120 rpm) at 25 °C.

3.2. Effects of Stirring Rates

The induction time for the salt precipitation in a standard stirring system is also affected by different lengths of magnetic stir bar used. As shown in Figure 3, $SrSO_4$ solutions at similar solution conditions (0.0015^2 M^2) were stirred at 120 rpm at 25 °C with different lengths of stirring rod. This change in length affected the induction time. It was found that longer magnetic stir bar length reduces the induction time for precipitation. However, comparison from Figure 3 showed something quite unexpected: the induction time starts fluctuating when magnetic stirring bar lengths of 3.5 cm and 5.5 cm were used. Under the same conditions the BCE system for the precipitation of solutions provides a longer induction time of 380 min. The solution in the BCE system has a stable induction time compared to a standard stirring system or even quiescent conditions. Different types of impellers show significantly different results in the precipitation process, in which parameters like different length change, line speed and the shear speed within the solution during stirring. All affect the precipitation process.[49]

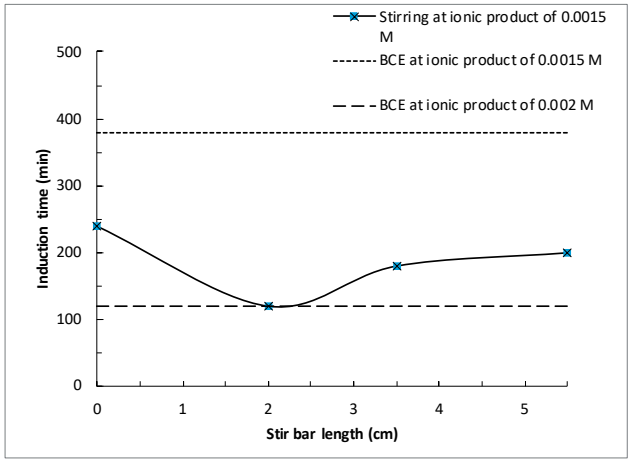

Figure 3. The induction time of $SrSO_4$ precipitation by simple stirring (120 rpm) with different stir bar length and using a BCE at 25 °C.

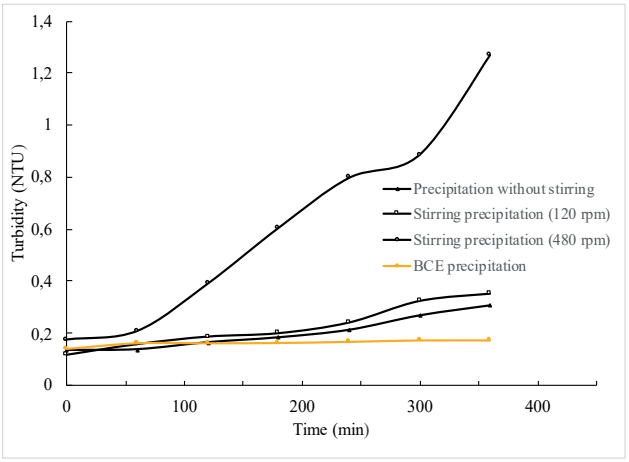

Figure 4. $SrSO_4$ precipitation at ionic product of 0.0015^2 M^2 (Supersaturation degree: 6.54) in a standard stirring process and a BCE monitored by turbidity measurements.

3.3. Comparison of $SrSO_4$ precipitation using the BCE and a standard stirring system

Figure 4 shows the precipitation results for 0.0015^2 M^2 $SrSO_4$ solutions in a standard stirring system with different speed of stirring and in the BCE system. In these experiments, particle growth by the precipitation process was monitored using turbidity measurements. The turbidity in a standard stirring system of 120 rpm shows similar behaviour to a salt solution without stirring. Both slowly reach onset precipitation (turbidity > 0.2). On the other hand, the salt solution that was placed in the same stirring system at 480 rpm significantly increased precipitation after 60 min. By comparison, the turbidity in the BCE system remained constant below 0.2 NTU for more than 350 min, even though the salt solution used in the BCE was at the same level of saturation. An increase in temperature will increase the solution solubility of $SrSO_4$.[50-52] Initially, it was expected that continuous water evaporation within the BCE will slowly increase the supersaturation level hence causing precipitation. However, based on the results given in Figures 3 and 4, the BCE system shows a clear inhibition effect on particle growth. The rising bubbles in the BCE show complex behaviour due to coalescence and non-coalescence and bubble shape and trajectory that rise with rotational oscillation effects in the salt solution.[53, 54] This behaviour appears to disturb the processes involved in particle growth, even in supersaturated solutions.

Low turbidity values do not indicate definitively the absence of particles in the sample, since the turbidimeter involves a light extinction method which may not be able to detect very small particles.[55, 56] Hence, the average size of $SrSO_4$ precipitated particles in the BCE and standard stirring processes were monitored using a Malvern zetasizer, as shown in Figure 5. Precipitated $SrSO_4$ particles were detected by a Malvern Zetasizer even at the initial point of mixing of the two solutions, with particles of around 0.3 μm, while the turbidity of the solution was found to be below 0.2 NTU. It was shown in a previous study that once particles become large, i.e. more than about 5 μm during the precipitation process, their presence can be correlated with an increase in solution turbidity.[57] As a possible explanation, the salt solutions of $Sr(NO_3)_2$ and Na_2SO_4 mixed at the beginning of the test might was not be fully homogenous, allowing local precipitation of $SrSO_4$ through a spontaneous heterogeneous process.[58] Numerous studies have been concerned with spontaneous precipitation processes, but no satisfactory explanation has yet been accepted.[59-63]

The results given in Figures 4 and 5 show that increases in solution turbidity is correlated with an increase in particle size. The average size of $SrSO_4$ particles was persistent with the SEM analysis given in Figure 7, in which the image of the particle changes from agglomerates to microrod/pod. The precipitation process in a stirring system led to broad size particle distribution, probably due to rapid reaction.[64] In comparison with $SrSO_4$ precipitation in the BCE system, the turbidity of solution remained below 0.2 NTU until 380 min and the average size of particle remained constantly below 1 μm. It can be seen from Figure 5 (a) that the BCE system successfully inhibits particle growth, compared to a standard stirring system. The results suggest that the BCE system for precipitation has the potential to be used as a method of controlled particle growth for the production of fine particles.

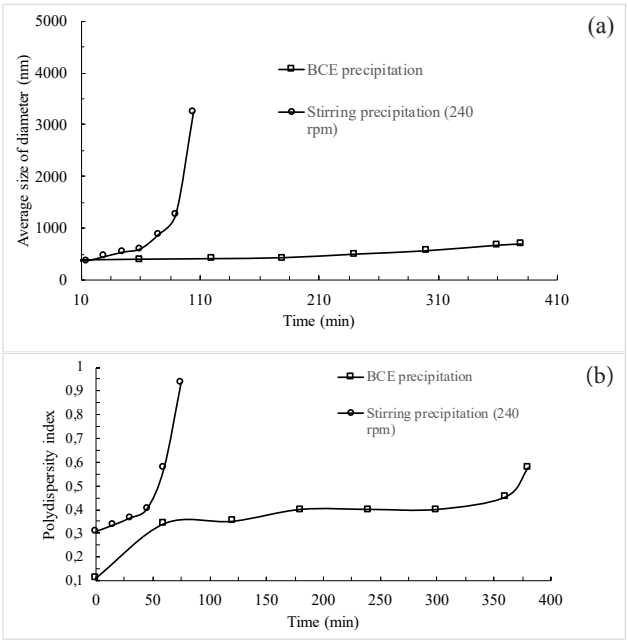

Figure 5. (a): $SrSO_4$ precipitation at ionic product of 0.0015^2 M^2 (Supersaturation degree: 6.54) in BCE and 240 rpm stirring system by average size at around 25 °C; (b): $SrSO_4$ precipitation at ionic product of 0.0015^2 M^2 (Supersaturation degree: 6.54) in BCE and 240 rpm stirring system studied by polydispersity index (PDI) measurements at around 25 °C.

The uniformity of $SrSO_4$ particles over time was based on the change in the Polydispersity Index (PDI) using the Malvern Zetasizer, as given in Figure 5(b). A PDI value close to 0 indicates the formation of a narrow range of particle sizes. For values that are close to 1, it correlates with a random distribution of sizes. The precipitates of $SrSO_4$ in the standard stirring system were expected to experience rapid growth and so a broader size distribution. After 45 mins, the PDI was around 0.5 for the standard stirring system, whereas $SrSO_4$ particles precipitated by the BCE system showed a gradual increase in the PDI value. It is clear that the BCE offers significant improvement in uniformity of particle growth and a controlled size distribution.

Figure 6 and Figure 7 show images of the particles of $SrSO_4$ formed in the precipitation process in the BCE system and standard stirring system, respectively. The images were captured from the initial mixing point and at 60 min of the BCE precipitation and at 0, 60 and 75 min of the standard stirring system. As can be seen, SEM images of the precipitates formed in the standard stirring system (Figure 7) show mixtures of microrods and flower-like shapes, with sizes ranging from 1.2 μm to 9.7 μm.

According to these results, with the same solution conditions as given in Figure 5 and Figure 6, the BCE system shows controlled and uniform particle growth compared to the standard stirring system. The pattern of the $SrSO_4$ particles observed, consisting of microrods and flower-like shaped particles were similar to previous studies on calcium sulphate.[26] The formation of $SrSO_4$ particle growth follows a "two-step formation mechanism", in which primary microcrystals are involved in the formation of monopods, followed by the continuous growth nucleation of monopods that leads to secondary microstructure growth, through the spontaneous aggregation of pods docking on planar structures.[65] The latter are formed due to their similar crystallographic orientation.[58]

The DLS measurements carried out for monitoring the particle size, gave further support to the inhibition effects in the BCE system, as shown in Figure 8, where

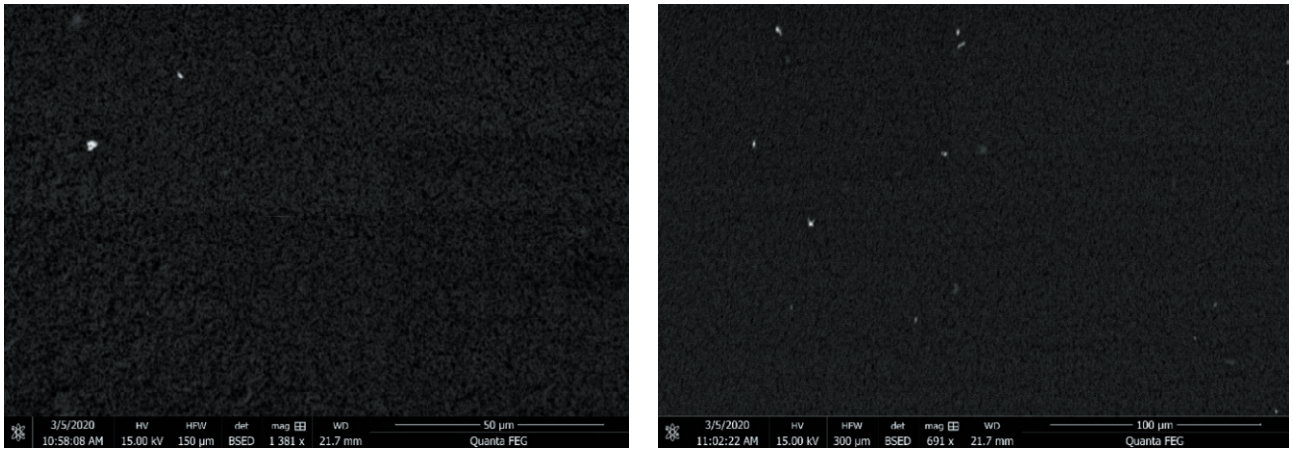

Figure 6. SEM image of $SrSO_4$ precipitated particles at an ionic product of 0.0015^2 M^2 in a BCE at 0 min (left), 60 min (right).

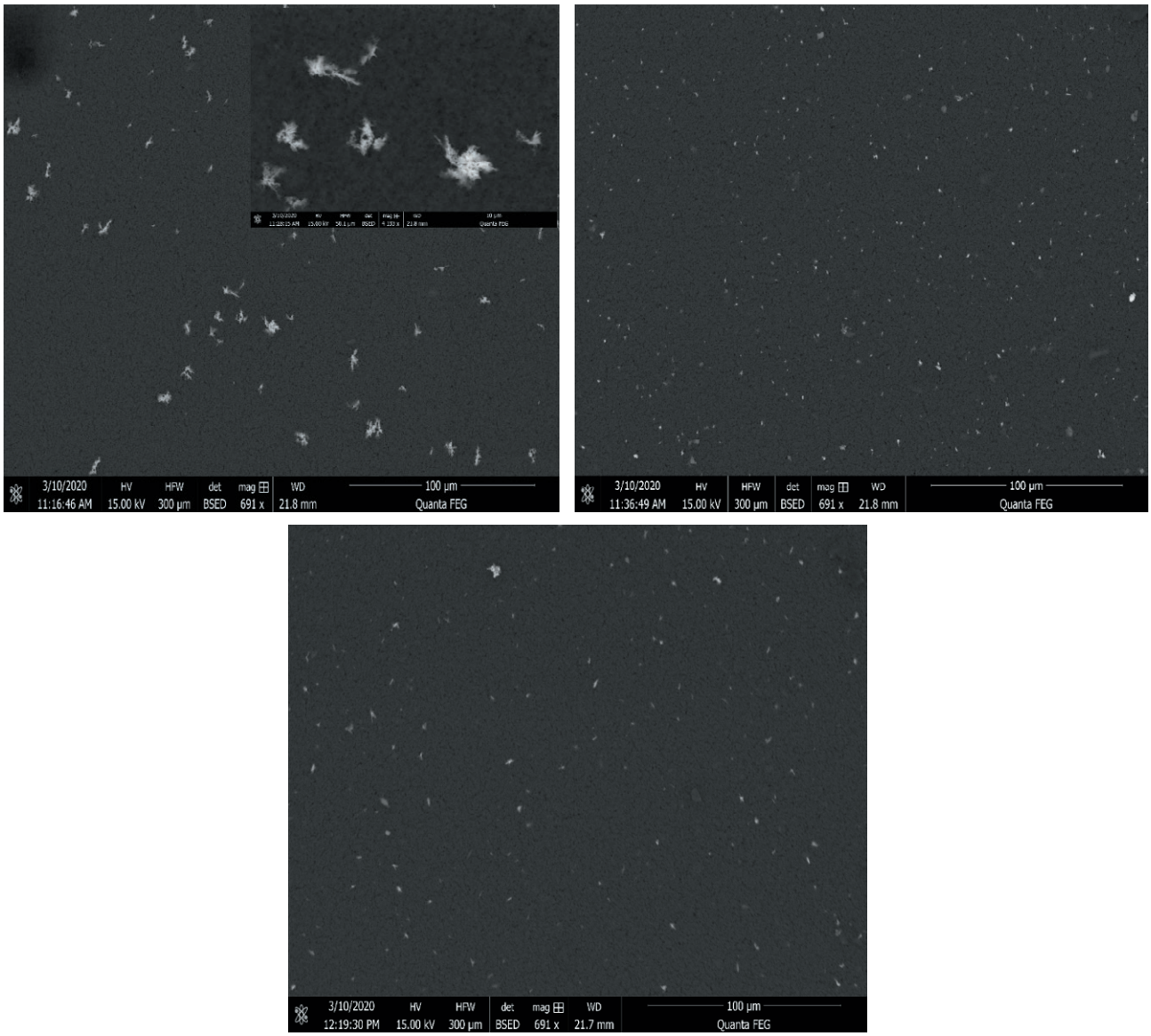

Figure 7. SEM image of $SrSO_4$ precipitated particles at an ionic product of 0.0015^2 M^2 in a standard stirring system at 0 min (a), 60 min (b) and 75 min (c).

the peak size at 180 min remained close to the initial peak. It was found that through a continuous process, the BCE was clearly able to produce fine particles in a specific size range due to the inhibition effect apparently inherent to the BCE process.

It might be thought that the effect of electrolytes on bubble coalescence inhibition[53,54] might also be related to the inhibition of precipitated particle growth. However, if there is a link it is unclear from the results presented here simply because the initial mixed salts were at concentrations significantly below those where bubble coalescence effects have previously been observed. Of course, only soluble mixed electrolytes have been studied for bubble coalescence effects but it would be a reasonable to assume that mixing $SrCl_2$ with Na_2SO_4 should be similar to mixing $CaCl_2$ with Li_2SO_4, both of which salts have been separately studied for their effects on bubble coalescence inhibition. For example, $CaCl_2$ has a transition concentration (i.e. corresponding to 50% coalescence) at about 0.04 M and Li_2SO_4 has a transition concentration at about 0.025 M.[54] Both these concentrations are well above even the highest concentrations (of 0.005 M) used in the present study and so would not be expected to significantly affect bubble coalescence in

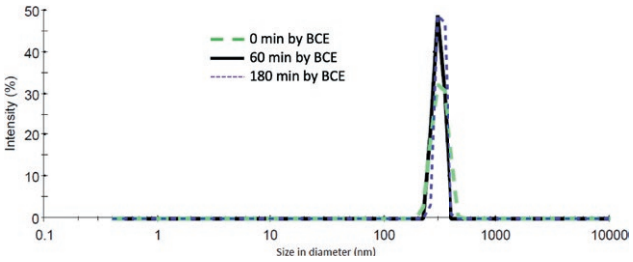

Figure 8. Size distribution of $SrSO_4$ precipitates at ionic product of 0.0015^2 M^2 in a BCE at 0 min, 60 min and 180 min.

the column, even though at higher concentration these mixed electrolytes would be expected to affect bubble coalescence.[66]

In this study the precipitation levels seen in the BCE process, even for supersaturated solutions, were very low and so no attempt was made to measure the particle yield, which would be very low. It might be possible, however, to continuously remove the fine particles using, for example, a membrane nano-filtration system to increase the product yield.

This study of the comparison between the BCE process and a standard stirring system, for $SrSO_4$ precipitates, was found to be similar to that reported earlier[26] for $CaSO_4.2H_2O$ precipitates. Both studies suggest that the BCE system, due to its inhibition of particle growth, can play an important role in precipitation control, especially in particle-growth-control applications and in industrial water treatment. In addition, the technique could be used in the production of fine particles for industrial applications in ceramics, catalysis, cosmetics, pharmaceuticals and in food products.[67]

4. CONCLUSIONS

A standard stirring system and a BCE system were compared for the precipitation of $SrSO_4$ particles from supersaturated solutions of $Sr(NO_3)_2$ and Na_2SO_4. The precipitation of $SrSO_4$ in both systems was monitored by turbidity measurements, Spectrex particle counting and a DLS Malvern Zetasizer, with particle morphologies observed using SEM. It was found that the BCE system, compared to the standard stirring system, had an inhibitory effect on the precipitation induction time and the precipitate growth rate; which allows for the production of particles over a wide size range, from nanometer to micrometer. The results obtained were found to be similar to those observed earlier with $CaSO_4.2H_2O$ precipitation, which leads to the proposition that this might be a general property of bubble column evaporators. The BCE system potentially offers useful applications in various industrial processes, such as in the treatment of wastewater and other industries that are required to produce fine particles in a controlled manner. Particle size distribution is a key parameter in quality control. This has been highlighted in various industries, especially from material-research and processing, fresco and paper restoration.

Our study opens up insights into curious phenomena by adding a new hidden and neglected variable, the role of dissolved gas in reactivity. How this plays out in detail we outline in the Appendix.

5. ACKNOWLEDGEMENTS

This research was supported by funding from Breakthrough Technologies and a UNSW scholarship for AWN.

6. REFERENCES

1. Z. Amjad, J. Albright, Strontium Sulfate Inhibition by Biopolymers and Synthetic Polymers, *Mater. Performance*, **2015**, *54*(12), 54-58.
2. Y.D. Yeboah, M.R. Saeed, A.K. Lee, Kinetics of strontium sulfate precipitation from aqueous electrolyte solutions, *J. Cryst. growth*, **1994**, 135(1-2), 323-330.
3. F.H. Butt, F. Rahman, U. Baduruthamal, Evaluation of SHMP and advanced scale inhibitors for control of $CaSO_4$, $SrSO_4$, and $CaCO_3$ scales in RO desalination, *Desalination*, **1997**, 109(3), 323-332.
4. H.M. Ezuber, Prediction of Strontium Sulfate Scale Formation in Oilfield Environment, *J. ASTM Int.*, **2007**, 4(6), 1-11.
5. C.C. Patton, Applied water technology, **1986**.
6. A.J. Essel, B.L. Carlberg, Strontium sulfate scale control by inhibitor squeeze treatment in the Fateh field, *J. Pet. Technol.*, **1982**, 34(06), 1-302.
7. J.C. Lindlof, K.G. Stoffer, A case study of seawater injection incompatibility, *J. Pet. Technol.*, **1983**, 35(07), 1-256.
8. M. Nassivera, A. Essel, Fateh field sea water injection-water treatment, corrosion, and scale control, In *Middle East Technical Conference and Exhibition*, Society of Petroleum Engineers, **1979**.
9. M.S.H. Bader, Sulfate removal technologies for oil fields seawater injection operations, *J. Pet. Sci. Eng.*, **2007**, 55(1-2), 93-110.
10. Z. Dai, A.T. Kan, F. Zhang, F. Yan, G. Ruan, N. Bhandari, M.B. Tomson, A Thermodynamic Model

for The Solution Density and Mineral Solubility Predictions up to 250 °C, 1,500 Bars for Na-K-Mg-Ca-Ba-Sr-Cl-CO_3-HCO_3-SO_4-CO_2 aq Systems. In *SPE International Oilfield Scale Conference and Exhibition*. Society of Petroleum Engineers.

11. F. Yan, F. Zhang, N. Bhandari, L. Wang, Z. Dai, Z. Zhang, M. Tomson, Adsorption and precipitation of scale inhibitors on shale formations, *J. Pet. Sci. Eng.*, **2015**, 136, 32-40.
12. C. Yan, A.T. Kan, W. Wang, F. Yan, L. Wang, M.B. Tomson, Sorption Study of Al-O (OH) Nanoparticle-Crosslinked Polymeric Scale Inhibitors and Their Improved Squeeze Performance in Porous Media. *SPE Journal*, **2014**, 19(04), 687-694.
13. R.W. Howarth, A. Ingraffea, T. Engelder, Natural gas: Should fracking stop?, *Nature*, **2011**, 477(7364), 271.
14. J. S. Al-Thuwaini, B. J. Burr, Encapsulated scale inhibitor treatment, In *Middle East Oil Show and Conference*. Society of Petroleum Engineers, **1997**.
15. A.B.B. Merdhah, A.A.M. Yassin, Calcium and Strontium Sulfate Scale Formation Due to Incompatible Water, *P. Int. Graduate Eng. Sci. (IGCES'08)*, **2008**, 23, 24.
16. J.D. Cogan, *The Removal of Barium, Strontium, Calcium and Magnesium from Hydraulic Fracturing Produced Water Using Precipitation with Traditional and Alternative Reactant Feedstocks* (Doctoral dissertation, Ohio University), **2016**.
17. L.O. Paugh, Marcellus shale water management challenges in Pennsylvania. In *SPE Shale Gas Production Conference*, Society of Petroleum Engineers, **2008**.
18. A. Taha, M. Amani, Water Chemistry in Oil and Gas Operations: Scales Properties and Composition, *Int. J. Org. Chem.*, **2019**, 9(3), 130-141.
19. J. Sohaili, H.S. Shi, N.H. Zardari, N. Ahmad, S.K. Muniyandi, Removal of scale deposition on pipe walls by using magnetic field treatment and the effects of magnetic strength, *J. Clean. Prod.*, **2016**, 139, 1393-1399.
20. J. Pichtel, Oil and gas production wastewater: Soil contamination and pollution prevention, *Appl. Env. Soil Sci.*, **2016**.
21. D. Place, Water Treatment Polymers, **2017**.
22. R. Bahar, M.N.A. Hawlader, Desalination: conversion of seawater to freshwater, *Energy (kWh/m3 4)*, **2013**, 9(1.8), 1-8.
23. W. Mark, The Guidebook to Membrane Desalination Technology: Reverse Osmosis, Nanofiltration and Hybrid Systems Process, Design, Applications and Economic. *L'Aquila Desalination Publications,* **2007**.
24. A. Ozverdi, M. Erdem, Cu^{2+}, Cd^{2+} and Pb^{2+} adsorption from aqueous solutions by pyrite and synthetic iron sulphide, *J. Hazard. Mater.*, **2006**, 137(1), 626-632.
25. M. Shahid, C. Fan, R.M. Pashley, Insight into the bubble column evaporator and its applications, *Int. Rev. Phys. Chem.*, **2016**, 1(135), 143-185.
26. C. Fan, R.M. Pashley, The controlled growth of calcium sulfate dihydrate (gypsum) in aqueous solution using the inhibition effect of a bubble column evaporator, *Chem. Eng. Sci.*, **2016**, 142, 23-31.
27. M. S. Atone, S. V. Moharil, S. M. Dhopte, P. L. Muthal, V. K. Kondawar, Synthesis and characterization of $SrSO_4$: Mo, Tb thermoluminescent phosphor. *physica status solidi (a)*, **1999**, 174(2), 521-526.
28. T. Murakami, J.H. Ouyang, K. Umeda, S. Sasaki, High-temperature friction properties of $BaSO_4$ and $SrSO_4$ powder films formed on Al_2O_3 and stainless steel substrates, *Mater. Sci. Eng., A*, **2006**, 432(1-2), 52-58.
29. R. Giorgi, C. Bozzi, L. Dei, C. Gabbiani, B.W. Ninham, P. Baglioni, Nanoparticles of $Mg(OH)_2$: synthesis and application to paper conservation, *Langmuir*, **2005**, 21(18), 8495-8501.
30. Y. Kimura, Rare earth phosphate particle and its production, *Japan Kokai Tokkyo Koho,* **1996**, JP H08-143305.
31. S.A. Khan, A. Gunther, M.A. Schmidt, K.F. Jensen, Microfluidic synthesis of colloidal silica, *Langmuir*, **2004**, *20*(20), 8604-8611.
32. T. Ogihara, M. Yabuuchi, T. Yanagawa, N. Ogata, K. Yoshida, N. Nagata, U. Maeda, Preparation of monodispersed, spherical ferric oxide particles by hydrolysis of metal alkoxides using a continuous tube-type reactor, *Adv. Powder Technol.*, **1997**, 8(1), 73-84.
33. M. Raudino, F. Sarri, D. Tatini, M. Ambrosi, G.D. Aloisi, B.W. Ninham, L. Dei, P.L. Nostro, The Effect of Temperature and Magnetic Field on the Precipitation of Insoluble Salts of Alkaline Earth Metals, *J. Solution Chem.*, **2020**, 49(3), 289-305.
34. M. A. Salman, M. Safar, G. Al-Nuwaibit, The Effect of Magnetic Treatment on Retarding Scaling Deposition, *The Online J. Sci. Technol.*, **2015**, 5(3), 62-77.
35. B. J. Mason, The nuclei of atmospheric condensation, Geofisica pura e applicata, **1957**, 36(1), 9-20.
36. P. A. Barata, M. L. Serrano, Salting-out precipitation of potassium dihydrogen phosphate (KDP). I. Precipitation mechanism, *J. Cryst. Growth*, **1996**, 160(3-4), 361-369.
37. D.F. Jacques, B.I. Bourland, A study of solubility of strontium sulfate, *Soc. Pet. Eng. J.*, **1983**, *23*(02), 292-300.
38. D. Feng, C. Aldrich, H. Tan, Treatment of acid mine water by use of heavy metal precipitation and ion exchange, *Miner. Eng.*, **2000**, 13(6), 623-642.

39. M. Li, *Removal of divalent cations from marcellus shale flowback water through chemical precipitation* (Doctoral dissertation, University of Pittsburgh), **2011**.
40. T. Chen, P. Chen, H. Montgomerie, T. Hagen, R. Benvie, Q. Guo, X. Yang, Do We Need Higher Dose Scale Inhibitors to Inhibit Scale under Turbulent Conditions? Insight into Mechanisms and New Test Methodology, In *SPE International Oilfield Scale Conference and Exhibition*, *Soc. Pet. Eng. J.*, **2014**.
41. F. Yan, N. Bhandari, F. Zhang, G. Ruan, Z. Dai, Y. Liu, M. Tomson, Scale Formation and Control Under Turbulent Conditions, In *SPE International Oilfield Scale Conference and Exhibition*, *Soc. Pet. Eng. J.*, **2016**.
42. F. Yan, Z. Dai, G. Ruan, H. Alsaiari, N. Bhandari, F. Zhang, M. Tomson, Barite scale formation and inhibition in laminar and turbulent flow: A rotating cylinder approach, *J. Pet. Sci. Eng.*, **2017**, 149, 183-192.
43. F. Yan, F. Zhang, N. Bhandari, G. Ruan, H. Alsaiari, Z. Dai, A. Kan, The Effect of Turbulence on Mineral Scale Control in Oilfield, In *SPE International Conference on Oilfield Chemistry*, *Soc. Pet. Eng. J.*, **2017**.
44. J. W. Mullin, *Crystallization*, Elsevier, **2001**.
45. A. Hina, G.H. Nancollas, Precipitation and dissolution of alkaline earth sulfates: kinetics and surface energy, *Rev. Miner. Geochem.*, **2000**, *40*(1), 277-301.
46. S.K. Hamdona, S.M. Hamza, Influence of polyphosphonates on the precipitation of strontium sulfate (Celestite) from aqueous solutions, *J. Taibah Uni. Sci.*, **2009**, 2(1), 36-43.
47. M. C. Van der Leeden, D. Kashchiev, G. M. Van Rosmalen, Effect of additives on nucleation rate, crystal growth rate and induction time in precipitation, *J. Cryst. Growth*, **1993**, 130(1-2), 221-232.
48. D. R. Lide, H. P. R. Fredrikse, CRC handbook of chemistry and physics, CRC Press, Boca Raton, FL. *CRC handbook of chemistry and physics, 75th ed. CRC Press, Boca Raton, FL,* **1994**.
49. W. Beckmann, *Crystallization: basic concepts and industrial applications*, John Wiley & Sons, **2013**.
50. D. F. Jacques, B. I. Bourland, A study of solubility of strontium sulfate, *Soc. Pet. Eng. J.*, **1983**, 23(02), 292-300.
51. E.J. Reardon, D.K. Armstrong, Celestite ($SrSO_{4\ (s)}$) solubility in water, seawater and NaCl solution, *Geochim. Cosmochim. Acta*, **1987**, 51(1), 63-72.
52. R. D. Howell, K. Raju, G. Atkinson, Thermodynamics of "scale" mineral solubilities. 4. Experimental measurements of strontium sulfate (s) in water and aqueous sodium chloride from 25 to 250 °C and from 1 to 500 bar, *J. Chem. Eng. Data*, **1992**, 37(4), 464-469.
53. V.S.J. Craig, B.W. Ninham, R.M. Pashley, Effect of electrolytes on bubble coalescence, *Nature*, **1993**, 364(6435), 317-319.
54. V. S. J. Craig, B. W. Ninham, R. M. Pashley, The effect of electrolytes on bubble coalescence in water, *J. Phys. Chem.*, **1993**, 97(39), 10192-10197.
55. N. Brown, Particle size analysis of large, transparent alumina trihydrate particles by turbidimetry, *Powder Technol.*, **1971**, 4(4), 232-234.
56. S. He, J. E. Oddo, M. B. Tomson, The Nucleation kinetics of strontium sulfate in NaCl solutions up to 6 m and 90 C with or without inhibitors, *J. Colloid Interface Sci.*, **1995**, 174(2), 327-335.
57. W. He, J. Nan, Study on the impact of particle size distribution on turbidity in water, *Desalination and Water Treat.*, **2012**, 41(1-3), 26-34.
58. I. X. Malollari, P. G. Klepetsanis, P. G. Koutsoukos, Precipitation of strontium sulfate in aqueous solutions at 25 °C, *J. Cryst. Growth*, **1995**, 155(3-4), 240-246.
59. A. E. Nielsen, Homogeneous nucleation in barium sulfate precipitation, *Acta Chemica Scandinavica*, 1961, 15(2), 441.
60. A. E. Austin, J. F. Miller, N. A. Richard, J. F. Kircher, Precipitation of calcium sulfate from sea water at high temperatures, *Desalination*, **1975**, 16(3), 331-344.
61. Z. Amjad, Environment Treatment & Control MP, **1989**.
62. F. H. Butt, F. Rahman, U. Baduruthamal, Evaluation of SHMP and advanced scale inhibitors for control of $CaSO_4$, $SrSO_4$, and $CaCO_3$ scales in RO desalination, *Desalination*, **1997**, 109(3), 323-332.
63. G. R. Campbell, G.H. Nancollas, Crystallization and dissolution of strontium sulfate in aqueous solution, *J. Phy. Chem.*, **1969**, *73*(6), 1735-1740.
64. M. Kawase, K. Miura, Fine particle synthesis by continuous precipitation using a tubular reactor, *Adv. Powder Technol.*, **2007**, 18(6), 725-738.
65. J. Sun, R. Sun, Z. Xia, H. Du, Facile room temperature morphology-controlled synthesis of $SrSO_4$ microcrystals, *Cryst. Eng. Comm.*, **2012**, 14(3), 1111-1116.
66. C. L. Henry, C. N. Dalton, L. Scruton, V.S.J Craig, Ion-specific coalescence of bubbles in mixed electrolyte solutions, *J. Phys. Chem.,* **2007**, (111), 1015-1023.
67. J. Toth, A. Kardos-Fodor, S. Halász-Péterfi, The formation of fine particles by salting-out precipitation, *Chem. Eng. Process.: Process Intensification*, **2005**, 44(2), 193-200.
68. B. W. Ninham, R. M. Pashley, P. Lo Nostro, Surface forces: Changing concepts and complexity with dissolved gas, bubbles, salt and heat, *Curr. Opin. Colloid Interface Sci.,* **2016**, 27, 25-32.

69. M. Taseidifar, J. Anthony, R.M. Pashley, Prevention of Cavitation in Propellers, *In press: Substantia: An International Journal of the History of Chemistry,* **2020**.
70. H. K. Kim, E. Tuite, B. Norden, B.W. Ninham, Coiondependence of DNA nuclease activity suggests hydrophobic cavitation as a potential source of activation energy Eur. *Phys. J. E*, **2001**, 4, 411–417.
71. S. V. Gudkov, G. A. Lyakhov, V.I. Pustovoy, I.A. Shcherbakov, Influence of Mechanical Effects on the Hydrogen Peroxide Concentration in Aqueous Solutions, *Phys Wave Phenom,* **2019**, 27(2), 141-144.
72. B. W. Ninham, P. Lo Nostro, Unexpected Properties of Degassed Solutions, *J. Phy. Chem. B,* **2020**, 124(36), 7872-7878.
73. A. E. Voinescu, D. Touraud, A. Lecker, A. Pfitzner, W. Kunz, B. W. Ninham, Mineralization of $CaCO_3$ in the Presence of Egg White Lysozyme, *Langmuir,* **2007**, 23, 12269-12274.
74. B. P. Reines, B.W. Ninham, Structure and function of the endothelial surface layer: unraveling the nanoarchitecture of biological surfaces, *Quarterly Rev. Biophys.,* **2019**, 52, 1–11.
75. A. G. Sanchis, R. M. Pashley, B. W. Ninham, Virus and bacteria inactivation by CO_2 bubbles in solution, *NPJ Clean Water,* **2019**, (2) Number 1.
76. A. G. Sanchis, L. Jin, Evaluation of the new energy-efficient hot bubble pilot plant (HBPP) for water sterilization from the livestock farming industry, *Water Resour. Ind.*, **2020**, 24, 100135.

APPENDIX
FACTORS CONTROLLING PRECIPITATION

The "reaction" Eq. (1) for the formation of particles is impeccably correct.

$$Sr^{2+}_{(aq)}+SO_4{}^{2-}_{(aq)}\rightleftarrows SrSO_{4(S)}$$

However, the reactants have no respect for equations on pieces of paper and something more inscrutable lies beneath it. We note first that the entire field of physical chemistry is undergoing revision due to sins of omission and commission at this time.[68] The problem of Hofmeister effects with all its consequences is on the way to resolution. But the more important issue is the omission in classical theory of the effects of dissolved gas. The omission is monumental in its consequences, a fact still only dimly perceived.

We showed the effects of cavitation on a propeller which is explored in detail in a paper in this Substantia Journal issue.[69] The reactions that produce propeller corrosion is due to the collapse of nanobubbles, that are accompanied by free radical production. The same free radicals are also produced by spontaneous cavitation in the active sites of an enzyme and are due to cooperative harnessing of all the weak van der Waals and other molecular forces to produce a chemical energy available to do the job.[70]

Nanobubbles containing reactive hydrogen peroxide are produced even by shaking, without any need for heavy sonication.[70,71]

In this paper both stirring at different speeds and turbulence accompanying the BCE process would therefore be expected to produce nanobubbles of different sizes and stability. These should also produce sites for the selective adsorption of both anions and cations and enhanced reactivity.

We have already discussed another related fundamental work that studies the effects of magnetic fields and temperature on the precipitation of alkaline earth metal salts.[33] The magnetic field seems too small an influence here. But who knows? Permanent magnets placed outside steel pipes prevent scaling. This works but no one knows why.

The effects of temperature are also large and specific in Ref [33] and that too can be put into the nanobubble causality camp. Water is generally agreed to lose its hydrogen bonding between 80-90 °C. So, our elusive nanobubbles will be different at higher temperatures, as will specific ion adsorption and reactivity.

Of all the different methods used to produce monodisperse nano or micro particles, the work Ref [29] is closest. In our study we used a mixture of

$$0.005M\ Sr(NO_3)_2 + 0.005\ M\ Na_2SO_4$$

and precipitated out particles of strontium sulphate. In Ref [29] the precipitated particles were $Mg(OH)_2$. The initial solution contained soluble salts of magnesium in a background of sodium hydroxide. The counterions of the magnesium source salts affect the size and the specific surface area of crystallites with a trend that follows a Hofmeister series of anions: (sulfate < chloride < nitrate < perchlorate). It was also shown that depending on the concentration of background salt the precipitated particles could vary in size from a micron to zero radius.

The two experiments are difficult to compare. With $Mg(OH)_2$ the background of indifferent anions are at high concentrations 0.2, 0.4, 1, and 2 M. The solutions were vigorously stirred as for our case. The same controlled variability in particle size can be achieved with sugars in solution.

The concentrations are well above the 'critical concentration' for bubble-bubble fusion inhibition.[53,54,66] So, it might be thought reasonable to assign the phenomena of size variability to 'water structure'.

By contrast, the situation for strontium sulfate here the concentrations were typically low at about 0.005 M and hence water structure cannot possibly be an issue.

This throws us firmly back into the wide-open arena of nanobubbles.

Our reference [72] brings the case into strong contention as a crucial, long-neglected hidden variable.

Finally, we remark on two matters that mineralization of calcium carbonate in the presence of proteins is probably the most used chemical reaction in nature by weight, being responsible for shells of all invertebrates.[73] This mineralization is of much interest too because of alarms about climate change.

Ref [73] is exceptionally important as it produced amorphous calcium carbonate for the first time. Ref [74] opens up a new arena too in medicine and biology.

Carbon dioxide foam of nanobubbles is the key component of a crucial new organ in the body, the Endothelial Surface Layer. It plays a key role in protection against viruses and cab and is being used industrially for sterilisation of water. See Editorial and Ref [75, 76].

Substantia
An International Journal of the History of Chemistry

Firenze University Press
www.fupress.com/substantia

Citation: M. Taseidifar, J. Antony, R.M. Pashley (2020) Prevention of Cavitation in Propellers. *Substantia* 4(2) Suppl.: 109-117. doi: 10.36253/Substantia-821

Data Availability Statement: All relevant data are within the paper and its Supporting Information files.

Competing Interests: The Author(s) declare(s) no conflict of interest.

Prevention of Cavitation in Propellers

Mojtaba Taseidifar[1], John Antony[2], Richard M. Pashley[1,*]

[1] *School of Science, UNSW Canberra, Northcott Drive, Canberra, Australia*
[2] *Dynamikx Pty Ltd, 169 Hampton Road, South Fremantle, WA, Australia*
*Corresponding author: r.pashley@adfa.edu.au

Abstract. It is well known that cavitation phenomena affect the efficiency of propellers. It is a major worldwide economic problem for the transport industry. The speed of fast, ocean going vessels is limited by cavitation effects on hydrofoils and propulsion systems. The main approaches by industry to mitigate the detrimental effects of cavitation on propellers is restricted to varying operating conditions, geometric design and employing wear resistant materials. We here develop a simple solution to the problem. It has been known for over a century that dissolved gases reduce the tensile strength of liquids by orders of magnitude. Degassing a liquid dramatically reduces its ability to cavitate. Propeller cavitation in ships and submarines is typically controlled by reducing rotation rate and/or blade pitch. We here demonstrate the astonishing fact that cavitation can be completely prevented by releasing degassed water adjacent to the low pressure side of a rotating propeller, without varying blade speed or pitch. Practical implementation is simple and cheap.

Keywords: cavitation, degassing, hollow fibre membrane, propeller.

1. INTRODUCTION

At the end of the 19th century it was realised that ships were not attaining their projected design speed. This was eventually found to be due to cavitation.[1] The effects of the collapse of a spherical cavity within a fluid were first considered by Besant in 1859.[2] Cavitation in fluids has been studied for over a century since this pioneering work and that of Reynolds in 1886 and Lord Rayleigh in 1917.[3] There are two main types: inertial cavitation, created by differences between boundary and bulk fluid flow in pumps, valves and propellers; and non-inertial cavitation, created by oscillatory processes such as simple shaking and sonication.[1] Cavitation also occurs in fine cavities between solid surfaces.[4] In many diverse processes, cavitation not only reduces the efficiency of fluid systems but the collapse of the created bubbles near surfaces creates shock waves. Shock waves create microjets which impinge upon a surface and create wear. The temperatures produced by the rapid collapse of a bubble can reach 20,000 degrees K, and can cause transient light emission or sonoluminescence, and initiate undesirable reactions in fluid components. The cavitation index C (σ or sometimes k) is used as a measure of cavitation potential and is defined as:[5]

$$C \equiv \frac{(p_r - p_v)}{\frac{1}{2}\rho V^2} \quad (1)$$

where p_r–p_v is the pressure difference due to dynamic effects of the fluid flow; p_r is the local (reduced reference pressure) and p_v the vapour pressure of the fluid (at that temperature). ρ is the density of the fluid and V the fluid velocity. In effect, the cavitation index is the ratio of the work done by the pressure to the work done by the fluid kinetic energy. The critical value of the index C_i is when cavitation inception occurs, and $C < C_i$ corresponds to conditions of advanced cavitation. The ability of a particular fluid to cavitate depends on the tensile strength of the fluid under the operating conditions. In general, $C >> 1$ makes cavitation increasingly unlikely.[6]

In fluid cavitation, it is generally assumed that local suction pressures just below the vapour pressure of a fluid, at a given temperature, will nucleate bubbles which then implode once local hydrostatic pressure returns. In practice, there is a significant additional barrier to the formation of cavities in the absence of suitable nucleation sites, and it is actually very difficult to cavitate pure liquids in clean, smooth vessels. Nano-sized cavities are usually the smallest structures which can be considered as a separate phase, and their growth or collapse controls the extent of cavitation.[4] The presence of dissolved atmospheric gases facilitates fluid cavitation. For example, water can dissolve close to 20 mL of atmospheric gases per litre and hydrocarbons typically absorb ten times more. The removal of these dissolved gases inhibits fluid cavitation.

In 1982, Israelachvili and Pashley[7] made the remarkable discovery that hydrophobic surfaces immersed in water were attracted to each other with a long-range (~10 nm) force much stronger than expected for van der Waals forces. They called this the 'long-range hydrophobic interaction'. Since that discovery, there have been many reports extending the range of the force, depending on surfaces and conditions, in some cases to a range of 300 nm. These observations created a problem for theoretical interpretation simply because the local effect of a hydrophobic, non-hydrogen bonding surface on water should only extend a few water molecules, at most. In 1985, Pashley et al.[4] noticed that a bridging cavity was formed when two solid hydrophobic surfaces were pulled apart in water, and later Christenson *et al.*[8] reported cavitation as two hydrophobic surfaces approached within a few nm, but before making contact. These observations led to the suggestion that the long-range hydrophobic interaction may be caused by the formation of bridging cavities between hydrophobic surfaces, giving a more reasonable explanation for the extraordinarily long range of the force.

Craig et al.[9] have given a thorough review of bulk and surface cavitation and its link to nanobubbles. Two recent studies[10, 11] have also considered the formation and applications of bulk nanobubbles.

If cavitation held hydrophobic surfaces together, then it follows that the inhibition of cavitation by removing dissolved atmospheric gases may indeed allow oil and water to mix. This idea was tested by Pashley (in 2003)[12] by studying the effects of degassing on the dispersion of oil droplets in water. Hydrocarbon oils such as decane immediately phase separated after shaking with water but, upon degassing, a fine stable dispersion was easily produced. This work demonstrated that cavitation also plays a central role in the dispersion of oil in water.

We note in passing that with colloidal systems involving electrolytes (DLVO) forces and Hofmeister effects change dramatically with removal of dissolved gas, a fundamental matter attracting much interest.

The presence of dissolved, non-polar gas molecules in a surrounding fluid, in equilibrium with the atmosphere, produces nucleation sites throughout this fluid. Both aqueous and non-aqueous fluids show similar effects, and, in addition, non-polar fluids have an increased capacity to dissolve non-polar gases relative to water. It has been demonstrated[13], and is elucidated upon in this work, that degassing a separate quantity of the fluid, and releasing it such that it flows directly onto a moving surface can completely prevent cavitation by providing a boundary layer of degassed fluid on the surface.

2. MATERIALS AND METHODS

2.1. Materials

Hollow fibre membranes were purchased from Membrana, Charlotte, USA (Model 2×6 Radial Flow Superphobic). A vacuum pump, Fossa FO 0015 A (Busch Sydney, Australia) was used for de-gassing. A diaphragm water pump (model: FloJet-D3732-E5011) was purchased from CreativePumps Australia. A Mettler-Toledo M700 process analysis system fitted with a type O2 4700 ppb module to detect dissolved oxygen levels in liquids in ppb, and fitted with a corresponding InPro 6900 dissolved oxygen electrode was obtained from Mettler-Toledo Ltd., Melbourne, Australia. Tap water with and without added salt (NaCl with 0.17 M) was used in all the experiments.

2.2. Methods

2.2.1. Membrane degassing for water and aqueous solutions

Hollow fibre hydrophobic membrane systems offer the most efficient commercial process for large scale degassing due to providing high surface area of contact per unit volume of fluid.[14] A photograph of the experimental setup used in this study is given in Figure 1. A strong vacuum is applied to the outside of a hollow fibre hydrophobic membrane or membrane array where the dissolved gases emerge, while the aqueous solution flows around a core of hollow fibres. The hollow fibre membranes are strongly hydrophobic (Teflon or polypropylene), and have small pores designed to prevent liquid water passing through them due to the high Laplace pressure of small diameter water/air interfaces. Only water vapour can exist in the pores and the high surface area membrane efficiently transfers water vapour and atmospheric gases out of aqueous solutions. This technique has been used to produce a continuous flow of water more than 99.5% degassed.

In these experiments, tap water was used to determine the effect of degassing on cavitation, and gases were removed from the tap water by pumping it through the membrane using a small diaphragm water pump while applying a vacuum to the inside of the hollow fibres in the membrane. The vacuum pump, with ultimate pressure ≤ 2.5×10^{-2} mbar was protected from exposure to water vapour by two 5 L pyrex glass tanks connected in series filled with pre-dried granular silica gel. The dissolved oxygen content, and thereby the level of degassing, was measured using an InPro 6900 Oxygen electrode with a detection limit of 1ppb in these studies.

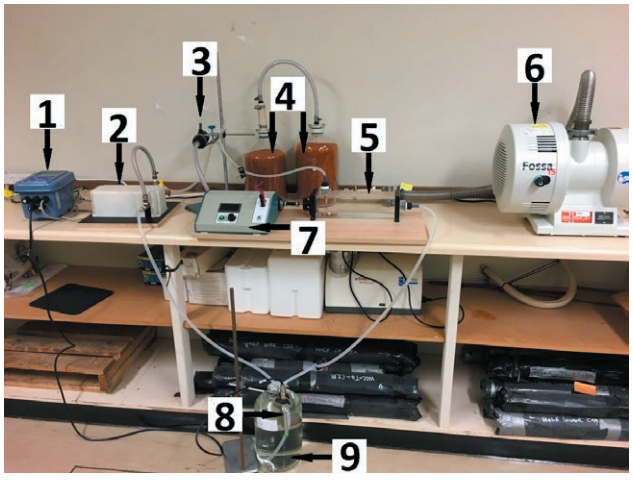

Figure 1. Photograph of the system used to study the effect of degassing on cavitation. (1) M700 process analysis system (to monitor DO levels); (2) Hollow fibre membrane; (3) Water pump; (4) Silica gel tanks; (5) Observation cell; (6) Vacuum pump; (7) Variable motor; (8) DO electrode; (9) Degassed water reservoir.

Cavitation was monitored visually using a Pentax K-5 II S camera aimed at an observation cell, shown in Figure 1. The observation cell (5) was a perspex housing (L: 300 mm, W: 65 mm and H: 65 mm) for a three-blade propeller (5 cm diameter) inside and two metal tubes sealed to the box – one to provide normal gassed water (tap water or salt water) and another one to provide degassed water.

3. RESULTS AND DISCUSSION

3.1. Theoretical prediction of the link between degassing and cavitation pressure

In fluid cavitation, it is generally assumed that local suction pressures just below the vapour pressure of the fluid, at a given temperature, will nucleate bubbles which then implode once local hydrostatic pressure returns. In practice, there is a significant additional barrier to the formation of cavities in the absence of suitable nucleation sites, and it is actually very difficult to cavitate pure liquids in clean, smooth vessels. Nano-sized cavities are usually the smallest structures which can be considered as a separate phase, and their growth or collapse controls the extent of cavitation.[12] Both homogeneous cavitation and heterogeneous nucleation cavitation in water are considered here, caused by the presence of inert dissolved atmospheric gas molecules throughout the bulk liquid phase.

The barrier to 'ideal' homogeneous cavitation can be estimated from a simple analysis of the formation of a nano-sized spherical cavity. The total energy E_T of a cavity of radius r is given by the sum of the negative work done by the suction pressure $-\Delta P$ on the cavity volume and the surface tension work done on creating the surface of the cavity. Thus, the total cavity energy is given by:

$$E_T=\frac{4}{3}\pi r^3(\Delta P)+4\pi r^2\gamma \quad (2)$$

A diagram of the behaviour expected for water is shown in Figure 2. Assuming that nm-sized cavities must form within pure water, the barrier to their formation is very high, of the order of 80 kT, which makes their formation difficult.

If we make the assumption that 1 nm is the critical radius of cavity formation, i.e. when $dE_T/dr = 0$, we can estimate the critical suction pressure from the Laplace equation:

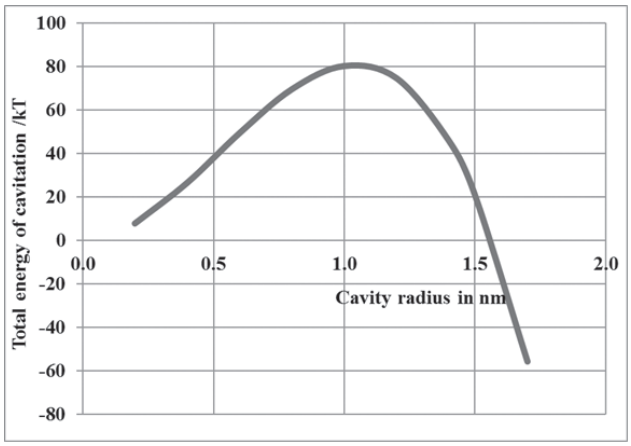

Figure 2. Theoretical calculation of the energy (in kT units) required to form a spherical cavity of radius r in pure water under ideal, de-gassed conditions, in the absence of nucleation sites, with an applied suction pressure of -1400 atm.

$$\Delta P = -\frac{2\gamma}{r_c} \tag{3}$$

This gives a critical suction pressure of about -1,440 atm for pure water or -493 atm for a typical hydrocarbon liquid. The largest suction pressure observed experimentally for degassed water was -1400 atm, which is close to theoretical predictions.[16]

In most practical situations, contaminants and 'real', rough surfaces facilitate the heterogeneous nucleation of cavities in water at much lower suction pressures than this. The presence of dissolved gases and hydrophobic groups also substantially reduce the cavitation pressure. Experimental cavitation pressures are typically about -1 atm for distilled water, saturated with air, since this is effectively the vapour pressure of water at room temperature. However, a suction pressure of -200 atm is required when the water is 99.98% de gassed according to[17]; see Figure 3. From these experimental results, it is clear that degassing water strongly inhibits cavitation, especially when degassed to greater than 99%. The disruptive presence of dissolved, non-polar gas molecules in the liquid water phase produces nucleation sites throughout the liquid.[4]

From solid state physics it is well known from studies of lattice dynamics in the harmonic approximation isotopes or impurities attract each other, a collective effective van der Waals interaction and associate into aggregates. The same happens in liquids. It is these that act as nucleation sites that connect adjoining nano sites. An equivalent result occurs with non-aqueous fluids, which also have an increased capacity to dissolve non polar gases relative to water.

A theoretical model has been developed to estimate the cavitation pressure p_c required to cause (heterogeneous) cavitation in water at a wide range of dissolved gas levels. The basic principle used is that the pressure required can be estimated from the change in activation energy $\Delta\mu$ required to transfer a dissolved gas molecule (e.g. N_2) from the aqueous phase to the gas phase. Since $\mu(g,w)$ will change with concentration of the dissolved gas in water x_g, i.e.:

$$\mu(g,w) = \mu^0(g,w) + kT\ln x_g \tag{4}$$

and since the gas-phase chemical potential will stay constant, the activation energy for the transfer from solution to gas phase will vary with concentration in the aqueous solution as:

$$\Delta\mu = kT\ln\left(\frac{x_g^s}{x_g}\right) \tag{5}$$

where x_g^s is the mole fraction of gas in water under standard atmospheric conditions (1 atm).

The cavitation pressure can then be estimated from the activation-energy equation:

$$p_c = p_0 \exp\left(\frac{\Delta\mu}{kT}\right) \tag{6}$$

where p_0 is the standard, i.e. saturated gas cavitation value, of 1 atm.

Hence, it follows that:

$$p_c = p_0\left(\frac{x_g^s}{x_g}\right) \tag{7}$$

Note that for air-equilibrated water, x_g^s is about 1.53×10^{-5}.

Also, note that this result reduces simply to:

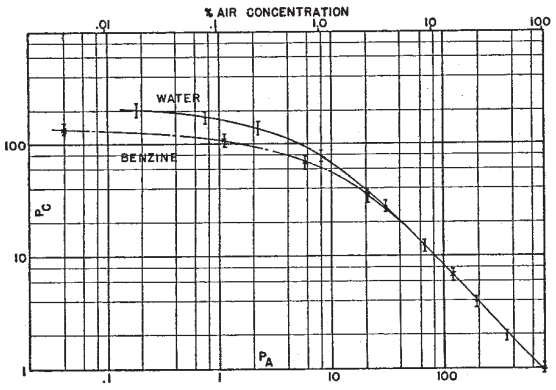

Figure 3. Experimental data showing the effect of de-gassed levels on the suction pressures required to produce cavitation in water and benzene. Reprinted with permission from Ref 16. Copyright 1954, Acoustic Society of America.

$$p_c(atm)=\left(\frac{100}{100-\%deG}\right) \quad (8)$$

This cavitation-pressure model will work for any liquid, since it is based entirely on gas solubility relative to a standard state. A graphical representation of this result is given in Figure 4 and Figure 5.

For the case of water, the model predicts that when the dissolved gas level is reduced to about 0.07% (or about 0.6 μM), the gas cavitation pressure equals that of pure water (note that at 20 °C, water in equilibrium with the atmosphere has 0.85 mM of dissolved gases: N_2, O_2, CO_2 and Ar). The pure water cavitation pressure is at its maximum and can be estimated using the Laplace equation with an estimated, critical cavity radius of 1 nm (eq. 3).

This gives a calculated (homogeneous) cavitation pressure of -1440 atm. This value agrees with the reported experimental value for pure (i.e. completely degassed) water of -1400 atm. These high suction pressures are also consistent with the basic (kinetic) model of condensed liquids, in which the repulsive ideal-gas pressure ($P = nRT/V$) is more than balanced by the cohesive molecular forces. For water at 20 °C, the 'ideal' repulsive molecular pressure P is 1353 atm. Cohesive pressures in liquid water must be higher than this. Thus, there is strong evidence for this high value for pure, completely degassed water.

This analysis strongly suggests that the Galloway data (1954)[17], shown in Figure 3, is correct at relatively low degassing levels (less than 99%) but that the cavitation pressures expected, for pure liquids, at higher levels of degassing was most likely not achieved in these experiments, probably due to the ubiquitous presence of contamination particles, which offer nucleation sites for cavity formation. Thus, the reported maximum of about -200 atm is much less than the theoretical prediction.

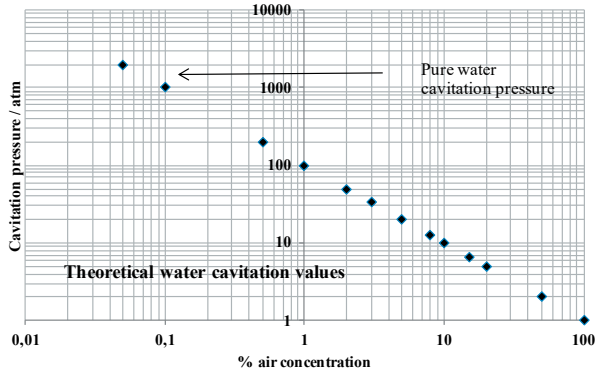

Figure 4. Calculated cavitation pressures for water obtained using Equation (8).

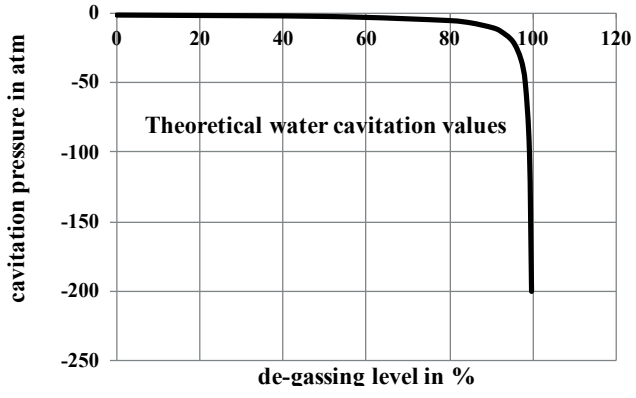

Figure 5. Effect of de-gassing on cavitation in water.

3.2. Experimental study of the prevention of propeller cavitation in degassed water

The cavitation created by a three-blade propeller with a maximum speed of 2960 rpm can be observed inside a water-filled perspex observation cell (Figure 6 and Figure 7). Tap water was pumped at 600 mL/min through the hollow fibre membrane whilst vacuum was applied to its outer housing. The M700 oxygen analysis system displayed the measured oxygen content in the water tank, which continuously decreased.

When seawater was subjected to compressive pressures in the 10–55 atm range, we found in earlier studies[18] that on release of this pressure through a needle valve, cavitation of dissolved gases occurred. It was found that degassing the seawater to above 99% completely prevented this cavitation and this was used[20] to improve the desalinated water product flow rate through a high pressure reverse osmosis system.

In these studies, it was found that by increasing the degassed level of the water, the speed of the propeller could be increased before cavitation was observed, as illustrated in Figure 8. The results of these rotation ate/degassing measurements are summarised in Table 1, which clearly shows that higher degassing levels produced higher cavitation pressures in the system (this data was obtained from the theoretical values for water cavitation in Figure 4). The experiments summarised in Table 1 were reproduced using a 0.5 M NaCl solution to simulate seawater. As an example, 70% degassing was found to be sufficient to prevent cavitation even at the maximum rotation rate of 2960 rpm. This degree of degassing corresponds to a cavitation pressure of about 3 atm, according to Eq. (8).

Figure 6. Photograph of the propeller used to study cavitation at the laboratory scale.

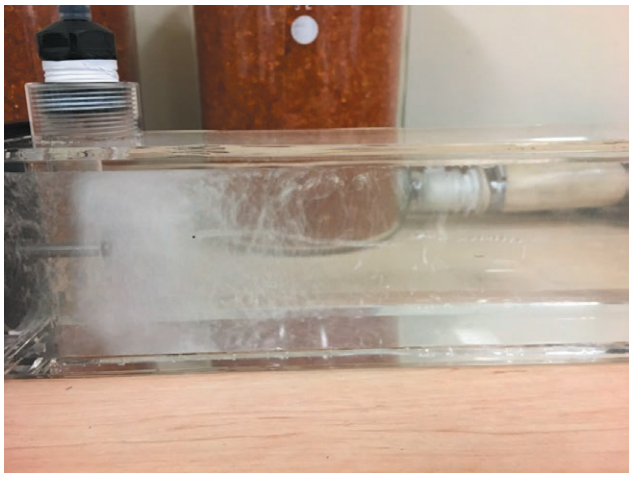

Figure 7. Cavitation occurring in air-equilibrated water at atmospheric pressure at a propeller rotation rate of 2960 rpm.

3.3. Prevention of cavitation using a local degassed aqueous environment

In these experiments, degassed water was introduced locally, close to the low pressure side of rotating propeller blades immersed in gas-equilibrated water. Inside the perspex observation cell, gassed tap water flowed at a rate of 8L/min through a bent metallic pipe (10mm diameter), and 80% degassed water was released through a vertical metallic pipe with suitable holes (4.4 mm diameter and with six holes on the side and one at the end of the pipe) at a flow rate of about 1/10th the background water flow-rate, as shown in Figure 9. With only gassed tap water flowing within the cell, visible cavitation occurred (Figure 9), but when a local flow of degassed water was released adjacent to the propeller blades, all cavitation ceased (Figure 10). These experiments were carried out at high rotation rates of 2300 rpm using a three-blade propeller. The cessation of the sound accompanying cavitation on starting the degassed water flow was also obvious and immediate.

Acoustic measurements also show that the noise level was reduced from 75 dB to 65 dB after releasing the degassed water behind the propeller, despite having another, additional, noise involved which was from the water pump releasing the degassed water. The observed drop in dB level, even with the additional pump noise, corresponds to a sound intensity decrease on releasing the degassed fluid, of 10x. Similar results were also obtained using a 0.5 M NaCl aqueous solution to simulate seawater.

Table 1. Experimental results of the de-gassing effects on cavitation observed for a rotating propeller completely immersed in de-gassed water.

Time (min)	De-gassing (%)	Cavitation pressure (atm)	Minimum rpm to start cavitation
0	0	1	–
5	19.7	1.3	148
10	27.8	1.5	592
15	36.9	1.6	1628
20	45.4	1.8	2072
30	56.0	2.8	2500
60	76.7	4	Not even with 2960
90	84.4	7	Not even with 2960
120	87.0	8	Not even with 2960

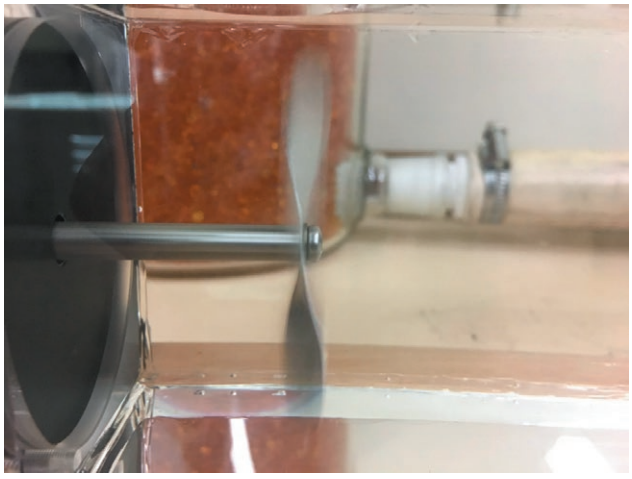

Figure 8. Complete cavitation prevention after gassed water was replaced with 70% de-gassed tap water (at 2960 rpm propeller).

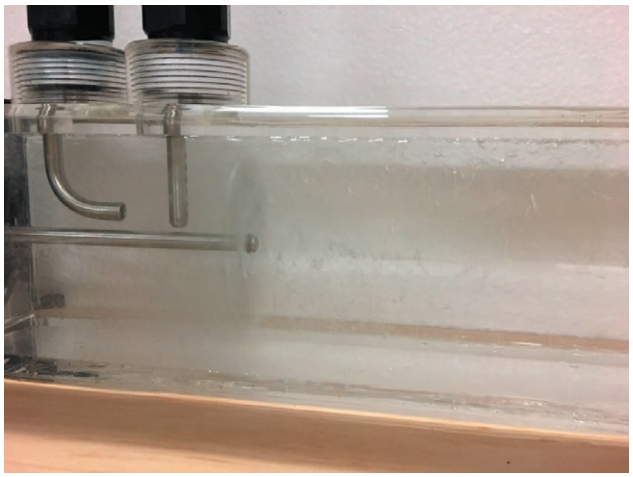

Figure 9. Cavitation occurring in flowing tap water at atmospheric pressure, i.e. in fully gassed water (at 2300 rpm).

Figure 10. Cavitation completely prevented in gassed tap water after flowing 80% de-gassed water directly onto the rotating propeller blades (at 2300 rpm).

3.4. Effects of degassed boundary layer films on a rotating propeller blade

When the flow of degassed water was terminated, it was observed that the cavitation effects remained absent for several seconds or 100-200 rotations of the propeller. This is consistent with the observation (shown in Figure 10) that release of degassed water onto the upper rotating propeller blade prevented cavitation effects through a full cycle of the blade. These observations support the view that coating a rotating propeller with a film of degassed fluid is sufficient to give protection against cavitation.

The lowest pressure regions on the low pressure side of a rotating propeller blade are at the edge and the tip

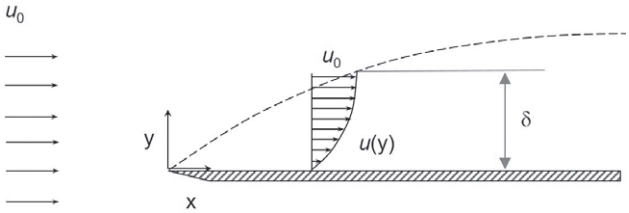

Figure 11. Schematic diagram of stationary or boundary-layer formation as a fluid flows over a flat solid surface (Adapted from David Weybourne (https://en.wikipedia.org/wiki/Boundary_layer_thick).

of the blade. For zero-slip conditions, water flow across a plate of length x (i.e. the propeller blade), will slow down to zero at the surface, as shown in Figure 11.

The experimental boundary layer equation can be used to calculate the thickness δ of the water layer next to the plate at which the incident flow velocity reaches 99% of the bulk water flow velocity:[19,20]

$$\delta = 5x/\sqrt{(R_e)} \tag{9}$$

where R_e is the Reynolds number. This situation is shown in Figure 11, illustrating the 'zero-slip' condition, in which the fluid velocity slows to zero on the surface. The Reynolds number of the fluid depends on the distance x the fluid has moved over the surface and these two parameters (R_e, x) determine the thickness δ of the boundary layer.[20]

The Reynolds number in this case is given by

$$R_e = (\rho V_\infty x)/\mu \tag{10}$$

where ρ is the density of water, V_∞ the bulk fluid velocity (i.e. the incident fluid velocity beyond the boundary layer), μ is the dynamic viscosity of water and x is the position on the surface.

Typically, R_e corresponding to laminar flow will be in the range 1000 to 5×10^5. For example, if R_e = 50,000, the boundary-layer water thickness d will be about 1.1 cm for an x value of 0.5 m. Much closer to the surface, say within 1% of the boundary layer thickness, the water moves only slowly relative to the solid surface: in a water layer of 110 μm thickness, the water flow velocity is about 10 cm/s.

Cavitation occurs when dissolved gas is present in a fluid such as water. For the diffusion of gas in one direction (x), the appropriate equation is Fick's second law in the form:[21]

$$\frac{\partial C}{\partial t} = D\frac{\partial^2 C}{\partial x^2} \tag{11}$$

where C is the solute concentration and D the diffusion coefficient. When completely degassed water is exposed to air at atmospheric pressure, a very thin layer will form rapidly at the surface which will be at the atmospheric dissolved gas concentration (of 0.85 mM). This layer will maintain its saturated concentration from then onwards (in equilibrium with the atmosphere), and the dissolved gas will subsequently diffuse further into the water beyond this layer. Thus, Fick's law must be solved for the boundary conditions $C = C_0$, when $x = 0$ for any value of t and $C_x = 0$ for $x > 0$ when $t = 0$. Also, $C_x = C_0$ for any value of x as t becomes very large. The solution to Fick's law under these conditions is:[21]

$$C = C_0 \left[1 - \mathrm{erf}\left(\frac{x}{2\sqrt{Dt}}\right)\right] \tag{12}$$

where the error function can be calculated using either tables or, as for the present calculation, using the series:[21]

$$\mathrm{erf}x = \frac{2}{\sqrt{\pi}} \int_0^x e^{-t^2} dt = \frac{2x}{\sqrt{\pi}} \left[1 - \frac{x^2}{1\times3} + \frac{x^4}{2\times1\times5} - \frac{x^6}{3\times2\times1\times7} + \cdots\right] \tag{13}$$

For oxygen and nitrogen gases in water the value of the diffusion coefficient D at 20 °C is about 2×10^{-5} cm^2/s and the saturated gas concentration, C_0 is about 0.85 mM. Using these values, the calculated results obtained show that for quiescent water that is in the almost stationary part of the boundary layer, closest to the solid surface, significant re-gassing of a degassed water film of about 100 μm thickness would take several seconds.

Thus, a transient coating of a boundary layer of degassed water on a rapidly rotating blade can be used to prevent cavitation effects for many subsequent rotations. This means that the amount of degassed water required to prevent or minimise cavitation can be substantially reduced, and the effect of cavitation minimisation can persist for a significant period of time e.g. a few or more seconds. The effect of reducing the occurrence of cavitation will persist until the stationary film drains as the blade rotates or until diffusion from the bulk fluid re-gasses the degassed film.

The effects of having a transient film of degassed fluid could be further optimised by having a periodic, controlled release of a positive, relatively high pressure flow of degassed fluid, released close to the rotating blades and timed to strike the leading edge on the negative pressure side. Once the de-gassed fluid strikes the blade, it would coat the face with degassed fluid (e.g. water) and form a boundary layer. The zero-slip boundary condition will ensure the retention of a degassed film on the rotating surface. Put another way, the degassed fluid could be periodically directed onto the surface using a pulsed flow to form the boundary layer. Use of a pulsed flow of degassed fluid may mean degassed fluid only needs to be released in a periodic fashion, such as every 1 in 100 rotations of the blade, or for only 1% of the time.

The leading edge of the rotating blade divides the incident flow into a high pressure stream on the nearly flat 'lower' face and a low pressure stream on the upper side of the blade. As the blade rotates, the film of degassed water will drain from the leading edge to the trailing edge of the blade, and suppress cavitation across the low pressure face. At the same time, dissolved gases within the flowing fluid (e.g. water) begin to diffuse into the degassed boundary layer. However, gas diffusion under effectively quiescent conditions next to the solid surface is relatively slow; for a 0.1 mm film, this re-gassing will take several seconds.

In addition to these effects, the centrifugal forces generated by the rotating blade will force the degassed boundary layer to flow towards the tip of the rotating blade, which will also help to prevent cavitation at this point, where it is often observed.

4. CONCLUSIONS

This study has demonstrated a new method for preventing cavitation at a surface that moves relative to a fluid. The method comprises directing a second fluid that is at least partially degassed towards the surface, where it will form a boundary layer. The boundary layer at least partially increases the negative pressure required to initiate cavitation at the surface, reducing the occurrence of cavitation during the relative movement. Collapse of the cavities formed during cavitation creates shockwaves, and hence microjets, which impinge upon surfaces, creating noise and causing wear, for example, on propeller blades. In these experiments, noise generation was completely suppressed, which suggests that wear could also be substantially reduced. Therefore, this process may help to reduce cavitation noise and wear and improve the efficiency of propeller-driven boats, ships and submarines.

5. ACKNOWLEDGEMENTS

The authors would like to acknowledge Mechanical Workshop staff at the School of Science at UNSW Canberra.

REFERENCES

1. H. Kato, Cavitation, in Advances in Marine hydrodynamics, *Computational mechanics publications*, **1996**.
2. C.E. Brennen, Cavitation and Bubble Dynamics, *Oxford University Press*, **1995**.
3. L. Rayleigh, VIII. On the pressure developed in a liquid during the collapse of a spherical cavity, *The London, Edinburgh, and Dublin Philosophical Magazine and Journal of Science*, **1917**, 34 (200), 94-98.
4. R. M. Pashley, P. M. McGuiggan, B. W. Ninham, D. F. Evans, Attractive forces between uncharged hydrophobic surfaces: direct measurements in aqueous solution, *Sci.*, **1985**, 229(4718), 1088-1089.
5. R. W. Johnson, *Handbook of Fluid Dynamics*, **1998**, CRC Press.
6. Z. Pan, A. Kiyama, Y. Tagawa, D. J. Daily, S. L. Thomson, R. Hurd, T. T. Truscott, Cavitation onset caused by acceleration, *Proc. Nat. Acad. Sci.*, **2017**, 114(32), 8470-8474.
7. J. N. Israelachvili, R. M. Pashley, The hydrophobic interaction is long range, decaying exponentially with distance, *Nature*, **1982**, 300(5890), 341-342.
8. H. K. Christenson, J. N. lsraelachvili, R. M. Pashley, Properties of Capillary Fluids at the Microscopic Level, *SPE Res. Eng.*, **1987**, 155-165.
9. M. Alheshibri, J. Qian, M. Jehannin, V.S.J. Craig, A history of nanobubbles, *Langmuir,* **2016**, 32, 11086−11100.
10. A. Agarwal, W. J. Ng, Y. Liu, Principle and applications of microbubble and nanobubble technology for water treatment, *Chemosphere*, **2011**, 84, 1175-1180.
11. Z. Fang, X. Wang, L. Zhou, L. Zhang, J. Hu, Formation and Stability of Bulk Nanobubbles by Vibration, *Langmuir,* **2020**, 36, 2264−2270.
12. R. M. Pashley, Effect of degassing on the formation and stability of surfactant-free emulsions and fine teflon dispersions, *J. Phys. Chem. B*, **2003**, 107(7), 1714-1720.
13. J. Antony, R. M. Pashley, M. Taseidifar, Prevention of Cavitation, *World Intellectual Property Organization*, **2018**, WO2018191790
14. M. Rzechowicz, R. M. Pashley, A membrane method for degassing nonaqueous liquids, *J. Colloid Interface Sci.*, **2006**, 298(1), 321-326.
15. M. Rzechowicz, R. M. Pashley, The effect of de-gassing on the efficiency of reverse osmosis filtration, *J. Membr. Sci.*, **2007**, 295(1), 102-107.
16. Q. Zheng, D.J. Durben, G.H. Wolf, C.A. Angell, Liquids at Large Negative Pressures: Water at the Homogeneous Nucleation Limit, *Sci.*, **1991**, 254(5033), 829-832.
17. W.J. Galloway, An Experimental Study of Acoustically Induced Cavitation in Liquids, *J. Acoust. Soc. Am.*, **1954**, 26(5) 849-857.
18. M.J. Francis, R.M. Pashley, M. Rzechowicz, The effects of feed water de-gassing on the permeate flux of a small scale SWRO pilot plant. *Desalination and Water Treat.*, **2011**, 25(1-3) 150-158.
19. J.H. Arakeri, P.N. Shankar, Ludwig Prandtl and boundary layers in fluid flow. *Resonance*, **2000**, 5(12) 48-63.
20. H. Schlichting, K. Gersten, Fundamentals of Boundary–Layer Theory, in Boundary-Layer Theory, *Springer Berlin Heidelberg: Berlin, Heidelberg,* **2017**, 29-49.
21. R. M. Pashley, M. Rzechowicz, L. R. Pashley, M. J. Francis, De-Gassed Water Is a Better Cleaning Agent, *J. Phys. Chem. B*, **2005**, 109(3) 1231-1238.

Substantia
An International Journal of the History of Chemistry

Firenze University Press
www.fupress.com/substantia

Citation: B.W. Ninham (2020) Postscript. *Substantia* 4(2) Suppl.: 119-121. doi: 10.36253/Substantia-1146

Data Availability Statement: All relevant data are within the paper and its Supporting Information files.

Competing Interests: The Author(s) declare(s) no conflict of interest.

Postscript

Barry W. Ninham

Department of Applied Mathematics, Research School of Physical Sciences, The Australian National University, Canberra, Australia
E-mail: barry.ninham@anu.edu.au

1348 was the year of the great plague in Europe. One third of the population died. A project into causes commissioned by the King of France from the best Doctors of Medicine of the premier Sorbonne University found out why. The plague, they discovered, was due to a rare conjunction of the planets Mars, Jupiter and Saturn.

That all made sense. These planets were associated with 3 of the 4 humours of the body, the balance of which determined health. Astrology was God-given in those Geocentric times. To dispute such a proof was tantamount to impiety.

Similar dogma attends the certainty of the science of each and every era. With time the theories of one generation evolve and are dismissed by the next as naïve, comparable with the book of Genesis. But not so credible!

Witness quantum entanglement.

This we know. Nonetheless current scientific theories are invariably defended as vigorously as the Bible is taken literally to be God's revealed truth by some fundamentalist believers. And so it is today.[1] Priests will be priests and professors will be professors.

We have reported on a suite of simple new water technologies, in desalination, in sterilisation, in heavy metal pollution and harvesting, in cavitation, in a new class of environmentally friendly surfactants, on control of slimes and sludges from mining and floods. All are cheap, scalable. All are desperately needed. Why were these not developed before?

The answer is that all depend on science[2] that does NOT fit into the standard dogmas of physical, colloid and surface chemistry. These theories we expect to be the enabling disciplines that underpin life sciences and chemical engineering sciences. In this, the physical sciences have signally failed. They have not done the job. The Greeks told us why. Of the four elements, fire, water, earth and air, we forgot about the air.

OUR THEORIES IGNORED DISSOLVED GAS IN WATER

The exemplar is the electrolyte ion pair specific bubble-bubble fusion interaction inhibition phenomenon.[3] It occurs around 0.17 M, precisely the

ionic strength of the blood. It has been known for a century, widely known for 40 years. Perhaps the simplest imaginable experiment, it cannot be explained by classical physical chemistry. The standard theories also omit specific ion (Hofmeister effects). All of our novel technologies depend on these things.

Concepts like pH and buffers, and pKa and osmotic pressure, activities, zeta potentials and membrane potentials, ion pumps, electrostatic forces, molecular recognition, antibody-antigen and enzyme specificity are part of the language and intuition of biology and electrochemistry.

The interpretation of such measurements that depend on a now outmoded astrology, flawed theories that omit the role of dissolved gas. "Hydrophobic" interactions go away when dissolved gas is removed.[4.] Similarly the theories omit or treat incorrectly specific ion effects. Simulation suffers from the same defects.

So what we think ought to be the relevant science in exploring new arenas is impotent. It is as handicapped as was that geocentric astrology of the good Doctors of Paris.

Our new technologies rely on unexplained effects associated with bubbles and dissolved gas. And as we proceeded it became clearer that we could begin to see the outline of something very new. The very effective sterilisation of water, killing of viruses and other pathogens by warm CO_2 in a column above 0.17 M, physiological concentration suggested more.[5,6] Nanobubbles of CO_2, oxygen and nitrogen under these conditions will also be stable and produce free radicals that drive not just enzymatic reactions,[7,8] but chemical reactivity generally.[9,10,11] And so it turns out. For example, the structure and function of the endothelial surface layer in physiology was revealed as a dynamic foam of CO_2 nanobubbles.[12] It complements the lung surfactant structure and its delivery of oxygen and nitrogen via nanobubbles.[13] The ESL protects tissue from invasions by pathogens and acts to destroy COVID viruses.[14]

The self-assembly of gas nanobubbles as a function of salt in bulk solution[4] and at surfaces mimics the same subtleties in self-assembly as surfactants[15,16] and provides the energy that drives chemical reactions.[7-11] The ubiquity of stable spontaneous nanobubbles that are sources of free radicals[17] adds a whole new flexibility to the rigidity and limitations of present antibody-antigen and enzyme substrate interaction ideas in immunology and biochemistry.

THESE THINGS IF ONLY DIMLY PERCEIVED, ARE NOW A LITTLE CLEARER

There remains the hurdle of Dean Swift's Confederacy of Dunces and their dialogue of the deaf. But if we ignore them, we can begin to see a scientific parallel for the Reverend Martin Luther King's Promised Land.

We remark finally that an excellent study of the effects of shaking and bubbles on inactivation of virues and bacteria as long ago as 1948.[18]

REFERENCES

1. B. W. Ninham, The Biological/Physical Sciences Divide and the Age of Unreason, *Substantia*, **2017**, 1 (1) 7- 24.
2. B. W. Ninham, R. M. Pashley, P. Lo Nostro, Surface forces: Changing concepts and complexity with dissolved gas, bubbles, salt and heat, *Curr. Opin. Colloid Interface Sci.*, **2016**, 27, 25-32.
3. V. S. J. Craig, B. W. Ninham, R. M. Pashley, The Effect of Electrolytes on Bubble Coalescence in Water, *J. Phys. Chem.* **1993**, 97 (39), 10192-10197.
4. B. W. Ninham and P. Lo Nostro, Unexpected Properties of Degassed Solutions, *J. Phys. Chem.*, **2020**, 124(36), 7872-7878.
5. A. G. Sanchis, R. M. Pashley, B. W. Ninham, Water sterilisation using different hot gases in a bubble column reactor, *J. Environ. Chem. Eng.,* **2018**, 6, 2651-2659.
6. A. G. Sanchis, R. M. Pashley, B. W. Ninham, Virus and bacteria inactivation by CO_2 bubbles in solution, *NPJ Clean Water*, **2019**, v 2 Number 1.
7. H.-K. Kim, E. Tuite, B. Nordén, B. W. Ninham, Co-ion dependence of DNA nuclease activity suggests hydrophobic cavitation as a potential source of activation energy, *Eur. Phy. J.*, **2001**, 4, 411-417.
8. B. Feng, R. P. Sosa, A. K. F. Mårtensson, K. Jiang, A. Tong, K.D. Dorfman, M. Takahashi, P. Lincoln, C. J. Bustamante, F. Westerlund, B. Nordén, Hydrophobic catalysis and a potential biological role of DNA unstacking induced by environment effects, *P. National Acad. Sci. United States of America*, **2019**, 116, 17169–34343.
9. M. E. Karaman, B. W. Ninham, R. M. Pashley, Effects of dissolved gas on emulsions, emulsion polymerization, and surfactant aggregation, *J. Phys. Chem.,* **1996,** 100 (38), 15503-15507.
10. M. Alfridsson, B. W. Ninham, S. Wall, Role of co-ion specificity and dissolved atmospheric gas in colloid interaction, *Langmuir*, **2000**, 16 (26), 10087-10091.
11. B. W. Ninham, K. Kurihara, O. I. Vinogradova, Hydrophobicity, Specific Ion Adsorption and Reactivity, *Colloids Surf., A: Physiochem. Eng. Aspects*, **1997,** 123-124, 7-12.
12. B. P. Reines, B. W. Ninham, Structure and function of the endothelial surface layer: unraveling the nano-

architecture of biological surfaces, *Quarterly Rev. Biophys.*, **2019**, 52, 1–11.
13. M. Larsson, K. Larsson, S. Andersson, J. Kakhar, T. Nylander, B. W. Ninham, P. Wollmer, The alveolar surface structure: Transformation from a liposome-like dispersion into a tetragonal CLP bilayer phase, *J. Dispersion Sci. Technol.*, **1999,** 20 (1&2), 1-12.
14. B. P. Reines, B. W. Ninham, Pulmonary intravascular coagulopathy in COVID-19 pneumonia, *Lancet Rheumatol.,* **2020**, 2(8), 458-459.
15. B. W. Ninham, K. Larsson, P. Lo Nostro, Two Sides of the Coin. Part 1. Lipid and surfactant self-assembly revisited, *Colloids Surf. B: Biointerfaces,* **2017**, 152, 326–338.
16. B. W. Ninham, K. Larsson, P. Lo Nostro, Two Sides of the Coin. Part 2. Colloid and Surface Science meets real Biointerfaces., *Colloids Surf. B: Biointerfaces*, **2107**, 159, 394-404.
17. N. F. Bunkin, B. W. Ninham, P. S. Ignatiev, V. A. Kozlov, A. V. Shkirin and A. V. Starosvetskiy, Long-Lived Nanobubbles of dissolved Gas in Aqueous Solutions of Salts and Eurythocyte Suspensions, *J. Biophotonics*, **2011**, 4 (3), 150–164.
18. M. H. Adams, Surface inactivation of bacterial viruses and of proteins, *J. Gen. Physiol.,* **1948**, 31(5), 417-431.

Finito di stampare da
Logo s.r.l. – Borgoricco (PD) – Italia

September 2020

No walls. Just bridges

Substantia

An International Journal of the History of Chemistry

Vol. 4 – n. 2
Suppl.

Table of contents